Functional Analysis of CASTOR in Vertebrate Cardiomyocyte Differentiation

Kathleen S. Christine

A dissertation submitted to the faculty of the University of North Carolina at Chapel Hill in partial fulfillment of the requirements for the degree of Doctor of Philosophy in the Department of Biology.

Chapel Hill
2009

Approved by:

Frank Conlon

Victoria Bautch

Stephen Crews

Mark Majesky

Joan Taylor

ABSTRACT

KATHLEEN S. CHRISTINE: Functional Analysis of CASTOR in Vertebrate Cardiomyocyte Differentiation
(Under the direction of Dr. Frank L. Conlon)

Cardiomyocyte differentiation is a complex coordination of cellular and molecular transformations which allows a mature cardiomyocyte to perform a specialized function within the chambered heart. Both intrinsic and extrinsic cues mediate the transition of a cardiomyocyte progenitor into a differentiated cardiomyocyte. However, very little is known about the molecular pathways that govern this differentiation process. In this thesis, we explore the regulation of differentiation in cardiomyocyte progenitors.

We identified a novel para-zinc finger transcription factor, CASTOR (CST), which is expressed within the cardiomyocyte progenitors immediately prior to the onset of cardiac differentiation. We show that CST is required for the differentiation of the ventral midline cardiomyocyte progenitor population and to regulate the proliferation of the differentiated lateral cardiomyocytes. In the absence of CST, this ventral midline cardiomyocyte population remains in the progenitor state. Fate mapping of the ventral midline cardiomyocyte progenitors

reveals that they ultimately contribute to the outer curvature of the future ventricle. However, the CST-depleted ventral midline cardiomyocyte progenitors overproliferate and remain as a coherent population of nonintegrated cells in the outer wall of the myocardium.

To begin to decipher how CST regulates cardiomyocyte differentiation, we performed a bacterial one-hybrid assay to determine that CST binds to a ten basepair DNA binding sequence CTAGTGGTGG. In addition, we used a cloning chromatin immunoprecipitation (ChIP) screen to identify direct transcriptional target genes of CST. We further show that CST may regulate the transcription of genes associated with cell growth control, cell migration and adhesion, Wnt signaling and myocardium patterning. This work provides insight into how CST may influence cardiomyocyte differentiation.

ACKNOWLEDGEMENTS

There are many people that I would like to thank for contributing both support and encouragement through the duration of this thesis. First, I would like to thank previous and current members of the Conlon lab: Chris Showell, Sarah Goetz, Yvette Langdon, Elizabeth Mandel, Daniel Brown, Erika Paden, Stephen Sojka, Kerry Dorr, Erin Kaltenbrun, Lauren Kuchenbrod and Jackie Swanik. Many of my lab mates have contributed scientific insight that has allowed my thesis to evolve over the years. In my opinion, one of the best qualities of the Conlon lab is the camaraderie. It has been enjoyable to come to work everyday when you are surrounded by people who can make you laugh. This is especially helpful and uplifting when experiments are not going as planned. I would also like to thank Mira Pronobis, a master's student who visited the Conlon lab for two months. Mira prepared over seven-hundred DNA preps for the cloning ChIP screen. I am very grateful for her efforts and her contribution to the success of this screen.

I owe a great deal of thanks to Frank Conlon for being an enthusiastic mentor. I was fortunate to have joined Frank's lab, and I could not have asked for a better experience. I feel that Frank has prepared me for my future endeavors as a scientist. Frank allowed me to have an enormous amount of

freedom with my research, for which I am very grateful. I feel that this environment has allowed me to develop the independence needed to be a successful scientist.

I would also like to thank my committee members: Vicki Bautch, Steve Crews, Mark Majesky and Joan Taylor. My committee has provided valuable insight and constructive discussions about my research.

Finally, I would also like to thank my family for all their constant support, understanding, and encouragement throughout the entirety of my education. I would especially like to thank my mother who instilled in me the value of hard work. She has taught me that achievements in life only come with hard work and perseverance. I also need to thank my husband, Jason Clayton. He has been incredibly supportive and encouraging. There have been times when I truly thought he was more versed in my work than I was. He has sat through countless practice talks and read many drafts of grants and manuscripts. I am very grateful for his insight and help in my thesis project.

TABLE OF CONTENTS

LIST OF FIGURES

LIST OF TABLES

LIST OF ABBREIVATIONS

Vertebrate CASTOR	CST
Drosophila CASTOR	dCAS
Cardiac Myosin Light Chain 2	CMLC2
Ventricular Myosin Heavy Chain	VMHC
Myosin Light Chain 1v	MLC1v
Fibroblast Growth Factor	FGF
Bone Morphogenesis Protein	BMP
β-galactosidase	β-gal
Outflow tract	OFT
Secondary heart field	SHF
Cardiac neural crest	cNC
Epithelial to mesenchymal transition	EMT
Epicardial-derived cells	EPDCs
Vascular Endothelial Growth Factor Receptor-2	VEGFR2
Platelet-Derived Growth Factor Receptor-β	PDGFRβ
Wilm's Tumor-1	WT-1
Retinoic acid	RA
Heat Shock Protein 27	HSP27
Atypical protein kinase C	aPCKλ
Atrial Natriuretic Factor	ANF
Hypoxia Inducible Factor 1alpha	Hif1α
Hunchback	Hb

Kruppel	Kr
POU homeobox transcription factor 1/2	Pdm
Neuroblasts	NB
Ganglion mother cell	GMC
Morpholino	MO
Tropomyosin	Tmy
Myosin Heavy Chain	MHC
Bacterial one-hybrid	B1H
DNA binding sequence	DBS
3-Aminotriazole	3-AT
Electromobility Shift Assay	EMSA
Chromatin Immunoprecipitation	ChIP
Planar Cell Polarity	PCP
Left Ventricular Non-Compaction	LVNC

Chapter 1

Introduction

Cardiogenesis involves a highly orchestrated series of events including specification, proliferation, migration, differentiation and morphogenesis. Disruption of any one of these steps has a tendency to result in a congenital heart defect. According to 2008 statistics, congenital heart defects are present in nine out of every one thousand live births. Consequently, 1.3 million Americans live with a congenital heart defect (Lloyd-Jones et al., 2008). While the most prevalent congenital heart defect involves defects in the ventral septum, many malformations result in valve defects that many not be detected until adulthood (Lloyd-Jones et al., 2008). To determine the causes of these congenital heart defects and generate treatments, the process of cardiogenesis must be better understood. Specifically, the mechanisms by which a naïve progenitor cell is instructed to become a functional cardiomyocyte are not fully known. Therefore, delineating these mechanisms will likely yield information that can be translated to the treatment of human cardiac disease.

Extensive cardiac research has greatly advanced the understanding of cardiogenesis; however, there remain significant gaps in knowledge of the

complex underpinnings of heart development. In particular, it is not known how a cardiomyocyte progenitor, for example, integrates positional cues to identify itself as a ventricle cardiomyocyte versus another type of cardiomyocyte. Moreover, it is not known how that cardiomyocyte progenitor differentiates into a specialized cardiomyocyte to perform one of many functions within the heart chamber. The primary focus of this thesis was to identify novel mechanisms of cardiomyocyte differentiation by characterizing a novel cardiac transcription factor, CASTOR, and the mechanism by which it functions.

VERTEBRATE HEART DEVELOPMENT

In all vertebrate species, the heart is the first organ to form. Despite interspecies differences in cardiac anatomy, the complex processes of cardiogenesis are highly conserved among vertebrates. Lineage tracing experiments in the mouse and chick have shown the cardiomyocyte progenitors originate from two bilateral populations of cells within the epiblast, lateral to the cranial portion of the primitive streak. During gastrulation, these cells are specified into the cardiac lineage as they undergo an epithelial to mesenchymal transition and ingress through the cranial portion of the primitive streak (Garcia-Martinez and Schoenwolf, 1993; Tam and Beddington, 1987; Tam et al., 1997). Similarly in *Xenopus*, blastomeres fated to contribute to the heart can be identified as early as the 32-cell stage. These cells reside in two populations located in the dorsal marginal zone on either side of the organizer (Cohen-Gould and Mikawa, 1996; Dale and Slack, 1987; DeHaan and Ursprung, 1965; Moody,

1987). During gastrulation, these cells are specified to the cardiac lineage (Antin et al., 1994; Nascone and Mercola, 1995; Sater and Jacobson, 1989).

Lineage tracing studies in the chick demonstrated that the cranial-caudal order in which the cardiac progenitors ingress through the primitive streak is maintained in the cranial-caudal organization of the cardiac progenitors in the future primary heart tube. This process is referred to as coalignment (Garcia-Martinez and Schoenwolf, 1993; Lopez-Sanchez et al., 2001; Rosenquist, 1970). Thus, the first cardiac progenitors that ingress though the cranial primitive streak give rise to the cranial region of the linear heart tube whereas the last cardiac progenitors to ingress through the middle of the primitive streak give rise to the caudal region of the linear heart tube. It remains unknown if coalignment exists in the mouse. In all vertebrate species, including the mouse, chick, frog, and fish, the cardiomyocyte progenitors migrate within the lateral plate mesoderm anteriorally and ventrally towards the anterior ventral midline of the embryo (Fishman and Chien, 1997; Kolker et al., 2000; Mohun et al., 2000; Sater and Jacobson, 1990).

As cardiomyocyte progenitor cells migrate, they become committed to a cardiac lineage. In several vertebrate species, including mouse, chick, frog and fish, the cardiomyocyte progenitor field is first molecularly distinguished by the expression of NKX2.5, GATA4, -5 and -6 (Charron and Nemer, 1999; Molkentin, 2000; Reiter et al., 1999; Schwartz and Olson, 1999). The molecular

determinants of cardiac induction are not entirely known. However, it is clear that secreted signals emanating from adjacent tissues create a delicate balance of pro- and anti-cardiogenic factors that define the cardiomyocyte progenitor field. In the mouse, Hedgehog signals emanating from the primitive streak and the underlying visceral endoderm is a pro-cardiogenic factor that serves as one of the earliest identified inducers of Nkx2.5 expression (Zhang et al., 2001). In addition, both Sonic and Indian Hedgehog upregulate the expression of BMP4 (Dyer et al., 2001). Meanwhile, studies in the chick show BMP4 and BMP2 secreted from the anterior endoderm juxtaposed to the cardiac region are potent inducers of the cardiac program. BMP4 and BMP2 are required to upregulate expression of Gata4 and Nkx2.5 (Schultheiss et al., 1997). To limit BMP-mediated cardiac induction, the BMP antagonists Noggin and Chordin emanate from the neural plate and notochord in mouse, chick and frog to inhibit the BMP pro-cardiac signals (Klingensmith et al., 1999; Nakajima et al., 2002; Sasai et al., 1994; Zimmerman et al., 1996). Additionally, Wnt-1 and Wnt-3a are secreted from the adjacent neural tissue in chick and frog to inhibit cardiac induction through the canonical Wnt signaling pathway (Schneider and Mercola, 2001; Tzahor and Lassar, 2001). However, to maintain balance, mesodermal expression of Wnt-11 in frog induces cardiomyocyte progenitors though the JNK-mediated, non-canonical Wnt pathway, which in turn inhibits anti-cardiogenic canonical Wnt signals from the adjacent neural tissue (Pandur et al., 2002). While there are many additional signals that regulate cardiac induction, it is clear

that cardiac transcription factors and signals secreted from surrounding tissues work together to delimit the cardiac field.

Cardiomyocyte progenitors in mouse and chick actively migrate as two bilateral sheets within the lateral mesodermal tissue. Progenitors migrate to the ventral midline in part by interacting with a fibronectin matrix deposited between the underlying ectoderm and overlying endoderm (Fig 1.1A) (George et al., 1993; Linask and Lash, 1986). The dependence on fibronectin for directional migration of the cardiomyocyte progenitors was corroborated with the zebrafish fibronectin mutant *natter*. In the absence of fibronectin in *natter* mutants, cardiomyocyte progenitors fail to migrate to the ventral midline resulting in cardia bifida, the formation of two independent hearts in the lateral aspect of the embryo. (Trinh and Stainier, 2004).

As demonstrated in the chick, during normal development, the two bilateral cardiomyocyte progenitor fields fuse across the midline to form a crescent-shaped cardiac field (Fig1.1A). The mesodermal tissue divides into the dorsal somatic mesoderm and the ventral cardiac mesoderm, which is where the cardiomyocyte progenitors are located (Linask, 1992). This cell sorting process gives rise to the lining of the pericardial cavity. Simultaneously, a population of cells segregates from the cardiomyocyte progenitor field and initiates expression of VE-cadherin (Fig 1.1A). This population of cardiac progenitor cells is thought to give rise to the endocardium in mouse and chick (Drake and Fleming, 2000;

Linask and Lash, 1993; Sugi and Markwald, 1996). Chick and mouse cardiomyocyte progenitors become polarized as they begin to express high levels of N-cadherin and β-catenin at apical adherens junctions (Fig 1.1A) (Linask et al., 2005; Radice et al., 1997). Subsequently, the lateral edges of the heart primordium migrate in association with the lateral walls of the forming foregut tube, enclosing the endocardial tissue. The tube then fuses dorsally to form the linear heart tube (Fig 1.1B).

Through a sequence of complex morphological movements, the linear heart tube undergoes right-ward looping (Fig 1.2) (Taber et al., 1995). Simultaneously, the cardiomyocyte progenitors undergo differentiation and chamber formation. This point of cardiogenesis coincides with the onset of cardiomyocyte terminal differentiation as evidenced by the appearance of the cardiac muscle-specific proteins in mouse, chick and frog, including Myosin Heavy Chain α, Myosin Light Chain 2a, and Troponin Ic (Chambers et al., 1994; Drysdale et al., 1994; Franco et al., 1999; Tokuyasu and Maher, 1987). The cardiomyocytes undergo myofibrillogenesis where the myofibrils become organized into sarcomeres, resulting in contractile cardiomyocytes. The linear heart tube continues to extend both cranially and caudally until it detaches and extends from the pharynx, forming the primary linear heart tube (Abu-Issa and Kirby, 2008).

Interestingly, migration of the bilateral cardiomyocyte progenitor fields and heart tube formation in zebrafish proceeds in a slightly different manner. As in higher vertebrates, the cardiac lineage is specified during gastrulation and migrates ventrally in two bilateral fields within the anterior lateral plate mesoderm towards the midline of the embryo (Stainier and Fishman, 1992; Stainier et al., 1993; Warga and Kimmel, 1990). In contrast to higher vertebrates, cardiomyocyte progenitors in zebrafish undergo differentiation during migration, prior to cardiac fusion (Yelon et al., 1999). During somatogenesis stage 13, the cardiomyocyte progenitors uniformly express Cardiac Myosin Light Chain 2 (CMLC2) throughout a majority of the NKX2.5 population (Yelon et al., 1999). A small NKX2.5 population adjacent to the notochord of the embryo does not initiate CMLC2 expression and is thought to not contribute to the myocardium (Serbedzija et al., 1998; Yelon et al., 1999). Simultaneously, the medial leading edges of the bilateral cardiomyocyte progenitor fields initiate expression of Ventricular Myosin Heavy Chain (VMHC). Further analysis demonstrates the $CMLC2^{+}/VMHC^{+}$ population defines ventricular cardiomyocytes, while the $CMLC2^{+}/VMHC^{-}$ population defines atrial cardiomyocytes (Yelon et al., 1999). The expression of these differentiation markers demonstrates the earliest molecular diversification of chamber-specific cardiomyocytes. However, this early pre-cardiac fusion differentiation is unique to zebrafish and absent in higher vertebrates.

As cardiogenesis proceeds in zebrafish, cardiac fusion commences as the two bilateral cardiac fields fuse across the midline at a posterior portion of the medial VMHC^{+} edges, creating a butterfly shape (Yelon et al., 1999). Subsequently, the medial anterior VMHC^{+} regions fuse, generating a lumen that projects dorsally. This dorsal projection of the VMHC expressing cardiomyocyte progenitors generates a shallow cone in the dorsal-ventral axis of the embryo (Stainier and Fishman, 1992). The cone then tilts posteriorly to the right, which in turn extends the heart tube and repositions the heart in the anterior-posterior axis of the embryo (Stainier and Fishman, 1992). This movement continues until the base of the cone coalesces into the tube, generating a linear heart tube oriented with a posterior ventricle and an anterior atrium. The linear heart tube undergoes subsequent movements, similar to cardiac looping, to reorient the ventricle anterior and to the right of the atrium (Stainier and Fishman, 1992). The chamber myocardium thickens as it undergoes concentric growth, in part due to signals emanating from the endocardium (Mably et al., 2006; Mably et al., 2003). The zebrafish heart later undergoes cardiac cushion formation to form valves between the ventricle and atrium (Hu et al., 2000).

Classical lineage and cell labeling studies in the chick have suggested that the anterior region of the heart originates from the addition of extracardiac cells from an unknown source between developmental stages 12 and 18 (de la Cruz et al., 1977; Viragh and Challice, 1973). In 2001, three independent investigations in the chick and mouse identified a cardiac progenitor population in

the anterior splanchnic mesoderm known as the anterior, or secondary, heart field (Cai et al., 2003; Kelly et al., 2001; Mjaatvedt et al., 2001; Waldo et al., 2001). Together, these studies establish the contribution of the anterior heart field population to the myocardial wall of the outflow region of the heart. However, it is intriguing that the anterior heart field has challenged the concept of separate heart fields and their contribution to the mature heart. To appreciate this evolution, one must first understand how the anterior heart field was identified.

In the mouse, the anterior heart field was initially identified using a gene trap method, in which a transgene consisting of nuclear *lacZ* downstream of a Myosin Light Chain 1v (MLC1v) 5' untranslated region randomly integrated upstream of the *fgf10* locus (Kelly et al., 2001). The *nlacZ* expression recapitulated endogenous FGF10 expression, presumably due to the positional effects of *fgf10* enhancers. Analysis of β-galactosidase (β-gal) expression in combination with endogenous FGF10 expression revealed that FGF10 marked the anterior splanchnic mesoderm medial to the earliest differentiated cardiomyocytes within the crescent at E7.5. By E8.5, cells expressing FGF10 and β-gal were displaced to positions anterior and dorsal to the anterior pole of the developing heart, within the splanchnic/pharyngeal mesoderm. By E9.5, bilateral streams of cells expressing β-gal progressively moved into the outflow tract (OFT) and the right ventricle. Interestingly, neither endogenous FGF10 nor the n*lacZ* transgene were expressed in the OFT or the right ventricle indicating that FGF10 expression is extinguished after cells are incorporated into the heart

as differentiated myocardium. The termination of FGF10 expression coincides with the initiation of α-Cardiac Actin in the OFT and the right ventricle myocardium (Kelly et al., 2001).

In chick, the OFT is composed of the proximal conus and the distal trunous. Mjaatvedt et al. labeled a region of the splanchnic mesoderm anterior and dorsal to the linear heart tube in stage 17 chick embryos with Mito Tracker fluorescent dye. These labeled cells gave rise to the cardiomyocytes in the distal conus and the entire truncus of the OFT (Mjaatvedt et al., 2001). Additionally, *in vitro* co-culture assays demonstrated that the proximal region of the developing heart (the right ventricle and the proximal conus) actively recruits anterior splanchnic mesodermal cells and is responsible for their differentiation (Mjaatvedt et al., 2001).

Waldo et al. identified a secondary heart field (SHF) in the chick (Waldo et al., 2001). Waldo et al. localized expression of NKX2.5 and GATA4 from stage 14 to stage 16 in the splanchnic mesoderm dorsal-caudal to the OFT and dorsal-anterior to the inflow tract of the heart. Mito Tracker fluorescent dye was used in stage 14 chick embryos to label cells within the NKX2.5/GATA4- expressing splanchnic mesoderm dorsal-caudal to the anterior (outflow) region of the heart tube. Labeled cells were found to ultimately reside in the proximal region of the conus, yet were not present in the distal truncus of the OFT (Waldo et al., 2001).

However, it is possible that the Mito Tracker dye did not extend to the region of the splanchnic mesoderm that would have populated the truncus.

Further analysis demonstrated that BMP2, which is required for proper differentiation of the primary cardiomyocytes of the linear tube, is co-expressed with NKX2.5 and GATA4 in the dorsal-caudal splanchnic mesoderm. BMP2 is also expressed in the distal myocardial end of the OFT. FGF8 was also shown to be expressed in the pharyngeal endoderm overlying the splanchnic mesoderm; however, FGF8 expression was extinguished at stage 18, coinciding with the completion of myocardial incorporation into the heart. Additionally, HNK-1, a portion of a cell surface glycoprotein that mediates cell-cell/matrix interactions, was expressed as SHF cells translocated into the OFT. As SHF cells differentiated into cardiomyocytes, HNK-1 expression was extinguished. It was concluded that the SHF (splanchnic mesoderm dorsal-caudal to the outflow region) is induced into the cardiac lineage, as evidenced by NKX2.5 and GATA4 expression. This could be an effect of the combinatorial action of BMP2 and FGF8. The SHF progenitor cells become migratory, as indicated by HNK-1 expression, and migrate into the outflow tract region. Within the OFT, these cells encounter increased levels of BMP2 at the distal rim of the myocardium. These high levels of BMP2 initiate the differentiation of SHF progenitor cells into cardiomyocytes of the OFT (Waldo et al., 2001).

The splanchnic mesoderm dorsocaudal to the OFT, the SHF, was also found to enter into the anterior cardiac region to contribute the distal outflow myocardium of the truncus at the level of the semilunar valves as well as the smooth muscle cells at the base of the great arterial vessels in chick (Waldo et al., 2005). However, this addition occurred at stage 22 to stage 28, hours later than the initial addition of SHF-derived myocardium to the proximal OFT (Waldo et al., 2001). The addition of the SHF myocardium to the OFT and the smooth muscle cells to the arterial vessels was impaired by unknown mechanisms in cardiac neural crest (cNC) ablated embryos (Yelbuz et al., 2002). The cNC cells originate from the neural tube in the somitic region of the embryo, where they migrate to the heart via the pharyngeal arches to form the aorticopulmonary septum, which separates the truncus into the ascending aorta and the pulmonary vein (Kirby et al., 1983). Since the SHF-derived smooth muscle cells abut the cNC-derived smooth muscle cells, it is intriguing to speculate that the cNC cells may recruit the SHF smooth muscle population.

Taken together, the anterior heart field in the mouse and chick located in the splanchnic mesoderm contribute cardiomyocytes to the outflow tract of the heart. However, there are differences between the two species that will likely be uncovered by future study. For example, in the mouse, the anterior heart field is broader, consisting of the splanchnic and pharyngeal mesoderm, which also contributes cardiomyocytes to the right ventricle. However, in the chick anterior heart field derived cardiomyocytes are not found in the right ventricle. It is

possible that if the investigators had labeled the splanchnic mesoderm at an earlier stage, perhaps stage 12, when myocardial accretion is initiated at the OFT, the anterior heart field could have contributed cardiomyocytes to the right ventricle. Interestingly, it is presently speculated that the secondary heart field is a subdomain of splanchnic mesodermal cells within the anterior heart field and therefore does not constitute an independent cardiac field. To definitively address this possibility, additional molecular markers of the anterior heart field are required, along with a more thorough understanding of the developmental gene networks that regulate its development.

Most molecular pathways shown to regulate anterior heart field contribution to the heart have been identified in the mouse. For example, a null mutation of Islet1 in mice results in the failure to extend the anterior pole of the OFT (Cai et al., 2003). Additionally, these mutants lack right ventricles and have reduced atrial tissue. Interestingly, similar to FGF10, Islet1 is expressed mediodorsal, yet contiguous to the differentiating cardiomyocyte progenitors of the primary heart field at E7.5. As the bilateral cardiomyocytes fuse at the ventral midline at E8.0, the progenitor field inverts such that the mediodorsal Islet1 cells reorient to be repositioned anterodorsal. In contrast, the leading migrating cardiomyocyte progenitors of the primary heart field reposition from a lateral to ventral position to fuse at the ventral midline (Cai et al., 2003). This reorientation of the primary and anterior heart fields also occurs in chick (Abu-Issa and Kirby, 2008). Islet1 expression is maintained in the splanchnic mesodermal cells of the

pharyngeal arches and the splanchnic mesenchyme ventral to the foregut endoderm (Cai et al., 2003).

Interestingly, fate mapping of the Islet1 population, presumably the anterior heart field, using Islet1-CRE to induce the expression of *lacZ,* revealed that the Islet1 population generated almost all of the OFT and right ventricle. In contrast to the lineage tracing in the chick, the Islet1 population also contributed 65% and 70% of the cardiomyocytes of the right and left atria, respectively. In addition, progeny of the Islet1 progenitors contribute approximately 20% of cells to the left ventricle. These cells were located in the inner wall of the left ventricle, the junctional region between the left and right ventricles (Cai et al., 2003). This finding suggests that anterior heart field (as defined by Islet1), along with left ventricular primary cardiomyocytes, generate the interventricular septum of the heart. Additional analysis suggests that Islet1 is required to maintain an undifferentiated state in the anterior heart field by promoting cell proliferation and survival. Islet1 is also required for the migration of the splanchnic mesoderm of the anterior heart field (Cai et al., 2003).

Mef2c, a MADS domain transcription factor, is a direct transcriptional target of Islet1 in the anterior heart field of the mouse (Dodou et al., 2004). Similar to the Islet1 mutant, Mef2c mutant mice have gross abnormalities of the OFT and the right ventricle (Lin et al., 1997). However, in contrast to Islet1, Mef2c is expressed in the OFT and the right ventricle of the murine heart (Lin et

al., 1997). The enhancer responsible for Islet1-dependent Mef2c transcription is also dependent on the presence of GATA4 (Dodou et al., 2004). In addition to Islet1-GATA4 dependent expression of Mef2c, Foxh1, a forkhead transcription factor, directly interacts with NKX2.5 to induce expression of Mef2c via an enhancer located less than 3 kb from the Islet1-GATA4 enhancer. This enhancer induces expression of Mef2c in both the anterior heart field, the OFT and right ventricle of the mouse heart (von Both et al., 2004). Interestingly, dHand, a basic helix-loop-helix transcription factor predominantly expressed in the right ventricle, is a downstream target of Mef2c in mouse (Lin et al., 1997). Therefore, it is plausible that Islet1-GATA4 and NKX2.5-Foxh1 interactions differentially initiate Mef2c expression in the anterior heart field and in the OFT and the right ventricle, respectively. Thus, dHand plays an important role in patterning of the right ventricle and OFT. Collectively, these data uncover a molecular pathway required for proper development of the right ventricle and OFT of the four-chambered heart.

Retrospective analysis identified regions colonized in E8.5 mouse hearts by clonally related cardiomyocytes by random intragenic recombination of a n*laacZ* reporter engineered into the *Cardiac Actin* locus (Meilhac et al., 2004). The analysis concluded that the heart was composed of two cell lineages, based on cellular regionalization within the cardiac tube. The first lineage generates the entirety of the left ventricle, as well as portions of the myocardium of the right ventricle, the atria and the atrioventricular canal. The second lineage generates

the entirety of the OFT, along with portions of the right ventricle, the atria and the atrioventricular canal (Meilhac et al., 2004). Therefore, while the left ventricle and OFT disseminate from the first and second field, respectively, all other segments of the heart contain a mixture of the two lineages. Notably, the second lineage nearly overlaps with the contribution of cells expressing Islet1 in the anterior heart field of the developing heart (Cai et al., 2003). It is speculated that cells of the second lineage mix with cells of the first lineage in the right ventricle, atria and atrioventricular canal prior to the breakdown of the dorsal mesocardium. This occurs when the splanchnic mesoderm (anterior heart field) is continuous with the dorsal aspect of the primary myocardium. Following the separation of the primary heart tube from the pharynx, the second lineage is contiguous only at the anterior and posterior poles of the heart tube, and therefore, contribute the entirety of the OFT.

This degree of intermingling of the two lineages argues against the existence of separate segmented heart fields. Rather, cardiomyocyte progenitors may have different responses to complex autonomous and non-autonomous patterning cues based on their position within a singular heart field. This hypothesis is strengthened by the finding that Islet1 protein is expressed throughout the entire cardiac lineage in an E7.5 mouse embryo, as it is in chick (Prall et al., 2007; Yuan and Schoenwolf, 2000). In the mouse, Islet1 expression is extinguished in differentiating NKX2.5 cardiomyocyte progenitors at E8.0 (Prall et al., 2007). Interestingly, Islet1 expression persists in the “primary heart field” in

the NKX2.5 null mouse (Prall et al., 2007). Therefore, it is possible that, as in the splanchnic mesoderm of the anterior heart field, Islet1 is at the top of the hierarchal gene regulatory network within primary and secondary cardiomyocyte progenitors to regulate their commitment and differentiation into the cardiac lineage.

While the contribution of the OFT and right ventricle from the anterior heart field continues to be actively investigated in the mouse and chick, there has been very little investigation of the frog anterior heart field. The idea of an anterior heart field in the frog is an interesting evolutionary question. Similar to higher vertebrates such as the mouse and chick, the frog heart, specifically in *Xenopus*, consists of two atria, a single ventricle and an OFT. However, the frog heart lacks a right ventricle. In contrast to zebrafish, frogs possess lungs that develop during metamorphosis of the tadpole. Therefore, the frog is an evolutionary intermediate between higher vertebrates that possess a sophisticated pulmonary circulatory system and lower vertebrates who support a rudimentary systemic circulatory system.

In the absence of a right ventricle, *Xenopus* maintains pulmonary circulation by using an evolved tiered blood flow system within the ventricle. Systemic deoxygenated blood enters the single ventricle of the *Xenopus* heart, where it is filtered through channel-like structures that maintain separation from incoming oxygenated blood. The deoxygenated blood is pumped in to the right

atria, where it exits the heart to be oxygenated in the lungs. Following oxygenation, the blood reenters the heart via the left atria. The oxygenated blood passes through the ventricle, where it again remains separated from the deoxygenated blood via the channels. The blood is then pumped out the ventricle to the systemic circulation.

In the frog, as in the mouse and chick, Islet1 expression overlaps expression of NKX2.5 during neurulation (Brade et al., 2007). The Islet1 and NKX2.5 regions separate when the NKX2.5 cardiomyocyte progenitors fuse at the ventral midline. Islet1 expression is restricted to the splanchnic mesoderm and pharyngeal endoderm anterior and dorsal to the NKX2.5 expressing linear heart tube. While Islet1 expression is not detected in the heart tube as it is undergoing cardiac looping, NKX2.5 expression is observed extending into the dorsal splanchnic mesoderm, overlapping with Islet1 expression (Brade et al., 2007). This expression pattern is highly similar to that found in both the mouse and chick, suggesting the possibility that the frog may possess an anterior heart field (Cai et al., 2003; Prall et al., 2007; Waldo et al., 2001). If Islet1 is depleted in the *Xenopus* embryo, the heart remains small and morphologically abnormal. However, there is a small rudiment resembling an OFT (Brade et al., 2007). The lack of adequate OFT markers hasten further analysis of the extent of OFT formation in the Islet1-depleted *Xenopus* embryo and its contribution from an anterior heart field.

Shortly before anterior heart field myocardial accretion to the anterior pole of the heart is complete, epicardium formation commences. The epicardium is derived from a protrusion, the proepicardium, that forms on the pericardial serosa overlying the septum transversum near the sinoatrial junction of the heart. In E9.0 mice, the proepicardial cells reach the heart by two pathways: one is by direct contact between proepicardium and myocardium, and the other is by vesiculation of the proepicardium and release of free-floating aggregates that attach to the dorsal wall of the heart (Komiyama et al., 1987; Rodgers et al., 2008). A similar process occurs in stage 14 chick and stage 37 frogs. However, in frogs, the proepicardial cells migrate to the dorsal wall of the heart over an extracellular matrix stalk that bridges the proepicardium and the heart (Hiruma and Hirakow, 1989; Jahr et al., 2008; Manner, 1992; Nahirney et al., 2003).

In the mouse, chick and frog, epicardial cells encase the heart, forming an epithelial sleeve that migrates from the back of the heart, over the apex of the ventricles, to the front of the heart. Its migration ceases after the OFT is covered. Production of extracellular matrix proteins including collagens, laminins, and fibronectin forms an interface between the epicardium and the myocardium, generating the subepicardium (Kalman et al., 1995; Tidball, 1992). In response to myocardial BMP2 and BMP4 signaling, epicardial cells subsequently undergo epithelial to mesenchymal transition (EMT) to populate the subepicardium (Morabito et al., 2001). These epicardial-derived cells (EPDCs) contribute endothelial cells and smooth muscle cells to the coronary vascular plexus, as

well as fibroblasts to the myocardium and the subepicardial space (Gittenberger-de Groot et al., 1998; Manner, 1999; Vrancken Peeters et al., 1999).

Data from embryonic stem cell cultures, quail-chick chimeras, and retroviral experiments have suggested that EPDCs are bipotential and differentiate into vascular endothelial and smooth muscle cells of the coronary vascular plexus in a temporal manner (Dettman et al., 1998; Mikawa and Fischman, 1992; Yamashita et al., 2000). Initial EMT produces EPDCs expressing Vascular Endothelial Growth Factor Receptor-2 (VEGFR2). In response to high levels of VEGF expression from the myocardium and the epicardium, $VEGF^{+}$ EPDCs differentiate into coronary vascular endothelial cells (Perez-Pomares et al., 1998a; Perez-Pomares et al., 1998b; Tomanek et al., 1999). Subsequently, a second wave of EMT produces EPDCs expressing Platelet-Derived Growth Factor Receptor-β (PDGFRβ). In response to PDGF emanating from the newly formed endothelial plexus, the EPDCs are recruited and differentiate into vascular smooth muscle cells of the coronary vasculature (Folkman and D'Amore, 1996; Shinbrot et al., 1994).

The epicardium also has a trophic effect on the myocardium, particularly in the ventricles. Prior to development of the epicardium in the mouse and chick, the ventricular chambers undergo the process of trabeculation. Trabeculation involves the formation of finger-like projections of cardiomyocytes that protrude into the cardiac jelly of the chamber in responds to signals from the endocardium,

particularly the growth factor Neuregulin (Kramer et al., 1996; Meyer and Birchmeier, 1995; Stratford et al., 1999). Trabeculae are more differentiated than cardiomyocytes of the outer wall, the compact zone. The compact zone of the ventricle is highly proliferative and its formation, referred to as compaction, coincides with the invasion of EPDCs expressing Wilm's Tumor-1 (WT-1) into the ventricle (Carmona et al., 2001; Gittenberger-de Groot et al., 1998). Interestingly, the invading EPDCs and the epicardium express Retinaldehyde-dehydrogenase-1 (RALDH2), the enzyme responsible for retinoic acid (RA) synthesis (Perez-Pomares et al., 2002; Xavier-Neto et al., 2000). The EPDCs, as well as the compact zone cardiomyocytes, express the RA receptor, RXRα (Kastner et al., 1994; Sucov et al., 1994). This molecular arrangement is thought to establish an autocrine loop, allowing the EPDCs and the compact zone cardiomyocytes to sustain proliferation and maintain an undifferentiated state relative to the trabeculae (Lavine et al., 2005; Xavier-Neto et al., 2000).

To sustain proliferation, the epicardium maintains Fibroblast Growth Factor (FGF) signaling in the compact zone by the RA pathway (Lavine et al., 2005). In mouse, RA induces the expression of FGF9 in the epicardium. FGF9 signaling via the FGFR1 and FGFR2 is essential in maintaining the proliferative capacity of the compact zone (Lavine et al., 2005). FGF2 and FGFR1 are highly expressed in the compact zone relative to the trabeculae, reflecting the differential mitotic index of the ventricular compartments (Pennisi et al., 2003). Additionally, studies in the chick demonstrate that the epicardium maintains the

expression of FGF2 and FGFR1 in the compact zone of the ventricle (Pennisi et al., 2003). It is not known if this is related to RA signaling.

REGULATION OF CARIDIAC DIFFERENTIATION

Differentiation is a process by which cardiomyocyte progenitors integrate intrinsic and extrinsic signals, resulting in maturation into a specialized cardiomyocytes, thus allowing them to perform functions characteristic of the region of the heart in which they ultimately reside. For proper differentiation of cardiomyocyte progenitors into functional cardiomyocytes, cardiomyocyte progenitors simultaneously undergo both cellular and molecular changes to form a chambered heart (Fig 1.1, 1.2).

Cell migration and Cell-Cell/Matrix Interactions

The expression of terminal differentiation proteins in the mouse, chick and frog, such as Myosin Heavy Chain α, Myosin Light Chain 2a, and Troponin Ic, coincide with the migration of the bilateral cardiomyocyte progenitor field to the ventral midline of the embryo (Chambers et al., 1994; Drysdale et al., 1994; Franco et al., 1999; Tokuyasu and Maher, 1987). However, mutations in the mouse and frog that prohibit migration of cardiomyocyte progenitors to the ventral midline do not necessarily inhibit cardiomyocyte differentiation. This suggests that differentiation is independent and separable from migration. For example, mice with a mutation in Nap1, a regulatory component of the WAVE complex that regulates the actin cytoskeleton, exhibit cardia bifida due to

destabilization of the WAVE complex. This in turn prevents cardiomyocyte progenitor migration (Rakeman and Anderson, 2006). However, the Nap1 mutant bifida hearts undergo morphogenesis and contract, suggesting differentiation occurs despite improper migration and cardiac fusion. A similar phenotype is seen in HSP27 (Heat Shock Protein 27)-depleted frog embryos (Brown et al., 2007). Despite the inhibition of proper cardiac fusion, the resulting two bilateral HSP27-depleted hearts do undergo differentiation as demonstrated by Myosin Heavy Chain and Troponin Ic expression.

Proper cardiomyocyte differentiation, independent of cardiomyocyte progenitor migration, is corroborated by multiple zebrafish mutants, including *casanova* (a novel SOX family transcription factor), *miles apart* (a sphingosine-1-phosphate receptor) and *one-eyed pinhead* (member of the EGF-CFC family) (Chen et al., 1996; Kikuchi et al., 2001; Kupperman et al., 2000; Stainier et al., 1996; Zhang et al., 1998). These three proteins are required for morphogenesis of the adjacent endoderm, as well as for creating a permissive environment for migration of the cardiomyocytes. In the absence of these proteins, the number of cardiomyocyte progenitors specified to the cardiac lineage is reduced. Subsequently, there is limited migration to the ventral midline of the embryo. Although this results in cardia bifida, the chamber myocardium does undergo differentiation (Chen et al., 1996; Stainier et al., 1996). However, as stated previously, zebrafish cardiomyocyte progenitors differentiate prior to cardiac migration and fusion. Therefore, differentiation would have already occurred.

Despite species variation, formation of a linear heart tube comprised of differentiated cardiomyocytes in the absence of proper fusion of the bilateral cardiac fields implies that cardiomyocyte differentiation is independent of cell migration and cardiac fusion.

Cell-cell contact is an essential component of cardiomyocyte differentiation. As mentioned above, at the time of fusion across the ventral midline, cardiomyocyte progenitors in the mouse, chick and frog epithelialize to form a single coherent sheet. In addition, it was demonstrated in chick that the cardiomyocyte progenitors polarize as they express calcium dependent N-Cadherin and β-Catenin at apical adherens junctions, while maintaining cell-matrix interaction via Fibronectin and integrins at their basal surfaces (Fig 1.1A) (Linask, 1992; Linask et al., 2005). While β-Catenin is a key downstream component of the canonical Wnt signaling pathway and essential for cardiogenesis, Fibronectin/integrin signaling as well as N-Cadherin, mediate myofibrillogenesis by aiding in proper alignment of the myofibrils at the plasma membrane of epithelialized cells (Luo and Radice, 2003).

The necessity of cell-cell contact has been verified with two zebrafish mutants, *heart and soul* and *glass onion* (Bagatto et al., 2006; Horne-Badovinac et al., 2001; Rohr et al., 2006; Stainier et al., 1996). The *heart and soul* zebrafish locus encodes an atypical protein kinase C (aPCKλ). In the absence of aPCKλ, tilting and elongation of the cardiac cone is impaired (Yelon et al., 1999). Further

analysis of the mutant phenotype determined aPCKλ is required to maintain epithelial integrity and polarization of the cardiomyocytes (Rohr et al., 2006). The *glass onion* zebrafish mutant locus encodes Cadherin2 (N-Cadherin) (Bagatto et al., 2006). Loss of Cadherin2 results in loosely organized cardiomyocytes with greatly reduced VMHC expression, suggesting N-cadherin is required for proper differentiation of the ventricular cardiomyocytes. Notably, the expression of CMLV, a differentiation marker of both the ventricle and the atrium, is properly expressed. However, the mutant heart does contract. Therefore, while disrupted cell epithelization does not entirely inhibit differentiation, it does appear to be required for initiation of early cardiomyocyte differentiation, particularly in the ventricle.

Proliferation

Additional cellular changes accompany cardiomyocyte differentiation. As the sheet of cardiomyocyte progenitors fold to form a linear heart tube, the entire heart tube consists of “primary” myocardium phenotypically characterized by negligible proliferation, low density of gap junction proteins, and slow conduction capacity (Christoffels et al., 2000; de Jong et al., 1992; Moorman et al., 1998). Shortly thereafter, as shown in the mouse, chick and frog, the ventral cardiomyocyte progenitors of the linear heart tube become specialized both molecularly and cellularly as they increase in size and begin to rapidly proliferate (Fig 1.1B) (Christoffels et al., 2000; Mohun, 2000; Soufan et al., 2006). This localized size expansion and proliferation forces the ventral side of the linear

heart tube to bulge out to form the primitive ventricle (Fig 1.2). Moreover, fate mapping of the ventral midline cardiomyocyte progenitors in both the chick and frog reveal the ventral midline cardiomyocyte progenitors of the linear heart tube ultimately contribute to the outer-most wall of the ventricle (Fig 1.1, 1.2) (Christine and Conlon, 2008; De La Cruz et al., 1989). This sequence of events is commonly referred to as the “ballooning” model of chamber formation and is thought to provide the means for cardiac looping (Christoffels et al., 2000). The newly formed chamber myocardium acquires chamber restricted expression of various transcription factors, high density of gap junctions and high conduction velocities (Christoffels et al., 2000). During cardiac looping, the dorsal cardiomyocytes of the linear heart tube reorganize to reside in the inner curvature of the chambered heart where they remain phenotypically in the primary myocardial state (Christoffels et al., 2000).

Detailed retrospective analysis of cardiomyocyte growth properties in mouse using the nuclear *laacZ* reporter in the *α-Cardiac Actin* locus has revealed that the chamber myocardium proliferates in an oriented manner along the transmural axis. Higher proliferation occurs in the compact zone of the ventricular chamber resulting in the myocardial thickening of the ventricular chamber (Meilhac et al., 2003). This oriented proliferation, referred to as coherent growth, is concomitant with oriented myofibrillogenesis. Similarly, in zebrafish, the ventricle myocardium proliferates in an oriented manner. The requirement for oriented coherent growth of the ventricle is highlighted by three zebrafish

mutants, *heart of glass*, *santa* and *valentine* (Stainier et al., 1996). *Heart of glass* encodes a novel transmembrane protein in the endocardium, while *santa* and *valentine* encode signaling cytoplasmic proteins Cerebral Cavernous Malformations (CCM)-1 and -2, respectively. These proteins are expressed in endothelial cells of the vasculature (Mably et al., 2006; Mably et al., 2003). All three mutants have distended single-layered ventricles, despite having the proper number of cardiomyocytes. Further analysis revealed that cardiomyocyte proliferation occurred along the anterior-posterior axis instead of the transmural axis, resulting in expansion of the chamber rather than concentric growth and thickening (Mably et al., 2006; Mably et al., 2003).

Regionalized Cardiac Gene Expression

Concomitant with the cellular modifications associated with differentiation, cardiomyocyte progenitors undergo molecular transformations to become specialized cardiomyocytes within the chambered heart. Multiple events occur simultaneously as the combinatorial effort of general cardiogenic factors, as well as chamber-specific factors, gradually restrict the potential of cardiomyocyte progenitors and facilitate the formation of regionalized chamber myocardium of the functional heart.

For proper maturation to occur, cardiomyocyte progenitors must maintain expression of the early cardiac transcription factors NKX2.5 and GATA4, -5 and -6. Numerous studies in the mouse, frog and fish determined that the endoderm is

a major source of secreted pro-cardiogenic factors that facilitate the maintenance of general cardiac transcription factor expression, including NKX2.5 and GATA4, -5 and -6 (Molkentin et al., 1997; Peterkin et al., 2003; Reiter et al., 2001; Shi et al., 2000; Walters et al., 2001). For example, in the frog and fish, endodermal expression of GATA6 is partially responsible for upregulation of BMP4 expression (Peterkin et al., 2003). BMP4 is then secreted from the endoderm, resulting in the upregulation of NKX2.5 in the cardiomyocyte progenitors (Peterkin et al., 2003; Shi et al., 2000; Walters et al., 2001). In the zebrafish, GATA5 is downstream of endodermal BMP signaling and is required in cardiomyocyte progenitors to increase NKX2.5 expression in the cardiac lineage (Reiter et al., 2001). The zebrafish mutant locus *faust* encodes GATA-5 (Reiter et al., 1999; Stainier et al., 1996). The *faust* mutant preferentially forms an atria, yet lacks a differentiated ventricular chamber (Reiter et al., 1999; Reiter et al., 2001). This may be a direct result of diminished expression of NKX2.5 in the ventricular cardiomyocyte progenitors. In the absence of sustained NKX2.5 expression, the cardiomyocyte progenitors fail to induce expression of Cardiac Actin, Myosin Light Chain and Troponin C and remain in a progenitor state (Shi et al., 2000; Walters et al., 2001).

The factors that determine specificity during this later stage of general cardiac transcription factor expression are not known. It is possible that local structural changes in chromatin mediate expression by allowing access to region-specific enhancers of the chamber-restricted genes. In zebrafish, the pandora

mutant loci encodes SPT6, a transcription elongation factor (Keegan et al., 2002). Homologues of SPT6 bind histones, particularly histone H3, and assemble nucleosomes *in vitro,* altering DNA accessiblity (Bortvin and Winston, 1996). Initial differentiation in the *pandora* mutant cardiomyocyte progenitors is inhibited. However, during formation of the cardiac cone, cardiomyocytes express low levels of CMLC2 and VMHC. This results in a heart that consists of a thin stalk of $VMHC^{+}$ ventricular cardiomyocytes and an atria-like chamber (Yelon et al., 1999). Although no *in vivo* targets of zebrafish SPT6 have been identified, it is intriguing to speculate that SPT6 regulates the timing of cardiomyocyte differentiation by modifying chromatin assembly and gene accessibility.

In the presence of sustained general cardiac transcription factor expression throughout the myocardium, how do cardiomyocyte progenitors progress molecularly from a state of primary myocardium to chamber myocardium? Detailed studies over the past decade have deciphered the morphogenic program of the developing chambered heart, particularly the ventricle, yet there is still more to be elucidated. For instance, in the mouse and chick, only after the initiation of cardiac looping, when the cardiomyocytes are distinguished morphologically and electrophysiologically as ventricle chamber myocardium, are chamber-restricted regulators expressed, including Atrial Natriuretic Factor (ANF), IRX4, Chisel, and Connexin 43 (Bruneau et al., 2000; Christoffels et al., 2000; Houweling et al., 2002; Minkoff et al., 1993; Palmer et al., 2001; Yamagishi et al., 2001). The transition from a contiguous sheet of

cardiomyocyte progenitors to a looped, chambered heart is suggestive of molecular pattering that governs differentiation within specific regions along the dorsoventral axis of the linear heart tube, particularly in the ventral region that will generate the future left ventricle.

However, very few known proteins are expressed exclusively in the ventral cardiomyocyte progenitors of the linear heart tube. One exception is the bHLH transcription factor eHand, which is expressed predominantly in the ventral cardiomyocyte progenitors of the linear heart tube in the mouse, frog and fish (Fig 1.1B) (Christoffels et al., 2000; Mohun, 2000; Thomas et al., 1998). Yet, very little is known of upstream and downstream mechanisms of eHAND function which would aid in deciphering mechanisms of differentiation in the dorsoventral axis of the linear heart tube. It has been suggested that Hif1α (Hypoxia Inducible Factor 1alpha) functions upstream of eHand, as knockout mice of Hif1α lack eHand expression. However, it is not known if Hif1α directly regulates eHand (Compernolle et al., 2003). If Hif1α is a regulator of eHand, this would suggest that an anoxic environment is required for cardiomyocyte differentiation. eHand does seem to be required to demarcate the limits of the left ventricle, as its expression is restricted to the left ventricle chamber myocardium in the mouse and chick (Srivastava, 1997; Srivastava et al., 1995).

Deciphering the mechanisms of cardiomyocyte differentiation requires more than determining where and when a regionally-restricted gene is

expressed. It is more intriguing to understand how these factors cooperate to activate and/or repress differentiation of chamber myocardium in a regionally-restricted manner. For example, GATA4 and NKX2.5 regulate transcription of multiple chamber myocardium differentiation genes. In mice and chick, GATA4 and NKX2.5 transcriptionally cooperate throughout the myocardium to induce the expression of Cardiac Actin (Sepulveda et al., 2002). However, numerous studies have demonstrated the requirement of cofactors that synergize with both GATA4 and NKX2.5 to limit expression of chamber-restricted genes. For example, in the mouse and chick, NKX2.5 and GATA4 synergize with TBX5, a T-box transcription factor expressed in the chamber myocardium of the atria and left ventricle, to upregulate ANF (Bruneau et al., 1999; Bruneau et al., 2001; Chapman et al., 1996; Hiroi et al., 2001; Plageman and Yutzey, 2004). TBX2, a T-box transcription factor expressed in the primary myocardium of the outflow tract, atrial ventricular canal, and inner curvature of the heart, forms a transcriptional complex with NKX2.5 which in turn inhibits TBX5 from binding NKX2.5, thus inhibiting expression of ANF in primary myocardium (Habets et al., 2002). Additionally, TBX2 directly represses expression of chamber myocardium genes such as Connexin 40, as well as N-MYC, to inhibit proliferation (Cai et al., 2005; Habets et al., 2002; Singh et al., 2005). Simultaneously, in the chamber myocardium, TBX20, a T-box transcription factor expressed throughout the chamber myocardium, directly activates expression of N-MYC within the mouse chamber myocardium, resulting in regionalized proliferation (Cai et al., 2005; Singh et al., 2005). The GATA4 - NKX2.5 – TBX5 - TBX20 – TBX2

cardiomyocyte differentiation program in part promotes the transition from primary linear heart tube myocardium to differentiated chamber myocardium (Fig 1.2). However, this gene network does not constitute the sole mechanism of differentiation in the chambered heart.

These are just a few examples that highlight the molecular complexities that exist to formulate regional identity within a cardiomyocyte progenitor population which then drives their differentiation into a chamber cardiomyocytes. They also underscore what remains to be discovered. While it is evident that both intrinsic and extrinsic mechanisms create regionalized diversity and complexity to form a functional heart, there remain large gaps in the understanding of the intricacies of cardiomyocyte differentiation. For example, given the chamber-specific expression of ANF, Chisel, and Connexin 40 in chamber myocardium, it is likely that their expression depends on the mediolateral and dorsoventral patterning of the newly fused cardiomyocyte progenitor field and the linear heart tube, respectively. However, eHand is one of very few transcription factors known to be expressed in a ventricularly-restricted fashion in the linear heart tube. In light of the transcriptional regulation of chamber-restricted genes by general cardiac transcription factor complexes, there may exist an additional level of complexity of cardiomyocyte differentiation in the form of unknown chamber specific cofactors. Therefore, it is necessary to identify more proteins involved in the early differentiation of the cardiomyocyte progenitors and determine the mechanisms by which they function. The remainder of this thesis

focuses on CASTOR, a zinc finger transcription factor previously shown to be required for the proper differentiation of a subset of neuronal progenitors in the *Drosophila* central nervous system.

CASTOR

CASTOR is a zinc-finger transcription factor that is required for proper differentiation of multiple tissue-specific progenitor populations (Christine and Conlon, 2008; Cui and Doe, 1992; Mellerick et al., 1992). Vertebrate CASTOR (CST) encodes a unique zinc finger protein. In each of the five CST zinc finger domains there is a classical TFIIIA Cys_2His_2 motif immediately proceeded by an additional Cys_2His_2 motif, creating a novel para zinc finger motif (Christine and Conlon, 2008; Liu et al., 2006; Miller et al., 1985; Vacalla and Theil, 2002). While vertebrate CST orthologues contain five para-zinc finger domains, only four para zinc fingers are present in *Drosophila* CASTOR (dCas) (Cui and Doe, 1992; Mellerick et al., 1992).

dCas was initially identified and shown to be required for the spatial and temporal patterning of neuronal precursors in the developing *Drosophila* central nervous system (Cui and Doe, 1992; Mellerick et al., 1992). Within the developing CNS, the stem cell-like neuroblast generates a unique and invariant lineage by asymmetrically dividing to generate a neuroblast and a ganglion mother cell which continues to further divide, giving rise to neurons and/or glia. The sequential expression of four transcription factors - Hunchback (Hb), Kruppel

(Kr), Pdm1/2, and Castor (dCas) – reflects the spatial and temporal birth order, as well as the identity of the neuroblasts. Hb is expressed in early born neuroblasts, Kr and Pdm1/2 (referred to as Pdm) are expressed in intermediate neuroblasts, while dCas is expressed in late-born neuroblasts (Fig 1.3) (Isshiki et al., 2001). This pattern of expression is tightly correlated with the spatial identity of the neuronal lineage. Early born Hb-expressing lineages are found within deep layers of the embryo, while late-born dCAS lineages remain in more superficial layers of the embryo (Isshiki et al., 2001; Pearson and Doe, 2003). In this way, the temporal and spatial expression cascade generates a stereotyped sequence of neuronal progeny, creating a multilayered neuron network within the embryo.

Multiple neuronal lineage studies have revealed the intricacies of how the neuroblast integrates spatial and temporal cues to generate the neuronal diversity defined by the expression cascade mentioned above. Misexpression studies show that each transcription factor in the cascade series initiates the expression of the succeeding transcription factor in a newly born neuroblast to progress the temporal identity window of the lineage (Fig 1.3). The expression of the new transcription factor then represses the expression of the previous transcription factor in the cascade (Isshiki et al., 2001). For example, Pdm is sufficient to drive the expression of dCas in the U5 motorneuron-generating neuroblast of the NB 7-1 lineage (Grosskortenhaus et al., 2006). Although Pdm acts alone to specify the previous U4 motorneuron lineage, Pdm and dCas act combinatorially in the subsequent NB to specify the U5 motorneuron lineage. As

dCas expression increases in the ensuing NB, dCas represses Pdm expression, thereby inducing the interneuron fate (Fig 1.3A). Consistent with this hypothesis, in the absence of dCas, Pdm is ectopically expressed due to its de-repression, resulting in excess U4 motorneurons at the expense of the Pdm/dCAS-positive U5 motorneurons, and possibly the interneurons as well (Grosskortenhaus et al., 2006). However, precocious dCas expression is insufficient to specify the U5 motorneuron fate, presumably due to repressed Pdm expression (Grosskortenhaus et al., 2006). It remains unknown if dCas alone is required to specify a neuronal identity in the NB 7-1 lineage due to a lack of an established interneuron lineage marker.

Hb and Kr are termed general temporal identity factors since they are both necessary and sufficient to specify the first and second temporal identities, respectively, in multiple neuronal lineages, including NB 7-1 and NB 3-1 (Fig 1.3A, B) (Isshiki et al., 2001; Tran and Doe, 2008). Initially, Pdm and dCas were defined as temporal identity factors when it was demonstrated that both were necessary and sufficient to specify the late-born identities in the NB 7-1 lineage (Fig 1.3A) (Grosskortenhaus et al., 2006). However, a detailed examination of the NB 3-1 neuronal lineage reveals that Pdm and dCas may not be general temporal identity factors as once thought. Despite being required for proper specification of late-born temporal identities in the NB 7-1 lineage, neither Pdm or dCas are directly required to specify the RP motorneuron identities in the NB 3-1 lineage (Fig 1.3B) (Tran and Doe, 2008). However, both are required to restrict

the previous temporal identity window by repressing the expression of the previous transcription factor (Tran and Doe, 2008). For example, Pdm is required to repress Kr expression in the RP5-generating NB; however, it is not sufficient to specify the RP5 lineage (Tran and Doe, 2008). In the successive interneuron-generating NB, dCas is required to repress Pdm expression for the proper advancement of the interneuron identity state (Fig 1.3B) (Tran and Doe, 2008). However, in the absence of an interneuron lineage marker, it has yet to be determined whether dCas is required for the specification of the late-born NBs responsible for producing interneurons. Therefore, dCas, as well as Pdm, are termed “timing factors” (Tran and Doe, 2008).

In addition to its role in generating neuronal diversity, dCas is also required for the proper development of adult brain structures. Cell clusters expressing dCas interact with neighboring cells expressing the *Drosophila* genes *linotte/derailed* and *no-bridge* in a non-cell autonomous fashion to control axonal outgrowth (Hitier et al., 2001). The gene *linotte/derailed* encodes a transmembrane receptor tyrosine kinase protein homologous to the mammalian RYK protein (Dura et al., 1995). This study suggests that dCas transcriptionally induces the expression of an unknown protein, allowing the dCas cell to respond to a signal originating from a neighboring cell expressing *linotte/derailed* and/or *no-bridge* (Hitier et al., 2001). Although much effort has led to the current understanding of the importance of dCas in generating neuronal diversity and

developing the adult brain, the mechanisms by which dCas functions are not known.

UV-induced protein-DNA crosslinking studies conclude that dCas binds genomic DNA (Kambadur et al., 1998). Cyclic amplification of DNA target selection demonstrated that dCas binds directly to a ten basepair consensus sequence [(G/C)C(C/T)(C/T)AAAAA(A/T)] (Kambadur et al., 1998). Analysis of the Pdm promoter identified an enhancer element containing the dCas DNA binding site. dCas binds this enhancer element both *in vitro* and *in vivo* to repress the transcriptional expression of Pdm (Kambadur et al., 1998). To date, the Pdm is the only identified direct transcriptional target of dCas.

Very little is known about vertebrate CST. Murine CST is expressed at E8.0 in the cardiomyocyte progenitor population of the linear tube and is continually expressed in the heart throughout development (Vacalla and Theil, 2002). However, this expression analysis does not exclude the possibly that CST is expressed earlier within the migrating specified cardiomyocyte precursor population. CST is expressed in the lateral neural folds. By E9.5, its expression is restricted to the dorsal neural tube adjacent to the roof plate. At E11.5, CST mRNA is also detected in the dorsal aspect of the eye, the nasal placode and other neuronal derivatives.

The human orthologue of CST has also been identified (Liu et al., 2006). Humans have two hCST proteins divergent in the 3' terminus. Human CST5 contains five zinc finger repeats, while hCST11, a product of alternative splicing, contains eleven zinc finger repeats. Northern blot analysis shows that both hCst5 and hCst11 are highly expressed in adult heart tissue. In addition, *in vitro* assays confirm that hCst mRNA is upregulated upon differentiation of myoblasts into myotubes (C2C12 cells) and neuroblastoma cells (KCNR cells) into neuronal-like cells.

DISSERTATION GOALS

Defining precise mechanisms of cardiomyocyte differentiation will provide valuable insight into the foundation of cardiogenesis as well as a possible basis for congenital cardiac diseases. Based on the function of dCAS to spatially and temporally regulate the differentiation of a subset of neuronal progenitor cells and the expression of murine CST in the linear heart tube, we sought to define a role for CST in the differentiation of a subset of cardiomyocyte progenitors using *Xenopus* as a model system. In Chapter 2, I characterize the requirement of vertebrate CST for the timely differentiation of a subset of cardiomyocyte progenitors at the ventral midline of the linear heart tube. Specifically, I show that CST is required at the ventral midline for their proper differentiation, while CST is required in more dorsally located cardiomyocyte progenitors to regulate cardiomyocyte proliferation. We go on to demonstrate by fate mapping analysis

for the first time in *Xenopus* that ventral midline cardiomyocyte progenitors ultimately reside in the outer curvature of the ventricle wall. In the absence of CST, the ventral midline cardiomyocyte progenitors remain in a progenitor state and fail to integrate into the mature heart. To begin to understand how CST mechanistically functions in the cardiomyocyte progenitors, Chapter 3 focuses on identifying the DNA binding site recognized by CST using a bacterial one-hybrid screen. No direct transcriptional targets of vertebrate CST have been identified. In effort to further define the molecular pathways by which CST functions in cardiogenesis, Chapter 4 focuses on a cloning ChIP screen to identify potential transcriptional targets of CST. Defining the molecular mechanisms regulated by CST will enhance the understanding of cardiomyocyte differentiation.

Figure 1.1 Cardiac fusion and linear tube formation of the vertebrate heart

(A) A schematic depiction of the heart subsequent to fusion of the bilateral cardiac fields (left) based on mouse (E7.5) and chick (stage 9) (ventral view with anterior to the top). Ventral midline cardiomyocytes (X) are located at the region of fusion. The transverse section (right) depicts cardiomyocyte progenitors undergoing apical-basal polarization and initiating differentiation into primary myocardium in response to maintained expression of general cardiac transcription factors (such as NKX2.5) by extrinsic signals from the overlying endoderm. Subsequent to cell sorting of the mesoderm, endocardial tissue begins to express endothelial specific VE-Cadherin. (B) A schematic depiction of the linear heart tube (left) in mouse (E8.0) and chick (stage 10) (ventral view with anterior to the top). The transverse section (right) illustrates the differentiation of the ventral cardiomyocytes into chamber myocardium and its localized patterning with the expression of eHand. The proliferation ventral chamber cardiomyocytes are larger in comparison to the smaller cardiomyocytes of the primary myocardium in the dorsal region of the linear heart tube.

A. Cardiac Fusion

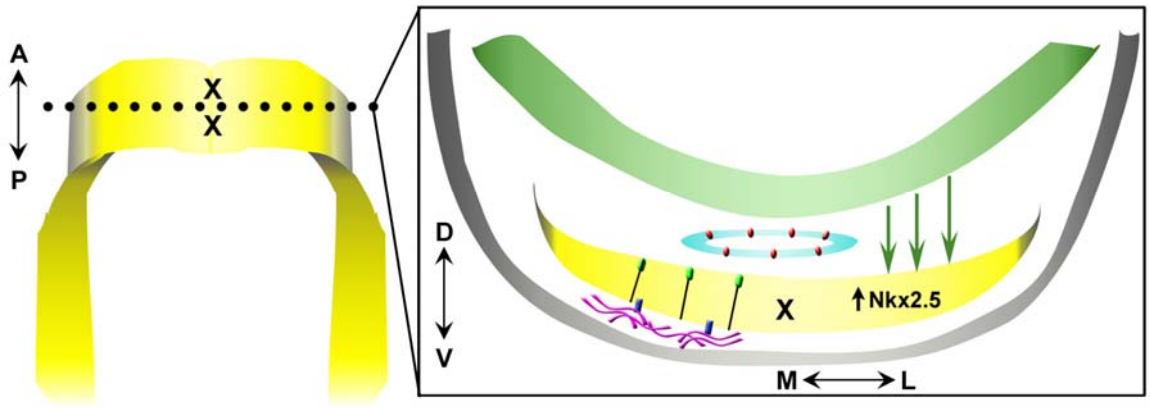

B. Linear Heart Tube

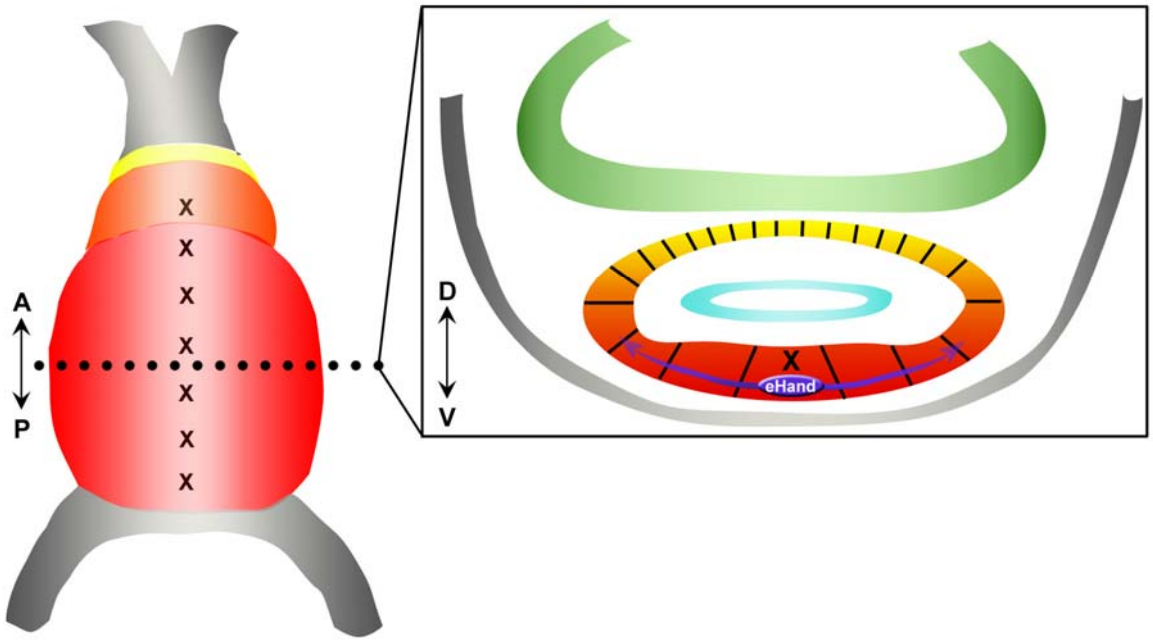

Primary Myocardium
Left Ventricle Chamber Myocardium
Right Venticle Chamber Myocardium
Endocardium
Endoderm
Ectoderm

X Ventral Midline Cardiomyocyte
Endodermal Signals
Fibronectin
VE-Cadherin
N-Cadherin/ β-Catenin
β1-Integrin

Figure 1.2 Differentiation of chamber myocardium during cardiac morphogenesis

Schematic depicting the early stages of cardiac looping and morphogenesis in mouse (E9.0) and chick (stage 11). General cardiac transcription factor (i.e. NKX2.5 and GATA4) complex with chamber specific transcription factors (i.e. TBX5) to initiate expression of chamber restricted genes (i.e. ANF). Chamber myocardium rapidly proliferates to extend the ventricular tissue in part under the control of TBX20 and its activation of N-Myc. After proliferation, the ventral midline cardiomyocyte progenitors (X) ultimately reside on the outer wall of the left ventricle. Simultaneously, the outflow tract, atrial ventricular canal and the inner curvature of the heart maintains a primary myocardial state in part by inhibiting chamber specific gene expression and maintaining low rates of proliferation in part by the transcriptional repressive affects of TBX2. AO – aorta, SV – sinus venosus, Primary myocardium: OFT – outflow tract, IC – inner curvature, AVC – atrial ventricular canal, Chamber myocardium: RV – right ventricle, LV – left ventricle, AT- atria.

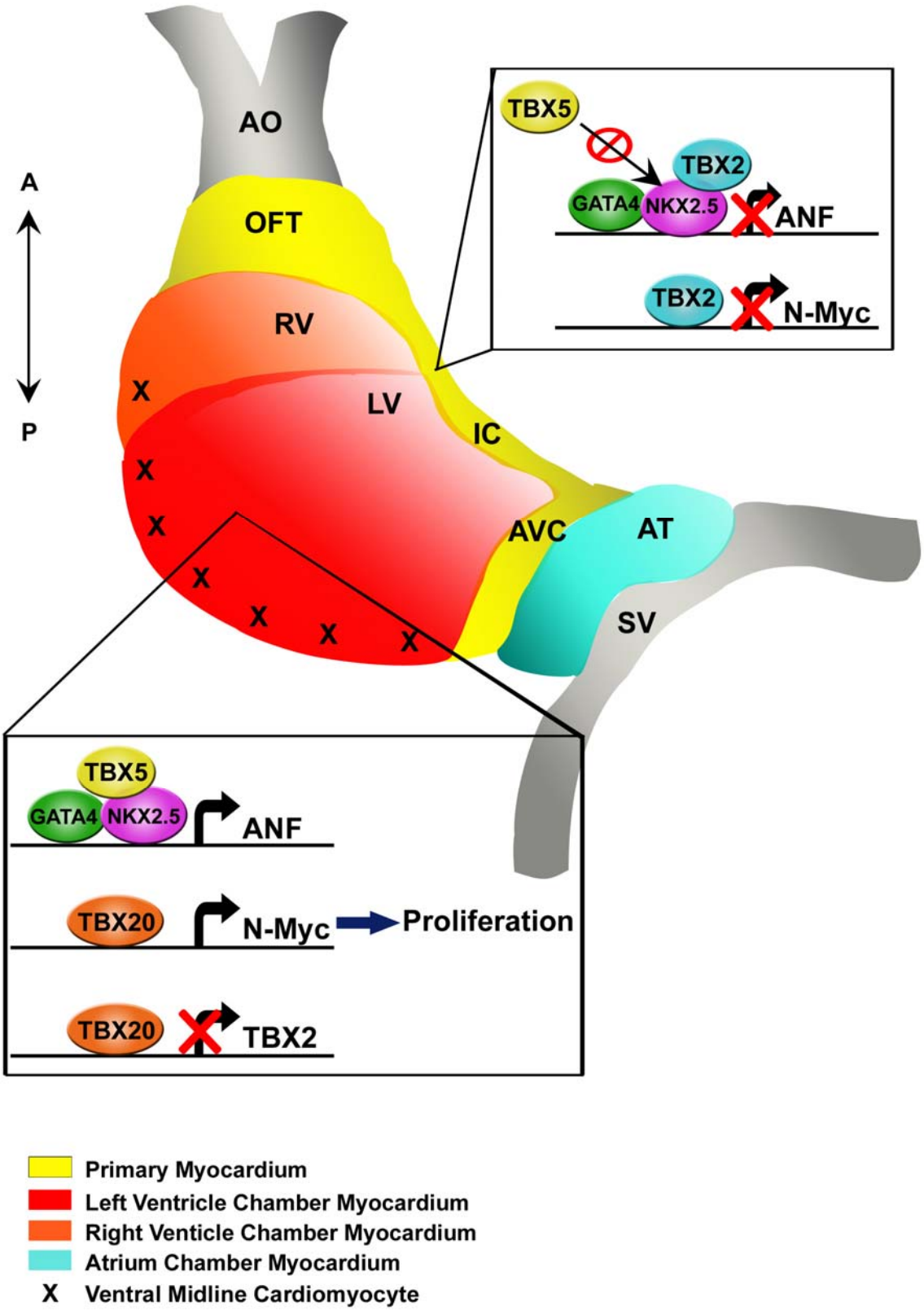
AO
A
P
OFT
RV
LV
IC
AVC
AT
SV
X
TBX5
GATA4
NKX2.5
ANF
TBX2
N-Myc
TBX20
Proliferation
Primary Myocardium
Left Ventricle Chamber Myocardium
Right Venticle Chamber Myocardium
Atrium Chamber Myocardium
Ventral Midline Cardiomyocyte

Figure 1.3 dCas is required for the specification of late born neuronal identities in the NB 7-1 and NB 3-1 lineages

Neuroblasts (NB) of the *Drosophila* central nervous system asymmetrically divide to generate an additional NB and a ganglion mother cell (GMC) which subsequently divides into two neuron and/or glia. NB lineages sequentially express four transcription factors that dictate the NB birth order – Hunchback (Hb), Krupple (Kr), Pdm 1/2 (Pdm), and Castor (dCas). Each transcription factor initiates the expression of the following transcription factor yet inhibits the expression of the previous transcription factor. (A) Temporal gene expression profile of the NB 7-1 lineage. The NB 7-1 lineage gives rise to five U type motorneurons followed by multiple interneurons. dCas is necessary in combination with Pdm to specify the late born U5 motorneuron derived from NB 5. dCas inhibits Pdm expression in NB 6 where it may specify the interneuron identity (no specific interneuron marker is presently available). (B) Temporal gene expression profile in the NB 3-1 lineage. The NB 3-1 lineage generates four RP type motorneurons followed by multiple interneurons. dCas is required to inhibit Pdm expression in NB 5 to close the previous temporal identity window. dCas may specify the interneurons derived from NB5. NB 4 expresses an unknown temporal identity transcription factor (?). Although Pdm is not required to specify the RP5 motorneurons, it is required to inhibit Kr expression in NB 4 and close the previous temporal identity window.

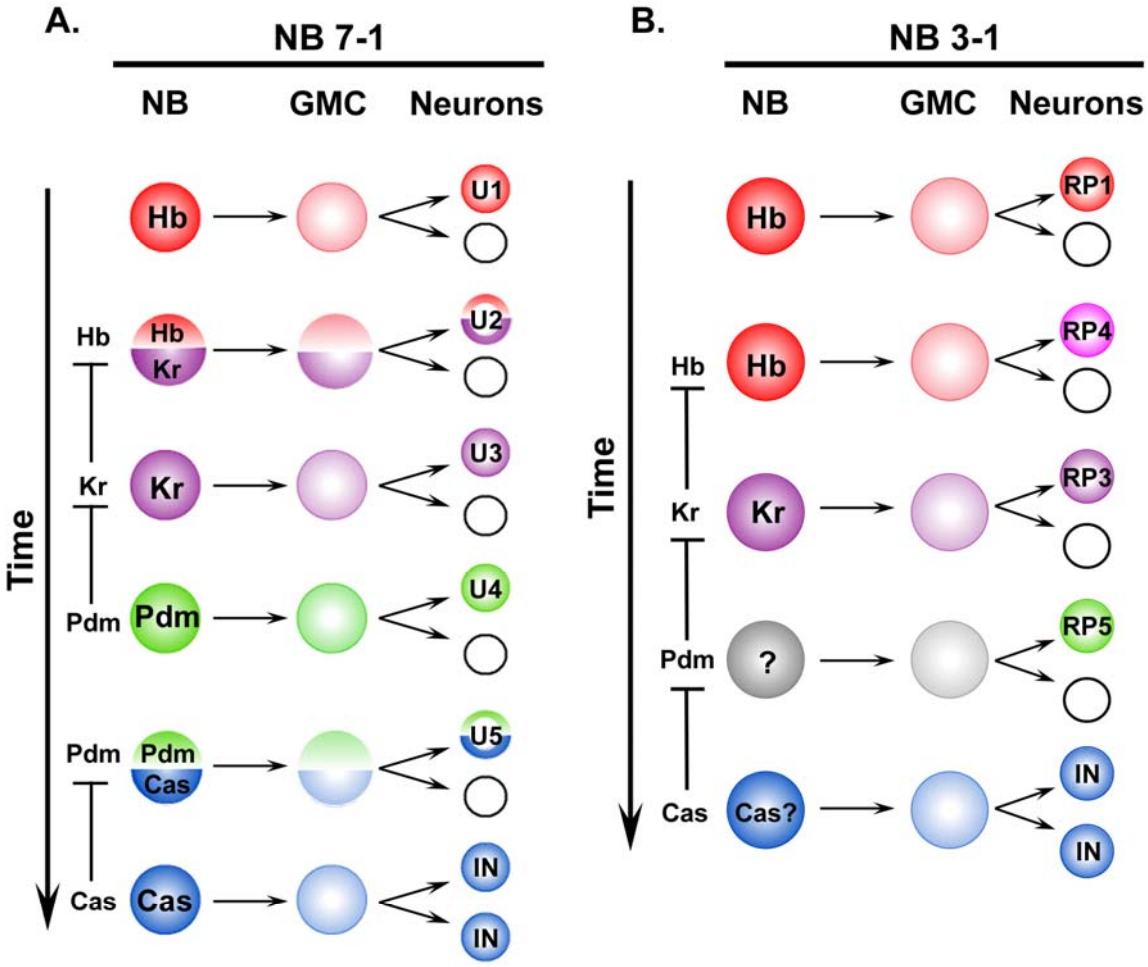
A.
NB 7-1
NB
GMC
Neurons
Time
Hb
Hb
Kr
Kr
Pdm
Pdm
Pdm
Cas
Cas
U1
U2
U3
U4
U5
IN
IN
B.
NB 3-1
NB
GMC
Neurons
Time
Hb
Hb
Kr
Pdm
Cas
Hb
Kr
?
Cas?
RP1
RP4
RP3
RP5
IN
IN

REFERENCES

Abu-Issa, R., and Kirby, M. L. (2008). Patterning of the heart field in the chick. Dev Biol *319*, 223-233.

Antin, P. B., Taylor, R. G., and Yatskievych, T. (1994). Precardiac mesoderm is specified during gastrulation in quail. Dev Dyn *200*, 144-154.

Bagatto, B., Francl, J., Liu, B., and Liu, Q. (2006). Cadherin2 (N-cadherin) plays an essential role in zebrafish cardiovascular development. BMC Dev Biol *6*, 23.

Bortvin, A., and Winston, F. (1996). Evidence that Spt6p controls chromatin structure by a direct interaction with histones. Science *272*, 1473-1476.

Brade, T., Gessert, S., Kuhl, M., and Pandur, P. (2007). The amphibian second heart field: Xenopus islet-1 is required for cardiovascular development. Dev Biol *311*, 297-310.

Brown, D. D., Christine, K. S., Showell, C., and Conlon, F. L. (2007). Small heat shock protein Hsp27 is required for proper heart tube formation. Genesis *45*, 667-678.

Bruneau, B. G., Bao, Z. Z., Tanaka, M., Schott, J. J., Izumo, S., Cepko, C. L., Seidman, J. G., and Seidman, C. E. (2000). Cardiac expression of the ventricle-specific homeobox gene Irx4 is modulated by Nkx2-5 and dHand. Dev Biol *217*, 266-277.

Bruneau, B. G., Logan, M., Davis, N., Levi, T., Tabin, C. J., Seidman, J. G., and Seidman, C. E. (1999). Chamber-specific cardiac expression of Tbx5 and heart defects in Holt-Oram syndrome. Dev Biol *211*, 100-108.

Bruneau, B. G., Nemer, G., Schmitt, J. P., Charron, F., Robitaille, L., Caron, S., Conner, D. A., Gessler, M., Nemer, M., Seidman, C. E., and Seidman, J. G. (2001). A Murine Model of Holt-Oram Syndrome Defines Roles of the T-Box Transcription Factor Tbx5 in Cardiogenesis and Disease. Cell *106*, 709-721.

Cai, C. L., Liang, X., Shi, Y., Chu, P. H., Pfaff, S. L., Chen, J., and Evans, S. (2003). Isl1 identifies a cardiac progenitor population that proliferates prior to differentiation and contributes a majority of cells to the heart. Dev Cell *5*, 877-889.

Cai, C. L., Zhou, W., Yang, L., Bu, L., Qyang, Y., Zhang, X., Li, X., Rosenfeld, M. G., Chen, J., and Evans, S. (2005). T-box genes coordinate regional rates of proliferation and regional specification during cardiogenesis. Development *132*, 2475-2487.

Carmona, R., Gonzalez-Iriarte, M., Perez-Pomares, J. M., and Munoz-Chapuli, R. (2001). Localization of the Wilm's tumour protein WT1 in avian embryos. Cell Tissue Res *303*, 173-186.

Chambers, A. E., Logan, M., Kotecha, S., Towers, N., Sparrow, D., and Mohun, T. J. (1994). The RSRF/MEF2 protein SL1 regulates cardiac muscle-specific transcription of a myosin light-chain gene in Xenopus embryos. Genes Dev *8*, 1324-1334.

Chapman, D. L., Garvey, N., Hancock, S., Alexiou, M., Agulnik, S. I., Gibson-Brown, J., Cebra-Thomas, J., Bollag, R., Silver, L. M., and Papaionnou, V. E. (1996). Expression of the T-box family genes, *Tbx1-Tbx5*, during early mouse development. Dev Dynam *206*, 379-390.

Charron, F., and Nemer, M. (1999). GATA transcription factors and cardiac development. Semin Cell Dev Biol *10*, 85-91.

Chen, J. N., Haffter, P., Odenthal, J., Vogelsang, E., Brand, M., van Eeden, F. J., Furutani-Seiki, M., Granato, M., Hammerschmidt, M., Heisenberg, C. P*., et al.* (1996). Mutations affecting the cardiovascular system and other internal organs in zebrafish. Development *123*, 293-302.

Christine, K. S., and Conlon, F. L. (2008). Vertebrate CASTOR is required for differentiation of cardiac precursor cells at the ventral midline. Dev Cell *14*, 616-623.

Christoffels, V. M., Habets, P. E., Franco, D., Campione, M., de Jong, F., Lamers, W. H., Bao, Z. Z., Palmer, S., Biben, C., Harvey, R. P., and Moorman, A. F. (2000). Chamber formation and morphogenesis in the developing mammalian heart. Dev Biol *223*, 266-278.

Cohen-Gould, L., and Mikawa, T. (1996). The fate diversity of mesodermal cells within the heart field during chicken early embryogenesis. Dev Biol *177*, 265-273.

Compernolle, V., Brusselmans, K., Franco, D., Moorman, A., Dewerchin, M., Collen, D., and Carmeliet, P. (2003). Cardia bifida, defective heart development and abnormal neural crest migration in embryos lacking hypoxia-inducible factor-1alpha. Cardiovasc Res *60*, 569-579.

Cui, X., and Doe, C. Q. (1992). ming is expressed in neuroblast sublineages and regulates gene expression in the Drosophila central nervous system. Development *116*, 943-952.

Dale, L., and Slack, J. M. (1987). Fate map for the 32-cell stage of Xenopus laevis. Development *99*, 527-551.

de Jong, F., Opthof, T., Wilde, A. A., Janse, M. J., Charles, R., Lamers, W. H., and Moorman, A. F. (1992). Persisting zones of slow impulse conduction in developing chicken hearts. Circ Res *71*, 240-250.

De La Cruz, M. V., Sanchez-Gomez, C., and Palomino, M. A. (1989). The primitive cardiac regions in the straight tube heart (Stage 9) and their anatomical expression in the mature heart: An experimental study in the chick embryo. J Anat *165*, 121-131.

de la Cruz, M. V., Sanchez Gomez, C., Arteaga, M. M., and Arguello, C. (1977). Experimental study of the development of the truncus and the conus in the chick embryo. J Anat *123*, 661-686.

DeHaan, R. L., and Ursprung, H. (1965). Organogenesis (New York: Holt, Rinehart Winston).

Dettman, R. W., Denetclaw, W., Jr., Ordahl, C. P., and Bristow, J. (1998). Common epicardial origin of coronary vascular smooth muscle, perivascular fibroblasts, and intermyocardial fibroblasts in the avian heart. Dev Biol *193*, 169-181.

Dodou, E., Verzi, M. P., Anderson, J. P., Xu, S. M., and Black, B. L. (2004). Mef2c is a direct transcriptional target of ISL1 and GATA factors in the anterior heart field during mouse embryonic development. Development *131*, 3931-3942.

Drake, C. J., and Fleming, P. A. (2000). Vasculogenesis in the day 6.5 to 9.5 mouse embryo. Blood *95*, 1671-1679.

Drysdale, T. A., Tonissen, K. F., Patterson, K. D., Crawford, M. J., and Kreig, P. A. (1994). Cardiac troponin I is a heart specific marker in the Xenopus embryo: Expression during abnormal heart heart morphogenesis. Dev Biol *154*, 432-441.

Dura, J. M., Taillebourg, E., and Preat, T. (1995). The Drosophila learning and memory gene linotte encodes a putative receptor tyrosine kinase homologous to the human RYK gene product. FEBS Lett *370*, 250-254.

Dyer, M. A., Farrington, S. M., Mohn, D., Munday, J. R., and Baron, M. H. (2001). Indian hedgehog activates hematopoiesis and vasculogenesis and can respecify prospective neurectodermal cell fate in the mouse embryo. Development *128*, 1717-1730.

Fishman, M. C., and Chien, K. R. (1997). Fashioning the vertebrate heart: earliest embryonic decisions. Development *124*, 2099-2117.

Folkman, J., and D'Amore, P. A. (1996). Blood vessel formation: what is its molecular basis? Cell *87*, 1153-1155.

Franco, D., Markman, M. M., Wagenaar, G. T., Ya, J., Lamers, W. H., and Moorman, A. F. (1999). Myosin light chain 2a and 2v identifies the embryonic outflow tract myocardium in the developing rodent heart. Anat Rec *254*, 135-146.

Garcia-Martinez, V., and Schoenwolf, G. (1993). Primitive-streak origin of the cardiovascular system in avian embryos. Dev Biol *15*, 706-719.

George, E. L., Georges-Labouesse, E. N., Patel-King, R. S., Rayburn, H., and Hynes, R. O. (1993). Defects in mesoderm, neural tube and vascular development in mouse embryos lacking fibronectin. Development *119*, 1079-1091.

Gittenberger-de Groot, A. C., Vrancken Peeters, M. P., Mentink, M. M., Gourdie, R. G., and Poelmann, R. E. (1998). Epicardium-derived cells contribute a novel population to the myocardial wall and the atrioventricular cushions. Circ Res *82*, 1043-1052.

Grosskortenhaus, R., Robinson, K. J., and Doe, C. Q. (2006). Pdm and Castor specify late-born motor neuron identity in the NB7-1 lineage. Genes Dev *20*, 2618-2627.

Habets, P. E., Moorman, A. F., Clout, D. E., van Roon, M. A., Lingbeek, M., van Lohuizen, M., Campione, M., and Christoffels, V. M. (2002). Cooperative action of Tbx2 and Nkx2.5 inhibits ANF expression in the atrioventricular canal: implications for cardiac chamber formation. Genes Dev *16*, 1234-1246.

Hiroi, Y., Kudoh, S., Monzen, K., Ikeda, Y., Yazaki, Y., Nagai, R., and Komuro, I. (2001). Tbx5 associates with Nkx2-5 and synergistically promotes cardiomyocyte differentiation. Nature Genetics *28*, 276-280.

Hiruma, T., and Hirakow, R. (1989). Epicardial formation in embryonic chick heart: computer-aided reconstruction, scanning, and transmission electron microscopic studies. Am J Anat *184*, 129-138.

Hitier, R., Chaminade, M., and Preat, T. (2001). The Drosophila castor gene is involved in postembryonic brain development. Mech Dev *103*, 3-11.

Horne-Badovinac, S., Lin, D., Waldron, S., Schwarz, M., Mbamalu, G., Pawson, T., Jan, Y., Stainier, D. Y., and Abdelilah-Seyfried, S. (2001). Positional cloning of heart and soul reveals multiple roles for PKC lambda in zebrafish organogenesis. Curr Biol *11*, 1492-1502.

Houweling, A. C., Somi, S., Van Den Hoff, M. J., Moorman, A. F., and Christoffels, V. M. (2002). Developmental pattern of ANF gene expression reveals a strict localization of cardiac chamber formation in chicken. Anat Rec *266*, 93-102.

Hu, N., Sedmera, D., Yost, H. J., and Clark, E. B. (2000). Structure and function of the developing zebrafish heart. Anat Rec *260*, 148-157.

Isshiki, T., Pearson, B., Holbrook, S., and Doe, C. Q. (2001). Drosophila neuroblasts sequentially express transcription factors which specify the temporal identity of their neuronal progeny. Cell *106*, 511-521.

Jahr, M., Schlueter, J., Brand, T., and Manner, J. (2008). Development of the proepicardium in Xenopus laevis. Dev Dyn *237*, 3088-3096.

Kalman, F., Viragh, S., and Modis, L. (1995). Cell surface glycoconjugates and the extracellular matrix of the developing mouse embryo epicardium. Anat Embryol (Berl) *191*, 451-464.

Kambadur, R., Koizumi, K., Stivers, C., Nagle, J., Poole, S. J., and Odenwald, W. F. (1998). Regulation of POU genes by castor and hunchback establishes layered compartments in the Drosophila CNS. Genes Dev *12*, 246-260.

Kastner, P., Grondona, J. M., Mark, M., Gansmuller, A., LeMeur, M., Decimo, D., Vonesch, J. L., Dolle, P., and Chambon, P. (1994). Genetic analysis of RXR alpha developmental function: convergence of RXR and RAR signaling pathways in heart and eye morphogenesis. Cell *78*, 987-1003.

Keegan, B. R., Feldman, J. L., Lee, D. H., Koos, D. S., Ho, R. K., Stainier, D. Y., and Yelon, D. (2002). The elongation factors Pandora/Spt6 and Foggy/Spt5 promote transcription in the zebrafish embryo. Development *129*, 1623-1632.

Kelly, R. G., Brown, N. A., and Buckingham, M. E. (2001). The arterial pole of the mouse heart forms from Fgf10-expressing cells in pharyngeal mesoderm. Dev Cell *1*, 435-440.

Kikuchi, Y., Agathon, A., Alexander, J., Thisse, C., Waldron, S., Yelon, D., Thisse, B., and Stainier, D. Y. (2001). casanova encodes a novel Sox-related protein necessary and sufficient for early endoderm formation in zebrafish. Genes Dev *15*, 1493-1505.

Kirby, M. L., Gale, T. F., and Stewart, D. E. (1983). Neural crest cells contribute to normal aorticopulmonary septation. Science *220*, 1059-1061.

Klingensmith, J., Ang, S. L., Bachiller, D., and Rossant, J. (1999). Neural induction and patterning in the mouse in the absence of the node and its derivatives. Dev Biol *216*, 535-549.

Kolker, S., Tajchman, U., and Weeks, D. L. (2000). Confocal Imaging of early heat development in Xenopus laevis. Dev Biol *218*, 64-73.

Komiyama, M., Ito, K., and Shimada, Y. (1987). Origin and development of the epicardium in the mouse embryo. Anat Embryol (Berl) *176*, 183-189.

Kramer, R., Bucay, N., Kane, D. J., Martin, L. E., Tarpley, J. E., and Theill, L. E. (1996). Neuregulins with an Ig-like domain are essential for mouse myocardial and neuronal development. Proc Natl Acad Sci U S A *93*, 4833-4838.

Kupperman, E., An, S., Osborne, N., Waldron, S., and Stainier, D. Y. (2000). A sphingosine-1-phosphate receptor regulates cell migration during vertebrate heart development. Nature *406*, 192-195.

Lavine, K. J., Yu, K., White, A. C., Zhang, X., Smith, C., Partanen, J., and Ornitz, D. M. (2005). Endocardial and epicardial derived FGF signals regulate myocardial proliferation and differentiation in vivo. Dev Cell *8*, 85-95.

Lin, Q., Schwarz, J., Bucana, C., and Olson, E. N. (1997). Control of mouse cardiac morphogenesis and myogenesis by transcription factor MEF2C. Science *276*, 1404-1407.

Linask, K. K. (1992). N-cadherin localization in early heart development and polar expression of Na+,K(+)-ATPase, and integrin during pericardial coelom formation and epithelialization of the differentiating myocardium. Dev Biol *151*, 213-224.

Linask, K. K., and Lash, J. W. (1986). Precardiac cell migration: fibronectin localization at mesoderm-endoderm interface during directional movement. Dev Biol *114*, 87-101.

Linask, K. K., and Lash, J. W. (1993). Early heart development: dynamics of endocardial cell sorting suggests a common origin with cardiomyocytes. Dev Dyn *196*, 62-69.

Linask, K. K., Manisastry, S., and Han, M. (2005). Cross talk between cell-cell and cell-matrix adhesion signaling pathways during heart organogenesis: implications for cardiac birth defects. Microsc Microanal *11*, 200-208.

Liu, Z., Yang, X., Tan, F., Cullion, K., and Thiele, C. J. (2006). Molecular cloning and characterization of human Castor, a novel human gene upregulated during cell differentiation. Biochem Biophys Res Commun *344*, 834-844.

Lloyd-Jones, D., Adams, R., Carnethon, M., De Simone, G., Ferguson, T. B., Flegal, K., Ford, E., Furie, K., Go, A., Greenlund, K.*, et al.* (2008). Heart Disease and Stroke Statistics--2009 Update. A Report From the American Heart Association Statistics Committee and Stroke Statistics Subcommittee. Circulation.

Lopez-Sanchez, C., Garcia-Martinez, V., and Schoenwolf, G. C. (2001). Localization of cells of the prospective neural plate, heart and somites within the

primitive streak and epiblast of avian embryos at intermediate primitive-streak stages. Cells Tissues Organs *169*, 334-346.

Luo, Y., and Radice, G. L. (2003). Cadherin-mediated adhesion is essential for myofibril continuity across the plasma membrane but not for assembly of the contractile apparatus. J Cell Sci *116*, 1471-1479.

Mably, J. D., Chuang, L. P., Serluca, F. C., Mohideen, M. A., Chen, J. N., and Fishman, M. C. (2006). santa and valentine pattern concentric growth of cardiac myocardium in the zebrafish. Development *133*, 3139-3146.

Mably, J. D., Mohideen, M. A., Burns, C. G., Chen, J. N., and Fishman, M. C. (2003). heart of glass regulates the concentric growth of the heart in zebrafish. Curr Biol *13*, 2138-2147.

Manner, J. (1992). The development of pericardial villi in the chick embryo. Anat Embryol (Berl) *186*, 379-385.

Manner, J. (1999). Does the subepicardial mesenchyme contribute myocardioblasts to the myocardium of the chick embryo heart? A quail-chick chimera study tracing the fate of the epicardial primordium. Anat Rec *255*, 212-226.

Meilhac, S. M., Esner, M., Kelly, R. G., Nicolas, J. F., and Buckingham, M. E. (2004). The clonal origin of myocardial cells in different regions of the embryonic mouse heart. Dev Cell *6*, 685-698.

Meilhac, S. M., Kelly, R. G., Rocancourt, D., Eloy-Trinquet, S., Nicolas, J. F., and Buckingham, M. E. (2003). A retrospective clonal analysis of the myocardium reveals two phases of clonal growth in the developing mouse heart. Development *130*, 3877-3889.

Mellerick, D. M., Kassis, J. A., Zhang, S. D., and Odenwald, W. F. (1992). castor encodes a novel zinc finger protein required for the development of a subset of CNS neurons in Drosophila. Neuron *9*, 789-803.

Meyer, D., and Birchmeier, C. (1995). Multiple essential functions of neuregulin in development. Nature *378*, 386-390.

Mikawa, T., and Fischman, D. A. (1992). Retroviral analysis of cardiac morphogenesis: discontinuous formation of coronary vessels. Proc Natl Acad Sci U S A *89*, 9504-9508.

Miller, J., McLachlan, A. D., and Klug, A. (1985). Repetitive zinc-binding domains in the protein transcription factor IIIA from Xenopus oocytes. Embo J *4*, 1609-1614.

Minkoff, R., Rundus, V. R., Parker, S. B., Beyer, E. C., and Hertzberg, E. L. (1993). Connexin expression in the developing avian cardiovascular system. Circ Res *73*, 71-78.

Mjaatvedt, C. H., Nakaoka, T., Moreno-Rodriguez, R., Norris, R. A., Kern, M. J., Eisenberg, C. A., Turner, D., and Markwald, R. R. (2001). The outflow tract of the heart is recruited from a novel heart-forming field. Dev Biol *238*, 97-109.

Mohun, T. J., Leong, L. M., Weninger, W. J., and Sparrow, D. B. (2000). The morphology of heart development in Xenopus laevis. Dev Biol *218*, 74-88.

Mohun, T. J., Leong, L.M., Weninger, W. J., and Sparrow, D. B. (2000). The Morphology of Heart Development in Xenopus laevis. Developmental Biology *218*, 74-88.

Molkentin, J. D. (2000). The zinc finger-containing transcription factors GATA-4, -5, and -6. Ubiquitously expressed regulators of tissue-specific gene expression. J Biol Chem *275*, 38949-38952.

Molkentin, J. D., Lin, Q., Duncan, S. A., and Olson, E. N. (1997). Requirement of the transcription factor GATA4 for heart tube formation and ventral morphogenesis. Genes Dev *11*, 1061-1072.

Moody, S. A. (1987). Fates of the blastomeres of the 32 cell *Xenopus* embryo. Dev Biol *122*, 300-319.

Moorman, A. F., de Jong, F., Denyn, M. M., and Lamers, W. H. (1998). Development of the cardiac conduction system. Circ Res *82*, 629-644.

Morabito, C. J., Dettman, R. W., Kattan, J., Collier, J. M., and Bristow, J. (2001). Positive and negative regulation of epicardial-mesenchymal transformation during avian heart development. Dev Biol *234*, 204-215.

Nahirney, P. C., Mikawa, T., and Fischman, D. A. (2003). Evidence for an extracellular matrix bridge guiding proepicardial cell migration to the myocardium of chick embryos. Dev Dyn *227*, 511-523.

Nakajima, Y., Yamagishi, T., Ando, K., and Nakamura, H. (2002). Significance of bone morphogenetic protein-4 function in the initial myofibrillogenesis of chick cardiogenesis. Dev Biol *245*, 291-303.

Nascone, N., and Mercola, M. (1995). An Inductive role for endoderm in *Xenopus* cardiogenesis. Development *121*, 515-523.

Palmer, S., Groves, N., Schindeler, A., Yeoh, T., Biben, C., Wang, C. C., Sparrow, D. B., Barnett, L., Jenkins, N. A., Copeland, N. G.*, et al.* (2001). The small muscle-specific protein Csl modifies cell shape and promotes myocyte fusion in an insulin-like growth factor 1-dependent manner. J Cell Biol *153*, 985-998.

Pandur, P., Lasche, M., Eisenberg, L. M., and Kuhl, M. (2002). Wnt-11 activation of a non-canonical Wnt signalling pathway is required for cardiogenesis. Nature *418*, 636-641.

Pearson, B. J., and Doe, C. Q. (2003). Regulation of neuroblast competence in Drosophila. Nature *425*, 624-628.

Pennisi, D. J., Ballard, V. L., and Mikawa, T. (2003). Epicardium is required for the full rate of myocyte proliferation and levels of expression of myocyte mitogenic factors FGF2 and its receptor, FGFR-1, but not for transmural myocardial patterning in the embryonic chick heart. Dev Dyn *228*, 161-172.

Perez-Pomares, J. M., Macias, D., Garcia-Garrido, L., and Munoz-Chapuli, R. (1998a). Immunolocalization of the vascular endothelial growth factor receptor-2 in the subepicardial mesenchyme of hamster embryos: identification of the coronary vessel precursors. Histochem J *30*, 627-634.

Perez-Pomares, J. M., Macias, D., Garcia-Garrido, L., and Munoz-Chapuli, R. (1998b). The origin of the subepicardial mesenchyme in the avian embryo: an immunohistochemical and quail-chick chimera study. Dev Biol *200*, 57-68.

Perez-Pomares, J. M., Phelps, A., Sedmerova, M., Carmona, R., Gonzalez-Iriarte, M., Munoz-Chapuli, R., and Wessels, A. (2002). Experimental studies on the spatiotemporal expression of WT1 and RALDH2 in the embryonic avian heart: a model for the regulation of myocardial and valvuloseptal development by epicardially derived cells (EPDCs). Dev Biol *247*, 307-326.

Peterkin, T., Gibson, A., and Patient, R. (2003). GATA-6 maintains BMP-4 and Nkx2 expression during cardiomyocyte precursor maturation. Embo J *22*, 4260-4273.

Plageman, T. F., Jr., and Yutzey, K. E. (2004). Differential expression and function of tbx5 and tbx20 in cardiac development. J Biol Chem *279*, 19026-19034.

Prall, O. W., Menon, M. K., Solloway, M. J., Watanabe, Y., Zaffran, S., Bajolle, F., Biben, C., McBride, J. J., Robertson, B. R., Chaulet, H.*, et al.* (2007). An Nkx2-5/Bmp2/Smad1 negative feedback loop controls heart progenitor specification and proliferation. Cell *128*, 947-959.

Radice, G. L., Rayburn, H., Matsunami, H., Knudsen, K. A., Takeichi, M., and Hynes, R. O. (1997). Developmental defects in mouse embryos lacking N-cadherin. Dev Biol *181*, 64-78.

Rakeman, A. S., and Anderson, K. V. (2006). Axis specification and morphogenesis in the mouse embryo require Nap1, a regulator of WAVE-mediated actin branching. Development *133*, 3075-3083.

Reiter, J. F., Alexander, J., Rodaway, A., Yelon, D., Patient, R., Holder, N., and Stainier, D. Y. (1999). Gata5 is required for the development of the heart and endoderm in zebrafish. Genes Dev *13*, 2983-2995.

Reiter, J. F., Kikuchi, Y., and Stainier, D. Y. (2001). Multiple roles for Gata5 in zebrafish endoderm formation. Development *128*, 125-135.

Rodgers, L. S., Lalani, S., Runyan, R. B., and Camenisch, T. D. (2008). Differential growth and multicellular villi direct proepicardial translocation to the developing mouse heart. Dev Dyn *237*, 145-152.

Rohr, S., Bit-Avragim, N., and Abdelilah-Seyfried, S. (2006). Heart and soul/PRKCi and nagie oko/Mpp5 regulate myocardial coherence and remodeling during cardiac morphogenesis. Development *133*, 107-115.

Rosenquist, G. C. (1970). Location and movements of cardiogenic cells in the chick embryo: the heart-forming portion of the primitive streak. Dev Biol *22*, 461-475.

Sasai, Y., Lu, B., Steinbeisser, H., Geissert, D., Gont, L. K., and De Robertis, E. M. (1994). Xenopus chordin: a novel dorsalizing factor activated by organizer-specific homeobox genes. Cell *79*, 779-790.

Sater, A. K., and Jacobson, A. G. (1989). The specification of heart mesoderm occurs during gastrulation in Xenopus laevis. Development *106*, 519-529.

Sater, A. K., and Jacobson, A. G. (1990). The restriction of the heart morphogenetic field in Xenopus laevis. Dev Biol *140*, 328-336.

Schneider, V. A., and Mercola, M. (2001). Wnt antagonism initiates cardiogenesis in Xenopus laevis. Genes Dev *15*, 304-315.

Schultheiss, T. M., Burch, J. B., and Lassar, A. B. (1997). A role for bone morphogenetic proteins in the induction of cardiac myogenesis. Genes Dev *11*, 451-462.

Schwartz, R. J., and Olson, E. N. (1999). Building the heart piece by piece: modularity of cis-elements regulating Nkx2-5 transcription. Development *126*, 4187-4192.

Sepulveda, J. L., Vlahopoulos, S., Iyer, D., Belaguli, N., and Schwartz, R. J. (2002). Combinatorial expression of GATA4, Nkx2-5, and serum response factor directs early cardiac gene activity. J Biol Chem *277*, 25775-25782.

Serbedzija, G. N., Chen, J. N., and Fishman, M. C. (1998). Regulation in the heart field of zebrafish. Development *125*, 1095-1101.

Shi, Y., Katsev, S., Cai, C., and Evans, S. (2000). BMP signaling is required for heart formation in vertebrates. Dev Biol *224*, 226-237.

Shinbrot, E., Peters, K. G., and Williams, L. T. (1994). Expression of the platelet-derived growth factor beta receptor during organogenesis and tissue differentiation in the mouse embryo. Dev Dyn *199*, 169-175.

Singh, M. K., Christoffels, V. M., Dias, J. M., Trowe, M. O., Petry, M., Schuster-Gossler, K., Burger, A., Ericson, J., and Kispert, A. (2005). Tbx20 is essential for cardiac chamber differentiation and repression of Tbx2. Development *132*, 2697-2707.

Soufan, A. T., van den Berg, G., Ruijter, J. M., de Boer, P. A., van den Hoff, M. J., and Moorman, A. F. (2006). Regionalized sequence of myocardial cell growth and proliferation characterizes early chamber formation. Circ Res *99*, 545-552.

Srivastava, D. (1997). Left, right ... which way to turn? Nat Genet *17*, 252-254.

Srivastava, D., Cserjesi, P., and Olson, E. N. (1995). A subclass of bHLH proteins required for cardiac morphogenesis. Science *270*, 1995-1999.

Stainier, D. Y., and Fishman, M. C. (1992). Patterning the zebrafish heart tube: acquisition of anteroposterior polarity. Dev Biol *153*, 91-101.

Stainier, D. Y., Fouquet, B., Chen, J. N., Warren, K. S., Weinstein, B. M., Meiler, S. E., Mohideen, M. A., Neuhauss, S. C., Solnica-Krezel, L., Schier, A. F.*, et al.* (1996). Mutations affecting the formation and function of the cardiovascular system in the zebrafish embryo. Development *123*, 285-292.

Stainier, D. Y., Lee, R. K., and Fishman, M. C. (1993). Cardiovascular development in the zebrafish. I. Myocardial fate map and heart tube formation. Development *119*, 31-40.

Stratford, T., Logan, C., Zile, M., and Maden, M. (1999). Abnormal anteroposterior and dorsoventral patterning of the limb bud in the absence of retinoids. Mech Dev *81*, 127-137.

Sucov, H. M., Dyson, E., Gumeringer, C. L., Price, J., Chien, K. R., and Evans, R. M. (1994). RXR alpha mutant mice establish a genetic basis for vitamin A signaling in heart morphogenesis. Genes Dev *8*, 1007-1018.

Sugi, Y., and Markwald, R. R. (1996). Formation and early morphogenesis of endocardial endothelial precursor cells and the role of endoderm. Dev Biol *175*, 66-83.

Taber, L. A., Lin, I. E., and Clark, E. B. (1995). Mechanics of cardiac looping. Dev Dyn *203*, 42-50.

Tam, P. P., and Beddington, R. S. (1987). The formation of mesodermal tissues in the mouse embryo during gastrulation and early organogenesis. Development *99*, 109-126.

Tam, P. P., Parameswaran, M., Kinder, S. J., and Weinberger, R. P. (1997). The allocation of epiblast cells to the embryonic heart and other mesodermal lineages: the role of ingression and tissue movement during gastrulation. Development *124*, 1631-1642.

Thomas, T., Yamagishi, H., Overbeek, P. A., Olson, E. N., and Srivastava, D. (1998). The bHLH factors, dHAND and eHAND, specify pulmonary and systemic cardiac ventricles independent of left-right sidedness. Dev Biol *196*, 228-236.

Tidball, J. G. (1992). Distribution of collagens and fibronectin in the subepicardium during avian cardiac development. Anat Embryol (Berl) *185*, 155-162.

Tokuyasu, K. T., and Maher, P. A. (1987). Immunocytochemical studies of cardiac myofibrillogenesis in early chick embryos. II. Generation of alpha-actinin dots within titin spots at the time of the first myofibril formation. J Cell Biol *105*, 2795-2801.

Tomanek, R. J., Ratajska, A., Kitten, G. T., Yue, X., and Sandra, A. (1999). Vascular endothelial growth factor expression coincides with coronary vasculogenesis and angiogenesis. Dev Dyn *215*, 54-61.

Tran, K. D., and Doe, C. Q. (2008). Pdm and Castor close successive temporal identity windows in the NB3-1 lineage. Development *135*, 3491-3499.

Trinh, L. A., and Stainier, D. Y. (2004). Fibronectin regulates epithelial organization during myocardial migration in zebrafish. Dev Cell *6*, 371-382.

Tzahor, E., and Lassar, A. B. (2001). Wnt signals from the neural tube block ectopic cardiogenesis. Genes Dev *15*, 255-260.

Vacalla, C. M., and Theil, T. (2002). Cst, a novel mouse gene related to Drosophila Castor, exhibits dynamic expression patterns during neurogenesis and heart development. Mech Dev *118*, 265-268.

Viragh, S., and Challice, C. E. (1973). Origin and differentiation of cardiac muscle cells in the mouse. J Ultrastruct Res *42*, 1-24.

von Both, I., Silvestri, C., Erdemir, T., Lickert, H., Walls, J. R., Henkelman, R. M., Rossant, J., Harvey, R. P., Attisano, L., and Wrana, J. L. (2004). Foxh1 is essential for development of the anterior heart field. Dev Cell *7*, 331-345.

Vrancken Peeters, M. P., Gittenberger-de Groot, A. C., Mentink, M. M., and Poelmann, R. E. (1999). Smooth muscle cells and fibroblasts of the coronary arteries derive from epithelial-mesenchymal transformation of the epicardium. Anat Embryol (Berl) *199*, 367-378.

Waldo, K. L., Hutson, M. R., Ward, C. C., Zdanowicz, M., Stadt, H. A., Kumiski, D., Abu-Issa, R., and Kirby, M. L. (2005). Secondary heart field contributes myocardium and smooth muscle to the arterial pole of the developing heart. Dev Biol *281*, 78-90.

Waldo, K. L., Kumiski, D. H., Wallis, K. T., Stadt, H. A., Hutson, M. R., Platt, D. H., and Kirby, M. L. (2001). Conotruncal myocardium arises from a secondary heart field. Development *128*, 3179-3188.

Walters, M. J., Wayman, G. A., and Christian, J. L. (2001). Bone morphogenetic protein function is required for terminal differentiation of the heart but not for early expression of cardiac marker genes. Mech Dev *100*, 263-273.

Warga, R. M., and Kimmel, C. B. (1990). Cell movements during epiboly and gastrulation in zebrafish. Development *108*, 581-594.

Xavier-Neto, J., Shapiro, M. D., Houghton, L., and Rosenthal, N. (2000). Sequential programs of retinoic acid synthesis in the myocardial and epicardial layers of the developing avian heart. Dev Biol *219*, 129-141.

Yamagishi, H., Yamagishi, C., Nakagawa, O., Harvey, R. P., Olson, E. N., and Srivastava, D. (2001). The combinatorial activities of Nkx2.5 and dHAND are essential for cardiac ventricle formation. Dev Biol *239*, 190-203.

Yamashita, J., Itoh, H., Hirashima, M., Ogawa, M., Nishikawa, S., Yurugi, T., Naito, M., Nakao, K., and Nishikawa, S. (2000). Flk1-positive cells derived from embryonic stem cells serve as vascular progenitors. Nature *408*, 92-96.

Yelbuz, T. M., Waldo, K. L., Kumiski, D. H., Stadt, H. A., Wolfe, R. R., Leatherbury, L., and Kirby, M. L. (2002). Shortened outflow tract leads to altered cardiac looping after neural crest ablation. Circulation *106*, 504-510.

Yelon, D., Horne, S. A., and Stainier, D. Y. (1999). Restricted expression of cardiac myosin genes reveals regulated aspects of heart tube assembly in zebrafish. Dev Biol *214*, 23-37.

Yuan, S., and Schoenwolf, G. C. (2000). Islet-1 marks the early heart rudiments and is asymmetrically expressed during early rotation of the foregut in the chick embryo. Anat Rec *260*, 204-207.

Zhang, J., Talbot, W. S., and Schier, A. F. (1998). Positional cloning identifies zebrafish one-eyed pinhead as a permissive EGF-related ligand required during gastrulation. Cell *92*, 241-251.

Zhang, X. M., Ramalho-Santos, M., and McMahon, A. P. (2001). Smoothened mutants reveal redundant roles for Shh and Ihh signaling including regulation of L/R symmetry by the mouse node. Cell *106*, 781-792.

Zimmerman, L. B., De Jesus-Escobar, J. M., and Harland, R. M. (1996). The Spemann organizer signal noggin binds and inactivates bone morphogenetic protein 4. Cell *86*, 599-606.

Chapter 2

Vertebrate CASTOR is required for differentiation of cardiac precursor cells at the ventral midline

Reprinted from Developmental Cell, Volume 14, Kathleen S. Christine and Frank L. Conlon, Vertebrate CASTOR Is Required for Differentiation of Cardiac Precursor Cells at the Ventral Midline, 616-623, 2008, with permission from Elsevier.

ABSTRACT

The CASTOR (CST) transcription factor was initially identified for its role in maintaining stem cell competence in the *Drosophila* dorsal midline. Here we report *Xenopus* CST affects cardiogenesis. In CST-depleted embryos, cardiomyocytes at the ventral midline arrest and are maintained as cardiac progenitors, while cells in more dorsal regions of the heart undergo their normal program of differentiation. Cardia bifida results from failed midline differentiation, even though cardiac cell migration and initial cell fate specification occur normally. Our fate mapping studies reveal that this ventral midline population of

cardiomyocytes ultimately gives rise to the outer curvature of the heart; however, CST-depleted midline cells over proliferate and remain a coherent population of nonintegrated cells positioned on the outer wall of the ventricle. These midline-specific requirements for CST suggest the regulation of cardiomyocyte differentiation is regionalized along a dorsal-ventral axis and that this patterning occurs prior to heart tube formation.

INTRODUCTION

Terminal differentiation of progenitor populations is initiated in response to alterations in growth factor signaling, which leads to an arrest in cell cycle progression and the transcription of tissue specific genes. In contrast to other cell types such as neural tissue and skeletal muscle, relatively little is known about the molecular pathways that trigger the onset of cardiomyocyte differentiation during heart development. Studies in tissue culture focusing on the ability of growth factors to drive the formation of cardiomyocytes from stem cells have identified numerous pathways that may be involved in cardiomyocyte differentiation (Guan and Hasenfuss, 2007; Liu et al., 2007); however, the transcriptional targets of these pathways or the endogenous role for their components during *in vivo* embryonic cardiomyocyte differentiation remains unclear. Furthermore, it is not known whether cardiomyocytes differentiate in a uniform manner in response to a single cue or if specific subsets of cardiomyocytes differentiate in response to different pathways.

To address these issues and to begin to identify the molecular pathways that function *in vivo* to regulate the onset of cardiomyocyte differentiation, we have characterized the *Xenopus* orthologue of *Castor* (*Cst*), a protein that regulates stem cell competence in *Drosophila* (Cui and Doe, 1992; Mellerick et al., 1992). In this report, we show that vertebrate *Cst* is expressed in the myocardial layer of the heart in a dorsal-to-ventral gradient and demonstrate that CST is required within a subset of cardiac progenitor cells for the initiation of cardiomyocyte differentiation at the ventral midline. Fate mapping of cardiac tissue indicates that cardiac progenitors at the ventral midline have a specific cell fate, giving rise to a population of cells in the outer curvature of the ventricle. In contrast, ventral midline cells depleted of CST over-proliferate and fail to integrate into cardiac muscle. Collectively, these studies demonstrate that CST is required for the proper timing of differentiation within a subset of cardiac progenitors that are fated to give rise to the outer curvature of the ventricle, and suggest that regulation of cardiomyocyte differentiation is regionalized along a dorsal-ventral axis prior to heart tube formation.

MATERIAL AND METHODS

Embryo collection and morpholinos

Preparation and collection of *X. tropicalis* and *X. laevis* was performed as described (Showell et al., 2006) and staged according to Nieuwkoop and Faber (Nieuwkoop and Faber, 1967). Sequences of *X.laevis Cstα, X.laevis Cstβ, X.tropicalis Cstα,* and *X.tropicalis Cstβ* have been assigned Accession No:

920664, 919693, 919695, and 919705 (Genbank), respectively. *Cst*-specific morpholinos were obtained from Gene Tools, LLC. Sequences of all morpholinos are available upon request. To demonstrate morpholino efficacy, RNA was extracted from homogenized stage 42 tadpoles in lysis buffer (Goetz et al., 2006) followed by RT-PCR.

Cst identification and characterization

RNA was extracted from embryos using Trizol (Invitrogen) and the 5' untranslated regions of *Cstα* and *Cstβ* was identified by 5'RLM RACE according to manufacturer's instructions with a *Cst*-specific primer. Coding DNA regions were determined by RT-PCR using primers based on regions of homology of murine *Cst* (Acc# XM_112612) to *X. tropicalis* genome available through the Joint Genomic Institute (http://genome.jgi-psf.org). *Cst* 3'untranslated region was determined by RT-PCR using primers designed from a *X. tropicalis* UniGene cluster (UniGene Str.46155) containing 3' untranslated region of *Cst*. Sequence conservation was analyzed using GeneDoc (www.psc.edu/biomed/genedoc) and synteny comparison by Metazome analysis (www.metazome.net).

Protein expression and cellular localization

Cstα and *Cstβ* cDNAs were cloned into pcDNA 3.1-V5/His TOPO vector (Invitrogen) and *in vitro* translated using TnT Coupled Reticulocyte Lysate System (Promega). Tagged proteins were detected by western blot using mouse

anti-V5 antibody (Invitrogen) and peroxidase-conjugated Affinity Pure donkey anti-mouse secondary antibody (Jackson Immunoresearch Laboratories). Cellular localization was determined by injecting 3 ng *Cstα*-V5 and *Cstβ*-V5 mRNA, prepared by mMessage *in vitro* Transcription System (Ambion). RNAs were injected at the one-cell stage. Embryos were cultured until Stage 32, fixed and sectioned as previously described (Goetz et al., 2006). Sections were stained with mouse anti-V5, Cy3-conjugated anti-mouse secondary antibody and DAPI (both Sigma) as previously described (Goetz et al., 2006). Sections were imaged on a Zeiss LSM410 confocal microscope.

Developmental temporal expression

RNA was extracted from homogenized embryos at indicated stages (10 embryos per stage) in lysis buffer (Goetz et al., 2006) followed by phenol:chloroform extraction. cDNA was synthesized with Superscript II reverse transcriptase (Invitrogen). Transcript specific PCR reactions were performed with Taq Polymerase using 1 µl of cDNA using the following PCR program: 94°- 3 min, 40 cycles of 94°- 30 sec, 55°- 30 sec, 72°- 2 min followed by 7 min of 72°. Forward primers were designed to unique regions of each *Cst* transcript and the reverse primer was designed to a common region of both transcripts spanning introns.

Developmental wholemount *in situ* hybridization

Wholemount *in situ* analysis and double detection wholemount *in situ* analysis was carried out as described (Harland, 1991) using α-sense RNA probes of *Nkx2.5* (Tonissen et al., 1994), *Tbx5* (Horb and Thomsen, 1999), *Tbx20* (Brown et al., 2003), *cardiac troponin I* (Logan and Mohun, 1993), *Sox2* (Kishi et al., 2000), *Endodermin* (Langdon et al., 2007), *Endocut* (Costa et al., 2003), and *Vito* [*Xenopus* EST clone XL043k17 (Costa et al., 2003)]. *in situ* hybridization of sectioned *Xenopus* heart and endoderm tissue was performed on 20 μm frozen sections using DIG-labeled antisense RNA probes followed by detection according to manufacture's protocol. For double *in situs* the protocol was modified so embryos were simultaneously analyzed with fluorosceine-labeled *Nkx2.5* probe and either *Cst* or *cardiac troponin I* DIG-labeled probe. Following incubation with α-fluorosceine alkaline phosphatase antibody, Nkx2.5 expression was detected using 175 μg/ml of magenta phosphate and 225 μg/ml tetrazolium red in AP buffer at 4° for 3-5 days. Embryos were washed three times in PBS incubated in 0.1M glycine-HCl pH2.2, 0.1% Tween-20 for 10 min at RT. DIG-labeled probes were detected as described. Embryos were bleached then photographed on a Leica MZF III fluorescent dissecting microscope. Stained embryos were prepared for 20 μm frozen sectioning in OTC freezing media. Sections were rinsed with PBS, coverslipped, and imaged on a Zeiss Axiovert 35 microscope.

Immunohistochemistry

Immunohistochemistry was carried out with mouse anti-myosin heavy chain, mouse anti-tropomyosin (Developmental Studies Hybridoma Bank) and rabbit anti-phospho-histone H3 (Cell Signaling) using Cy3 anti-rabbit, Cy3 anti-mouse, and Alexa 488 anti-mouse as described (Goetz et al., 2006). Embryos were cleared in 2:1 benzyl benzoate: benzyl alcohol and viewed on a Leica MZFIII fluorescence dissecting microscope. Sections were imaged on a Nikon Eclipse E800 fluorescent microscope.

SYBR Green quantitative PCR

RNA was isolated from Stage 29 embryos (10 embryos per condition) using Trizol (Invitrogen) and purified using an RNeasy column (Qiagen) according to manufacture's protocol. cDNA synthesis with 1 µg of RNA was performed with random primers using SuperScript II reverse transcriptase (Invitrogen) according to manufacture's protocol. Expression levels were assessed by quantitative PCR using SYBR Green Master Mix (Sigma) on a Rotogene 3000. Primers (19-21 bp) were designed for each mRNA to amplify a 100-121 bp product. Prior to quantitative PCR analysis, primer sets were tested by standard PCR and analyzed by 2.5% agarose gel electrophoresis to determine amplification of a single PCR product. GAPDH was used as the housekeeping gene. Reactions with 5 µl of a 1:60 dilution of the cDNA were heated to 94° for 2 minutes, followed by 50 cycles of 94°, 15 seconds; 55°, 15 seconds; 72°, 20 seconds. Following amplification, melting curves were

generated to verify presence of a single amplification product. Each sample was analyzed in triplicate with a corresponding minus-RT control. Five samples (N=5) per condition were analyzed. Analysis generated Ct values based on thresholds determined by Rotogene 3000 software. Data was analyzed by the Pfaffl method (Pfaffl et al., 2002) and represented as relative fold change +/- S.E.M.

Fate Mapping

Fertilized embryos were injected at one-cell stage with either Cst MOs or control MOs as described (Goetz et al., 2006). Stage 29 GFP-positive embryos were embedded in 3% methyl-cellulose and injected with 0.3 nl of 1mM Mito Tracker Red CMXRos (Molecular Probes) at the ventral midline 5.5 mm from the posterior boundary of the cement gland. Two hours post-injection, embryos were analyzed and scored for incorporation into GFP-positive cardiac tissue. Stage 35 and 45 hearts were dissected in 1x Modified Barths Solution (MBS) and placed in 1x MBS supplemented with 0.1M KCl to arrest contraction. Stage 35 labeled-clones were scored based on anterior-posterior axis and inner-outer curvature of the heart and Stage 45 based on location of labeled-clones in the atrium or ventricle. Transgenic animals expressing cardiac actin-GFP were a generous gift from Dr. Tim Mohun (Latinkic et al., 2002).

Statistical Methods

Morpholino injections were performed on greater then fifteen batches of embryos. Similar results were seen in each experiment. Statistical differences of

cell counts between injected embryos were determined using one-tailed, unpaired t-tests. Number of embryos used in each experiment is noted in the results.

RESULTS

Cst is Expressed in the Myocardium Prior to the Onset of Cardiomyocyte Differentiation

To begin to identify the molecular pathways that are involved in the decisions of cardiac progenitor cells to proliferate or differentiate, we have focused on the vertebrate orthologues of *Castor* (*Cst*), a known regulator of stem cell competence in *Drosophila*. We have identified two alternatively 5-prime spliced variants of vertebrate *Castor* (*Cstα* and *Cstβ*) from *Xenopus laevis* (*X. laevis*) as well as *Xenopus tropicalis* (*X. tropicalis*) (Fig 2.1A, S2.1A). Synteny and sequence analysis confirmed that these are the true orthologues of jawed vertebrate and *Drospholia Castor* (Fig S2.1B-D). *in vitro* translation of CSTα and CSTβ give proteins of the expected size (Fig S2.1E). Injection of mRNAs into *Xenopus* show CSTα and CSTβ both localize to the nucleus in *Xenopus* tissue (Fig S2.1F-G). RT-PCR analysis with *Cstα* and *Cstβ* specific primers (Fig S2.2A) indicate *Cstα* is expressed at the onset of neurulation (Stage13) whereas *Cstβ* is expressed slightly later (Stage15) with both transcripts continuing to be expressed throughout embryonic development. Using a probe common to *Cstα* and *Cstβ*, shows a nearly identical spatial pattern of expression in *X. laevis* and *X. tropicalis* (Fig 2.1B, S2.2B-K, S2.3), with *Cst* expression first observed at the

dorsal midline in the developing hindbrain region of the embryo (Fig S2.2B) (Stage 13) and by early tailbud stage in the developing somites (Fig 2.1B). By early tailbud stage (Stage 27) we also observe expression of *Cst* in the heart primordium (Fig 2.1B) during the period when the bilateral heart fields begin to fuse across the ventral midline and at Stage 29 find *Cst* co-expressed with the cardiac maker *Nkx2.5* throughout the heart tube (Fig 2.1B-C, S2.4). On more detailed analysis, we observe *Cst* expression within the myocardial layer of the heart in a dorsal to ventral gradient (Fig 2.1D). We further note that onset and maintenance of *Cst* expression is not disrupted in TBX5, TBX20 or HSP27 depleted embryos (Brown et al., 2007; Brown et al., 2005) suggesting CST is not a downstream component of these pathways (data not shown).

CST is Required for Heart Development

To determine the requirement for CST in development, both CSTα and CSTβ were depleted using morpholinos that block splicing of a common conserved region of the transcripts located between exon 8 (ex8D MO) and exon 9 (ex9A MO) (Fig S2.5A). These splice junction morpholinos, referred to collectively as CstMO, abrogate proper splicing of both pre-mRNAs and introduce a stop codon after the second amino acid following exon 8. CstMO, but not a five nucleotide mis-matched CstMO, properly target *Cst* until at least tadpole stage (Stage 42) as shown by RT-PCR with the CstMO giving an amplified product that is larger than control-MO injected embryos by the size of the corresponding intron (679bp) (Fig 2.1K). Cloning and sequencing of

respective PCR bands confirmed that they were the expected products derived from the *Cst* locus. Together, these data demonstrate that CstMO depletes the embryo of CSTα and CSTβ until at least Stage 42.

Examination of CST-depleted embryos indicate that they are indistinguishable from control MO-injected embryos until Stage 41 when fluid begins to accumulate over the dorsal fin (Fig 2.1J) and they have small, compact hearts (Fig 2.1G-J). Shortly thereafter (Stage 42), CST-depleted embryos develop a ventral edema (Fig S2.6) and die when sibling embryos develop to Stage 46. Despite the normal appearance of earlier CST-depleted tadpole stage embryos (Stage 37) (Fig 2.1G-H), upon closer examination, CST-depleted hearts had improperly looped giving the overall appearance of a twisted kinked tube (Fig 2.1L) when examined by MHC staining. *Cst*-specific morpholinos against the 5' regions of *Cstα* and *Cstβ* (Fig S2.5B) gave identical results confirming that the phenotype is due to depletion of CSTα and CSTβ. This strongly implies that any protein associated with the *Cst* splice junction morpholinos is non-functional rather than acting as a dominant negative protein. These data demonstrate that CST is required for early cardiac development in *Xenopus*.

CST is Required for the Onset of Cardiomyocyte Differentiation at the Ventral Midline

Since *Cst* is first expressed in heart primordium at Stage 27, the abnormal heart morphology at tadpole Stage 37 is likely a consequence of an earlier

requirement for CST in cardiac development. During the process of early cardiogenesis, specified cardiac progenitor cells migrate towards the ventral midline where they meet (Stage 26) and fuse at the ventral midline (Stage 29). Cardiomyocytes then undergo epithelialization, initiate the expression of cardiac structural genes, and begin myofibrillogenesis. To determine when CST is required in heart development, *in situ* analysis was performed on control and CST-depleted embryos with a panel of early cardiac markers that include *Nkx2.5*, *Tbx5*, *Tbx20, Gata4, Gata5, and Gata6*. No alteration in temporal or spatial expression of any of these markers was observed between control and CST-depleted embryos up to Stage 29 (Fig 2.2A-L, S2.7) suggesting that CST is not required for the determination, migration, or, most critically, fusion of cardiac precursor cells.

To determine if CST is required for cardiomyocyte differentiation, wholemount antibody staining was conducted with antibodies against MHC (Fig 2.2M-U) and tropomyosin (Tmy; Fig 2.2V-Y). Although CST-depleted embryos have a single normal sized continuous cardiac field that uniformly expresses *Nkx2.5*, *Tbx5*, *Tbx20*, *Gata4, Gata5, and Gata6* (Fig 2.2A-L, S2.7), we found that CST-depleted embryos fail to initiate cardiac differentiation at the ventral midline (Fig 2.2M-O, V-W). We confirmed that the cells at the ventral midline are Nkx2.5 positive by double wholemount *in situ* analysis with *Nkx2.5*- and *cardiac troponin I*-specific probes (Fig 2.2Z-B'). Additionally, we find CST-depleted hearts have architectural defects including distention along the left-right axis in the ventral

region of the embryo (Fig 2.2N-O, D'). These results collectively suggest that CST is required within a six hour period of heart development between Stage 27 and Stage 29 for proper differentiation of a subset of cardiomyocyte progenitors at the ventral midline.

To verify that alteration in heart morphology in CST-depleted embryos is associated with a failure of ventral cardiomyocytes to undergo differentiation, we determined the total number of differentiated cardiomyocytes in control and CST-depleted heart tissue staining with DAPI, to mark cell nuclei, and anti-MHC, to mark differentiated cardiomyocytes (Fig 2.2C'-E'). Consistent with a failure of the ventral midline cells to express MHC, there is a significant reduction in the number of terminally differentiated cardiomyocytes in CST-depleted hearts relative to control hearts, 525.90±42.16 versus 690.5±19.76 respectively (Fig 2.2E'). We further note that this decrease is not a reflection of a role for CST in cardiac cell survival since we observed no increase in the total number of cardiac cells that were positive for TUNEL or the apoptotic marker Capase-3 during these stages (data not shown). Taken together, these data demonstrate a role for CST in cardiac differentiation at the ventral midline and suggest that regulation of cardiomyocyte differentiation is regionalized along the dorsal-ventral axis.

Failure of the cardiac cells in CST-depleted embryos to uniformly differentiate across the ventral midline leads to a bifurcation of the developing linear heart tube by slightly later stages (Stage 32) (Fig 2.2Q-R, Y). Similar to

genetic mutants in zebrafish which lead to cardia bifida, e.g. *natter, miles apart, mtx, bon* (Chen et al., 1996; Sakaguchi et al., 2006; Stainier et al., 1996), severity of the bifida ranges from extreme phenotypes (30% penetrance) (Fig 2.2R,Y) in which CST-depletion results in two separate linear heart tubes, to moderate phenotypes (60% penetrance) (Fig 2.2Q) that manifest as two heart fields joined along the ventral midline either posteriorly or along the length of the heart field to form an irregular heart tube. Variation in linear heart tube formation ultimately disrupts the morphogenic movements of the heart tube, resulting in a secondary cardiac looping defect seen in the chambered heart (Stage 37) (Fig 2.2T-U). An identical cardiac phenotype is observed when a combination of morpholinos targeting the 5' UTR of *Cstα* and *Cstβ* is injected (Fig. S2.5C). Taken together, these results imply that, in contrast to other cardia bifida phenotypes, CST depletion causes a bifurcation of the heart due to lack of uniform differentiation of cardiomyocytes across the midline.

CST-Depletion Does Not Affect Endoderm Formation or Patterning, Components of the Extracellular Matrix, or Cardiac Polarity

Signals from the endoderm are required for proper cardiac midline development (Chen et al., 1996; Stainier et al., 1996). However, we are unable to detect *Cst* expression within the endoderm or endodermal derivatives over the periods in which we observe the phenotype in CST-depleted embryos (Fig 2.1B, S2.2). To further exclude the possibility that the inability of cardiomyocytes to differentiate at the ventral midline in CST-depleted embryos is a secondary

consequence of alterations in the formation, maintenance or patterning of endodermal tissue, endodermal markers *Endodermin*, *Sox2*, *Endocut* and *Vito* were assayed for spatial expression by *in situ* analysis in both wholemount and sectioned embryos, and for quantitative expression by SYBR Green quantitative PCR (Fig 2.3). No alterations in spatial or quantitative expression of any endodermal markers were observed in CST-depleted embryos, further suggesting CST is not required for the proper formation, maintenance or patterning of endodermal tissue.

To determine if CST functions in a tissue-autonomous fashion, we assayed for alteration in components of the extracellular matrix (fibronectin and fibrillin), cardiomyocyte polarity (β-catenin) and endocardium/BMP signaling (SMAD1/5/8). No alteration in the staining pattern of any of these markers was observed between control MO and CstMO derived hearts (data not shown). Collectively, these data demonstrate that the midline defect as a consequence of CST-depletion are due to a block or delay in cardiomyocyte differentiation and are not a secondary consequence of alterations in cardiac migration or polarity. Moreover, these results suggest that the phenotype of CST-depletion is not associated with inappropriate activation of the canonical Wnt pathway or inactivation of the BMP2/4/7 pathway.

Fate Mapping of Cardiac Ventral Midline Cells

Collectively, our results imply cardiomyocytes at the ventral midline have a fate different from that of neighboring cardiomyocyte progenitors. To determine the ultimate fate of these cardiomyocytes at the ventral midline, we conducted fate mapping studies at the time when we first detect a phenotype in CST-depleted embryos; i.e. when cardiac progenitors have fused at the anterior ventral midline (Stage 29). Using anatomical landmarks and a cardiac actin-GFP (CA-GFP) transgenic reporter host strain of *Xenopus* to unambiguously identify cardiac tissue, we injected MitoTracker dye into the ventral midline of control MO-injected CA-GFP positive embryos (Fig 2.4A-B), identified by GFP expression in the developing somites. We then scored embryos that incorporated the dye into the underlying mesoderm. Broadly consistent with studies in chick (Abu-Issa and Kirby, 2007; De La Cruz et al., 1989; Moreno-Rodriguez et al., 2006), we find that by the stage at which the heart initiates chamber morphogenesis, cardiomyocytes derived from the ventral midline give rise to cells that occupy positions in the medial outer curvature of the heart (Stage 35) (Fig 2.4C, E-I). At later stages, during the period after completion of chamber and valve formation (Stage 45) cells preferentially colonize the outer curvature of the mature ventricle and to a lesser extent, the atrium (Fig 2.4D, V-Z).

CST-Depleted Cardiac Ventral Midline Cells Fail to Integrate Into the Mature Heart

To further establish the role of CST in cardiac midline development, and to confirm that cells that occupy a position in cardiac ventral midline in CST-depleted embryos are cardiomyocyte progenitors, we fate mapped ventral midline cells in CA-GFP embryos in which we depleted CST. In stark contrast to results from wildtype embryos, ventral midline cells in CST-depleted embryos preferentially give rise to cells that occupy positions in the posterior midline of the developing heart (Fig 2.4J-N). Interestingly, we also found a portion of fated CST-depleted ventral midline cells located in a posterior undifferentiated ventricular cleft (Fig 2.4O-S). Although we often observe that CST-depleted ventral midline cells are delayed but not blocked in cardiomyocyte differentiation, in all case cells fail to integrate into the heart and remain as a condensed population of cells attached to the outer ventricular wall (Fig 2.4V-Z).

CST is Required for the Regulation of Cardiomyocyte Proliferation

We observe from our fate mapping studies at later stages that CST-depleted labeled ventral midline cells consistently give rise to a much larger population of cells relative to controls (Fig 2.4 compare Y with D'). Consistent with this observation, we find cardiomyocytes undergoing differentiation in the more dorsal regions of the CST-depleted hearts have a significant increased mitotic index (Fig S2.8). Collectively these data imply that CST plays a critical

role in regulating the proliferation and onset of differentiation of cardiac progenitors.

DISCUSSION

Our findings collectively imply that cardiomyocytes do not differentiate in a uniform manner and strongly suggest that cells in the ventral region of the heart field differentiate in response to localized signals. Our results further imply that cardiomyocytes differentiate along a dorsal-ventral axis before the onset of terminal cardiomyocyte differentiation, thus, cardiac progenitor fates appear to be determined prior to the formation of the linear heart tube.

We observe that the requirement for CST in cardiomyocyte differentiation is within a subset of cardiac progenitor cells in which *Cst* is expressed. What then limits CST function to the ventral midline? One possibility is that CST functions redundantly with other transcription factors in regulating cardiomyocyte differentiation in more dorsal regions of the heart; however, CST binds DNA through a unique para-zinc finger domain (Mellerick et al., 1992). Similar to studies in *Drosophila*, we are unable to identify any protein in genomes of *Xenopus*, chick or mammals which contains a similar domain suggesting CST acts on an exclusive set of transcriptional targets. Based on these observations, our phenotypic analysis of cardiac tissue depleted of CST, and by inference with *Drosophila* (Kambadur et al., 1998), we hypothesize that CST activity is regulated by as yet, unidentified factors. Consistent with this proposal, we have

shown that over-expression of CST throughout the embryo leads to cellular defects only in tissue types which normally express CST (data not shown).

We note that our fate mapping studies of early *Xenopus* hearts are consistent with those performed in chick showing that cardiac progenitors at the ventral midline preferentially give rise to terminally differentiated cardiomyocytes in the outer ventricular wall (De La Cruz et al., 1989; Moreno-Rodriguez et al., 2006). Studies in chick further demonstrated that cardiomyocyte progenitors at the ventral midline are derived from the cephalic mesoderm; i.e. the anterior heart field. Therefore, it is intriguing to speculate that the regulation of CST activity restricts its role to cardiac cell derived from the anterior heart field.

In light of the role for CST in cardiac differentiation and its high degree of sequence conservation and expression between vertebrates (Liu et al., 2006; Vacalla and Theil, 2002), it will be interesting in the future to examine the relationship between CST and congenital heart disease and cardiac hypertrophy.

AKNOWLEDGEMENTS

This work is supported by grants to FLC from the NIH/NHLBI, R01 HL075256 and R21 HL083965. KSC is a trainee in the Integrative Vascular Biology program supported by T32HL69768 from the NIH. We are extremely grateful to Suk-won Jin, Dazhi Wang, Larysa Pevny, Cam Patterson, Mark Peifer

and Mark Majesky for their helpful discussions and critical reading of the manuscript.

Figure 2.1 CST is required for vertebrate heart development.

(A) Predicted schematic representation of CSTα and CSTβ proteins; nuclear localization signal (yellow), zinc finger repeats (red), serine-rich region (red). (B-F) Wholemount *in situ* analysis of Stage 27 (early tailbud), Stage 32 (tailbud), and Stage 36 (early tadpole) embryos using a *Cst*-specific probe common to *Cstα* and *Cstβ*. (B lateral view with anterior to the left, C and D ventral and dorsal views, respectively, with anterior to the top). (D) and (F) Transverse sections of wholemount *in situ* Stage 36 embryos through (D) the heart and (F) the hindbrain: hindbrain (hb), somites (s), heart primordium (hp), heart (h), myocardium (m), endocardium (en), commissural neurons (c). (G-J) Representative (G,I) control MO and (H,J) CstMO embryos. (G) Stage 32 control MO and (H) CstMO embryos are indistinguishable. (I) Stage 41 control MO and (J) CstMO embryos. CST-depleted embryos present with dorsal fin edema and no gross ventral region abnormalities. (K) RT-PCR analysis of Stage 42 tadpole injected at the one-cell stage with the CstMO demonstrating inhibition of proper slicing of *Cst* pre-mRNA. Control MO (Con MO) and 5-mismatch MO (5-mis MO) are negative controls. (L) Wholemount MHC antibody staining of tadpole Stage 37 CST-depleted embryos (lateral views with anterior to the left); inflow tract (i), ventricle (v), outflow tract (o). Scale bars: B-C = 0.5 mm, G = 1 mm, D & L = 100 μm.

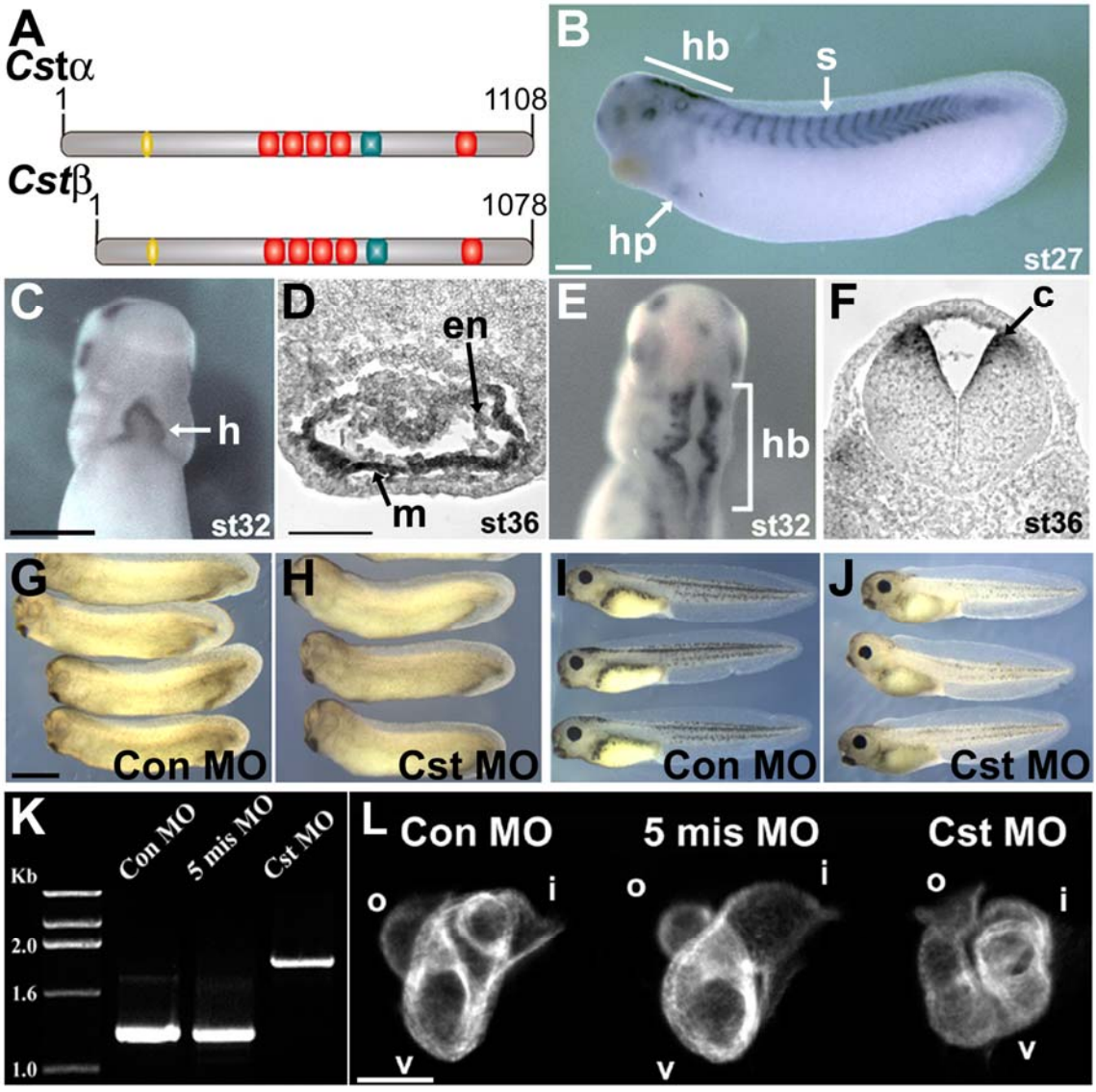
A
Cstα
1
1108
Cstβ
1
1078
B
hb
s
hp
st27
C
h
st32
D
en
m
st36
E
hb
st32
F
c
st36
G
Con MO
H
Cst MO
I
Con MO
J
Cst MO
K
Con MO
5 mis MO
Cst MO
Kb
2.0
1.6
1.0
L
Con MO
5 mis MO
Cst MO
o
i
v

Figure 2.2 CST is required for cardiomyocyte differentiation at the ventral midline.

(A-L) Wholemount *in situ* analysis with early cardiac markers *Nkx2.5* (A,B,G,H), *Tbx5* (C,D,I,J), and *Tbx20* (E,F,K,L), of tailbud Stage 26 and 29 control and CST-depleted embryos (ventral view with anterior to the top). Cardiac progenitors have properly migrated and completely fused across the ventral midline. (M-U) Wholemount MHC antibody staining at Stage 29 (onset of cardiac differentiation), Stage 32 (completion of linear heart tube formation), and Stage 37 (chamber formation) (ventral view with anterior to the top). (M) Stage 29 control MO embryos and (N-O) CST-depleted embryos. (P) Stage 32 control MO embryos and (Q-R) CST-depleted embryos display varying degrees of cardia bifida of the linear heart tube upon CST depletion. (S) Stage 37 control MO embryos and (T-U) CST-depleted embryos display morphological consequence of CST depletion on chamber formation. (V-Y) Wholemount Tmy antibody staining of Stage 29 and 32 (V,X) control MO and (W,Y) CST-depleted embryos demonstrate lack of differentiation is not specific to MHC. (Z-B') Simultaneous detection of cardiac progenitor cells and differentiated cardiac cells in a Stage 29 CST-depleted embryo. (Z-A') Wholemount double *in situ* analysis using a *Nkx2.5*-specific probe (pink) to mark cardiac progenitor cells and *Cardiac troponin I*-specific probe (blue) to mark differentiated cardiac cells in (Z) control MO and (A') CST-depleted embryos. (B') Magnified image of the cardiac region in the CST-depleted embryo in panel A'. (C'-D') Transverse sections of Stage 29 (C') control MO and (D') CST-depleted embryos stained with MHC antibody and DAPI.

Brackets highlight the lack of differentiation at the ventral midline. (E') Quantification of differentiated cardiomyocytes determined by counting the total MHC-positive cells derived from serial sectioned embryos. Bars represent the average of at least six embryos per condition +/- SEM. *, $p<0.01$. Representative images are derived from a single experiment, all experiments were repeated at least twice with independent batches of embryos. Scale bars: C = 0.5 mm, S & X = 100 μm, C' = 200 μm.

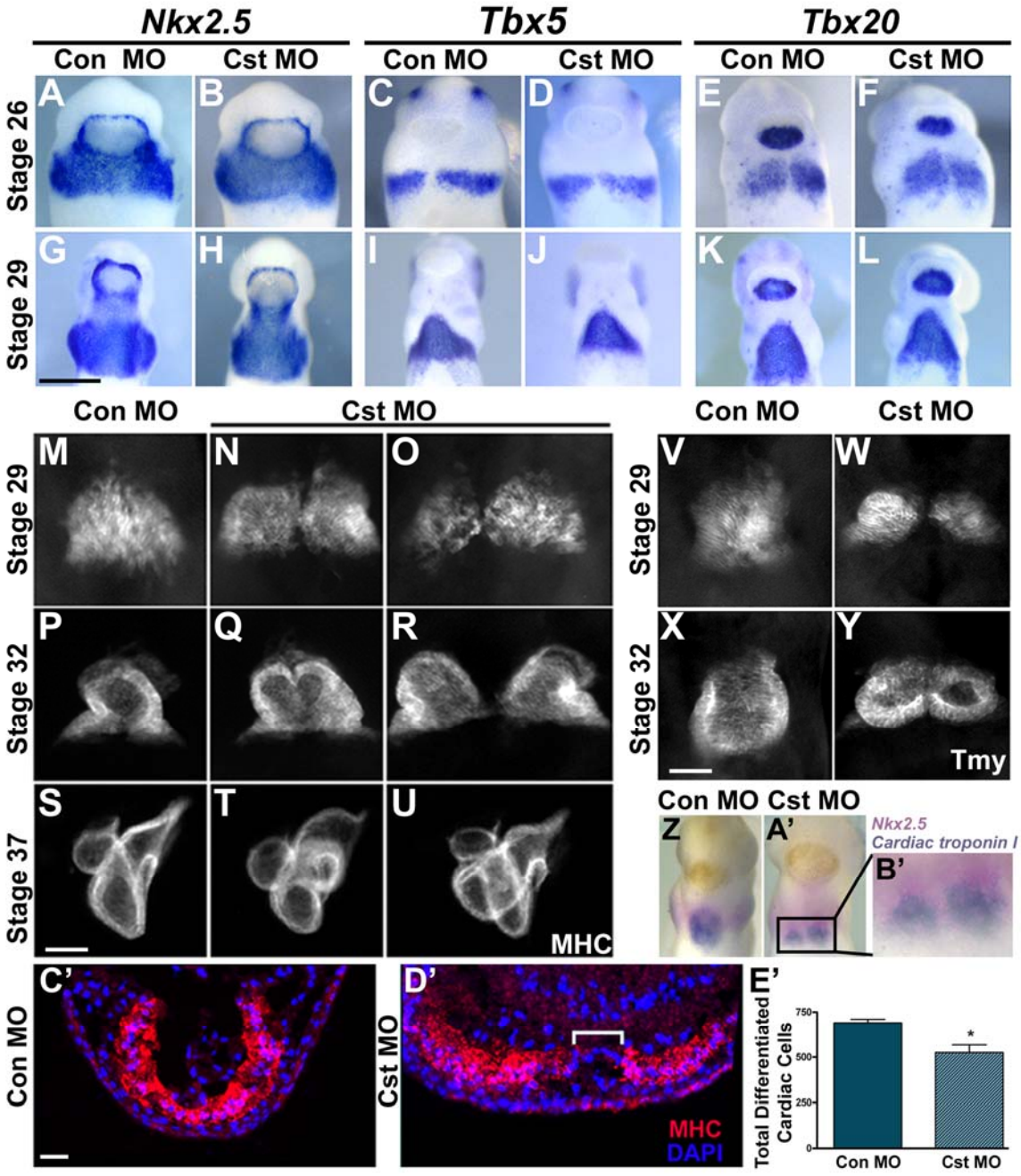
Nkx2.5
Tbx5
Tbx20
Con MO
Cst MO
Stage 26
Stage 29
Stage 32
Stage 37
A
B
C
D
E
F
G
H
I
J
K
L
M
N
O
P
Q
R
S
T
U
MHC
V
W
X
Y
Tmy
Z
A'
B'
Nkx2.5
Cardiac troponin I
C'
D'
MHC
DAPI
E'
Total Differentiated Cardiac Cells
750
500
250
0
*

Figure 2.3 CST is not required for formation or patterning of endodermal tissue.

(A) Schematic representation of endodermal tissue markers that demarcate pharyngeal endoderm (*Sox2* and *Endodermin*), ventral midgut (*Vito* and *Endodermin*) and posterior endoderm (*Endocut*). (B) Relative expression levels of endodermal markers *Sox2, Vito, Endodermin,* and *Endocut* in Stage 29 CST-depleted embryos (N=5) relative to control MO embryos (N=5) using *GAPDH* as the housekeeping gene. Bars represent the relative expression levels ± SEM. (C-F) Wholemount *in situ* analysis of endodermal markers (C) *Sox2,* (D) *Vito,* (E) *Endodermin,* and (F) *Endocut* in Stage 29 (top) control MO and (bottom) CST-depleted embryos (lateral views with anterior to the left). (G-I) *in situ* analysis of endodermal and cardiac markers on adjacent transverse sections through the cardiac region of (top) control MO and (bottom) CST-depleted Stage 29 embryos. (G) *Sox2* and *Nkx2.5* expression on adjacent sections demonstrating proper expression within pharyngeal tissue of CST-depleted embryos. (H) *Endodermin* and *Tbx20* expression on adjacent sections demonstrating proper relative spatial expression within the cardiac tissue and endoderm of the embryo.

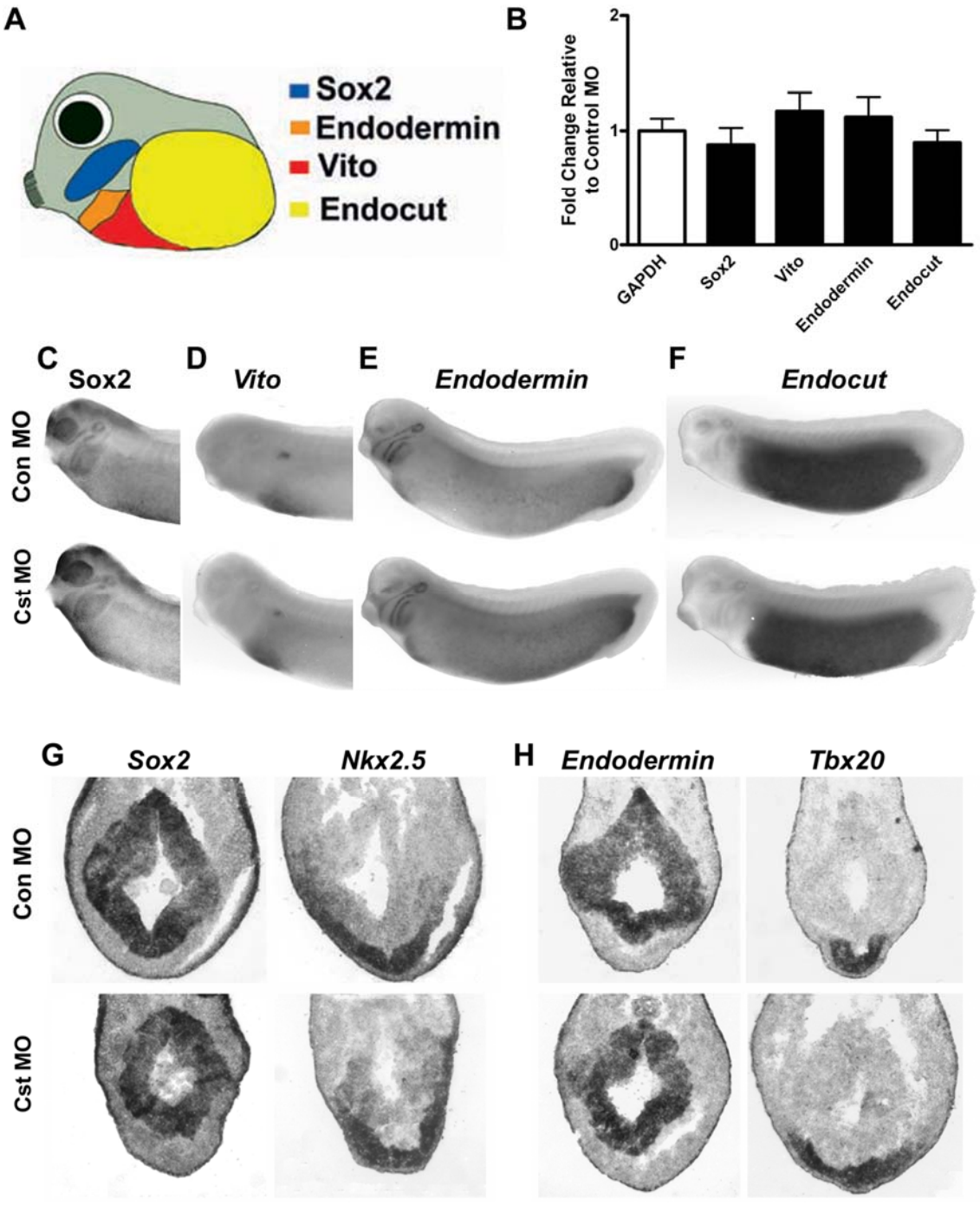
A
Sox2
Endodermin
Vito
Endocut
B
Fold Change Relative to Control MO
2
1
0
GAPDH
Sox2
Vito
Endodermin
Endocut
C
Sox2
D
Vito
E
Endodermin
F
Endocut
Con MO
Cst MO
G
Sox2
Nkx2.5
H
Endodermin
Tbx20
Con MO
Cst MO

Figure 2.4 Fate mapping cardiac ventral midline cells.

(A) Brightfield image of a living cardiac actin-GFP transgenic embryo injected with MitoTracker at Stage 29 along the ventral midline 5.5mm posterior to the cement gland (CG). (B) Fluorescent image of the same embryo demonstrating the location of incorporated MitoTracker into cells at the ventral midline (ventral views with anterior to the top). Fluorescence anterior to site of injection is reflection off the surface of the live embryo. (C,D) Tabulation of the location of MitoTracker-labeled cardiac cells of control MO and CST-depleted embryo at (C) midtailbud Stage 35 and (D) tadpole Stage 45. Images of CA-GFP transgenic control MO-injected and CST-depleted (E-H, J-M, O-U) Stage 35 and (V-Y, A'-D') Stage 45 dissected hearts. (F,K,P,T,U,Z) Corresponding images of GFP expression. (G,L,Q,X,C') Corresponding images of fated MitoTracker-labeled cardiac ventral midline cells. (H,M,R,U,Y,D') Merged images of GFP and fated MitoTracker-labeled ventral midline cells. (T,U) Note the fated ventral midline cells in a pocket of undifferentiated (GFP-negative) cardiomyocytes. (I,N,S,Z,E') Schematics representing fate of the cardiac ventral midline cells to the outer curvature of the ventricle in (I) Stage 35 and (Z) Stage 45 control MO-injected hearts. CST-depleted fated ventral midline cells located in the (N) posterior midline or (S) in an undifferentiated cleft in the outer ventricular myocardium in Stage 35 CST-depleted hearts and (E') in a condensed mass of cells on the outer ventricle in Stage 45 CST-depleted hearts.

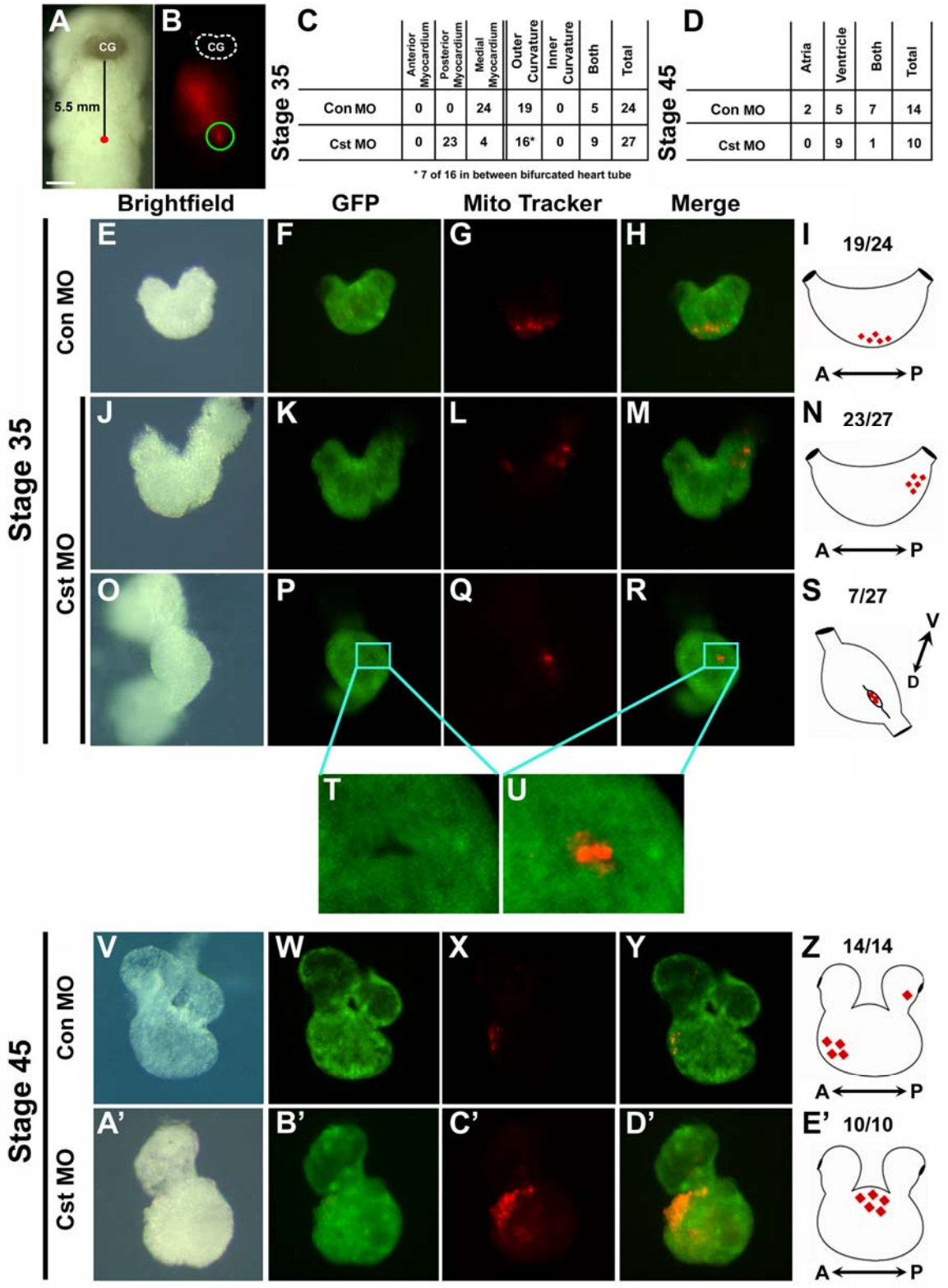
A
CG
5.5 mm
B
CG
C
Stage 35
Anterior Myocardium
Posterior Myocardium
Medial Myocardium
Outer Curvature
Inner Curvature
Both
Total
Con MO 0 0 24 19 0 5 24
Cst MO 0 23 4 16* 0 9 27
* 7 of 16 in between bifurcated heart tube
D
Stage 45
Atria
Ventricle
Both
Total
Con MO 2 5 7 14
Cst MO 0 9 1 10
Brightfield
GFP
Mito Tracker
Merge
Stage 35
Con MO
Cst MO
E
F
G
H
I
19/24
A
P
J
K
L
M
N
23/27
A
P
O
P
Q
R
S
7/27
V
D
T
U
Stage 45
Con MO
Cst MO
V
W
X
Y
Z
14/14
A
P
A'
B'
C'
D'
E'
10/10
A
P

Figure S2.1 Identification and characterization of Xenopus CST.

(A) Predicted genomic locus structure of *Xenopus Cstα* and *Cstβ* (5' to 3', not to scale). Exons are shown in boxes with the corresponding size given in basepairs. Exons in gray depict those containing the zinc finger repeats, and the sizes of intervening introns are indicated beneath each intron. Alternative splicing of the 5' regions is also indicated. (B,C) Table showing the evolutionary conservation of the full length CST amino acid sequence (B) and the zinc finger repeats (repeats 1-4) (C). The percentage of identical amino acids (identity) and the percentage of conservative substitutions (similarity) are given for comparison between CST proteins of *X. tropicalis*, hCST (human), mCST (mouse), predicted gCST (chicken), and dCAS (*Drosophila*). (D) Syntenic relationship between vertebrate *Cst* genomic loci using Metazome blast analysis. (E) Western blot analysis of CSTα-V5 and CSTβ-V5 *in vitro* translation. Both CST proteins run at the predicted size of 148 kDa. (F,G) CSTα and CSTβ cellular localization. Transverse confocal images of CSTα-V5 and CSTβ-V5 injected Xenopus embryos at Stage 32. Histological sections were stained with a V5 antibody (Red) to visualize the CST proteins and with DAPI (Blue) to identify the nucleus. Scale bar indicates 10μm.

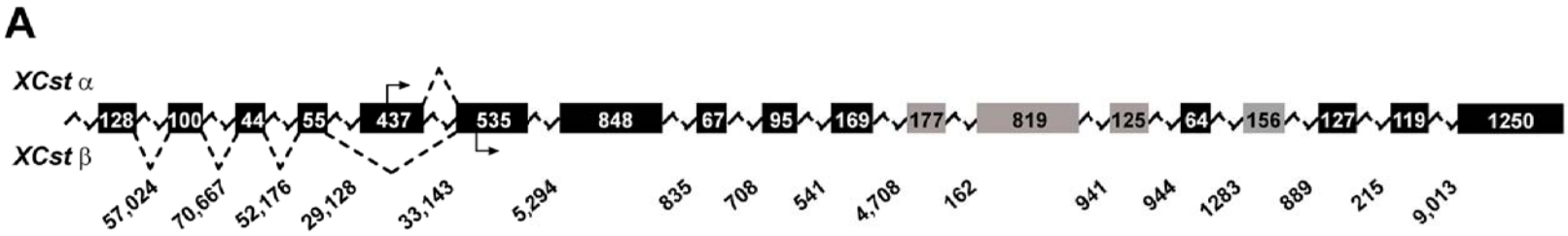

B

		X. trop CST	hCST	mCST	gCST	dCAS
X. laevis CST	% Identity	93	61	60	67	11
	% Similarity	96	69	70	77	17

C

		X. trop CST	hCST	mCST	gCST	dCAS
X. laevis CST	% Identity	100	99	98	99	49
	% Similarity	100	99	99	100	65

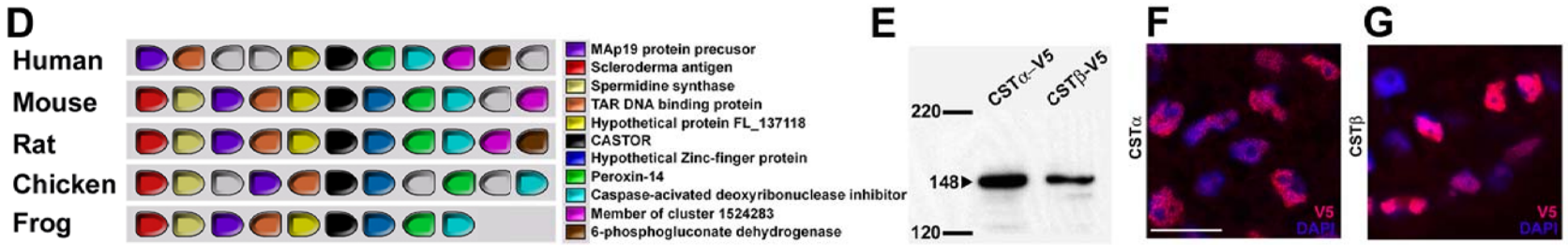

Figure S2.2 *Xenopus laevis Cst* developmental and spatial expression.

(A) Developmental time course of *X. laevis Cstα* and *Cstβ* expression by RT-PCR of egg lysate (maternal transcripts), whole embryo ranging from Stage 10 (gastrulation) to Stage 42 (late tadpole), and adult heart. *Ef1α* is used as a positive control. (B-K) Whole mount *in situ* hybridization of Stage 14 (neurula) to Stage 40 (tadpole) embryos using a *Cst*-specific probe common to both *Cstα* and *Cstβ*. B,C are dorsal views with anterior to the left. D-H, and J are lateral views with anterior to the left: hindbrain (hb), presomitic mesoderm (psm), somites (s), heart primordium (hp), eye (e), otic vesicle (ot), nasal placode (np), trigeminal ganglion (tg), facial placodes (p), heart (h), kidney (k), vascular vitelline network (vvn).

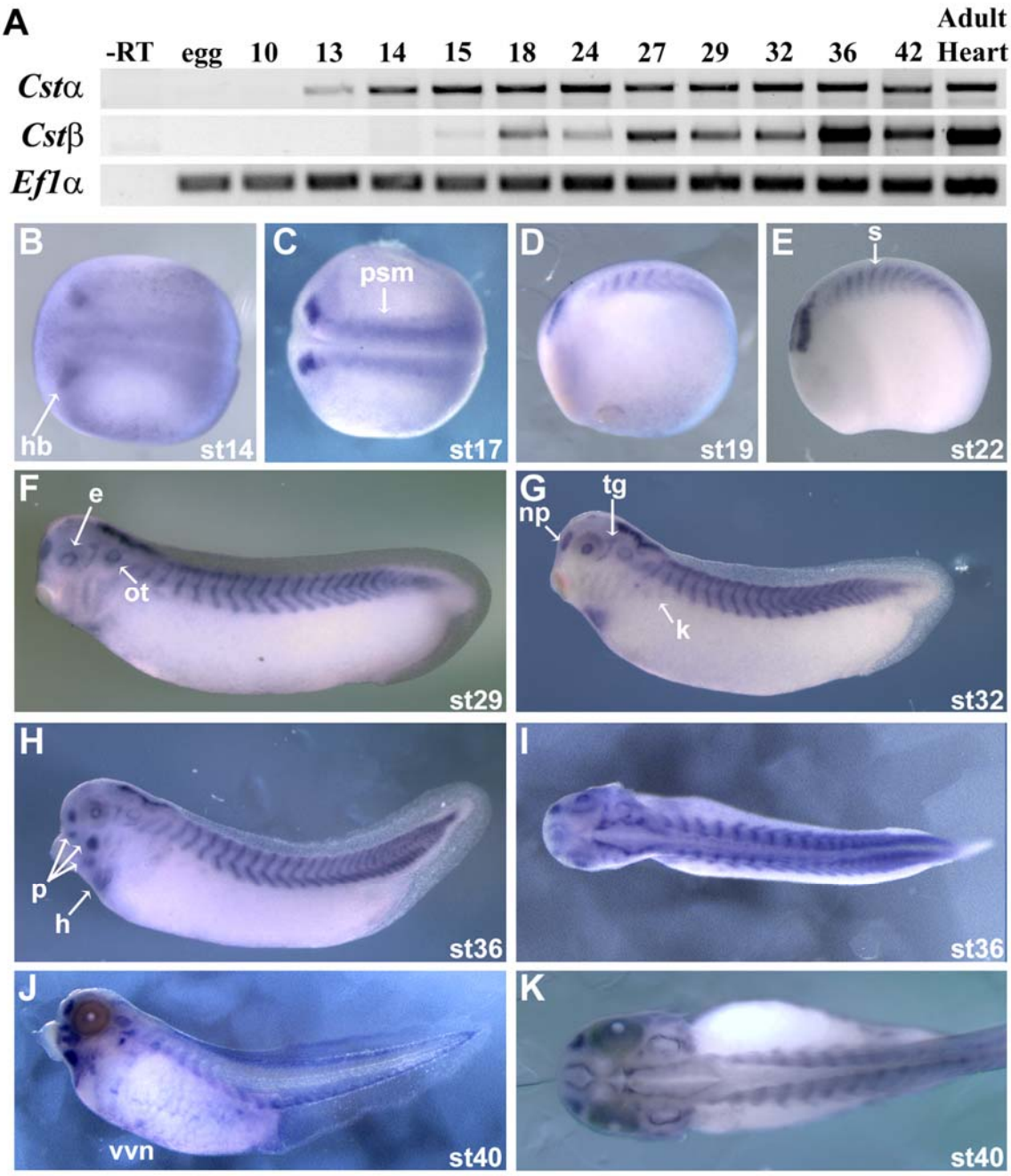
A
-RT
egg
10
13
14
15
18
24
27
29
32
36
42
Adult Heart
Cstα
Cstβ
Ef1α
B
hb
st14
C
psm
st17
D
st19
E
s
st22
F
e
ot
st29
G
tg
np
k
st32
H
p
h
st36
I
st36
J
vvn
st40
K
st40

Figure S2.3 *Xenopus tropicalis Cst* spatial expression.

Whole mount *in situ* hybridization of *Cst* in *X. tropicalis* of Stage 14 (neurula) to Stage 40 (tadpole) embryos using a Cst-specific probe common to both *Cstα* and *Cstβ*. A is an anterior view. B-F, I-J are lateral views with anterior to the left. G is a ventral view with anterior to the top. H is a dorsal view with anterior to the left. hindbrain (hb), presomitic mesoderm (psm), somites (s), heart primordium (hp), otic vesicle (ot), nasal placode (np), facial placodes (p), heart (h), kidney (k), vascular vitelline network (vvn).

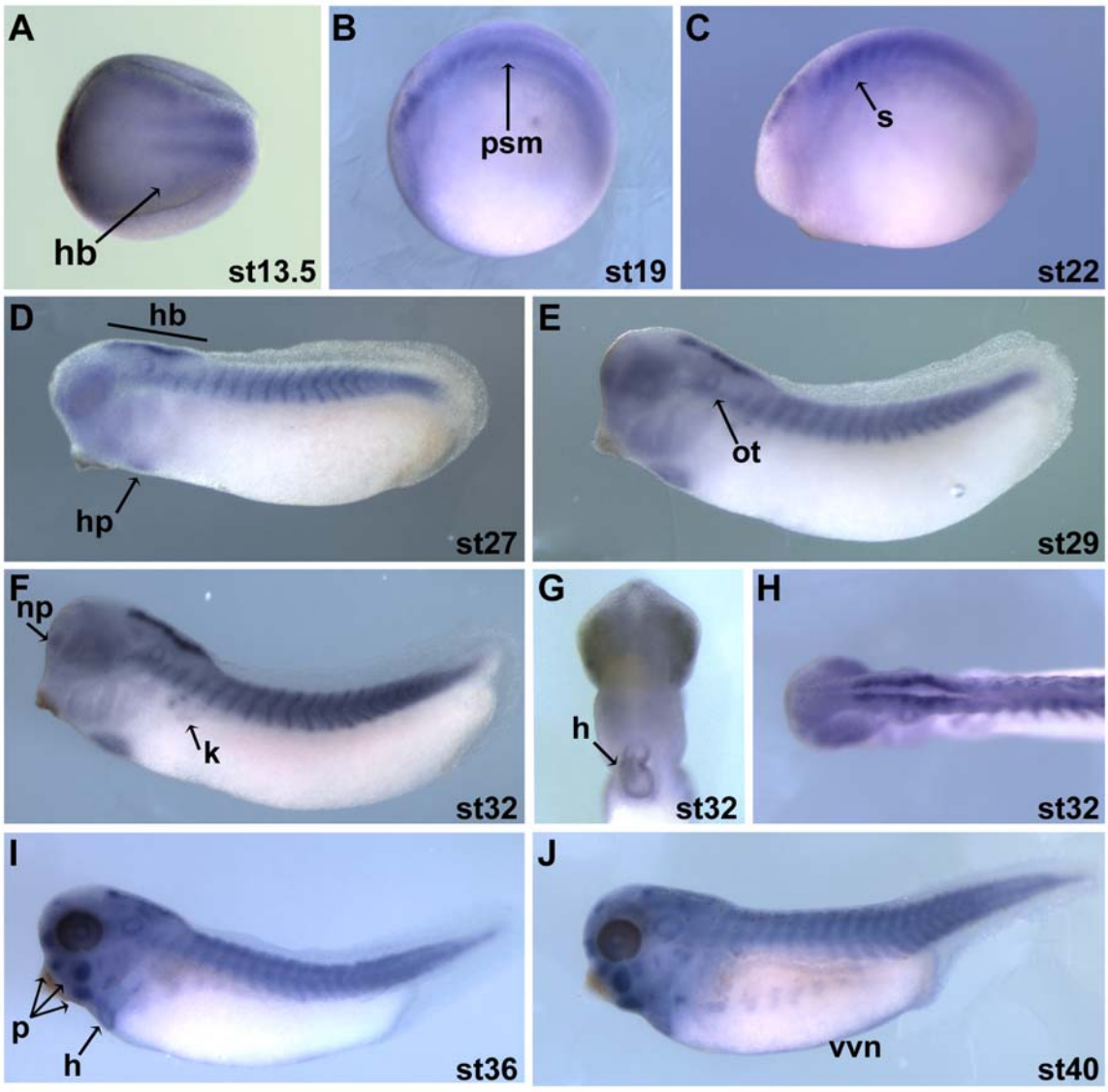
A
hb
st13.5
B
psm
st19
C
s
st22
D
hb
hp
st27
E
ot
st29
F
np
k
st32
G
h
st32
H
st32
I
p
h
st36
J
vvn
st40

Figure S2.4 *Xenopus Cst* is expressed throughout the linear heart tube.

Whole mount double *in situ* hybridization of Stage 29 embryos using a *Nkx2.5*-specific probe (pink) to mark the cardiac field and a *Cst*-specific probe (blue). Left panel is a lateral view with anterior to the left. Right panel is a ventral view with anterior to the top.

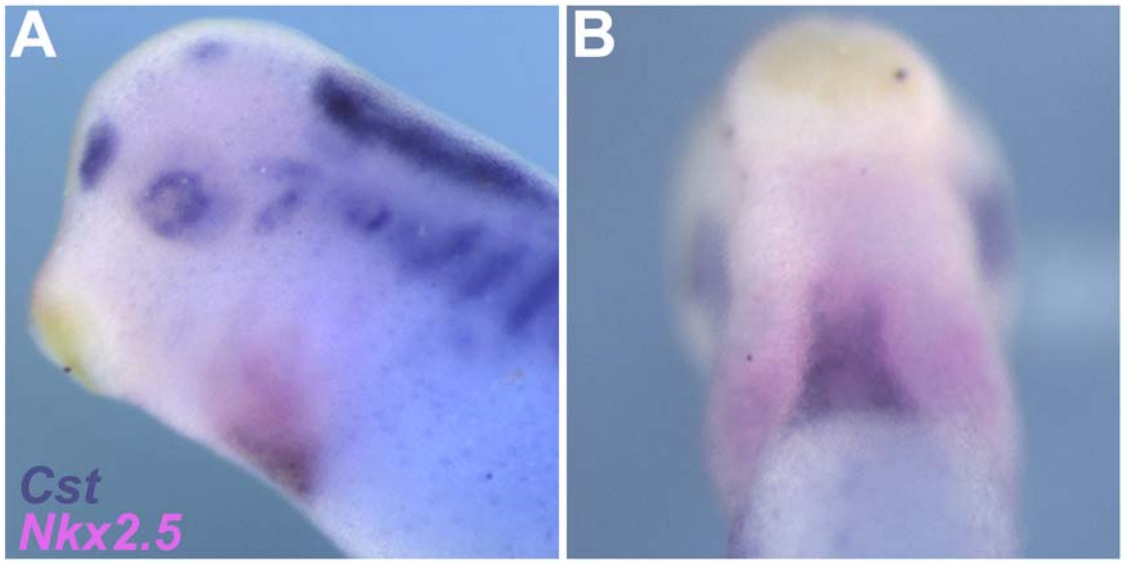

Figure S2.5 Morpholino design and phenotype.

(A) Position of the *Cst* splice junction morpholinos relative to the pre-mRNA transcripts targeting the donor the exon 8 (ex8D MO) and the acceptor of exon 9 (ex9A MO), referred collectively as CstMO. (B) Position of the *Cst*-5′ UTR morpholinos (red) relative to the *Cstα* and *Cstβ* cDNA transcripts. (C-D) Whole mount antibody staining with anti-MHC of Stage 32 control MO (C) and Cstα/β MO (D) embryos (ventral view) indicating an identical cardia bifida phenotype is obtained with both the CstMO (splice MO) as the Cstα/β MO (5′ UTR MO). Scale bar: C = 100 μm.

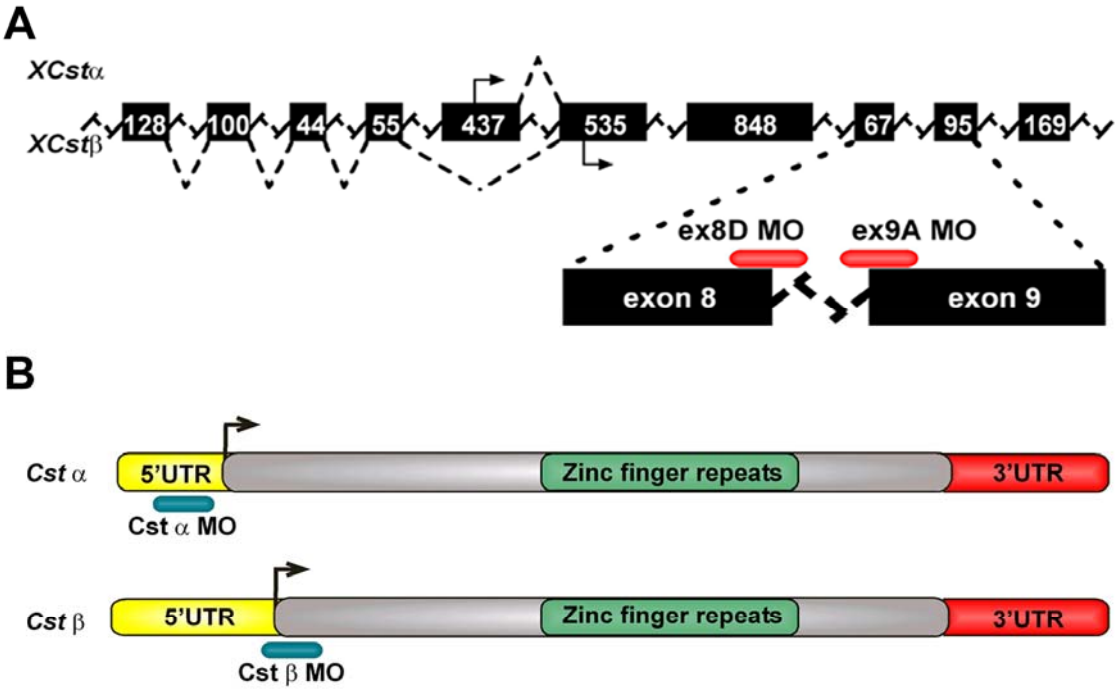
A
XCstα
XCstβ
128
100
44
55
437
535
848
67
95
169
ex8D MO
ex9A MO
exon 8
exon 9
B
Cst α
5'UTR
Zinc finger repeats
3'UTR
Cst α MO
Cst β
5'UTR
Zinc finger repeats
3'UTR
Cst β MO

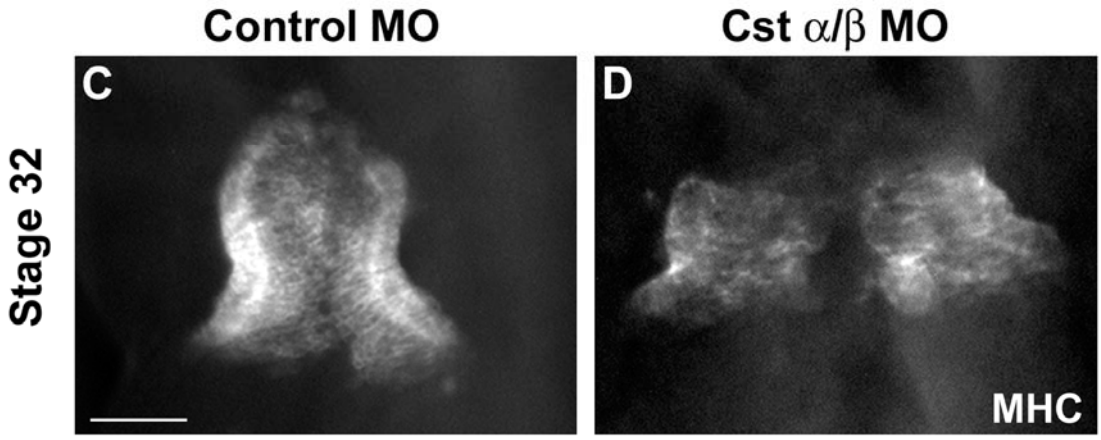
Control MO
Cst α/β MO
Stage 32
C
D
MHC

Figure S2.6 Statistics of Ventral Edema in CST-depleted embryos.

Distribution of incidences of ventral edema in control and CST-depleted embryos from Stage 37 to Stage 42. Graph represents one batch of 56 embryos. Analysis was performed with two independent experiments.

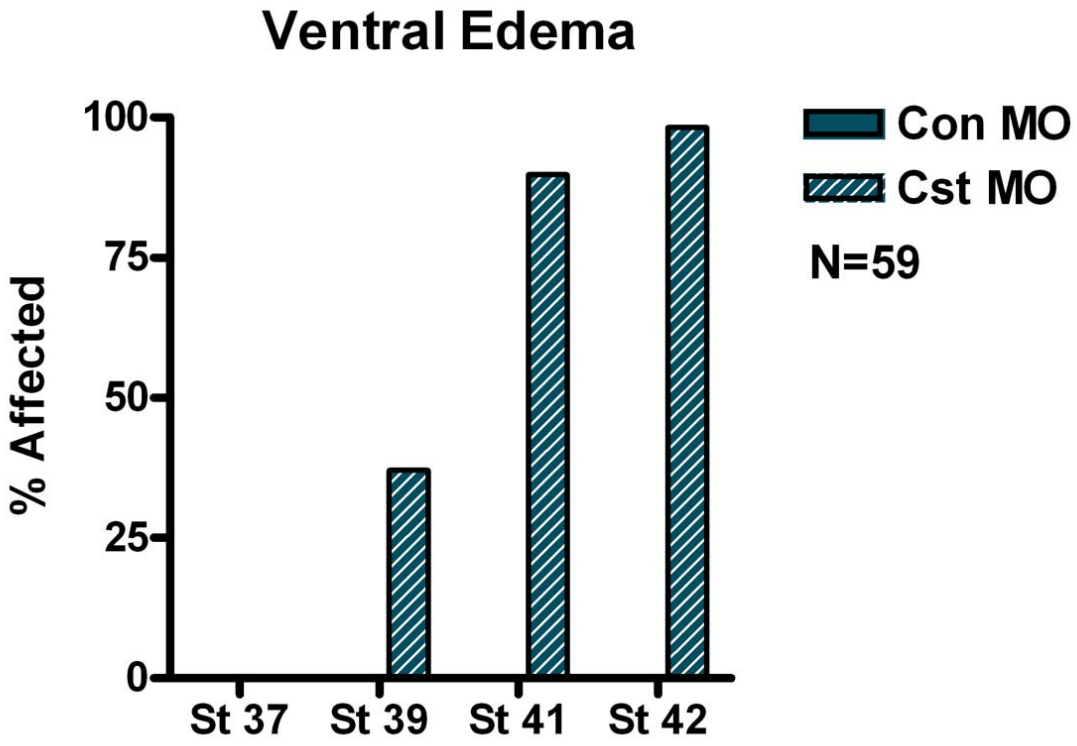

Figure S2.7 CST is not required for expression of *Gata4*, *Gata5*, or *Gata6*. Whole mount *in situ* hybridization of Stage 29 control MO and CST-depleted embryos demonstrating proper expression of (A,B) *Gata4*, (C,D) *Gata5*, and (E,F) *Gata6*. Ventral views with anterior to the top.

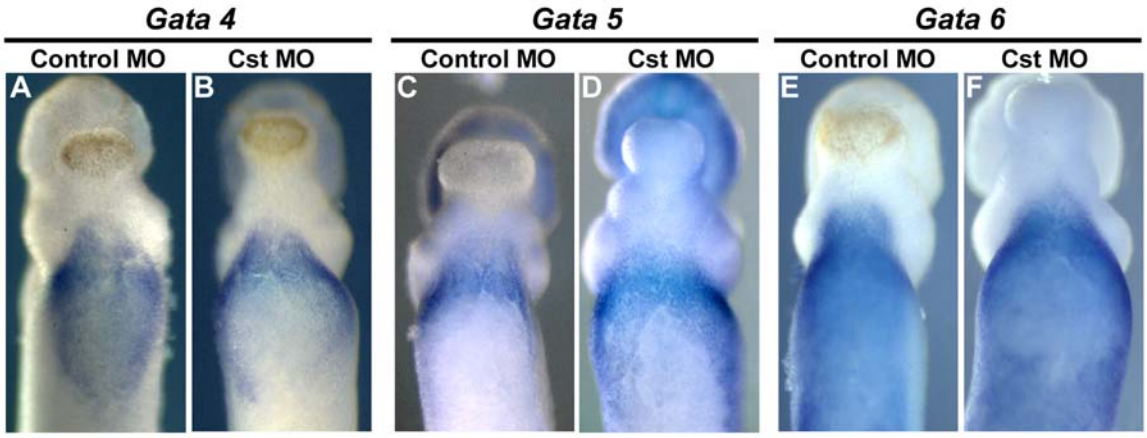

Figure S2.8 CST is required for proper cell growth of cardiomyocytes dorsal to the cardiac ventral midline.

(A) Representative transverse sections of Stage 29 control MO (top) and CstMO (bottom) injected embryos stained with MHC antibody to mark differentiated cardiomyocytes, phospho-histone H3 (pH3) antibody to mark cardiac cells in the M-phase of the cell cycle, and DAPI. Bracket highlights undifferentiated cardiac ventral midline cells. (B) CST-depleted differentiated cardiomyocytes have an increased mitotic index at Stage 29. Quantification of the mitotic index was determined by calculating the percentage of pH3-positive differentiated cardiomyocytes. Bars represent the average of at least three embryos per condition +/- SEM. *, p<0.01; Scale bars: 200 μm.

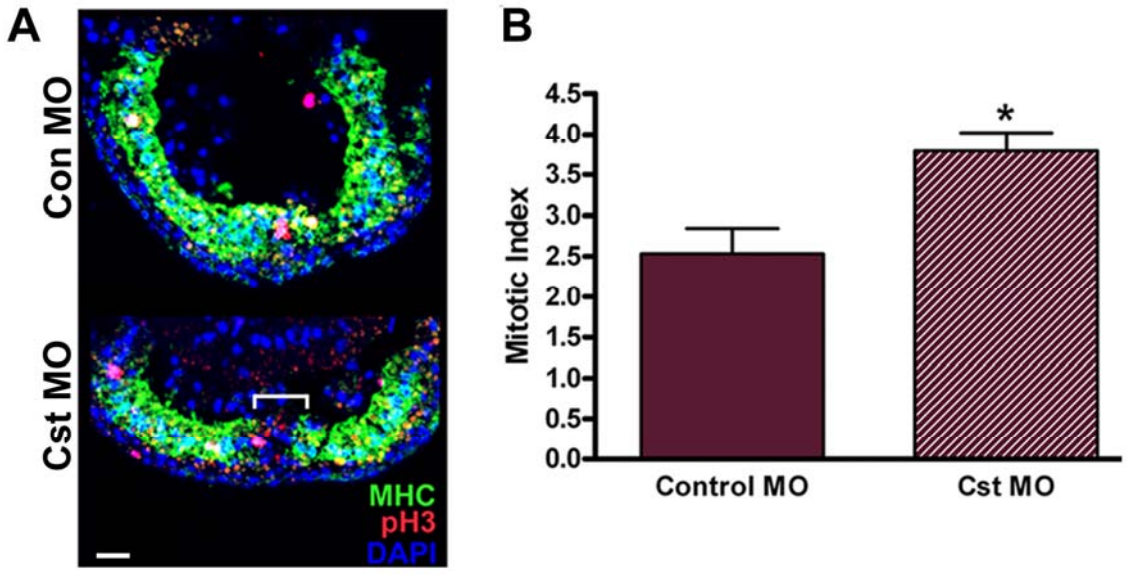

REFERNCES

Abu-Issa, R., and Kirby, M. L. (2007). Heart field: from mesoderm to heart tube. Annu Rev Cell Dev Biol *23*, 45-68.

Brown, D. D., Binder, O., Pagratis, M., Parr, B. A., and Conlon, F. L. (2003). Developmental expression of the Xenopus laevis Tbx20 orthologue. Dev Genes Evol *212*, 604-607.

Brown, D. D., Christine, K. S., Showell, C., and Conlon, F. L. (2007). Small heat shock protein Hsp27 is required for proper heart tube formation. Genesis *45*, 667-678.

Brown, D. D., Martz, S. N., Binder, O., Goetz, S. C., Price, B. M. J., Smith, J. C., and Conlon, F. L. (2005). Tbx5 and Tbx20 act synergistically to control vertebrate heart morphogenesis. Development *132*, 553-563.

Chen, J. N., Haffter, P., Odenthal, J., Vogelsang, E., Brand, M., van Eeden, F. J., Furutani-Seiki, M., Granato, M., Hammerschmidt, M., Heisenberg, C. P.*, et al.* (1996). Mutations affecting the cardiovascular system and other internal organs in zebrafish. Development *123*, 293-302.

Costa, R. M., Mason, J., Lee, M., Amaya, E., and Zorn, A. M. (2003). Novel gene expression domains reveal early patterning of the Xenopus endoderm. Gene Expr Patterns *3*, 509-519.

Cui, X., and Doe, C. Q. (1992). ming is expressed in neuroblast sublineages and regulates gene expression in the Drosophila central nervous system. Development *116*, 943-952.

De La Cruz, M. V., Sanchez-Gomez, C., and Palomino, M. A. (1989). The primitive cardiac regions in the straight tube heart (Stage 9) and their anatomical expression in the mature heart: An experimental study in the chick embryo. J Anat *165*, 121-131.

Goetz, S. C., Brown, D. D., and Conlon, F. L. (2006). TBX5 is required for embryonic cardiac cell cycle progression. Development *133*, 2575-2584.

Guan, K., and Hasenfuss, G. (2007). Do stem cells in the heart truly differentiate into cardiomyocytes? J Mol Cell Cardiol *43*, 377-387.

Harland, R. M. (1991). In situ hybridization: an improved whole mount method for Xenopus embryos. Meth Cell Biol *36*, 675-685.

Horb, M. E., and Thomsen, G. H. (1999). Tbx5 is essential for heart development. Development *126*, 1739-1751.

Kambadur, R., Koizumi, K., Stivers, C., Nagle, J., Poole, S. J., and Odenwald, W. F. (1998). Regulation of POU genes by castor and hunchback establishes layered compartments in the Drosophila CNS. Genes Dev *12*, 246-260.

Kishi, M., Mizuseki, K., Sasai, N., Yamazaki, H., Shiota, K., Nakanishi, S., and Sasai, Y. (2000). Requirement of Sox2-mediated signaling for differentiation of early Xenopus neuroectoderm. Development *127*, 791-800.

Langdon, Y. G., Goetz, S. C., Berg, A. E., Swanik, J. T., and Conlon, F. L. (2007). SHP-2 is required for the maintenance of cardiac progenitors. Development.

Latinkic, B. V., Cooper, B., Towers, N., Sparrow, D., Kotecha, S., and Mohun, T. J. (2002). Distinct enhancers regulate skeletal and cardiac muscle-specific expression programs of the cardiac alpha-actin gene in Xenopus embryos. Dev Biol *245*, 57-70.

Liu, L., Zhang, X., Qian, B., Min, X., Gao, X., Li, C., Cheng, Y., and Huang, J. (2007). Over-expression of heat shock protein 27 attenuates doxorubicin-induced cardiac dysfunction in mice. Eur J Heart Fail.

Liu, Z., Yang, X., Tan, F., Cullion, K., and Thiele, C. J. (2006). Molecular cloning and characterization of human Castor, a novel human gene upregulated during cell differentiation. Biochem Biophys Res Commun *344*, 834-844.

Logan, M., and Mohun, T. (1993). Induction of cardiac muscle differentiation in isolated animal pole explants of Xenopus laevis embryos. Development *118*, 865-875.

Mellerick, D. M., Kassis, J. A., Zhang, S. D., and Odenwald, W. F. (1992). castor encodes a novel zinc finger protein required for the development of a subset of CNS neurons in Drosophila. Neuron *9*, 789-803.

Moreno-Rodriguez, R. A., Krug, E. L., Reyes, L., Villavicencio, L., Mjaatvedt, C. H., and Markwald, R. R. (2006). Bidirectional fusion of the heart-forming fields in the developing chick embryo. Dev Dyn *235*, 191-202.

Nieuwkoop, P. D., and Faber, J. (1967). Normal Table of *Xenopus laevis* (Daudin) (Amsterdam: North Holland).

Pfaffl, M. W., Horgan, G. W., and Dempfle, L. (2002). Relative expression software tool (REST) for group-wise comparison and statistical analysis of relative expression results in real-time PCR. Nucleic Acids Res *30*, e36.

Sakaguchi, T., Kikuchi, Y., Kuroiwa, A., Takeda, H., and Stainier, D. Y. (2006). The yolk syncytial layer regulates myocardial migration by influencing extracellular matrix assembly in zebrafish. Development *133*, 4063-4072.

Showell, C., Christine, K. S., Mandel, E. M., and Conlon, F. L. (2006). Developmental expression patterns of Tb x 1, Tb x 2, Tb x 5, and Tb x 20 in Xenopus tropicalis. Dev Dyn *235*, 1623-1630.

Stainier, D. Y., Fouquet, B., Chen, J. N., Warren, K. S., Weinstein, B. M., Meiler, S. E., Mohideen, M. A., Neuhauss, S. C., Solnica-Krezel, L., Schier, A. F.*, et al.* (1996). Mutations affecting the formation and function of the cardiovascular system in the zebrafish embryo. Development *123*, 285-292.

Tonissen, K. F., Drysdale, T. A., Lints, T. J., Harvey, R. P., and Krieg, P. A. (1994). XNkx-2.5, a Xenopus gene related to Nkx-2.5 and tinman: evidence for a conserved role in cardiac development. Dev Biol *162*, 325-328.

Vacalla, C. M., and Theil, T. (2002). Cst, a novel mouse gene related to Drosophila Castor, exhibits dynamic expression patterns during neurogenesis and heart development. Mech Dev *118*, 265-268.

Chapter 3

Identification of the *Xenopus* CASTOR DNA binding sequence

ABSTRACT

Previous work revealed an integral role for CASTOR (CST) in the differentiation of cardiomyocyte progenitors specifically located at the ventral midline of the linear heart tube (Christine and Conlon, 2008). Yet no information exist as to how vertebrate CST functions during development. We have utilized a bacterial one-hybrid assay to determine the DNA binding sequence recognized by vertebrate CST. While vertebrate CST did not bind the previously identified DNA binding sequence of the *Drosophila* orthologue, it did recognize a novel 10 basepair DNA binding sequence (C/A)(T/A)A(G/C)TGGT(G/C)G. These studies present the first investigations into the molecular function of vertebrate CST. Together with further proposed analysis, this information will begin to decipher the role of vertebrate CST in development.

INTRODUCTION

Inherent characteristics of a DNA-binding transcription factor include the affinity and specificity to the DNA sequence that it recognizes to activate and/or repress transcription. Therefore, identifying the DNA binding sequence (DBS) associated with a transcription factor potentially allows for analysis of regulatory regions of tissue-specific genes to build a more comprehensive understanding of gene regulatory networks driving development. We previously identified vertebrate CASTOR (CST) and characterized its role in regulating differentiation of a subset of cardiomyocyte progenitors in the developing heart (Christine and Conlon, 2008). However, the mechanism by which CST regulates differentiation has yet to be determined.

Vertebrate CST encodes a novel zinc finger transcription factor, consisting of four tandem para-zinc fingers followed by a fifth additional C-terminal para-zinc finger. Each para-zinc finger consists of a classical Cys_2-His_2 motif originally characterized in the *Xenopus* TFIIIA transcription factor immediately preceded by an additional Cys_2-His_2 motif (Christine and Conlon, 2008; Miller et al., 1985). Analysis of the CST para-zinc fingers yields a highly conserved motif – **Cys**-X_4-**Cys**-X_6-**His**-(F/Y)-**His**-**Cys**-X_4-**Cys**-X_4-(F/Y)-X_5-ψ-X_2-**His**-X_3-**His**, where X can be any amino acid and ψ is a hydrophobic residue. Additionally, the entire amino acid sequence of the zinc finger repeats is 100-98% identical in the vertebrate CST orthologues (Christine and Conlon, 2008).

The DBS of the *Drosophila* orthologue of CST, known as dCas, has been previously identified by cyclic amplification of selected targets (Kambadur et al., 1998). This technique yielded a 10 basepair consensus DBS [(G/C)C(C/T)(C/T)AAAAA(A/T)] of which mutational analysis demonstrated that the A-T rich core is essential for dCas DNA binding. Moreover, the dCas DBS is present within the proximal promoter of Pdm-1, a POU homeobox transcription factor (Kambadur et al., 1998). dCas and Pdm-1 are essential components of developmental pathways in the *Drosophila* central nervous system. Together dCas and Pdm specify the temporal identity of the neuroblast 7-1 lineage U5-type motorneurons (Grosskortenhaus et al., 2006). However, in a subsequent neuroblast, the expression of Pdm-1 is repressed to regulate the specification of the interneuron identity. Both *in vivo* and *in vitro* studies reveal dCas directly binds the consensus DBS within the Pdm-1 promoter resulting in its extinguished expression in the late born interneuron-generating neuroblast (Kambadur et al., 1998). To date, Pdm-1 is the sole direct transcriptional target of dCas.

In contrast, not a single direct transcriptional target of vertebrate CST has been identified. However, based on the differences between dCas and the vertebrate CST orthologues, it is feasible that vertebrate CST may recognize a different DBS. For example, the amino acid sequence of the vertebrate CST zinc finger domains is only 49% identical to that of dCas (Christine and Conlon, 2008). Additionally, vertebrate CST orthologues contain a single fifth zinc finger domain C-terminal to the four tandem zinc finger domains that is not present in

dCas. It is conceivable that the fifth zinc finger domain is required for homodimerization and/or recruitment of cofactors which could in turn alter DNA binding specificity. How the variance of the amino acid sequence and the fifth zinc finger domain affect DNA binding specificity and/or affinity of vertebrate CST remains unknown.

To begin to dissect the molecular pathway by which CST functions, we have used a bacterial one-hybrid (B1H) screen to determine the vertebrate CST DBS (Meng et al., 2005). The B1H system consists of three components: 1) a bait vector containing the DNA binding domain (DBD) of a transcription factor of interest cloned in-frame to the alpha subunit of RNA polymerase; 2) a purified prey library containing randomized 18-mers that mimic DNA binding sequences upstream of two selection reporters, the HIS3 and URA3 yeast genes; and finally, 3) a bacterial selection strain depleted of the *E. coli* homologues of the yeast HIS3 and URA3 genes (Fig 3.1). If the DBD of the transcription factor recognizes and binds to a target DNA sequence in the prey library reporter vector, the alpha subunit of the DBD fusion protein recruits RNA polymerase to the *lac* promoter of the prey library reporter vector to activate the expression of the HIS3 reporter gene. Cells grown on plates containing 3-aminotriazole (3-AT), a competitive inhibitor of histidine, allows only clones with a positive interaction to survive. Following the isolation of the prey library plasmid from surviving clones, the DBS is sequenced and identified.

Utilizing the B1H approach affords advantages over the traditional methods of Pollock and Treisman (Pollock and Treisman, 1990) or yeast one-hybrid screens (Li and Herskowitz, 1993). Once a library of sufficient diversity is produced, one can rapidly screen a very diverse profile of DNA binding sequences. Unlike the Pollock and Treisman method of multiple rounds of PCR amplification of *in vitro* bound purified, active protein-DNA complexes, the B1H assay requires only one round of selection in which the only limitation in the number of possible DNA binding sequences screened in one assay is the bacterial transformation efficiency. Therefore, unlike a yeast one-hybrid screen, the B1H assay has the ability to screen a minimum of 10^8 DNA binding sequences in under two weeks time. Additionally, the power of this selection relies on a low copy bait vector (~10 copies/cell) and an extremely low copy prey vector (~6 copies/cell), a feature that alleviates false interactions due to overabundance and proximity of the bait and prey that plagues the traditional methods. Finally, this method eliminates the need for associated cofactors since the alpha subunit fusion protein directly recruits RNA polymerase to drive transcription.

In this study, we have used the B1H assay system to determine if vertebrate CST binds the previously identified dCas DBS found within the Pdm-1 promoter. Additionally, we performed the B1H assay with vertebrate CST and the purified prey library to determine if vertebrate CST has affinity to a novel DBS.

MATERIALS AND METHODS

B1H Assay Components

Plasmids pB1H2 (bait vector – Ampicilin resistance), pB1H1 (bait vector – Chloramphenicol resistance), pH3U3 (prey library backbone – Kanamycin resistance), pB1H1-*Zif268*, pH3U3-*Zif268*DBS, and the *E. coli* USO∆*hisB*∆*pyrF* bacterial strain were generously provided by Dr. Scot Wolfe.

DNA binding domain constructs

The DNA binding domain of *Xenopus* CST was subcloned into the KpnI and AvrII of pB1H1 (Ampicilin). The CST DBD construct (pB1H2-CSTDBD) contains 621 amino acid residues, twelve amino acids N-terminal to the first zinc finger domain to the translational termination codon located 45 amino acids C-terminal of the fifth zinc finger. The DBD of *Drosophila* Cas was also subcloned into the pB1H1 (Ampicilin). The dCas DBD construct (pB1H2-dCasDBD) contains 256 amino acid residues, ten amino acids N-terminal to the first zinc finger domain to 28 amino acids C-terminal of the fourth zinc finger domain.

Generation of the purified prey library

A 56 bp oligo (purchased from Integrated DNA Technologies) containing an 18 bp randomized region flanked by a 5' NotI and a 3' AscI restriction site was extended with the following conditions: 10 units GO Taq Flexi, 1x GO Taq buffer (Promega), 2nmol dNTPs (Invitrogen), 1nmol 18 bp randomized prey oligo, 3 nmol complimentary (to 3' end of 18 bp randomized prey oligo) extension oligo.

Extension reaction took place using the following program: 94°, 3.5 minutes; 50°, 5 minutes; 72°, 15 minutes. Double stranded oligo product was ran on a 4% agarose gel in TAE. The double stranded (DS) prey DNA was excised and isolated by electroelution for one hour at 100 V in 1000 dalton molecular weight cutoff dialysis tubing (GE Healthcare). Following ethanol precipitation, the DS prey DNA was sequentially restriction digested by AscI and NotI (each - 37°, overnight). Digested DS prey library digested DNA was ran on a 4% agarose gel, electroeluted and ethanol precipitated. Seventeen large scale 20 µl ligations of 0.5 µg DS prey library digested DNA and 1 µg AscI/NotI digested pH3U3 (ratio determined empirically) using Ligation Kit (Stratagene) with 40 U of ligase were incubated a 4° for two days. The ligation reactions were pooled, ethanol precipitated and resuspended in 21 µl of water. The entire ligated product was transformed into 1200 µl XL-Blue1 electrocompetent cells (20 – 60 µl electroporation reactions) using a BioRad Gene Pulser electroporator at 1.70 kVolts, 200 Ω, 25 µFarads. Electroporated cells were resuspended in 940 µl pre-warmed SOC and subsequently added to 100 ml of pre-warmed SOC. Transformants were recovered for one hour at 37°, 250 rpm generating a prey library estimated to contain approximately $1.67x10^8$ unique clones. The library was then expanded for four hours at 37°, 250 rpm in 2xYT broth containing Kanamycin. Prey library plasmids were isolated using a Midi DNA plasmid prep (Invitrogen).

To generate a purified prey library, approximately $2x10^8$ prey library clones were electroporated into the USO∆*hisB*∆*pyrF* bacterial strain. Following one hour recovery in pre-warmed SOC at 37°, 250 rpm, cells were centrifuged for ten minutes at room temperature in a benchtop clinical centrifuge and resuspended in 2XYT broth with Kanamycin. The cells were incubated one hour at 37°, 250 rpm. Transformants were pelleted and washed three times with 2XYT broth, plated and challenged to grow on ten 245 mm x 245 mm YM plates containing 2 mM 5-fluoroorotic acid. $8.8x10^7$ surviving purified prey library clones were recovered in 15 ml of 2XYT broth followed by plasmid isolation using the Midi DNA plasmid prep (Invitrogen).

Binding site selection

To identify a DBS, 1 µg bait construct and 3.6 µg purified prey library were electroporated at 1.70 kVolts, 200 Ω, 25 µFarads into 60 µl of the USO∆*hisB*∆*pyrF* bacterial strain. After addition of 940 µl pre-warmed SOC, transformants were recovered for one hour at 37°, 250 rpm. Cells were pelleted in a benchtop clinical centrifuge for 10 minutes at room temperature and subsequently resuspended in 5 mls NM media supplemented with 0.1% histidine, Ampicilin (or Chloramphenicol) and Kanamycin. Transformats grew one hour at 37°, 250 rpm, and were subsequently pelleted and washed three times in NM media. After the final wash, cells were divided among four 150 mm NM- Amplicin (or Chloramphenicol) plates containing 0.1% histidine, 1 mM, 2 mM or 4 mM 3-

AT. Plates were inverted and incubated at 37° for about 20 hours. Prey library plasmids of surviving clones were isolated and sequenced.

Analysis of DNA binding Site

Unique 18 bp regions were analyzed for overrepresented motifs using MEME (http://meme.sdsc.edu/meme4/cgi-bin/meme.cgi) and BioProspector (http://ai.stanford.edu/~xsliu/BioProspector/). DBS identified by MEME or BioProspector to contribute to an overrepresented motif were imported into WebLOGO (http://weblogo.berkeley.edu/logo.cgi) to generate a sequence logo.

RESULTS

The prey library of the B1H assay contains an 18 bp randomized region 56 bp 5' to the weak *lac* promoter that drives the expression of histidine and uracil (Fig 3.1). To successfully identify the vertebrate CST DBS, the prey library has to have the capacity to represent as many DBS as possible. The raw prey library generated for this study is estimated to contain $1.7x10^8$ unique clones. This degree of complexity statistically represents the likelihood of containing every possible sequence combination within a 13 bp DBS, which is adequate to identify the DBS of most transcription factors (i.e. dCas DBS is 10 bp). To remove self-activating plasmids from the prey population, the raw library was challenged to grow in the presence of 5-fluoroorotic acid, a compound that is rendered toxic by the uracil biosynthesis pathway. The recovered surviving population is the purified prey library.

To demonstrate the efficacy of the purified prey library, the B1H assay was performed with the previously characterized classical zinc finger transcription factor *Drosophila* Zif268 (Christy and Nathans, 1989; Meng et al., 2005). Screening $5x10^8$ purified prey library clones (3X the library complexity) in the USO∆*hisB*∆*pyrF* bacterial strain on minimal media containing 0.1% histidine, 1 mM, 2 mM and 4 mM 3-AT resulted in a dose-dependent decrease in the number of surviving clones reflecting the increasing stringency of the selection (Fig 3.2A). Of the surviving clones, ten unique clones were isolated, sequenced and analyzed using the MEME software. Analysis of the 18 bp randomized regions generated an alignment consisting of seven of the ten clones that produced a 9 bp consensus motif strikingly similar to the published Zif268 DBS of "GCG(G/T)GGGCG" (Fig 3.2B) (Christy and Nathans, 1989; Meng et al., 2005). With successful detection of the Zif268 DBS, the purified prey library is a reliable source to decipher the vertebrate CST DBS using the B1H assay system.

Many transcription factors, especially zinc finger proteins, function in a modular fashion with each domain functioning independently (Jamieson et al., 2003; Meng et al., 2007; Urnov et al., 2005). Therefore, the CST DBD bait was constructed using C-terminal region of *Xenopus* CST consisting of the first zinc finger domain to the translational termination codon 45 amino acids C-terminal to the fifth zinc finger domain (Fig 3.3A). In similar fashion, the dCas DBD bait was constructed to consist of its four tandem zinc finger domains (Figure 3.3B). Eliminating non-DNA binding regions of a transcription factor alleviates potential

problems such as codon bias and toxicity in *E. coli*. To confirm proper expression of the α-RNA Polymerase subunit DBD fusion proteins, the expression of both the CST and dCas bait proteins were induced in the USO∆*hisB*∆*pyrF* bacterial strain. Utilizing the FLAG epitope within the linker of the bait proteins, western analysis demonstrated proper expression of the CST DBD fusion protein (Fig 3.3C). However, the dCas DBD fusion protein failed to be expressed (Data not shown). This may be due to rare codon usage which can be alleviated by substituting synonymous codons preferred by *E. coli* in the future.

To determine whether vertebrate CST binds the previously identified dCas DBS, a dCas DBS prey plasmid was generated consisting of the 10 bp dCas DBS (CCTCAAAAAA) flanked by four randomly chosen nucleotides to maintain the 18 bp interval (Kambadur et al., 1998). When the CST DBD fusion bait vector and the dCas DBS prey vector were introduced into the B1H system, there were no surviving clones on any of the 3-AT selection plates indicating vertebrate CST does not bind the dCas DBS in the context of the B1H assay. In parallel, the B1H assay was conducted with the CST DBD fusion bait and the purified prey library. This assay resulted in a dose-dependent survival of clones on 1 mM, 2 mM, and 4mM 3-AT. Of the 414 surviving clones on the 4 mM 3-AT selection plate, 73 clones were isolated, sequence and analyzed. Seventeen unique 18 bp randomized DNA binding regions were analyzed using BioProspector software. Of the seventeen analyzed, seven clones aligned to generate a consensus DBS

of (C/A)(T/A)A(G/C)TGGT(G/C)G (Fig 3.4A). The position weight matrix renders the nucleotide most probable at each position of the DBS (CTAGTGGTGG) which is also depicted in a sequence logo (Fig 3.4B, C).

Interestingly, two of the seven aligned sequences contained the sequence CTAGTGGTGG within completely unique 18 bp randomized DNA binding regions. To be sure this sequence did not self-activate and escape previous 5-fluoroortic acid selection, the prey library plasmid was isolated and reintroduced into the USO∆*hisB*∆*pyrF* bacterial strain and challenged to grow in the presence of 5-fluoroortic acid. As expected, the bacteria survived, demonstrating the prey plasmid was not self-activating. To ascertain whether the CST/CTAGTGGTGG binding interaction tolerates increasing doses of the histidine inhibitor, the CST DBD bait vector and the CTAGTGGTGG-containing prey plasmid was re-introduced into the USO∆*hisB*∆*pyrF* bacterial strain and challenged to grow under 3-AT selection. The CST/ CTAGTGGTGG binding interaction responded to the selection in a dose-dependent fashion suggesting CST binds the putative CST DBS with a measurable affinity (Fig 3.5).

DISCUSSION

Previous work has demonstrated that CST is required for the proper differentiation of a subpopulation of cardiomyocyte progenitors at the ventral midline of the heart (Christine and Conlon, 2008). To begin to address the

biological mechanism of CST, we have used a bacterial one-hybrid assay to determine the DNA binding site of CST.

We have generated a representative purified prey library with a complexity sufficient to detect as large as a 13 bp DBS. Since many zinc finger domains function independently, we utilized the DBD of CST consisting of the C-terminal portion from the first zinc finger domain to the translational termination codon (Jamieson et al., 2003; Meng et al., 2007; Urnov et al., 2005). In the context of the B1H assay system, CST recognizes a 10 bp DBS - (C/A)(T/A)A(G/C)TGGT(G/C)G. Interestingly, the sequence CTAGTGGTGG was identified twice in two independent, unique prey plasmids, invoking confidence in the putative CST DBS. Additionally, the dose-dependent survival of the bacteria containing the CST DBD and the CTAGTGGTGG-containing prey plasmid suggests that CST binds this DBS with an affinity to overcome as much as 4 mM 3-AT, a competitive inhibitor of histidine. As an indirect measure, this suggests the CST/CTAGTGGTGG interaction binds with an affinity that produces an amount of histidine in excess to the concentration of the 3-AT inhibitor. This finding allows for further characterization of the CST DBS by mutational analysis which would assess CST's specificity (tolerance of nucleotide variation) as well as affinity (strength of the binding interaction). For example, the CST DBS sequence logo indicated the adenosine at position 3 and the guanidine at position 10 may be essential for CST DBS recognition. If mutated, it would be

interesting to ascertain whether CST would continue recognize and bind the altered DBS.

A more direct assessment of the specificity and affinity of CST to the putative DBS is to perform a similar mutational analysis using either Electromobility Shift Assay (EMSA) or the PHERAstar assay system. This high-throughput analysis directly measures binding affinity of proteins to a DBS by measuring the intrinsic spin of a fluorescent-labeled DBS probe free in solution relative to the spin of the fluorescent-labeled DBS probe bound to a protein of interest. This analysis will be conducted with full length CST to directly determine the binding affinity to the consensus DBS identified by the B1H assay as well as mutated variants to assess the specificity of CST DNA binding recognition.

Significantly, vertebrate CST did not bind the dCas DBS in the context of the B1H assay. Since dCas contains only the first four tandem zinc finger domains, it is intriguing to speculate that the fifth C-terminal vertebrate zinc finger domain may influence vertebrate CST DNA binding recognition. It has been documented that tandem zinc finger domains are required for DNA recognition, while single zinc finger domains are thought to contribute secondary structure for DNA recognition (Wolfe et al., 2000). Therefore, a deletion series of the CST DBD (i.e. removal of the fifth zinc finger domain or the serine-rich region flanked by the fourth and fifth zinc finger domains) will be useful to investigate contribution of each region to CST DNA binding recognition. It is also plausible,

for example, the fifth C-terminal zinc finger domain is required for dimerization to itself or a transcriptional cofactor which in turn modifies the three-dimensional configuration of the four tandem zinc finger domains for DNA binding recognition. If it is discovered that CST heterodimerizes to a transcriptional cofactor, the B1H assay system could be utilized to investigate the affect of heterodimerization on CST DBS specificity and affinity. Since two α-subunits are present in the RNA Polymerase complex, CST and the cofactor can be expressed as independent α-subunits fusion proteins in the B1H assay. This procedure was successful in reproducing the previously identified DBS for the *Drosophila* core-binding factor α/β, Runt/Big Brother heterocomplex (Melnikova et al., 1993; Meng et al., 2005). It is possible homo- and/or heterodimerization of CST could modify either the specificity and/or the affinity of CST to DNA.

In addition to EMSA assays presently being conducted with full length CST and the consensus DBS, transcriptional assay will also be conducted in 293T cells to confirm CST DNA binding recognition to the consensus DBS in the context of a mammalian cell. Utilizing the basic and SV40 enhancer luciferase reporter in the transcriptional assays affords the ability to determine whether CST binds the DBS to activate and/or repress transcription. This will be an interesting finding since dCas is reported to act as a transcriptional repressor (Grosskortenhaus et al., 2006).

While further validation studies are necessary, we have identified the putative vertebrate CST DNA binding sequence using a bacterial one-hybrid assay system. We further established that vertebrate CST does not interact with the previously reported dCas DBS. This is an interesting finding considering vertebrate CST evolved to contain a fifth single C-terminal zinc finger domain that is not present in dCas. The influence of the additional fifth zinc finger domain on DNA recognition as well as transcriptional activation and/or repression capabilities is the focus of active investigation. These studies are the first biochemical investigation of vertebrate CST function and will increase understanding the role of vertebrate CST in development.

Figure 3.1 Overview of the bacterial one-hybrid assay

Schematic depiction of the B1H assay. The prey library construct containing the HIS3 and URA3 selection reporters downstream of the *lac* promoter. Interaction of the CST DBD alpha subunit fusion protein recognizes a DNA sequence in the 18 bp randomized DNA region, the alpha subunit will recruit RNA polymerase to the *lac* promoter to activate transcription of *HIS3* and *URA3*, allowing the bacterial clone to survive on minimal media plates containing 3-AT, a competitive inhibitor of histidine.

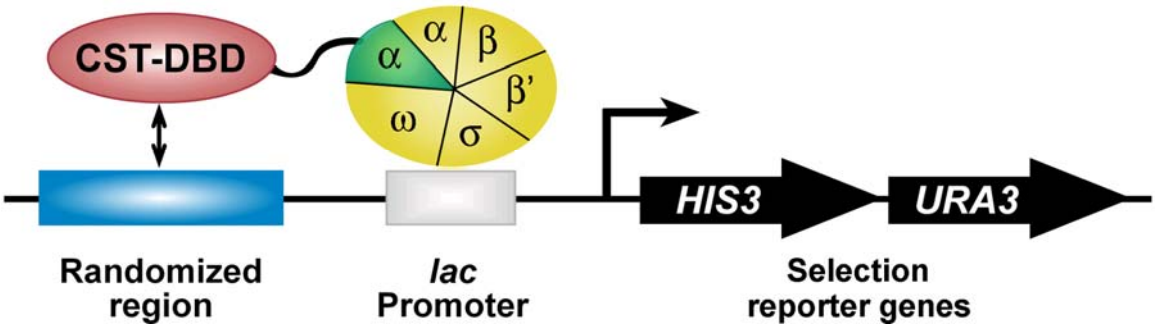

Figure 3.2 Validation of the purified prey library

The purified prey library successfully determined the DBS of *Drosophila* Zif268. (A) Dose-dependent survival of bacterial clones containing the Zif268 DBD and the purified prey library challenged to grow on increasing concentrations of 3-AT. (B) The sequence logo generated based on an alignment of seven 18 bp randomized regions. The consensus sequenced determined with the purified prey library in the B1H assay is very similar to the previously published Zif268 DBS.

A

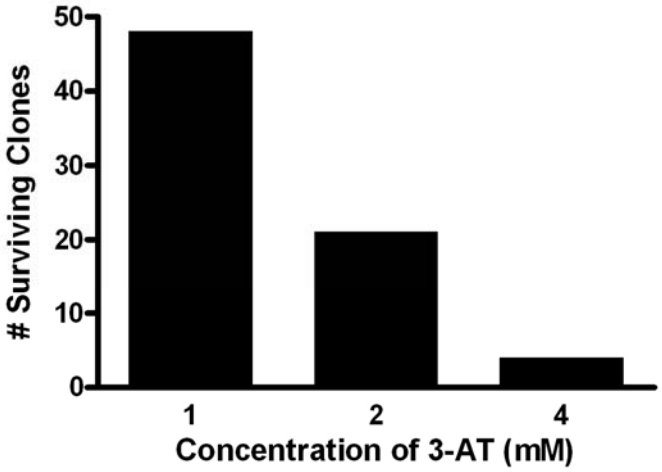
50
40
30
20
10
0
Surviving Clones
1
2
4
Concentration of 3-AT (mM)

B


2
1
0
bits
5′
1
2
3
4
5
6
7
8
9
10
3′

Figure 3.3 CST and dCAS DNA binding domain constructs for the B1H assay

(A) Schematic showing the region of *Xenopus* CST expressed as bait in the B1H assay. The CST DBD α-subunit fusion protein contains the C-terminal portion of CST from the first zinc finger domain (red) to the translational termination codon, including the serine rich region (blue). (B) Schematic showing the region of dCas expressed as bait in the B1H assay. The dCas DBD α-subunit fusion protein contains the four tandem zinc finger domains (red). (C) Western blot analysis of induced expression of vertebrate CST α-subunit fusion protein expressed in the USOΔ*hisB*Δ*pryF* bacterial strain using an anti-FLAG antibody. Yellow region – nuclear localization signal, Green triangle – FLAG epitope, Un – Uninduced, PI – Post Induction.

A

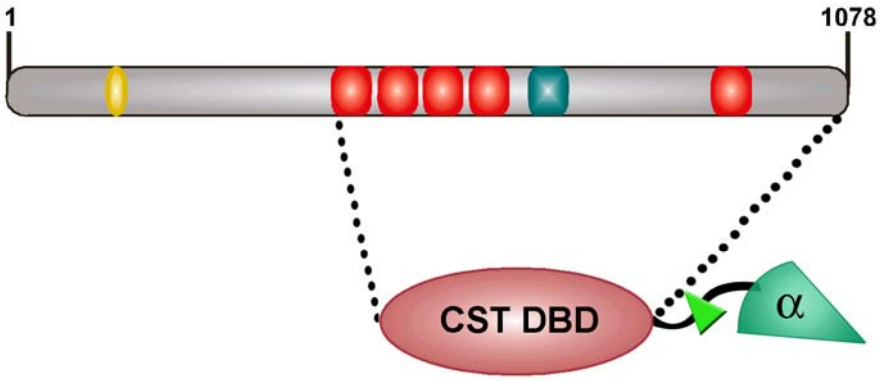
1
1078
CST DBD
α

B

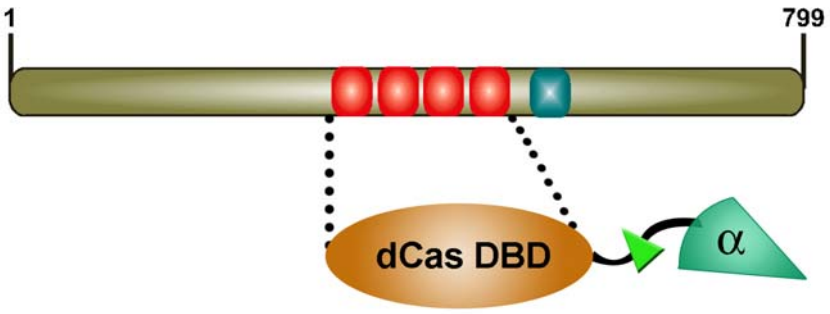
1
799
dCas DBD
α

C

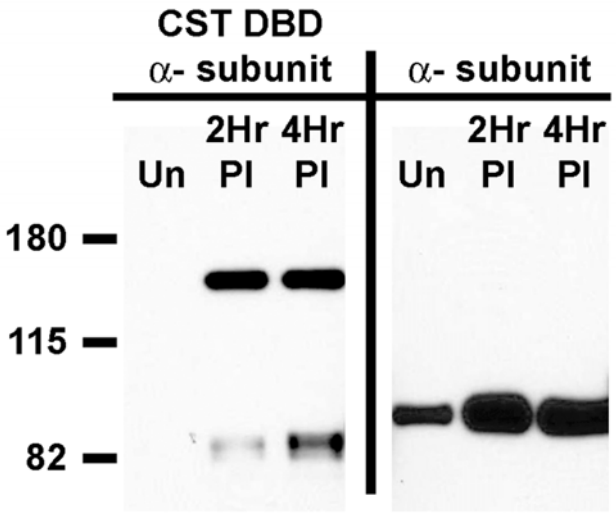
CST DBD
α- subunit
α- subunit
2Hr 4Hr
Un Pl Pl
2Hr 4Hr
Un Pl Pl
180
115
82

Figure 3.4 Vertebrate CST DBS determined by B1H assay

(A) Alignment of seven 18 bp randomized regions isolated from bacterial clones containing the CST DBD α-subunit fusion protein and the purified prey library that survived in the presence of 4 mM 3-AT. The aligned 10 bp DBS were used for further analysis. (B) Position weight matrix of the 10 bp DBS demonstrating the probability of each nucleotide at each of the ten positions. The most likely nucleotide is highlighted in red. This analysis generates a CST consensus DBS of CTAGTGGTGG. Note – sequences 1 and 2 in A contain this consensus DBS in two independent, unique 18 bp randomized regions. (C) Sequence logo of the vertebrate CST DBS created from the aligned regions highlighted in A.

A

Sequence			
1	TTCTGTC	CTAGTGGTGG	G
2	TATA	CTAGTGGTGG	AGGT
3		ATAGTCGCCG	GATGTGTA
4	TGACGAAC	AAAGTCGTGG	
5	ATTTAGCG	CAAATGGTTG	
6	ATG	CTACTGATCG	CACAA
7	AGTAATAC	CAACGGGGGG	

B

Position	A	C	G	T	Con
1	28.45	69.54	0.99	1.03	C
2	42.16	0.99	0.99	55.87	T
3	97.00	0.99	0.99	1.03	A
4	1.03	42.12	55.83	1.03	G
5	1.03	0.99	14.70	83.29	T
6	1.03	42.12	55.83	1.03	G
7	28.45	0.99	69.54	1.03	G
8	1.03	14.70	28.41	55.87	T
9	14.74	28.41	55.83	1.03	G
10	1.03	0.99	96.96	1.03	G

C

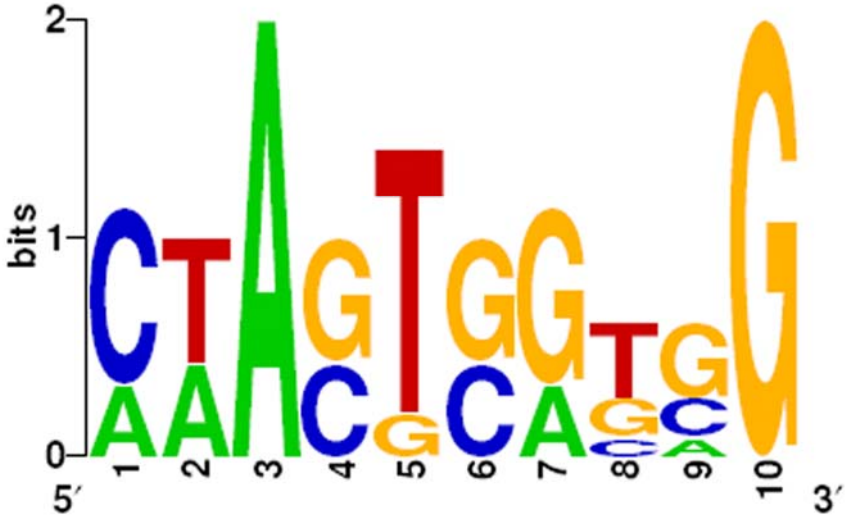

Figure 3.5 Vertebrate CST recognizes the CTAGTGGTGG binding motif

The CST DBD α-subunit fusion protein and the CTAGTGGTGG-containing prey plasmid was reintroduced into the USOΔ*hisB*Δ*pyrF* bacterial strain and challenged to grow on minimal media containing increasing concentrations of 3-AT. The dose-dependent decrease in the survival of clones validates the CTAGTGGTGG-containing prey plasmid interaction with the CST DBD.

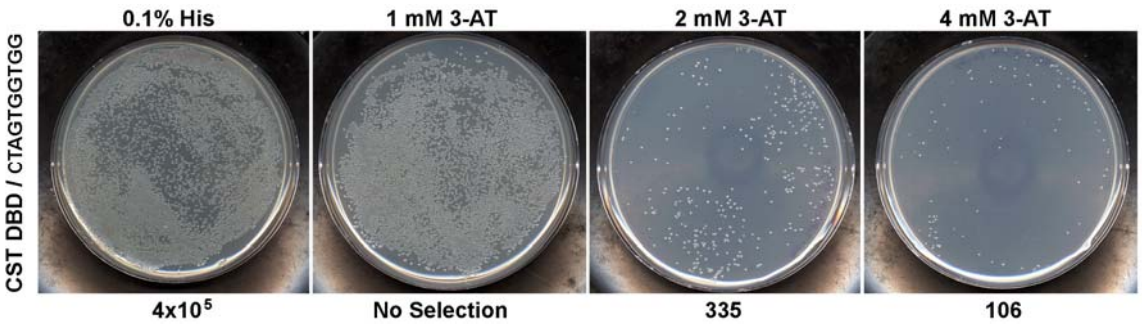

REFERENCE

Christine, K. S., and Conlon, F. L. (2008). Vertebrate CASTOR is required for differentiation of cardiac precursor cells at the ventral midline. Dev Cell *14*, 616-623.

Christy, B., and Nathans, D. (1989). DNA binding site of the growth factor-inducible protein Zif268. Proc Natl Acad Sci U S A *86*, 8737-8741.

Grosskortenhaus, R., Robinson, K. J., and Doe, C. Q. (2006). Pdm and Castor specify late-born motor neuron identity in the NB7-1 lineage. Genes Dev *20*, 2618-2627.

Jamieson, A. C., Miller, J. C., and Pabo, C. O. (2003). Drug discovery with engineered zinc-finger proteins. Nat Rev Drug Discov *2*, 361-368.

Kambadur, R., Koizumi, K., Stivers, C., Nagle, J., Poole, S. J., and Odenwald, W. F. (1998). Regulation of POU genes by castor and hunchback establishes layered compartments in the Drosophila CNS. Genes Dev *12*, 246-260.

Li, J. J., and Herskowitz, I. (1993). Isolation of ORC6, a component of the yeast origin recognition complex by a one-hybrid system. Science *262*, 1870-1874.

Melnikova, I. N., Crute, B. E., Wang, S., and Speck, N. A. (1993). Sequence specificity of the core-binding factor. J Virol *67*, 2408-2411.

Meng, X., Brodsky, M. H., and Wolfe, S. A. (2005). A bacterial one-hybrid system for determining the DNA-binding specificity of transcription factors. Nat Biotechnol *23*, 988-994.

Meng, X., Thibodeau-Beganny, S., Jiang, T., Joung, J. K., and Wolfe, S. A. (2007). Profiling the DNA-binding specificities of engineered Cys2His2 zinc finger domains using a rapid cell-based method. Nucleic Acids Res *35*, e81.

Miller, J., McLachlan, A. D., and Klug, A. (1985). Repetitive zinc-binding domains in the protein transcription factor IIIA from Xenopus oocytes. Embo J *4*, 1609-1614.

Pollock, R., and Treisman, R. (1990). A sensitive method for the determination of protein-DNA binding specificities. Nuc Acids Res *18*, 6197-6204.

Urnov, F. D., Miller, J. C., Lee, Y. L., Beausejour, C. M., Rock, J. M., Augustus, S., Jamieson, A. C., Porteus, M. H., Gregory, P. D., and Holmes, M. C. (2005). Highly efficient endogenous human gene correction using designed zinc-finger nucleases. Nature *435*, 646-651.

Wolfe, S. A., Nekludova, L., and Pabo, C. O. (2000). DNA recognition by Cys2His2 zinc finger proteins. Annu Rev Biophys Biomol Struct *29*, 183-212.

Chapter 4

Identification of novel CASTOR transcriptional targets in cardiogenesis

ABSTRACT

Vertebrate CASTOR (CST) is required for proper differentiation of a subset of cardiomyocyte progenitors at the ventral midline of the heart. Moreover, CST is required to regulate proliferation of cardiomyocyte progenitors lateral to the ventral midline. To date, no transcriptional targets of vertebrate CST have been identified. To begin to elucidate the biological pathways in which CST is active, we have used a cloning chromatin immunoprecipitation (ChIP) screen to identify direct transcriptional targets of vertebrate CST. This analysis has generated a pool of putative CST transcriptional targets which are now undergoing a secondary validation screen. The majority of the putative CST targets have been associated with major biological pathways, suggesting a potential role for CST in regulating cell growth, cell adhesion, Wnt signaling pathways and chamber myocardium patterning.

INTRODUCTION

Cardiomyocyte differentiation is regulated in part by the initiation of transcription of unique, spatially and temporally restricted proteins. Previously, we identified a role for CASTOR (CST) in mediating differentiation of a subset of cardiomyocyte progenitors located at the ventral midline of the linear heart tube (Christine and Conlon, 2008). In the absence of CST, the ventral midline cardiomyocyte progenitors remain in a premature state and fail to differentiate in a timely manner. The remaining cardiomyocyte progenitor population undergoes differentiation; however, a portion of the cardiomyocytes remain in a hyperproliferative state (Christine and Conlon, 2008). The dual nature of the CST phenotype suggests the presence of spatially unique transcriptional targets in the cardiomyocyte progenitors. To understand the biological functions regulated by CST, we set out to identify novel direct transcriptional targets of CST.

In the absence of a *Xenopus* genomic DNA ChIP, we chose to identify direct transcriptional targets of CST using a cloning chromatin immunoprecipitation (ChIP) screen. Unlike a reverse ChIP assay, which is used to investigate the interaction of a protein with a predetermined gene of interest using PCR amplification, the cloning ChIP method is an unbiased approach that entails isolating the CST-DNA complexes by immunoprecipitation and subsequently subcloning the target DNA fragments. This method has been used successfully to identify novel direct transcriptional targets of the SOX2 and E2F

transcription factors in development (Taranova et al., 2006; Weinmann et al., 2001).

In this study, we generated a CST-specific antibody to perform the cloning ChIP screen on both early tailbud stage 27 – 29 *Xenopus tropicalis* whole embryos and heart-enriched regions of early tailbud stage 27 – 29 *Xenopus tropicalis* embryos. The cloning ChIP screen has generated a pool of potential CST transcriptional targets that are in the process of being validated.

MATERIALS AND METHODS

Xenopus CST antibodies

Polyclonal antibodies against CST were generated in rabbits at Covance, Inc. Antibodies were raised against a maltose binding protein (MBP)-8x-histinde epitope fused in-frame to the C-terminal fragment of CST containing the amino acids on the immediate C-terminal side of the fourth zinc finger domain and extending to and including the translation termination codon. The antigen fusion protein was expressed in *E. coli* and purified by nickel Sepharose chromatography. CST-specific antibodies were affinity-purified.

Xenopus tropicalis embryo and tissue collection

Xenopus tropicalis females were stimulated to ovulate by pre-priming with 10U human chorionic gonadotropin (hCG) followed by priming 20 h later with 200 units of hCG. Embryos were fertilized *in vitro* and cultured in 0.1x Marc's Modified

Ringer's buffer. Embryos were collected at early tailbud stage 27 – 29. Heart-enriched regions of the embryos were collected by dissecting posterior to the pharyngeal region and anterior to the gut endoderm. Following dissection, the tissue was rinsed in cold phosphate-buffered saline (PBS) and incubated in 1% formaldehyde containing protease inhibitors (Complete Mini Protease tablets, Roche) for 1 h at room temperature to crosslink protein-DNA complexes. Batches of 50 cross-linked embryos or heart-enriched regions were incubated in 0.125M glycine in PBS for 10 min at room temperature followed by three washes with PBS. Samples were flash-frozen in a dry ice/ethanol bath and stored at -80°C.

Cloning Chromatin Immunoprecipitation

Sixty whole embryos and 400 heart-enriched regions were used for the cloning ChIP screen. Samples were lysed in 800 µl cell lysis buffer (50 mM Tris-HCl pH 8.0 containing 2 mM EDTA, 0.1% NP-40, 10% glycerol and the Complete Mini Protease Inhibitor cocktail) for 10 min on ice with vigorous pipetting. Nuclei were pelleted by centrifuging at 2500 rpm for 5 min at 4°C. The cell lysis supernatant was removed and the nuclei pellets were washed with ice-cold PBS. Nuclei were resuspended in 200 µl nuclei lysis buffer (50 mM Tris-HCl pH 8.0 containing 10 mM EDTA, 1% SDS and the Complete Mini Protease Inhibitor cocktail) for 10 min on ice with vigorous pipetting. Four hundred microliters of IP dilution buffer (20 mM Tris-HCl pH 8.0 containing 2 mM EDTA, 150 mM NaCl, 1% Triton-X100 and the Complete Mini Protease Inhibitor cocktail) were added to the samples to adjust the volumes for sonication. Whole-embryo samples were

sonicated to generate DNA fragments of approximately 4 kb with the Branson Digital Sonifier at an amplitude of 20% for two cycles of 30 s each (1 s on / 0.5 s off). Samples of heart-enriched tissue were sonicated for one additional cycle of 15 s (1 s on / 0.5 s off). After each cycle, the sample was placed in a dry ice/ethanol bath for 5 s followed by a 2-min incubation on ice. Samples were centrifuged at 15,000 rpm for 10 min at 4°C. Supernatants were removed to fresh tubes and pellets were discarded. Samples were pre-cleared for 2 h at 4°C by incubation with protein A/G beads (Santa Cruz) that have been blocked in 5% bovine serum albumin (BSA) in PBS with rotation. To reduce the concentration of SDS prior to immunoprecipitation, 400 µl of IP dilution buffer was added to the pre-cleared samples. Five micrograms of affinity-purified anti-CST antibody were added to the pre-cleared samples and incubated overnight at 4°C with rotation. To immobilize antibody-bound CST-DNA complexes, 50 µl of BSA-blocked protein A/G beads were added and incubated for 2 h at 4°C with rotation. The CST-DNA-bead complexes were washed with 1 ml IP dilution buffer three times for 15 min each at 4°, followed by three 2-min washes with 1 ml IP dilution buffer at room temperature and two 2-min washes with 1 ml TE buffer at room temperature; all washes were done with constant rotation. All samples were centrifuged between washes at 4000 rpm for 1.5 min at the temperature of the previous wash. To elute the CST-DNA complexes, beads were washed at 65°C with 150 µl elution buffer (50 mM Tris-HCl pH 8.0 containing10 mM EDTA and 1% SDS) and gently vortex-mixed every 2 min for 10 min. This procedure was repeated once and the eluates were pooled and treated with 30 µg RNaseA

(Sigma) at 37°C for 3 h. Crosslinking was reversed by incubating samples in 280 mM NaCl overnight at 65°C in a hybridization oven to reduce condensation. Samples were treated with 20 µg Proteinase K (Sigma) for 4 h at 55°C in a hybridization oven. The samples were sequentially extracted with phenol:cholorform and chloroform, ethanol-precipitated in the presence of 37.5 µg linear acrylamide and 500 mM NaCl and incubated overnight at -80°C. DNA was pelleted by centrifugation at 15000 rpm for 15 min at 4°C. The pellets were washed with 70% ethanol followed by centrifugation at 15000 rpm for 5 min spin at 4°C. DNA was air-dried for approximately 10 min and resuspended in 35.5 µl of water. The entire DNA sample was digested with *Nla*III (New England Biolabs) in a 50 µl reaction mixture overnight at 37° in a PCR machine to reduce condensation. Digested DNA was purified by ethanol precipitation in the presence of 37.5 µg linear acrylamide and 370 mM NaCl overnight at -80°C. DNA was pelleted by centrifugation at 15000 rpm at 4°C for 15 min. Pellets were washed with 70% ethanol followed by centrifugation at 15000 rpm for 5 min at 4°C. DNA was air-dried for approximately 10 min and resuspended in 5 µl of water. The entire 5 µl *Nla*III-digested DNA sample was ligated into 100 ng *Sph*I-(New England Biolabs) digested pUC19 in a 10 µl reaction mixture for 2 d at 4°C using the DNA ligation kit (Stratagene). Two-microliter aliquots of ligation products were transformed into 25 µl aliquots of NEB10β electrocompetent cells at 1.7 kV, 200 Ω and 25 µF using the BioRad Gene Pulser. Transformants were suspended in 975 µl pre-warmed SOC and recovered for 1 h at 37°C. Transformants were plated on seven 150-mm LB plates containing 100 µg/ml

ampicillin and 100 µg/ml β-galactosidase (β-gal) (Sigma) and incubated overnight at 37°C. White transformants were cultured and plasmids were isolated using a standard DNA isolation protocol. Plasmid DNA was resuspended in 30 µl water and sequenced using the M13 Forward primer.

Transcriptional target annotation

CST target DNA sequences between the two *Nla*III restriction sites were first assessed by BLAT analysis using the UCSC *Xenopus tropicalis* Genome Browser (http://genome.ucsc.edu, August 2005 assembly) to identify their locations within the scaffolds of the *Xenopus tropicalis* genome. A positive identification was defined as a 100% homology match between the CST target DNA and a single genomic scaffold region. Complete homology to multiple scaffolds identified the target DNA as a repetitive sequence. The DNA scaffold location coordinates were imported into the Joint Genome Institute *Xenopus tropicalis* v4.1 database (http://genome.jgi-psf.org/Xentr4/Xentr4.home.html). The genomic scaffold was scanned for the nearest gene up to 100 kb 5' and 3' to the CST target DNA.

RESULTS

The success of the CST cloning ChIP screen depends on an antibody with high specificity and affinity for CST. Therefore, a CST-specific polyclonal antibody that targets the C-terminal portion of the protein was generated (Fig 4.1A). Following affinity purification, the CST-specific antibody was used to

immunoprecipitate *in vitro* translated V5 epitope-tagged CST (Christine and Conlon, 2008). The CST-specific antibody successfully immunoprecipitated CST-V5 while rabbit pre-immune serum did not (Fig 4.1B). However, the CST cloning ChIP screen requires immunoprecipitation of endogenous CST. To confirm that the antibody also specifically recognizes endogenous CST, the anti-CST antibody was used to immunoprecipitate endogenous CST from an adult *Xenopus tropicalis* heart (Fig 4.1C).

The CST cloning ChIP screen was implemented in a slightly different manner than in previous studies utilizing a cloning ChIP screen (Taranova et al., 2006; Weinmann and Farnham, 2002); here the screen was modified to allow subcloning of the CST target DNAs in the most efficient manner. The genomic DNA was sheared to fragments of approximately 4 kb; this is four times larger than used in previous studies. Following isolation of immunoprecipitated DNA, *Nla*III, a four-base pair DNA restriction enzyme, was used to digest the DNA to fragments of approximately 400 to 40 bp. *Nla*III digestion provided a 5' overhang compatible with the overhang of the restriction enzyme *Sph*I. The *Sph*I recognition sequence is located within the multiple cloning site of the pUC19 vector, and therefore, ligation of the *Nla*III-digested CST target DNA into *Sph*I-digested pUC19 provided an efficient method to subclone the CST target DNA and screen positive clones by blue/white β-gal selection. However, this cloning method slightly complicates the analysis and validation of the CST-bound DNA. Since the 4 kb CST target DNA wasreduced to 400 to 40 bp fragments, it is

possible that the DNA fragments isolated by this approach do not represent the region of DNA bound by CST. Therefore, validation of the CST target DNAs must include analysis of DNA 4 kb upstream and downstream of the isolated CST target DNA. However, independent isolation of CST target DNAs that are located within 4 kb of each other will provide supporting evidence that the nearby gene is a genuine transcriptional target of CST.

To validate the modified CST cloning ChIP screen, a pilot analysis was completed using 30 *Xenopus tropicalis* stage 27 – 29 embryos. The whole-embryo CST cloning ChIP screen generated approximately 47,000 clones, of which 112 clones were analyzed. Ten CST target DNAs were located within an intronic region of a gene, while 11 CST target DNAs were found within 10 kb of a nearby gene. A high yet expected number of clones - 35 of 112 - contained repetitive DNA while 12 CST target DNAs were not identified within the *Xenopus tropicalis* genome. Seven of the 112 CST target DNAs were identified within the genome; however, in the case of these seven DNAs, there were no genes within 100 kb of upstream or downstream of the isolated DNA.

Because *Cst* mRNA is expressed within the hindbrain and other neuronal derivatives, it is reasonable to assume that CST may regulate transcription of neuronal genes (Christine and Conlon, 2008). Therefore, it is not surprising that analysis of the CST target DNAs revealed eight genes associated with neuronal cell processes (Table 4.1).

To enrich for CST cardiac transcriptional targets, the CST cloning ChIP screen was performed on 400 dissected *Xenopus tropicalis* stage 27 – 29 heart-enriched regions. This developmental window was chosen based on the observation that *Cst* mRNA expression is initiated within the cardiomyocyte progenitors at stage 27 and that the cardiac phenotype first appears in stage 29 CST-depleted embryos (Christine and Conlon, 2008). This screen produced approximately 840 clones of which 602 have been sequenced, analyzed and annotated. Sixty-one CST target DNAs were located within introns and 50 were located within 10 kb of a nearby gene. Two hundred ninety-six additional CST target DNAs were identified in the genome; however, they were located at a distance greater than 10 kb from the nearest gene. Forty-seven of the 296 CST target DNAs located at a distance greater than 100 kb from any gene were identified in the genome. Of the 602 CST target DNAs analyzed, 77 were repetitive DNA and 71 were not identified within the *Xenopus tropicalis* genome.

Further analysis of the CST target DNAs indentified two genes represented by multiple hits to two independent regions of DNA, the genes encoding Wnt-1 inducible signaling pathway 1 (Wisp1) and the N-myc downstream regulated gene 1 (Ndrg1). Of the 110 putative CST targets that were identified by CST target DNAs located in an intron or within 10 kb of a nearest gene, 12 putative targets were represented by multiple hits to the same CST target DNA region. Seventeen putative CST targets were represented by multiple hits to the same DNA region located beyond 10 kb of the nearest gene. However,

due to the large distances between the CST target DNAs and the corresponding genes, these putative targets were not further analyzed. The 110 putative CST transcriptional targets identified by CST target DNAs lying within an intron or within 10 kb of another gene were further investigated to determine whether they are expressed in the myocardium and/or endocardium of the developing heart in vertebrate species (Table 4.2). The putative CST targets were further categorized into broad developmental pathways, all of which are involved in cardiogenesis. Table 4.2 provides the initial characterization of putative CST targets organized in a hierarchy based on documented cardiac expression in vertebrate species.

DISCUSSION

The CST cloning ChIP screen has generated a pool of putative CST targets with documented expression in the heart of vertebrate species (Table 4.2). The putative targets have been further categorized based on their involvement in major developmental pathways that are integral to cardiogenesis, including cell growth, migration and adhesion, the Wnt signaling pathway, tissue patterning, cell and tissue structural, and metabolism. Although further validation is required to determine if these are bona fide CST transcriptional targets, the putative targets and their established roles in development provides insight into the potential function of CST in cardiogenesis.

CST is required for the differentiation of cardiomyocyte progenitors at the ventral midline immediately following cardiac fusion (Christine and Conlon, 2008). Interestingly, the ventral midline cardiomyocyte progenitor population mediates the fusion of the two bilateral cardiac fields. These leading edge cells must sense the environmental signals to detect the approaching opposed cardiac field, halt migration and establish cell-cell contact to form a single coherent cardiac field while simultaneously commencing differentiation and rapid proliferation to form the primitive ventricle. While the signals and corresponding pathways that influence the initial contact and fusion of the cardiac fields into one coherent cardiac field are not entirely understood, it is intriguing that the CST cloning ChIP screen identified multiple genes implicated in mediating cell-cell and/or cell-matrix contact and migration. Despite the occurrence of cardiac fusion in CST-depleted embryos, it is plausible that CST activates and/or represses a gene(s) that are instructive or responsive to environmental cues to mediate cardiac fusion. CST may be required to mediate cell-cell adhesion and/or inhibit further migration of the ventral midline cardiomyocyte progenitor population subsequent to cardiac fusion. In the absence of CST, the integrity of fusion and cohesiveness within the ventral midline cardiomyocyte progenitor population may be jeopardized resulting in inhibition of differentiation.

Properly orchestrated cell growth is essential in the developing heart, especially during the temporal window in which CST functions. Cardiomyocyte progenitors rapidly proliferate during migration to the ventral midline. Once

cardiac fusion occurs, the ventral cardiomyocytes undergo coherent growth and rapid proliferation along the perpendicular axis of the heart tube to form the multilayered ventricle chamber (Meilhac et al., 2003; Soufan et al., 2006). In the absence of CST, a population of differentiated cardiomyocytes lateral to the ventral midline have an increased mitotic index (Christine and Conlon, 2008). However, it has not been determined whether these cells are proliferating aberrantly or whether they are arrested in the M-phase of the cell cycle, either of which could prevent these cells from differentiating properly. Notably, while there is a significant decrease in the number of differentiated cardiomyocytes in CST-depleted hearts, the decrease may not be entirely accounted for by the reduced number of undifferentiated ventral midline cardiomyocyte progenitors. Therefore, it is possible that the lateral cardiomyocytes with an increased mitotic index are also undifferentiated and will undergo excessive proliferation in the subsequent coherent growth phase of ventral chamber formation. Notably, the ventricular myocardium appears strikingly thicker in mid-tailbud stage 33 CST-depleted embryos, suggesting that unrestrained proliferation is occurring when coherent growth should be taking place (unpublished results). The cloning ChIP screen identified multiple cell growth-associated putative CST targets. Interestingly, with one exception (Jumonji domain containing 1A), all identified putative CST targets associated with cell growth were also associated with the cell growth-inhibiting p53 pathway (Table 4.2). The repression and/or activation of these putative targets by CST may account in part for the hyperproliferation of the lateral

cardiomyocytes and the lack of differentiation of the ventral midline cardiomyocyte progenitors in the CST-depleted embryos.

The cloning ChIP screen also implicates CST in the Wnt signaling pathway. The canonical Wnt pathway involves the binding of canonical Wnts to their frizzled receptors which results in the inhibition of GSK3β. GSK3β inhibition releases β-catenin, which then relocates to the nucleus to associate with TCF/LEF transcription factors to mediate transcription of Wnt target genes. The non-canonical Wnt pathway involves activation of JNK downstream of RhoA and Rac, which mediates β-catenin-independent signaling. This non-canonical Wnt pathway is commonly referred to as the planar cell polarity (PCP) pathway and is associated with oriented cell division and convergence-extension cell movements. Canonical Wnt signaling emanating from neural tissue is thought to inhibit cardiac specification as the cardiomyocyte progenitors migrate from the primitive streak to the ventral midline of the embryo. Simultaneously, the non-canonical Wnt pathway promotes commitment to the cardiac lineage by inhibiting canonical Wnt signaling. Wnt2a and Wnt8a, canonical Wnts, are expressed in the linear heart tube in mouse, but surprisingly, data obtained using the β-catenin transgene reporter mouse line indicate that canonical Wnt signaling does not occur in the linear heart tube (Jaspard et al., 2000; Maretto et al., 2003; Monkley et al., 1996). It is possible that these canonical Wnt ligands also interact in non-canonical Wnt pathways; however, further investigation is necessary to test this hypothesis. Interestingly, Wnt2a and Wnt3a have been demonstrated to induce

cardiac differentiation in murine embryonic stem cells (Deb et al., 2008; Monkley et al., 1996). Conditional knock-out of β-catenin in the Islet1-Cre mouse line demonstrates that canonical Wnt signaling is also required for the specification and proliferation of the anterior heart field (Cohen et al., 2007; Lin et al., 2007). Therefore, canonical Wnt signaling appears to have multiple roles in cardiogenesis: inhibiting cardiac specification, maintaining proliferation of the anterior heart field cardiomyocyte progenitors, and regulating cardiomyocyte differentiation. Results of the CST cloning ChIP screen suggest that CST may repress the transcription of canonical Wnt targets such as NBL4 or Wisp1 in the linear heart tube to induce differentiation. Further validation is needed to test this hypothesis.

The non-canonical PCP Wnt pathway is also required for proper migration of the cardiomyocyte progenitors to the ventral midline in *Xenopus*. Wnt11R, a non-canonical Wnt, is expressed within the migrating cardiomyocyte progenitors just prior to cardiac fusion at the ventral midline (Garriock et al., 2005). Pharmacological inhibition studies have shown that Wnt11R regulates migration of the cardiac fields to the ventral midline through a JNK-mediated pathway (Garriock et al., 2005). It would be interesting to determine if the non-canonical Wnt pathway also participates in coherent growth of the ventricle chamber myocardium since the PCP pathway is associated with oriented cell proliferation and the time at which the non-canonical Wnt pathway is active in the cardiomyocyte progenitors coincides with the initiation of coherent myocardial

growth (Ciruna et al., 2006; Meilhac et al., 2003). Downstream components of the PCP pathway, Shisa2 and/or Prickle1, were identified in the cloning ChIP screen as putative transcriptional targets of CST. If these genes are expressed in the linear heart tube, further investigation will determine if CST regulates their transcription to mediate the PCP pathway in cardiomyocytes.

Formation of a functional cardiac chamber requires not only the induction of chamber-specific gene expression but also the repression of cardiac genes specific to adjacent areas of the forming heart, thus maintaining boundaries between chambers. Interestingly, Msx1 was identified as a putative transcriptional target of CST in the cloning ChIP screen. Msx1 is a homeobox transcription factor that directly interacts with the T-box transcription factor TBX3 to repress the expression of connexin 43 in the primary myocardium of the atrioventricular canal (Boogerd et al., 2008). Msx1 is also required for the survival of the anterior heart field progenitors (Chen et al., 2007). It will be interesting to determine if Msx1 expression is transcriptionally repressed by CST in the ventricular chamber myocardium. It is also possible that CST is expressed in the anterior heart field progenitors where it can regulate Msx1 expression.

Validation of the putative CST transcriptional targets will be prioritized based on selected criteria. Highest priority will be given to putative targets that were identified by multiple hits to independent genomic regions. Thus far, this includes Wisp1 and Ndrg1. The second group of putative targets to be

investigated will be those that were identified multiple times within the same genomic region. These include Msx1, jumonji domain containing 1A, troponin T type3, NBL4, and cyld (Table 4.2). Next, the CST target DNAs located within 4 kb of a gene will be analyzed to determine if they contain any of the six CST DNA binding sequence (DBSs) that contribute to the CST consensus DBS identified in Chapter 3. If a CST DBS is identified in any of the target DNAs, those putative targets will receive a higher priority for validation. The CST target DNAs located within 4 kb of a gene will also be analyzed for phylogenetic conservation. DNA regions conserved among *Xenopus*, mouse and human are likely to be regulatory enhancer regions of genes that are targeted by transcription factors. Therefore, the conserved regions can also be analyzed for the presence of known DBSs of cardiac transcription factors such as NKX2.5, GATA, SRF and Tbox proteins. Those putative CST targets that have phylogenetically conserved regions will be given priority for validation, particularly if the CST or other cardiac transcription factor DBS is identified within those regions. Finally, the putative CST targets associated with major developmental pathways such as those involving cell proliferation, migration/adhesion, patterning and the Wnt pathway will also be validated.

To begin the secondary validation screen, the spatial and temporal expression patterns of the putative CST targets will be assessed in wildtype and CST-depleted *Xenopus* embryos by *in situ* hybridization. If CST transcriptionally regulates the putative target, its temporal and spatial expression pattern in the

CST-depleted embryo may be altered relative to wildtype embryos. For example, if CST is required in the primitive ventricle to repress expression of a tumor suppressor gene to permit chamber myocardium proliferation, the putative CST target may by ectopically expressed in the ventricular chamber myocardium in the CST-depleted embryo. While *in situ* hybridization studies will assess the spatial and temporal expression of the putative targets, SYBR Green quantitative PCR will be used to assess the level of expression of the putative CST target in wildtype and CST-depleted dissected heart-enriched regions. Altered expression levels will indicate if CST is repressing or activating transcription of the putative CST target. If a commercial antibody is available for any of the putative CST targets, whole mount antibody staining and western analysis will be performed to assess the spatiotemporal pattern and level of protein expression.

The putative CST targets that show altered expression in the CST-depleted embryo will undergo further validation by *in vitro* transcriptional assays. The CST target DNAs and associated phylogenetically conserved regions will be subcloned into a luciferase reporter construct and transfected with CST into 293T cells. Using a standard luciferase reporter construct, CST should increase luciferase transcription if CST acts on the target DNA as a transcriptional activator. In contrast, when using a luciferase reporter construct containing an SV40 enhancer that increases basal levels of luciferase expression, transcriptional repression would result in decreased luciferase expression if CST acts on the target DNA as a transcriptional repressor. If the putative CST target is

associated with a cellular pathway, appropriate assays will be conducted to validate a role for CST in its regulation. For example, the TOP-FLASH luciferase reporter construct consists of multiple TCF/LEF binding sites for β-catenin/TCF-mediated transcription and, therefore, serves as a readout for the canonical Wnt signaling pathway. If CST-depletion results in altered expression of a gene in the canonical Wnt signaling pathway, a TOP-FLASH luciferase assay can be conducted to determine the effect of altered expression of the target on β-catenin/TCF-mediated transcription.

In validating a transcriptional target of CST, it will be essential to demonstrate CST-mediated transcriptional activation/repression of the target *in vivo*. If it is determined, based on the assays described above, that CST activates the expression of a particular transcriptional target, antisense morpholinos will be designed to deplete the transcriptional target to determine if the CST target-depleted embryo phenocopies the CST-depleted embryo. If CST represses the target, CST target mRNA will be injected into the embryo to achieve overexpression. Ideally, this would also phenocopy the CST-depleted cardiac phenotype. However, this approach is problematic in that depletion or overexpression of a gene may cause either embryonic lethality or disruption of other aspects of development, precluding the ability to assess similarities of the cardiac phenotypes. To circumvent this obstacle, a transgene (Tg) containing the region of CST target DNA, with or without 4 kb of flanking DNA determined by the *in vitro* analysis to be required for CST activation or repression, can be

cloned upstream of a DsRed reporter and integrated into the genome of the embryo. Following initial cleavage, Cst morpholino or *Cst* mRNA can be injected into both cells of the embryo. The levels of DsRed expression can be compared in the CST-depleted/Tg or CST over-expressing/Tg embryos to levels in the embryos harboring the Tg alone. Ideally, the DsRed expression would increase in the CST-depleted/Tg embryo and decrease in the CST over-expressing/Tg embryos if CST acted as a transcriptional repressor. In contrast, DsRed expression would decrease in the CST-depleted/Tg embryo and increase in the CST-overexpressing/Tg embryos if CST acted as a transcriptional activator. This would be an ambitious experiment accompanied by its own challenges; however, it would provide functional *in vivo* relevance to the role of CST on the transcription of its putative target.

The cloning ChIP screen generated a pool of putative CST targets and further analysis is underway to determine whether these genes are bona fide CST transcriptional targets. Moreover, the design of the validation analysis will provide insight into the mechanism(s) by which CST regulates the expression of its targets and determine whether it functions as a transcriptional activator and/or a transcriptional repressor. Given the nature of the putative targets and the biological pathways which they are associated, this validation screen will provide the first illustration of a role for vertebrate CST in an established developmental pathway.

ACKNOWLEDGEMENTS

I would like to sincerely thank Ms. Mira Pronobis for her assistance in the CST cloning ChIP screen. Mira is a talented undergraduate who had joined our lab for two months while visiting from Germany. In this time, she single-handedly isolated and sequenced over six hundred clones. Her effort highly contributed to the success of the CST cloning ChIP screen.

Figure 4.1 Generation of a CST-specific antibody

(A) Schematic of CST demonstrating the region of the protein used to develop the polyclonal CST-specific antibody (green). The antigen consisted of the C-terminal portion of CST immediately following the fourth zinc finger domain including the serine-rich region (blue) and the fifth zinc finger domain (red) to the translation termination codon. (B) Western blot analysis of immunoprecipitated *in vitro* translated CST-V5 with the CST-specific antibody and pre-immune rabbit serum. (C) Western blot analysis of immunoprecipitated endogenous CST with the CST-specific antibody and pre-immune serum from adult *Xenopus tropicalis* heart tissue. Red arrow indicates the position of the endogenous CST protein.

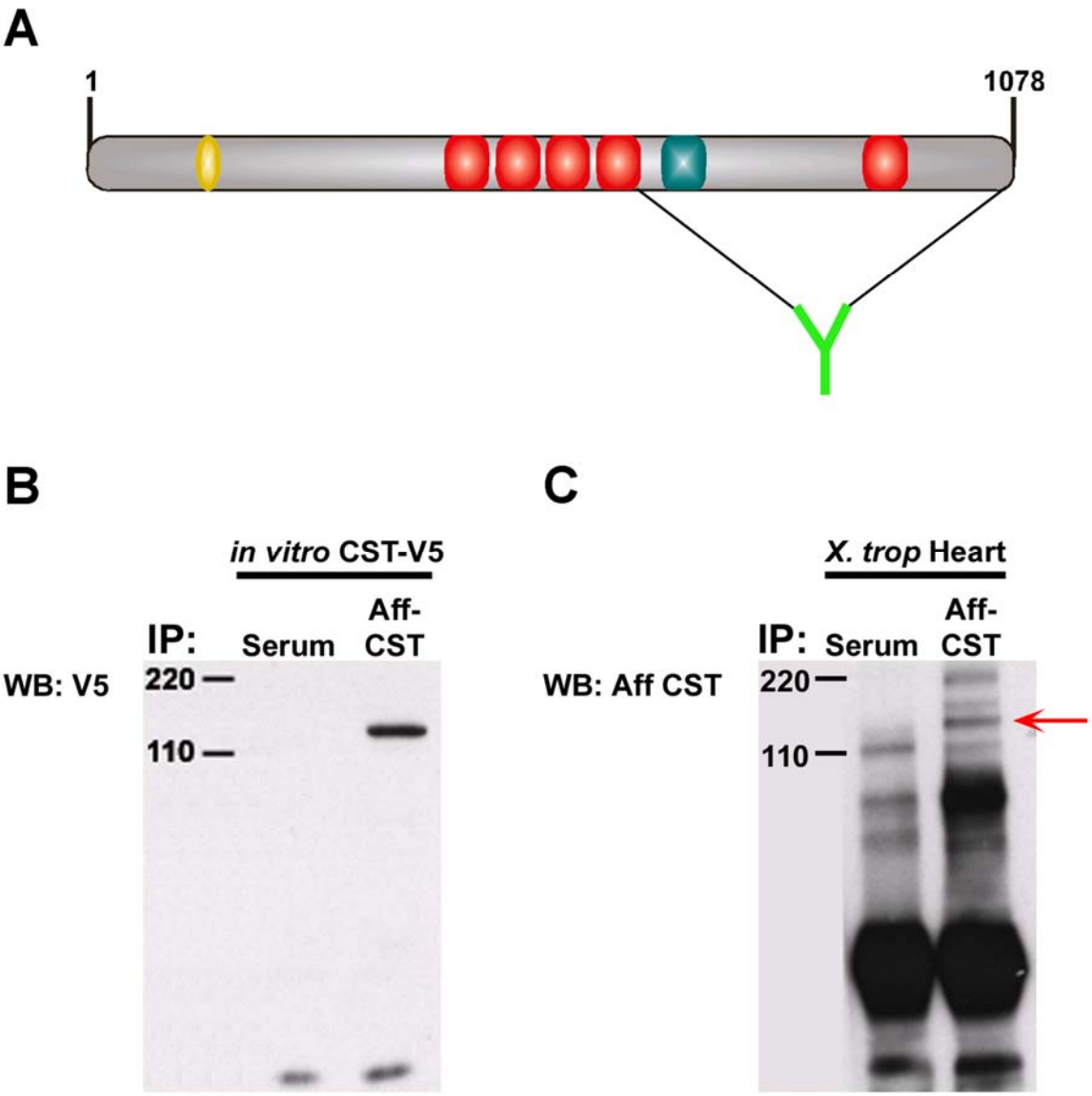
A
1
1078
B
in vitro CST-V5
IP:
Serum
Aff-CST
WB: V5
220
110
C
X. trop Heart
IP:
Serum
Aff-CST
WB: Aff CST
220
110

Table 4.1 Putative CST transcriptional targets from a whole embryo cloning ChIP screen

Putative CST transcriptional targets identified in the whole *Xenopus troplicalis* embryo cloning ChIP screen associated with development of the central nervous system. The distance of the putative CST target relative to the CST target DNA isolated in the cloning ChIP screen is documented as internal (found within an intron of the gene), 3' or 5' ± 4 kb.

Putative CST Target	CST Target DNA location	Function	References
Transcription factor 4 (TCF4)	Internal	bHLH/E-protein – required for differentiation of pontine neuronal progenitors in the dorsal hindbrain	Flora et al., 2007
Intersectin 2	Internal	Cytoplasmic protein – Expressed in the brain and involved in clathrin-mediated endocytosis	Seifert et al., 2007
Chondrolectin	Internal	C-type lectin transmembrane protein – expressed in brain	Weng et al., 2003
Hunington Interacting Protein 1 (HIP1)	Internal	Endocytic protein – Pro-apoptotic factor in hippocampal neuronal progenitors	Kang et al., 2005
Neuronal Leucine-Rich Repeat Protein 4 (NLRR4)	6800 bp 5'	Transmembrane protein – associated with long-distance learning and memory retention	Bando et al., 2005
EPH receptor B1 (Ephb1)	28,561 bp 5'	Tyrosine-protein kinase receptor – mediate cell-contact-dependent repulsion of neuronal outgrowths of the hindbrain	Wilkinson DG, 2000
Neural Cell Adhesion Molecule 2 (NCAM2)	40,341 bp 5'	Transmembrane protein – involved in guidance of olfactory sensory neurons	Kulahin et al., 2008
Leukemia Inhibitory Factor Receptor (LIF-R)	40,649 bp 3'	Transmembrane protein – promotes the self-renewal of a subpopulation ventricular zone precursors in the ventral forebrain	Gregg et al., 2005

Table 4.2 Putative CST transcriptional targets from the heart-enriched tissue cloning ChIP screen

Putative CST targets identified in the cloning ChIP screen using heart-enriched regions from stage 27-29 *Xenopus tropicalis* embryos. Putative CST targets listed are associated with cardiac expression and are categorized according to their involvement in developmental pathways. If the gene was identified multiple times in the screen, (#X) follows the gene name. The distance of the putative CST target relative to the CST target DNA isolated in the cloning ChIP screen is documented as internal (found within an intron of the gene), 3' or 5' ± 4 kb. Expression in the myocardium and/or endocardium in vertebrate species is documented: h – human, m – mouse, m^A – mouse adult heart, c – chick, ND – not determined. If documented with "Heart", no distinction between myocardium and endocardium in the literature.

Putative CST Target	CST Target DNA location	Function	Expressed in Myo/Endocardium	References
Cell Growth Pathways				
N-myc Downregulated Gene1 (Ndrg1) (3X-2 independent)	3743 bp 3'	Cytoplasmic protein – tumor suppressor, upregulated in terminally differentiating cells, direct transcriptional target of p53	Heart (c, h)	Tian et al., 2008 Qu et al., 2002 Zhang et al., 2007
Jumonji Domain Containing 1A (2X)	Internal	Histone Demethylase stimulated in hypoxic conditions	Heart (h, m)	Knebel et al., 2006 Wellmann et al., 2008
Cyld (2x)	8075 bp 5'	Tumor suppressor – interferes with activation of proto-oncogene Bcl(3) and CyclinD1 to limit cell proliferation	ND	Massoumi et al., 2007
MDM2	4868 bp 3'	E3 Ubiquitin Ligase - cell survival factor – inhibits pro-apoptotic factor p53	Myocardium (m)	Grier et al., 2006
MDM4	Internal	E3 Ubiquitin Ligase - cell survival factor – inhibits pro-apoptotic factor p53	Myocardium (m)	Xiong et al., 2007
Cyclin L2	16 bp 3'	Induces G0/G1 arrest and apoptosis	ND	Hong-li et al., 2007
Inhibitor of Growth 1 (Ing1)	309 bp 5'	Tumor suppressor factor – cofactor of p53 for cell growth inhibition and apoptosis	ND	Walzak et al., 2008
Gli2	3680 bp 3'	Hedgehog signaling effector – promotes cell proliferation, inhibits p53 tumor suppressor accumulation	Heart (h)	Abe et al., 2008 Katoh et al., 2008
Migration & Adhesion				
Plexin A2	Internal	Co-receptor of Semaphorin 3C – expressed in migratory and postmigratory cardiac neural crest cells	Heart (m)	Brown et al., 2001
EGF-like Domain 7 (Egfl7)	Internal	Secreted factor associated with ECM – creates permissive environment for endothelial progenitors	Endocardium (m)	Parker et al., 2004
Neurexin 3	Internal	Transmembrane protein – involved in cell-cell and cell-matrix adhesion	Heart (h)	Occhi et al., 2002
FAT-J	Internal	Cadherin – involved in cell-cell adhesion and oriented cell division (Planar Cell Polarity [PCP] Pathway)	Heart (h,m)	Hong et al., 2004 Rock et al., 2005
Wnt Signaling Pathway				
Wnt1 Induced Secreted Pathway 1 (Wisp1) (3X-2 indpendent)	Internal & 2867 bp 3'	Connective Tissue Growth Factor – downstream target of Wnt1-β-catenin pathway, mediates proliferation and prevents apoptosis and cell migration	Myocardium (m)	Colston et al., 2007 Soon et al., 2003 Su et al., 2002
Novel Band 4.1-like Protein 4 (NBL4) (2X)	6788 bp 5'	Membrane associated protein – downstream of β-catenin-TCF pathway, may interact at plasma membrane and cytoskeleton & be involved in cell polarity and/or proliferation	Heart (h)	Ishiguro et al., 2000
Shisa 2	Internal	Endoplasmic reticulum protein – inhibits FGF and Wnt signaling by retaining receptors in the ER , tissue maturation	Heart (c)	Hedge et al., 2008 Nagano et al., 2006
Prickle 1	Internal	LIM domain protein – involved in PCP pathway, axon guidance and convergence extension cell movements	Heart (c)	Cooper et al., 2008 Okuda et al., 2007

Table 4.2 - Continued

Putative CST Target	CST Target DNA location	Function	Expressed in Myo/Endocardium	References
Patterning				
Msx1 (2X)	8775 bp 5'	Homeobox transcription factor – inhibits chamber myocardial genes in primary myocardium and proliferation of OFT myocardium and post-migratory cNC cells, promotes AV cushion formation	Myocardium (m) Endocardium (c, m)	Chan-Thomas et al., 1993 Chen et al., 2007 Chen et al., 2008 Boogerd et al., 2008 Robert et al., 1989
ALK2 / ACVR1	9351 bp 5'	BMP Receptor Type I – required for cNC cell migration, expression of Msx1 in OFT and AV cushion formation	Myocardium (m) Endocardium (m)	Kaartinen et al., 2004 Wang et al., 2005
Structural Proteins				
Troponin T Type 3 (Tnnt3) (2X)	4654 bp 5'	Fast twitch skeletal Troponin T	No	Huang et al., 2008 Stefancsik et al., 2003
Myosin 5C	Internal	Motor protein – actin-based membrane trafficking	Heart (h)	Rodriguez et al., 2002
Metabolism				
Cytochrome b5 (2X)	Internal	Hemoprotein – involved in lipid metabolism and cholesterol biosynthesis	Ubiquitous	Borgese et al., 1993
Cytochrome b5 reductase isoform 2 (2X)	10,000 bp 3'	flavoenzyme family of dehydrogenases-electron transferases	Ubiquitous	Borgese et al., 1993
Cytochrome C Oxidase subunit VIII-Heart specific isoform	3859 bp 3'	Terminal enzyme of respiratory electron chain – required for cellular energy production	Heart (h)	Rizzuto et al., 1989

REFERENCES

Abe, Y., Oda-Sato, E., Tobiume, K., Kawauchi, K., Taya, Y., Okamoto, K., Oren, M., and Tanaka, N. (2008). Hedgehog signaling overrides p53-mediated tumor suppression by activating Mdm2. Proc Natl Acad Sci U S A *105*, 4838-4843.

Bando, T., Sekine, K., Kobayashi, S., Watabe, A. M., Rump, A., Tanaka, M., Suda, Y., Kato, S., Morikawa, Y., Manabe, T., and Miyajima, A. (2005). Neuronal leucine-rich repeat protein 4 functions in hippocampus-dependent long-lasting memory. Mol Cell Biol *25*, 4166-4175.

Boogerd, K. J., Wong, L. Y., Christoffels, V. M., Klarenbeek, M., Ruijter, J. M., Moorman, A. F., and Barnett, P. (2008). Msx1 and Msx2 are functional interacting partners of T-box factors in the regulation of Connexin43. Cardiovasc Res *78*, 485-493.

Borgese, N., D'Arrigo, A., De Silvestris, M., and Pietrini, G. (1993). NADH-cytochrome b5 reductase and cytochrome b5 isoforms as models for the study of post-translational targeting to the endoplasmic reticulum. FEBS Lett *325*, 70-75.

Brown, C. B., Feiner, L., Lu, M. M., Li, J., Ma, X., Webber, A. L., Jia, L., Raper, J. A., and Epstein, J. A. (2001). PlexinA2 and semaphorin signaling during cardiac neural crest development. Development *128*, 3071-3080.

Chan-Thomas, P. S., Thompson, R. P., Robert, B., Yacoub, M. H., and Barton, P. J. (1993). Expression of homeobox genes Msx-1 (Hox-7) and Msx-2 (Hox-8) during cardiac development in the chick. Dev Dyn *197*, 203-216.

Chen, Y. H., Ishii, M., Sucov, H. M., and Maxson, R. E., Jr. (2008). Msx1 and Msx2 are required for endothelial-mesenchymal transformation of the atrioventricular cushions and patterning of the atrioventricular myocardium. BMC Dev Biol *8*, 75.

Chen, Y. H., Ishii, M., Sun, J., Sucov, H. M., and Maxson, R. E., Jr. (2007). Msx1 and Msx2 regulate survival of secondary heart field precursors and post-migratory proliferation of cardiac neural crest in the outflow tract. Dev Biol *308*, 421-437.

Christine, K. S., and Conlon, F. L. (2008). Vertebrate CASTOR is required for differentiation of cardiac precursor cells at the ventral midline. Dev Cell *14*, 616-623.

Ciruna, B., Jenny, A., Lee, D., Mlodzik, M., and Schier, A. F. (2006). Planar cell polarity signalling couples cell division and morphogenesis during neurulation. Nature *439*, 220-224.

Cohen, E. D., Wang, Z., Lepore, J. J., Lu, M. M., Taketo, M. M., Epstein, D. J., and Morrisey, E. E. (2007). Wnt/beta-catenin signaling promotes expansion of Isl-1-positive cardiac progenitor cells through regulation of FGF signaling. J Clin Invest *117*, 1794-1804.

Colston, J. T., de la Rosa, S. D., Koehler, M., Gonzales, K., Mestril, R., Freeman, G. L., Bailey, S. R., and Chandrasekar, B. (2007). Wnt-induced secreted protein-1 is a prohypertrophic and profibrotic growth factor. Am J Physiol Heart Circ Physiol *293*, H1839-1846.

Cooper, O., Sweetman, D., Wagstaff, L., and Munsterberg, A. (2008). Expression of avian prickle genes during early development and organogenesis. Dev Dyn *237*, 1442-1448.

Deb, A., Davis, B. H., Guo, J., Ni, A., Huang, J., Zhang, Z., Mu, H., and Dzau, V. J. (2008). SFRP2 regulates cardiomyogenic differentiation by inhibiting a positive transcriptional autofeedback loop of Wnt3a. Stem Cells *26*, 35-44.

Flora, A., Garcia, J. J., Thaller, C., and Zoghbi, H. Y. (2007). The E-protein Tcf4 interacts with Math1 to regulate differentiation of a specific subset of neuronal progenitors. Proc Natl Acad Sci U S A *104*, 15382-15387.

Garriock, R. J., D'Agostino, S. L., Pilcher, K. C., and Krieg, P. A. (2005). Wnt11-R, a protein closely related to mammalian Wnt11, is required for heart morphogenesis in Xenopus. Dev Biol *279*, 179-192.

Gregg, C., and Weiss, S. (2005). CNTF/LIF/gp130 receptor complex signaling maintains a VZ precursor differentiation gradient in the developing ventral forebrain. Development *132*, 565-578.

Grier, J. D., Xiong, S., Elizondo-Fraire, A. C., Parant, J. M., and Lozano, G. (2006). Tissue-specific differences of p53 inhibition by Mdm2 and Mdm4. Mol Cell Biol *26*, 192-198.

Hedge, T. A., and Mason, I. (2008). Expression of Shisa2, a modulator of both Wnt and Fgf signaling, in the chick embryo. Int J Dev Biol *52*, 81-85.

Hong, J. C., Ivanov, N. V., Hodor, P., Xia, M., Wei, N., Blevins, R., Gerhold, D., Borodovsky, M., and Liu, Y. (2004). Identification of new human cadherin genes using a combination of protein motif search and gene finding methods. J Mol Biol *337*, 307-317.

Huang, Q. Q., Feng, H. Z., Liu, J., Du, J., Stull, L. B., Moravec, C. S., Huang, X., and Jin, J. P. (2008). Co-expression of skeletal and cardiac troponin T decreases mouse cardiac function. Am J Physiol Cell Physiol *294*, C213-222.

Ishiguro, H., Furukawa, Y., Daigo, Y., Miyoshi, Y., Nagasawa, Y., Nishiwaki, T., Kawasoe, T., Fujita, M., Satoh, S., Miwa, N.*, et al.* (2000). Isolation and characterization of human NBL4, a gene involved in the beta-catenin/tcf signaling pathway. Jpn J Cancer Res *91*, 597-603.

Jaspard, B., Couffinhal, T., Dufourcq, P., Moreau, C., and Duplaa, C. (2000). Expression pattern of mouse sFRP-1 and mWnt-8 gene during heart morphogenesis. Mech Dev *90*, 263-267.

Kaartinen, V., Dudas, M., Nagy, A., Sridurongrit, S., Lu, M. M., and Epstein, J. A. (2004). Cardiac outflow tract defects in mice lacking ALK2 in neural crest cells. Development *131*, 3481-3490.

Kang, J. E., Choi, S. A., Park, J. B., and Chung, K. C. (2005). Regulation of the proapoptotic activity of huntingtin interacting protein 1 by Dyrk1 and caspase-3 in hippocampal neuroprogenitor cells. J Neurosci Res *81*, 62-72.

Katoh, Y., and Katoh, M. (2008). Integrative genomic analyses on GLI2: mechanism of Hedgehog priming through basal GLI2 expression, and interaction map of stem cell signaling network with P53. Int J Oncol *33*, 881-886.

Knebel, J., De Haro, L., and Janknecht, R. (2006). Repression of transcription by TSGA/Jmjd1a, a novel interaction partner of the ETS protein ER71. J Cell Biochem *99*, 319-329.

Kulahin, N., and Walmod, P. S. (2008). The Neural Cell Adhesion Molecule NCAM2/OCAM/RNCAM, a Close Relative to NCAM. Neurochem Res.

Li, H. L., Wang, T. S., Li, X. Y., Li, N., Huang, D. Z., Chen, Q., and Ba, Y. (2007). Overexpression of cyclin L2 induces apoptosis and cell-cycle arrest in human lung cancer cells. Chin Med J (Engl) *120*, 905-909.

Lin, L., Cui, L., Zhou, W., Dufort, D., Zhang, X., Cai, C. L., Bu, L., Yang, L., Martin, J., Kemler, R*., et al.* (2007). Beta-catenin directly regulates Islet1 expression in cardiovascular progenitors and is required for multiple aspects of cardiogenesis. Proc Natl Acad Sci U S A *104*, 9313-9318.

Maretto, S., Cordenonsi, M., Dupont, S., Braghetta, P., Broccoli, V., Hassan, A. B., Volpin, D., Bressan, G. M., and Piccolo, S. (2003). Mapping Wnt/beta-catenin signaling during mouse development and in colorectal tumors. Proc Natl Acad Sci U S A *100*, 3299-3304.

Massoumi, R., and Paus, R. (2007). Cylindromatosis and the CYLD gene: new lessons on the molecular principles of epithelial growth control. Bioessays *29*, 1203-1214.

Meilhac, S. M., Kelly, R. G., Rocancourt, D., Eloy-Trinquet, S., Nicolas, J. F., and Buckingham, M. E. (2003). A retrospective clonal analysis of the myocardium reveals two phases of clonal growth in the developing mouse heart. Development *130*, 3877-3889.

Monkley, S. J., Delaney, S. J., Pennisi, D. J., Christiansen, J. H., and Wainwright, B. J. (1996). Targeted disruption of the Wnt2 gene results in placentation defects. Development *122*, 3343-3353.

Nagano, T., Takehara, S., Takahashi, M., Aizawa, S., and Yamamoto, A. (2006). Shisa2 promotes the maturation of somitic precursors and transition to the segmental fate in Xenopus embryos. Development *133*, 4643-4654.

Occhi, G., Rampazzo, A., Beffagna, G., and Antonio Danieli, G. (2002). Identification and characterization of heart-specific splicing of human neurexin 3 mRNA (NRXN3). Biochem Biophys Res Commun *298*, 151-155.

Okuda, H., Miyata, S., Mori, Y., and Tohyama, M. (2007). Mouse Prickle1 and Prickle2 are expressed in postmitotic neurons and promote neurite outgrowth. FEBS Lett *581*, 4754-4760.

Parker, L. H., Schmidt, M., Jin, S. W., Gray, A. M., Beis, D., Pham, T., Frantz, G., Palmieri, S., Hillan, K., Stainier, D. Y*., et al.* (2004). The endothelial-cell-derived secreted factor Egfl7 regulates vascular tube formation. Nature *428*, 754-758.

Qu, X., Zhai, Y., Wei, H., Zhang, C., Xing, G., Yu, Y., and He, F. (2002). Characterization and expression of three novel differentiation-related genes belong to the human NDRG gene family. Mol Cell Biochem *229*, 35-44.

Rizzuto, R., Nakase, H., Darras, B., Francke, U., Fabrizi, G. M., Mengel, T., Walsh, F., Kadenbach, B., DiMauro, S., and Schon, E. A. (1989). A gene specifying subunit VIII of human cytochrome c oxidase is localized to chromosome 11 and is expressed in both muscle and non-muscle tissues. J Biol Chem *264*, 10595-10600.

Robert, B., Sassoon, D., Jacq, B., Gehring, W., and Buckingham, M. (1989). Hox-7, a mouse homeobox gene with a novel pattern of expression during embryogenesis. Embo J *8*, 91-100.

Rock, R., Schrauth, S., and Gessler, M. (2005). Expression of mouse dchs1, fjx1, and fat-j suggests conservation of the planar cell polarity pathway identified in Drosophila. Dev Dyn *234*, 747-755.

Rodriguez, O. C., and Cheney, R. E. (2002). Human myosin-Vc is a novel class V myosin expressed in epithelial cells. J Cell Sci *115*, 991-1004.

Seifert, M., Ampofo, C., Mehraein, Y., Reichrath, J., and Welter, C. (2007). Expression analysis of human intersectin 2 gene (ITSN2) minor splice variants showing differential expression in normal human brain. Oncol Rep *17*, 1207-1211.

Soon, L. L., Yie, T. A., Shvarts, A., Levine, A. J., Su, F., and Tchou-Wong, K. M. (2003). Overexpression of WISP-1 down-regulated motility and invasion of lung cancer cells through inhibition of Rac activation. J Biol Chem *278*, 11465-11470.

Soufan, A. T., van den Berg, G., Ruijter, J. M., de Boer, P. A., van den Hoff, M. J., and Moorman, A. F. (2006). Regionalized sequence of myocardial cell growth and proliferation characterizes early chamber formation. Circ Res *99*, 545-552.

Stefancsik, R., Randall, J. D., Mao, C., and Sarkar, S. (2003). Structure and Sequence of the Human Fast Skeletal Troponin T (TNNT3) Gene: Insight Into the Evolution of the Gene and the Origin of the Developmentally Regulated Isoforms. Comp Funct Genomics *4*, 609-625.

Su, F., Overholtzer, M., Besser, D., and Levine, A. J. (2002). WISP-1 attenuates p53-mediated apoptosis in response to DNA damage through activation of the Akt kinase. Genes Dev *16*, 46-57.

Taranova, O. V., Magness, S. T., Fagan, B. M., Wu, Y., Surzenko, N., Hutton, S. R., and Pevny, L. H. (2006). SOX2 is a dose-dependent regulator of retinal neural progenitor competence. Genes Dev *20*, 1187-1202.

Tian, Y., Xu, M., Fu, Y., Yuan, A., Wang, D., Li, G., Liu, G., and Lu, L. (2008). Mapping and expression analysis of chicken NDRG1 and NDRG3 genes. Biochem Genet *46*, 677-684.

Walzak, A. A., Veldhoen, N., Feng, X., Riabowol, K., and Helbing, C. C. (2008). Expression profiles of mRNA transcript variants encoding the human inhibitor of growth tumor suppressor gene family in normal and neoplastic tissues. Exp Cell Res *314*, 273-285.

Wang, J., Sridurongrit, S., Dudas, M., Thomas, P., Nagy, A., Schneider, M. D., Epstein, J. A., and Kaartinen, V. (2005). Atrioventricular cushion transformation is mediated by ALK2 in the developing mouse heart. Dev Biol *286*, 299-310.

Weinmann, A. S., Bartley, S. M., Zhang, T., Zhang, M. Q., and Farnham, P. J. (2001). Use of chromatin immunoprecipitation to clone novel E2F target promoters. Mol Cell Biol *21*, 6820-6832.

Weinmann, A. S., and Farnham, P. J. (2002). Identification of unknown target genes of human transcription factors using chromatin immunoprecipitation. Methods *26*, 37-47.

Wellmann, S., Bettkober, M., Zelmer, A., Seeger, K., Faigle, M., Eltzschig, H. K., and Buhrer, C. (2008). Hypoxia upregulates the histone demethylase JMJD1A via HIF-1. Biochem Biophys Res Commun *372*, 892-897.

Weng, L., Hubner, R., Claessens, A., Smits, P., Wauters, J., Tylzanowski, P., Van Marck, E., and Merregaert, J. (2003). Isolation and characterization of chondrolectin (Chodl), a novel C-type lectin predominantly expressed in muscle cells. Gene *308*, 21-29.

Wilkinson, D. G. (2000). Eph receptors and ephrins: regulators of guidance and assembly. Int Rev Cytol *196*, 177-244.

Xiong, S., Van Pelt, C. S., Elizondo-Fraire, A. C., Fernandez-Garcia, B., and Lozano, G. (2007). Loss of Mdm4 results in p53-dependent dilated cardiomyopathy. Circulation *115*, 2925-2930.

Zhang, A. H., Rao, J. N., Zou, T., Liu, L., Marasa, B. S., Xiao, L., Chen, J., Turner, D. J., and Wang, J. Y. (2007). p53-dependent NDRG1 expression induces inhibition of intestinal epithelial cell proliferation but not apoptosis after polyamine depletion. Am J Physiol Cell Physiol *293*, C379-389.

Chapter 5

Discussion and Future Directions

Differentiation of cardiomyocyte progenitors proceeds in a specific temporal and spatial manner to program cardiomyocytes for specialized functions within the developed heart. However, there remains significant deficiency in our understanding of the regulation of cardiomyocyte differentiation. This dissertation lays the foundation for a novel mechanism of cardiomyocyte differentiation involving CASTOR (CST), a unique para-zinc finger transcription factor. These studies have investigated the role of CST within the cardiomyocyte progenitor population. CST is required for the differentiation of the ventral midline cardiomyocyte progenitors. In an effort to further characterize the role of CST in cardiomyocyte differentiation and elucidate the molecular mechanism by which it functions, two screens were employed to 1) determine the DNA binding sequence (DBS) recognized by CST to regulate transcription and 2) to identify direct transcriptional targets of CST within cardiomyocytes of the developing heart.

CST is required for cardiomyocyte progenitor differentiation

The *Drosophila* orthologue of vertebrate CST, dCas, is required for the spatial and temporal differentiation of a subset of neuronal progenitors within the developing central nervous system (Cui and Doe, 1992; Mellerick et al., 1992). In addition, the murine orthologue of CST is expressed in the heart of the developing mouse embryo (Vacalla and Theil, 2002). Therefore, CST was an excellent candidate to study to further our understanding of the regulatory mechanisms that mediate the temporal and spatial differentiation of cardiomyocyte progenitors.

Chapter 2 characterizes the temporal and spatial expression of *Cst* in *Xenopus*. *Cst* expression is initiated in the cardiomyocyte progenitors at early tailbud stage 27 as the bilateral heart fields migrate toward the ventral midline. CST depletion using morpholinos demonstrated that CST is required in a subset of cardiomyocytes at the ventral midline for their timely differentiation, immediately following fusion of the bilateral cardiac fields (tailbud stage 29). Fate mapping of ventral midline cardiomyocytes demonstrated that these cells ultimately contribute to the outer wall of the ventricle. In contrast, CST-depleted ventral midline cardiomyocytes remained in an undifferentiated progenitor state as an unincorporated, hyperproliferative mass near the inflow region of the chambered heart. Interestingly, this hyperproliferation is consistent with an increased mitotic index of cardiomyocytes located in the dorsolateral differentiated cardiomyocyte population adjacent to the undifferentiated ventral

midline cardiomyocyte progenitors at stage 29. This analysis has provided the first characterization of a role for CST in vertebrate heart development.

Molecular mechanism of CST function

Chapters 3 and 4 detail how CST may regulate differentiation. This was especially important given that no molecular pathways have been identified for vertebrate CST. Additionally, CST is a novel zinc finger transcription factor in that each of the five zinc finger domains contains a classical Cys_2-His_2 immediately preceded by an additional Cys_2-His_2 motif, generating a novel para-zinc finger domain. Therefore, the identification of any molecular characteristics of this novel transcription factor is unprecedented.

In Chapter 3, results from the bacterial one-hybrid assay performed to identify the DBS of vertebrate CST are presented. Vertebrate CST recognizes a 10 bp consensus DBS – (C/A)(T/A)A(G/C)TGGT(G/C)G. However, vertebrate CST did not bind the previously identified dCAS DBS – (G/C)C(C/T)(C/T)AAAAA(A/T) (Kambadur et al., 1998). These data suggest that the fifth zinc finger domain, which is only found in vertebrate CST, may modulate DNA binding recognition. It is also possible the fifth zinc finger binds to coordinates the three-dimensional configuration of the other four consecutive zinc finger domains for DNA binding or engages the binding of cofactors that modulate DNA binding specificity. How this domain contributes to DBS specificity and/or affinity will be investigated actively in future experiments.

The identification of direct transcriptional targets of CST is critical for determining which molecular pathway(s) it regulates to direct cardiomyocyte differentiation. Chapter 4 presents a cloning chromatin immunoprecipitation (ChIP) screen which identified twenty-three putative CST transcriptional targets that have been previously shown previously to be expressed in cardiac tissue of vertebrate species. Interestingly, a majority of these putative CST targets are implicated in cell cycle and cell growth control, cell migration and adhesion, Wnt signaling and myocardium patterning. Although these putative CST targets are presently being validated, they do provide insight into how CST may influence cardiomyocyte differentiation.

The potential role of CST in cardiomyocyte cell adhesion

Cell migration and adhesion are essential components of cardiogenesis. Cardiomyocyte progenitors migrate as bilateral epithelial sheets to the ventral midline and fuse to become a single coherent epithelial cardiac field. Upon formation of the linear heart tube, the ventral cardiomyocytes undergo morphogenesis as they proliferate to form the chambers of the heart while maintaining cell-cell contact to preserve the integrity of the cardiac tissue.

It is intriguing that the ventral midline cardiomyocyte progenitors are affected in the CST-depleted embryo. The ventral midline cardiomyocytes are present at the leading edge of the migrating bilateral cardiac fields. They must respond to the environmental cues to detect the approaching, opposed cardiac

field, halt migration and establish cell-cell contact to form a single coherent cardiac field while simultaneously commencing differentiation and rapid proliferation to form the primitive ventricle. Therefore, it is possible that CST regulates the transcription of genes that are instructive or responsive to environmental cues to mediate the fusion of the bilateral cardiac field. Although cardiac fusion in the absence of CST has been demonstrated exhaustively, the adhesive properties of the CST-depleted ventral midline cardiomyocyte progenitors may be altered, resulting in excessive or insufficient cohesiveness that could lead to improper intercalation with the opposing leading edge cells. Interestingly, in the most severely affected CST-depleted hearts, it appears as though the leading edges appear to fuse at the ventral midline yet continue to migrate, forcing the leading edges of the bilateral cardiac progenitor fields into the interior regions of the ventricle chamber. This hypothesis argues that the CST mediates the cohesive properties of the ventral midline cardiomyocytes that facilitate their ability to differentiate. This notion is consistent with the fate mapping studies that demonstrated that the CST-depleted ventral midline cardiomyocyte progenitors remain in a progenitor state clustered near the posterior inflow region of the mature heart. This is in contrast to wildtype ventral midline cardiomyocyte progenitors that extend along the anterior-posterior axis of the outer ventricular myocardium in the mature heart.

The potential role of CST in cardiomyocyte cell growth and survival

The cloning CST ChIP screen also revealed putative CST targets implicated in cell growth. Properly orchestrated cell growth is essential in the developing heart, especially during the temporal window in which CST functions. Interestingly, all but one of the eight putative CST targets involved in cell growth were associated with the tumor suppressor p53. p53 is a transcriptional activator that mediates cell growth arrest, DNA repair and apoptosis in response to DNA damage and cellular stress (Danilova et al., 2008). p53 arrests progression of the S- and M-phases of the cell cycle by inhibiting cyclin dependent kinase 2 (CDK2) and cell division cycle 2 (CDC2), respectively (Dulic et al., 1994; Milner et al., 1990). However, p53 is tightly regulated to maintain low expression levels in part by MDM2-mediated ubiquitin-based degradation (Grier et al., 2006). MDM2 and MDM4 were both identified as putative CST targets in the cloning ChIP screen. Since both mediate degradation of p53, it is possible that CST upregulates the expression of these proteins to maintain low levels of p53 in cardiomyocytes (Grier et al., 2006; Xiong et al., 2007). This may partially explain the increase in mitotic index of the CST-depleted cardiomyocytes. In the absence of CST, and thereby reduced levels of MDM2 and MDM4, p53 levels may rise and inhibit CDC2, arresting the cardiomyocytes in the M-phase of the cell cycle. Notably, there was no increase in apoptosis of differentiated cardiomyocytes at tailbud stage 29 when an increased mitotic index in dorsolateral cardiomyocytes was observed. Comparison of the cell cycle profile of isolated CST-depleted heart-enriched regions versus wildtype by determining the expression levels of

p53 and established cell cycle-specific markers would be informative (Goetz et al., 2006). However, caution must be taken in evaluating the cell cycle profile results since cardiac tissue can not be isolated from the surrounding tissue at this stage of development. Although there is no detectable level of CST expression in the anterior endoderm, which appears unaffected in the CST-depleted embryo, molecular perturbations may affect the anterior endoderm in the CST-depleted embryo that could in turn alter the cell cycle profile. Additionally, the large number of cells may mask the detection of an altered cell cycle profile within the relatively small number of affected CST-depleted cells. Despite these potential setbacks, these experiments may still provide insight into the potential role of CST in cell cycle control.

A second hypothesis for the increased mitotic index of the dorsolateral CST-depleted cardiomyocytes is that the cells are not arrested in M-phase but are aberrantly hyperproliferating. Once cardiac fusion occurs, the ventral cardiomyocytes undergo coherent growth, rapidly proliferating along the perpendicular axis of the heart tube to form the multilayered ventricle chamber (Meilhac et al., 2003; Mohun, 2000; Soufan et al., 2006). Coherent growth is associated with oriented cell division along the transmural axis that, in concert with trophic signals from the overlying epicardium, forms the compact zone of the ventricle (Meilhac et al., 2003). Hyperproliferation of the dorsolateral CST-depleted cardiomyocytes could affect this coherent growth in the ventricular myocardium. As noted in Chapter 4, the ventricle myocardium of the CST-

depleted mid-tailbud stage 33 embryo appears thicker than its wildtype counterpart. This is suggestive of unrestrained proliferation, perhaps due to the hyperproliferation of the dorsolateral CST-depleted cardiomyocytes. This may in part be due to altered expression of the cell cycle/growth putative CST targets noted earlier. However, numerous Wnt pathway-associated components were also identified in the cloning ChIP screen. Canonical Wnt signaling has been documented to maintain the proliferative state of the anterior heart field cardiomyocyte progenitors in the mouse (Cohen et al., 2007; Lin et al., 2007). Previous studies have also shown that ES cells require canonical Wnt signaling for proper differentiation into cardiomyocytes (Deb et al., 2008; Monkley et al., 1996). Although these Wnt pathway-associated putative CST targets are being validated, it is intriguing that the canonical Wnt pathway is associated with phenotypes of the two subpopulations of affected CST-depleted cardiomyocytes, the hyperproliferative dorsolateral cardiomyocytes and the undifferentiated ventral midline cardiomyocyte progenitors.

The potential role of CST in non-canonical Wnt signaling

The non-canonical Wnt pathway is associated with the planar cell polarity (PCP) pathway, which acts through JNK downstream of RhoA and Rac to mediate β-catenin-independent signaling. Studies in *Xenopus* demonstrate that the PCP pathway mediated by Wnt11R and JNK is active in cardiomyocyte progenitors as the bilateral cardiac fields fuse (Garriock et al., 2005). Strikingly, the phenotype of the Wnt11R-depleted heart is very similar to that of the CST-

depleted heart (Christine and Conlon, 2008; Garriock et al., 2005). In the Wnt11R-depleted frog heart, the fusion of the bilateral cardiac fields is perturbed, resulting in their leading edges protruding into the interior of the ventricle. In the most severely affected hearts, Wnt11R-depletion results in cardia bifida. Additionally, the ventricular myocardial wall is thicker due to increased extracellular space between the cardiomyocytes at midtailbud stage 34. Therefore, Wnt11R and its associated downstream effectors are required in the linear tube to establish and maintain cell adhesion through the PCP pathway (Garriock et al., 2005). The similarity in the phenotypes of the CST-depleted and the Wnt11R-depleted hearts suggests CST may also mediate cell-cell adhesion, as suggested earlier through the non-canonical Wnt/PCP pathway.

The PCP pathway is also responsible for oriented cell division during developmental processes, such as in the *Drosophila* wing (Doyle et al., 2008). Therefore, determination of whether CST is required for coherent growth of the ventricular chamber myocardium, as well as whether this growth depends on the PCP pathway, would be interesting. With the hyperproliferation of the dorsolateral CST-depleted cardiomyocytes, the thickening of the ventricular myocardium at mid-tailbud stage 33 and the observed similarities with the non-canonical Wnt11R phenotypes, CST is likely involved in restricting coherent growth of the myocardium through the PCP pathway. Two putative CST targets, Shisa2 and Prickle1, are associated with the non-canonical Wnt/PCP pathway. A direct contribution of the non-canonical Wnt/PCP pathway to coherent growth of

the chamber myocardium has not been examined since depletion of components of this pathway results in gastrulation defects and early lethality.

Xenopus provides an excellent system in which to test the role of CST in coherent growth of the ventricular chamber myocardium and its dependence on the non-canonical Wnt/PCP pathway. To begin, early tailbud stage 29 heart-enriched regions would be excised and analyzed for differences in phosphorylated JNK between CST-depleted and CST-overexpressing cardiac explants relative to wildtype controls. Significant differences would suggest that CST is involved in the non-canonical Wnt pathway. If a difference in phosphorylated JNK is observed, explants of wildtype, CST-depleted and CST-overexpressing heart region could be excised at early tailbud stage 26 and cultured in a commercially available JNK inhibitor that prevents phosphorylation/activation of JNK and, therefore, the non-canonical Wnt pathway (Garriock et al., 2005; Langdon et al., 2007). These treated explants would be analyzed at stage 29 to determine if the wildtype JNK inhibitor-treated explant is phenotypically similar to the untreated CST-depleted or CST-overexpressing hearts (i.e. lack of ventral midline cardiomyocyte progenitor differentiation, hyperproliferation of dorsolateral cardiomyocytes and overall morphology), suggesting that CST may mediate non-canonical Wnt signaling. In addition, levels of phosphorylated JNK would be compared in the untreated CST-depleted/overexpressing and untreated wildtype hearts. If CST activates the non-canonical Wnt/PCP pathway, the phosphorylated JNK levels would be lower in

the CST-depleted hearts and higher in the CST-overexpressing hearts that the wildtype controls. Likewise, if CST repressed the non-canonical Wnt/PCP pathway, the levels of phosphorylated JNK would be increased in the CST-depleted hearts and decreased in the CST-overexpressing hearts relative to wildtype controls. Comparison of untreated and JNK inhibitor-treated CST-depleted cardiac explants at midtailbud stage 33 would determine if the thickening of the ventricular chamber myocardium is due to altered non-canonical Wnt signaling.

To test whether CST and/or the non-canonical Wnt pathway are associated with coherent growth, JNK inhibitor-treated CST-depleted and wildtype explants would be injected with fluorescent-labeled MitoTracker in the ventral cardiomyocytes of the linear heart tube at early tailbud stage 29 and cultured until mid-tailbud stage 33 and late tailbud stage 37. Transverse sections of the explants would be analyzed for the MitoTracker-labeled cells to determine the orientation of their proliferation from the compact zone into the trabeculae of the ventricle. If CST is required for coherent growth, proliferation of the MitoTracker labeled cells along the transmural axis would be perturbed in the CST-depleted hearts. Incorporating the JNK inhibitor-treated hearts in this experiment would determine the contribution of the non-canonical Wnt/PCP pathway in coherent growth of the heart. Likewise, to determine whether the non-canonical Wnt/PCP pathway is required for coherent growth, the MitoTracker-labeled cells along the transmural axis in the JNK inhibitor-treated explants would

be analyzed and compared to those in untreated wildtype explants. If perturbed, this result would suggest that the non-canonical Wnt/PCP pathway mediates coherent growth of the ventricle chamber myocardium. If both CST and the non-canonical Wnt/PCP pathway are associated with coherent growth, JNK inhibitor-treated CST-overexpressing explants and its untreated counterpart could be injected with MitoTracker and analyzed as previously mentioned. If CST-mediated coherent growth is regulated through the non-canonical Wnt/PCP pathway, the proliferation of the MitoTracker-labeled cells would be altered along the transmural axis of the ventricle chamber myocardium in the JNK inhibitor-treated CST-overexpressing cardiac explant. Results from this analysis would have considerable impact on identifying a functional role and molecular pathway for CST in heart development.

The potential role of CST in the anterior heart field

The sparse number of hyperproliferative cardiomyocytes relative to the differentiated cardiomyocyte population suggests that they may be incorporated into the linear heart tube from the anterior heart field prior to dorsal closure of the linear heart tube and its separation from the pharynx/anterior endoderm. This hypothesis is supported by lineage tracing of the Islet1-anterior heart field-derived cardiomyocytes, which revealed that 20% of the left ventricle in the mouse originated from the anterior heart field (Cai et al., 2003). However, Islet1-positive anterior heart field-derived cardiomyocytes were never located in the outer left ventricular wall, which arises from the ventral midline cardiomyocytes in

the chicken and frog (Christine and Conlon, 2008; De La Cruz et al., 1989). Although the existence of the anterior heart field has not been definitively established in *Xenopus*, it is possible that the hyperproliferative dorsolateral cardiomyocytes in the CST-depleted heart are derived from an anterior heart field cardiomyocyte progenitor population and that CST is required to establish and/or maintain their differentiation. In the absence of CST, these cardiomyocytes escape cell growth control. Expression of Islet1 is similar in the frog, mouse and chick, suggesting that an anterior heart field does exist in the frog (Brade et al., 2007; Cai et al., 2003; Mjaatvedt et al., 2001). If the frog anterior heart field is added to the linear heart tube as it is in the mouse or chick, expression of Islet1 and FGF10, markers of the anterior heart field, would most likely be extinguished immediately as they upregulate developmental programs characteristic of primary cardiomyocytes including NKX2.5 (Kelly et al., 2001; Prall et al., 2007). Therefore, in the absence of lineage tracing of the Islet1-expressing cells in *Xenopus*, it would be very difficult to prove the hypothesis that the hyperproliferative CST-depleted dorsolateral cardiomyocytes were derived from an anterior heart field. Because of this, the role of CST in the anterior heart field will be addressed in the mouse in future experiments.

Future Directions

This dissertation has provided a foundation for investigating the mechanism by which CST regulates cardiomyocyte differentiation. However, many additional aspects of CST remain to be addressed. For example, we will

analyze the gene expression profile of CST-depleted hearts by cDNA microarray analysis. A cDNA microarray analysis with CST-depleted heart-enriched regions at early tailbud stage 27-28, when CST expression is initiated in the cardiomyocyte progenitors, will potentially provide more transcriptional targets of CST. Although many of the misregulated cDNAs observed could be an indirect consequence of CST-depletion, cDNA microarray analysis has the added benefit of providing insight into CST-mediated molecular pathways based on their altered regulation in CST-depleted tissue.

The dual nature of the CST-depleted cardiomyocyte indicates that CST mediates unique molecular mechanisms within these cells in a spatial and temporal manner. Therefore, it is likely that the specificity of CST function in different cardiomyocyte populations is regulated through interactions with spatially-restricted cofactors. To address this possibility, a yeast two-hybrid screen has been performed with full length CST. This screen has identified two candidate cofactors, Maskin and WRB. Maskin is an acidic coiled-coil domain protein that promotes cell proliferation in the frog by anchoring mitotic spindles to the centrosome of mitotic cells (Albee and Wiese, 2008). The human orthologue of Maskin, TACC3, directly binds directly to FOG1 (Friend of GATA 1) to sequester it in the cytoplasm and inhibit differentiation of the erythroid and megakaryocytic lineages (Garriga-Canut and Orkin, 2004; Sadek et al., 2003). WRB, a tryptophan-rich basic protein, is a candidate gene identified in a region of DNA associated with congenital cardiac defects in Down syndrome patients

(Egeo et al., 1998). WRB is expressed in the endocardial lineage of the fetal heart and in the adult heart (Egeo et al., 1998). However, the role of WRB and Maskin in cardiogenesis is presently unknown and currently being investigated. To isolate additional cofactors, mass spectroscopy will be used to identify cofactors that immunoprecipitate with endogenous CST from *Xenopus* heart-enriched tissue. This provides the additional benefit of identifying endogenous tissue-specific cofactor-CST interactions, which will provide insight into the molecular mechanisms regulated by CST.

Having focused thus far on downstream pathways of CST, it is also necessary to identify upstream regulators of *Cst* expression. To do this, the CST promoter will be identified based on its ability to drive expression of an eGFP transgenic reporter in endogenous CST-expression domains of the heart in the *Xenopus* embryo. Regions of the CST promoter can then be analyzed by mutagenesis to identify the minimal enhancer regions sufficient to drive CST expression in early cardiomyocyte progenitors. These enhancer regions will be further analyzed in available databases, such as TRANSFAC, to identify transcription factor DNA binding sites, which will provide insight into how *Cst* expression is regulated within the cardiomyocyte.

Thus far, we have discussed the characterization of CST in the context of *Xenopus.* However, it is essential to characterize the role of CST in a mammalian system in an effort to translate these findings to human cardiac disease research.

Therefore, two CST mouse strains are presently being constructed. The first strain utilizes the Cre-*loxP* system such that *loxP* sites are inserted surrounding an exon common to both CST isoforms to create a null CST allele when crossed to a transgenic mouse strain expressing a tissue-specific Cre recombinase. For example, the floxed CST mice will be crossed to Nkx2.5-cre transgenic mice to create a null allele of CST in all cells that express Nkx2.5. Upon obtaining homozygous floxed mice ($CST^{fl/fl}$) through breeding, CST will be effectively absent in the cardiomyocytes of the mouse heart. These animals will allow us to examine the role of CST in Nkx2.5-expressing tissues, including the heart and the pharyngeal arches. Similar breeding crosses can be conducted with Myosin Heavy Chain α-cre and Islet1-cre mice to examine the role of CST in the primary and anterior heart fields, respectively.

A second mouse strain has a tamoxifen-inducible Cre recombinase knocked-in to a coding exon of CST, enabling Cre recombinase expression under the endogenous CST promoter in the presence of tamoxifen. The advantage of this CST allele is that it can be crossed to the ROSA26-lacZ indicator mouse strain to lineage-trace CST-expressing cardiomyocytes and their progeny at different stages of heart development. These tamoxifen-inducible CST-cre mice can also be crossed to $CST^{fl/fl}$ mice to generate a tamoxifen-inducible CST knockout strain at different stages of development. For example, CST can be removed at E8.0 when it is expressed in cardiac progenitors of the cardiac crescent or at later gestational time points to determine a later role for

this factor in cardiogenesis. Tamoxifen-inducible CST-cre recombinase mice can also be crossed to the heterozygous floxed CST mice ($CST^{fl/+}$) to observe dosage effects of CST on cardiac development.

With the above CST knockout mice, we will be able to determine the function of CST in mammalian cardiogenesis during discrete periods of development. We hypothesize that the role of CST will be conserved in cardiomyocyte differentiation based on its conserved expression of CST in the developing mouse heart. Investigation of CST in the mouse lends itself to techniques that are otherwise unavailable at this time in *Xenopus*. For example, to compliment the work presented in this dissertation, identification of additional transcriptional targets can be more readily ascertained by performing ChIP-chip, namely CST chromatin immunoprecipitation followed by genomic DNA chip analysis. Identification of additional CST transcriptional targets by genomic chip analysis will likely provide more putative targets in comparison to the cloning ChIP screen and will greatly advance our understanding of how CST regulates cardiomyocyte differentiation. Investigation of CST in the mouse also allows for the isolation and manipulation of CST-expressing primary cardiomyocytes *in vitro*. For example, to investigate the hypothesis that CST regulates cardiomyocyte cell growth, these primary cardiomyocytes could be sorted by flow cytometry and then analyzed for their cell cycle profile. Likewise, the primary cardiomyocytes could be supplemented with growth factors to determine potential upstream signaling pathways that may regulate CST function in

cardiogenesis. Most importantly, these CST knockout mouse will serve as a model to investigate the function of CST in the human population. The cardiac defects observed in these mice will provide valuable information that may implicate CST as a candidate gene associated with a human congenital cardiac defect and/or syndrome.

Human CST is located in the 1p36 region of chromosome 1 approximately 8.6 Mbp from the telomeric region. Human patients with a 10.5-11.1 Mbp terminal deletion of 1p36 on chromosome 1 present with left-ventricular non-compaction (LVNC) and Epstein's anomaly (Kurosawa et al., 2005; Saito et al., 2008). LVNC is characterized as excessive ventricular trabeculation with deep intertrabecular recesses which is hypothesized to be due to abnormal endocardial function (Finsterer et al., 2006; Xing et al., 2006). Epstein's anomaly is a malformation of the tricuspid valve between the right atrium and right ventricle resulting in regurgitation of deoxygenated blood between the two chambers and hampered delivery of the deoxygenated blood to the lungs. Since CST is within this deleted chromosomal segment, CST is a candidate gene for mutation leading to LVNC and Epstein's anomaly. However, finer mapping of the chromosomal region is necessary to determine the gene(s) responsible for these cardiomyopathies.

CASTOR as a therapeutic agent

Zinc finger transcription factors, specifically the Cys_2-His_2 type, are at the forefront of molecular therapeutics. Zinc finger domains are now being used to

synthesize novel engineered artificial transcription factors that are designed to manipulate the genome (Blancafort and Beltran, 2008). Based on crystal structure analysis, most Cys_2-His_2 zinc finger domains make three DNA contacts through the α-helix, while the two β-sheets maintains a three-dimensional structure, in part, by coordinating a zinc ion (Wolfe et al., 2000). Together with crystal structure analysis, DNA binding sequences (DBS) of many zinc finger transcription factors have provided a library of zinc finger domains and their associated DBS. The independent modular nature of zinc finger domains has promoted the engineering of artificial zinc finger transcription factors composed of multiple zinc finger domains with the anticipation of creating a protein that can specifically target a predetermined DNA sequence within the genome. To provide specificity to the artificial factor, they are usually composed of multiple zinc finger domains in an effort to increase the size of the DBS to approximately 16 bp (Blancafort and Beltran, 2008). As a result, non-specific binding is greatly reduced. The artificial zinc finger transcription factors have been designed to alter the transcriptome of a cell by attaching effector domains. Thus far, transcriptional activators, repressors, DNA methyltransferases and endonucleases have been used successfully to modify the genome and/or alter transcription of endogenous target genes. For example, DBSs in the promoter, as well as the 5’ and 3’ untranslated region, of VEGF were targeted by artificial zinc finger transcription factors resulting in the upregulation of VEGF-A transcription in HEK293 cells and in the ears of mice, where it promoted new blood vessel growth (Liu et al., 2001; Rebar et al., 2002). An artificial VEGF-A

factor is being tested currently in clinical trials for promotion of blood vessel growth to alleviate peripheral arterial disease (Klug, 2005).

This technology can also be used in gene therapy applications to replace a defective gene by homologous recombination. Homologous recombination within a targeted locus is more efficient in the presence of nearby double-stranded DNA breaks. Therefore, site-specific nucleases that target the damaged locus in close proximity to the restriction sequence have been engineered onto an artificial factor. In this manner, the mutation associated with the human X-linked Severe Combined Immune Deficiency (SCID) syndrome was corrected by homologous recombination in 15% of somatic K562 cells (Klug, 2005).

The uniqueness of the para-zinc finger domains of CST makes them attractive candidates for incorporation into artificial zinc finger transcription factor libraries. Additionally, the potential ability of CST to coordinate two zinc ions may provide an advantage, such as stability and/or specificity, over the classical Cys_2-His_2 zinc finger domain. To do this, the crystal structure of the para-zinc finger domains of CST would need to be resolved to identify the amino acids that establish contact with the DBS determined in Chapter 3. If CST does indeed regulate cell growth and/or cell adhesion, its DBS may be found in the endogenous promoter or untranslated regions of dysregulated genes in cancer and/or cardiovascular disease. Likewise, if the para-zinc finger configuration provides an advantage for artificial zinc finger transcription factors, the five para-

zinc fingers could be manipulated to forge specificity to a predetermined DBS to alter expression of a gene of interest. Therefore, CST in the context of an artificial zinc finger transcription factor may provide a future therapeutic treatment for human disease in the future.

REFERENCES

Albee, A. J., and Wiese, C. (2008). Xenopus TACC3/maskin is not required for microtubule stability but is required for anchoring microtubules at the centrosome. Mol Biol Cell *19*, 3347-3356.

Blancafort, P., and Beltran, A. S. (2008). Rational design, selection and specificity of artificial transcription factors (ATFs): the influence of chromatin in target gene regulation. Comb Chem High Throughput Screen *11*, 146-158.

Brade, T., Gessert, S., Kuhl, M., and Pandur, P. (2007). The amphibian second heart field: Xenopus islet-1 is required for cardiovascular development. Dev Biol *311*, 297-310.

Cai, C. L., Liang, X., Shi, Y., Chu, P. H., Pfaff, S. L., Chen, J., and Evans, S. (2003). Isl1 identifies a cardiac progenitor population that proliferates prior to differentiation and contributes a majority of cells to the heart. Dev Cell *5*, 877-889.

Christine, K. S., and Conlon, F. L. (2008). Vertebrate CASTOR is required for differentiation of cardiac precursor cells at the ventral midline. Dev Cell *14*, 616-623.

Cohen, E. D., Wang, Z., Lepore, J. J., Lu, M. M., Taketo, M. M., Epstein, D. J., and Morrisey, E. E. (2007). Wnt/beta-catenin signaling promotes expansion of Isl-1-positive cardiac progenitor cells through regulation of FGF signaling. J Clin Invest *117*, 1794-1804.

Cui, X., and Doe, C. Q. (1992). ming is expressed in neuroblast sublineages and regulates gene expression in the Drosophila central nervous system. Development *116*, 943-952.

Danilova, N., Sakamoto, K. M., and Lin, S. (2008). p53 family in development. Mech Dev *125*, 919-931.

De La Cruz, M. V., Sanchez-Gomez, C., and Palomino, M. A. (1989). The primitive cardiac regions in the straight tube heart (Stage 9) and their anatomical expression in the mature heart: An experimental study in the chick embryo. J Anat *165*, 121-131.

Deb, A., Davis, B. H., Guo, J., Ni, A., Huang, J., Zhang, Z., Mu, H., and Dzau, V. J. (2008). SFRP2 regulates cardiomyogenic differentiation by inhibiting a positive transcriptional autofeedback loop of Wnt3a. Stem Cells *26*, 35-44.

Doyle, K., Hogan, J., Lester, M., and Collier, S. (2008). The Frizzled Planar Cell Polarity signaling pathway controls Drosophila wing topography. Dev Biol *317*, 354-367.

Dulic, V., Kaufmann, W. K., Wilson, S. J., Tlsty, T. D., Lees, E., Harper, J. W., Elledge, S. J., and Reed, S. I. (1994). p53-dependent inhibition of cyclin-dependent kinase activities in human fibroblasts during radiation-induced G1 arrest. Cell *76*, 1013-1023.

Egeo, A., Mazzocco, M., Sotgia, F., Arrigo, P., Oliva, R., Bergonon, S., Nizetic, D., Rasore-Quartino, A., and Scartezzini, P. (1998). Identification and characterization of a new human cDNA from chromosome 21q22.3 encoding a basic nuclear protein. Hum Genet *102*, 289-293.

Finsterer, J., Stollberger, C., and Blazek, G. (2006). Neuromuscular implications in left ventricular hypertrabeculation/noncompaction. Int J Cardiol *110*, 288-300.

Garriga-Canut, M., and Orkin, S. H. (2004). Transforming acidic coiled-coil protein 3 (TACC3) controls friend of GATA-1 (FOG-1) subcellular localization and regulates the association between GATA-1 and FOG-1 during hematopoiesis. J Biol Chem *279*, 23597-23605.

Garriock, R. J., D'Agostino, S. L., Pilcher, K. C., and Krieg, P. A. (2005). Wnt11-R, a protein closely related to mammalian Wnt11, is required for heart morphogenesis in Xenopus. Dev Biol *279*, 179-192.

Goetz, S. C., Brown, D. D., and Conlon, F. L. (2006). TBX5 is required for embryonic cardiac cell cycle progression. Development *133*, 2575-2584.

Grier, J. D., Xiong, S., Elizondo-Fraire, A. C., Parant, J. M., and Lozano, G. (2006). Tissue-specific differences of p53 inhibition by Mdm2 and Mdm4. Mol Cell Biol *26*, 192-198.

Kambadur, R., Koizumi, K., Stivers, C., Nagle, J., Poole, S. J., and Odenwald, W. F. (1998). Regulation of POU genes by castor and hunchback establishes layered compartments in the Drosophila CNS. Genes Dev *12*, 246-260.

Kelly, R. G., Brown, N. A., and Buckingham, M. E. (2001). The arterial pole of the mouse heart forms from Fgf10-expressing cells in pharyngeal mesoderm. Dev Cell *1*, 435-440.

Klug, A. (2005). Towards therapeutic applications of engineered zinc finger proteins. FEBS Lett *579*, 892-894.

Kurosawa, K., Kawame, H., Okamoto, N., Ochiai, Y., Akatsuka, A., Kobayashi, M., Shimohira, M., Mizuno, S., Wada, K., Fukushima, Y.*, et al.* (2005). Epilepsy and neurological findings in 11 individuals with 1p36 deletion syndrome. Brain Dev *27*, 378-382.

Langdon, Y. G., Goetz, S. C., Berg, A. E., Swanik, J. T., and Conlon, F. L. (2007). SHP-2 is required for the maintenance of cardiac progenitors. Development.

Lin, L., Cui, L., Zhou, W., Dufort, D., Zhang, X., Cai, C. L., Bu, L., Yang, L., Martin, J., Kemler, R.*, et al.* (2007). Beta-catenin directly regulates Islet1 expression in cardiovascular progenitors and is required for multiple aspects of cardiogenesis. Proc Natl Acad Sci U S A *104*, 9313-9318.

Liu, P. Q., Rebar, E. J., Zhang, L., Liu, Q., Jamieson, A. C., Liang, Y., Qi, H., Li, P. X., Chen, B., Mendel, M. C.*, et al.* (2001). Regulation of an endogenous locus using a panel of designed zinc finger proteins targeted to accessible chromatin regions. Activation of vascular endothelial growth factor A. J Biol Chem *276*, 11323-11334.

Meilhac, S. M., Kelly, R. G., Rocancourt, D., Eloy-Trinquet, S., Nicolas, J. F., and Buckingham, M. E. (2003). A retrospective clonal analysis of the myocardium reveals two phases of clonal growth in the developing mouse heart. Development *130*, 3877-3889.

Mellerick, D. M., Kassis, J. A., Zhang, S. D., and Odenwald, W. F. (1992). castor encodes a novel zinc finger protein required for the development of a subset of CNS neurons in Drosophila. Neuron *9*, 789-803.

Milner, J., Cook, A., and Mason, J. (1990). p53 is associated with p34cdc2 in transformed cells. Embo J *9*, 2885-2889.

Mjaatvedt, C. H., Nakaoka, T., Moreno-Rodriguez, R., Norris, R. A., Kern, M. J., Eisenberg, C. A., Turner, D., and Markwald, R. R. (2001). The outflow tract of the heart is recruited from a novel heart-forming field. Dev Biol *238*, 97-109.

Mohun, T. J., Leong, L.M., Weninger, W. J., and Sparrow, D. B. (2000). The Morphology of Heart Development in Xenopus laevis. Developmental Biology *218*, 74-88.

Monkley, S. J., Delaney, S. J., Pennisi, D. J., Christiansen, J. H., and Wainwright, B. J. (1996). Targeted disruption of the Wnt2 gene results in placentation defects. Development *122*, 3343-3353.

Prall, O. W., Menon, M. K., Solloway, M. J., Watanabe, Y., Zaffran, S., Bajolle, F., Biben, C., McBride, J. J., Robertson, B. R., Chaulet, H.*, et al.* (2007). An Nkx2-5/Bmp2/Smad1 negative feedback loop controls heart progenitor specification and proliferation. Cell *128*, 947-959.

Rebar, E. J., Huang, Y., Hickey, R., Nath, A. K., Meoli, D., Nath, S., Chen, B., Xu, L., Liang, Y., Jamieson, A. C.*, et al.* (2002). Induction of angiogenesis in a mouse model using engineered transcription factors. Nat Med *8*, 1427-1432.

Sadek, C. M., Pelto-Huikko, M., Tujague, M., Steffensen, K. R., Wennerholm, M., and Gustafsson, J. A. (2003). TACC3 expression is tightly regulated during early differentiation. Gene Expr Patterns *3*, 203-211.

Saito, S., Kawamura, R., Kosho, T., Shimizu, T., Aoyama, K., Koike, K., Wada, T., Matsumoto, N., Kato, M., Wakui, K., and Fukushima, Y. (2008). Bilateral perisylvian polymicrogyria, periventricular nodular heterotopia, and left ventricular noncompaction in a girl with 10.5-11.1 Mb terminal deletion of 1p36. Am J Med Genet A *146A*, 2891-2897.

Soufan, A. T., van den Berg, G., Ruijter, J. M., de Boer, P. A., van den Hoff, M. J., and Moorman, A. F. (2006). Regionalized sequence of myocardial cell growth and proliferation characterizes early chamber formation. Circ Res *99*, 545-552.

Vacalla, C. M., and Theil, T. (2002). Cst, a novel mouse gene related to Drosophila Castor, exhibits dynamic expression patterns during neurogenesis and heart development. Mech Dev *118*, 265-268.

Wolfe, S. A., Nekludova, L., and Pabo, C. O. (2000). DNA recognition by Cys2His2 zinc finger proteins. Annu Rev Biophys Biomol Struct *29*, 183-212.

Xing, Y., Ichida, F., Matsuoka, T., Isobe, T., Ikemoto, Y., Higaki, T., Tsuji, T., Haneda, N., Kuwabara, A., Chen, R.*, et al.* (2006). Genetic analysis in patients with left ventricular noncompaction and evidence for genetic heterogeneity. Mol Genet Metab *88*, 71-77.

Xiong, S., Van Pelt, C. S., Elizondo-Fraire, A. C., Fernandez-Garcia, B., and Lozano, G. (2007). Loss of Mdm4 results in p53-dependent dilated cardiomyopathy. Circulation *115*, 2925-2930.

Appendix 1

Developmental expression patterns of *Tbx1, Tbx2, Tbx5* and *Tbx20* in *Xenopus tropicalis*

Developmental Expression Patterns of *Tbx1, Tbx2, Tbx5* and *Tbx20* in *Xenopus tropicalis*, Chris Showell, Kathleen S. Christine, Elizabeth M. Mandel, and Frank Conlon, Developmental Dynamics, Volume 235, 1623-1630, 2006. Reprinted with permission of Wiley-Liss, Inc. a subsidiary of John Wiley & Sons, Inc.

ABSTRACT

T-box genes have diverse functions during embryogenesis and are implicated in several human congenital disorders. Here we report the identification, sequence analysis and developmental expression patterns of four members of the T-box gene family in the diploid frog *Xenopus tropicalis*. These four genes – *Tbx1*, *Tbx2*, *Tbx5* and *Tbx20* – have been shown to influence cardiac development in a variety of organisms, in addition to their individual roles in regulating other aspects of embryonic development. Our results highlight the high degree of evolutionary conservation between orthologues of these genes in *X.tropicalis* and other vertebrates, both at the molecular level and in their

developmental expression patterns, and also identify novel features of their expression. Thus, *X.tropicalis* represents a potentially valuable vertebrate model in which to further investigate the functions of these genes through genetic approaches.

INTRODUCTION

DNA-binding transcription factors encoded by several members of the T-box gene family have been shown to have both cell-autonomous and non-cell autonomous roles in controlling the development of the heart during embryogenesis (Plageman and Yutzey, 2005; Stennard et al., 2005). These roles appear to be conserved during evolution and, in some cases, their importance is highlighted by the association between mutations in these factors and the incidence of human congenital heart defects (Mandel et al., 2005; Packham and Brook, 2003; Ryan and Chin, 2003). In addition, the same genes have been shown to be required for the proper development of other tissues and organs, such as the eye (*Tbx5*) (Koshiba-Takeuchi et al., 2000) and ear (*Tbx1*) (Liao et al., 2004; Lindsey et al., 2001; Moraes et al., 2005; Piotrowski et al., 2003; Raft et al., 2004), while other T-box genes have key roles in regulating early embryonic patterning (Showell et al., 2004).

Xenopus is a valuable model organism in which to investigate the molecular and genetic regulation of organogenesis in general and heart development in particular, and reverse genetic approaches have recently been

developed to isolate mutant alleles in specific genes of interest in the diploid frog *Xenopus (Silurana) tropicalis*. In comparison with the zebrafish (*Danio rerio*), *Xenopus* cardiac morphology is more similar to that of humans, including septation of the atrium into left and right chambers (Hu et al., 2000; Mohun et al., 2000). Also, the accessibility of the embryo throughout development and the high fecundity of the frog are significant advantages over the mouse, both in embryological analysis and in genetic screening.

The genes analyzed here – *Tbx1, Tbx2, Tbx5 and Tbx20* – are all known to play important roles in regulating normal cardiac development. *TBX1* lies within a critical region of human chromosome 22 (22q11.2) that is deleted in patients with DiGeorge syndrome, and loss of Tbx1 function in the mouse mimics the severe morphological defects of the outflow tract of the heart that are seen in DiGeorge patients (Jerome and Papaioannou, 2001; Lindsay et al., 2001). Similarly, mutations in the human *TBX5* gene are associated with Holt-Oram syndrome, affecting atrioventricular septation, the cardiac conduction system and the development of the upper limbs (Basson et al., 1997; Li et al., 1997). *Tbx5* has been shown to act in concert with *Tbx20* at the molecular level to control cardiac morphogenesis (Brown et al., 2005). Conversely, *Tbx5* and *Tbx2* appear to function within distinct domains of the developing heart, contributing to the patterning of the early heart tube and its subsequent morphological regionalization. A number of recent studies have also demonstrated a requirement for *Tbx20* function for proper regulation of *Tbx2* expression within

the developing heart (Cai et al., 2005; Singh et al., 2005; Stennard et al., 2005). As a preliminary step in investigating the molecular basis of their developmental roles through genetic analysis in the emerging model organism *Xenopus tropicalis*, we have identified cDNA clones containing full-length coding sequences corresponding to these four T-box genes, determined the structure of their genomic loci *in silico*, and characterized their spatial expression patterns over a wide range of stages during embryogenesis. Our results demonstrate the high degree of sequence conservation of T-box gene orthologues in *Xenopus tropicalis*
and highlight both conserved and previously undescribed aspects of their embryonic expression.

MATERIAL AND METHODS

Identification and isolation of cDNA clones

cDNA clones TNeu106g11, TGas050k23 and TTpA031n09, encoding *X.tropicalis* orthologues of Tbx1, Tbx2 and Tbx20 respectively, were identified by searching a database of *X.tropicalis* expressed sequence-tagged clones derived from oligo-dT primed cDNA libraries specific to several developmental stages (www.sanger.ac.uk; (Gilchrist et al., 2004)). Specifically, nucleotide sequences from the 5' ends of the coding regions of the corresponding *X.laevis* orthologues (*Tbx1* Genbank Acc. # AF526274; *Tbx2* Genbank Acc. # AB023815; *Tbx20* Genbank Acc. # AY154394) were used to BLAST search (Altschul et al., 1990) for *X.tropicalis* clones containing the predicted translation start codon and which

were therefore likely to contain full-length cDNAs. The clones were obtained (MRC Geneservice) and the cDNA inserts were sequenced. A cDNA encoding Tbx5 was cloned by low-stringency RT-PCR, using total RNA template from stage 13-20 *X.tropicalis* embryos. Primers were designed based on sequences flanking the *X.laevis Tbx5* coding sequence (forward: 5'-GAAGATCTATGGCGGACACAGAGGAGGCT-3'; reverse: 5'-GAGAGATCTACGCTGTTTTCATTCCAGTCTGG-3'). The resulting product was cloned into *pcDNA3.1* (Invitrogen Corp.). All cDNA sequences are deposited in Genbank (*Tbx1* accession # DQ124205; *Tbx2* accession # DQ124206; *Tbx5* accession # DQ124207; *Tbx20* accession # DQ124208).

In silico analysis

To identify genomic sequence scaffolds corresponding to *Tbx1*, *Tbx2*, *Tbx5* and *Tbx20*, the corresponding cDNA sequences were used to search the *X.tropicalis* draft genome sequence (versions 2.0 and 3.0) using the BLAST algorithm (Altschul et al., 1990) (DoE Joint Genome Institute). Pairwise sequence alignments and analyses of sequence conservation of conceptually translated proteins were performed using GeneDoc (www.psc.edu/biomed/genedoc).

Embryo collection and *in situ* hybridization

X.tropicalis embryos were collected following natural single-pair mating between animals from a partially inbred (F6) line (NASCO). Males and females were pre-primed with ten units of human chorionic gonadotropin (hCG; SIGMA)

twenty hours before being primed with an additional two hundred units. One hour after priming, males and females were paired and allowed to mate for approximately five hours in shallow water at 25ºC. Embryos and unfertilized eggs from successful matings were collected, treated with 2% cysteine hydrochloride to remove their jelly coat, and sorted. Embryos were cultured at 25ºC in sterilized water from our aquatic system and staged according to criteria set out in the Normal Table of *Xenopus laevis* (Nieuwkoop and Faber, 1967).

A 908bp *KpnI-XhoI* fragment of the *Tbx1* EST clone was subcloned into *pBluescript-KS* and this construct was linearized with *Acc657* to generate a template for in situ hybridization probe synthesis. Template for *Tbx2* probe synthesis was produced by linearizing the full-length cDNA clone described above using *HindIII*. The *Tbx5* cDNA was cut from *pcDNA3.1-Tbx5* by *NotI-SpeI* digest and sub-cloned into *pBluescript-KS* to generate a probe template construct that was subsequently linearized with *NotI*. To generate a template for *Tbx20* probe synthesis, a 565bp *SalI-NotI* fragment from the *Tbx20* EST clone was sub-cloned into *pBluescript-KS* and the construct linearized using *SalI*. In situ hybridizations were performed according to a standard protocol (Sive et al., 2000) with the following exceptions: Fixed embryos were devitellinized by enzymatic treatment with collagenase A (Roche Applied Science), proteinase K and hyaluronidase (SIGMA) (Islam, 1996). No further proteinase K treatment was performed. Embryos were pre-hybridized overnight (approx. 15 hours) and the RNase treatment step prior to antibody incubation was omitted (Khokha et al.,

2002). After staining with BM Purple alkaline phosphatase substrate (Roche Diagnostics), embryos were re-fixed in 1X MEM salts containing 10% formamide and then dehydrated in methanol.

Where necessary, embryos were cleared in 2:1 benzyl benzoate:benzyl alcohol (SIGMA). Embryos were photographed on a Leica M-series stereomicroscope (Leica Microsystems Ltd.) using the Spot Advanced image capture system (Diagnostic Instruments Inc.) and edited using Photoshop 7.0 (Adobe Systems Inc.).

Cryosectioning

For cryosectioning, embryos were embedded in gelatin using a method modified from Stern and Holland (Izpisúa-Belmonte et al., 1993). Following *in situ* hybridization, embryos were fixed in 4% paraformaldehyde in PBS and incubated overnight at 4ºC in 30% sucrose/PBS (w/v). The embryos were then pre-warmed to 38ºC before being transferred to 15% sucrose/PBS containing 7.5% gelatin (~300 Bloom; SIGMA) at 38ºC. Embryos were incubated in gelatin for a minimum of thirty minutes before being transferred to specimen molds (Tissue-Tek; Sakura Finetek U.S.A., Inc.). Embedded embryos were stored at 4ºC prior to cryosectioning. Sections were taken at a thickness of 20µm. Gelatin was rinsed from the sections using PBS at 38ºC before mounting in aqueous mounting medium (Faramount; DakoCytomation).

RESULTS AND DISCUSSION

Sequence analysis of *Xenopus tropicalis* T-box gene orthologues

cDNA clones corresponding to *Tbx1*, *Tbx2* and *Tbx20* were identified by BLAST searches within a database of *Xenopus tropicalis* expressed sequence tags and a clone containing the translation initiation codon was obtained and sequenced for each gene. A cDNA encoding the *X.tropicalis* orthologue of Tbx5 was cloned by RT-PCR and sequenced. These cDNA sequences were used to search the *X.tropicalis* draft genome sequence (DoE Joint Genome Institute) for genomic scaffolds containing the corresponding loci. The cDNA sequences were then mapped onto the genomic locus sequences and the exon/intron boundaries were identified based on consensus sequences for eukaryotic splice donor and acceptor sites (Stemple et al., 1996).

All four *Xenopus tropicalis* cDNA clones exhibit a very high degree of sequence identity when compared with their *Xenopus laevis* orthologues, particularly within their coding regions. The 1389nt open reading frame within the 3065bp *Tbx1* cDNA is 94% identical to that of *Xenopus laevis Tbx1* (Genbank Acc. # AF526274) (89% identity in untranslated regions). The degrees of identity and similarity between the conceptually translated *Xenopus tropicalis Tbx1* coding sequence and several vertebrate orthologues are shown in Table A1.1. The results of our analysis of the genomic *Tbx1* locus are shown in Figure A1.1a.

The 3510bp *Tbx2* cDNA identified here contains a 2055nt open reading frame with 94% identity to *Xenopus laevis Tbx2* (Genbank Acc. # AB032941) (86% identity in untranslated regions). Table A1.1 shows the degrees of identity and similarity between conceptually translated *Xenopus tropicalis* Tbx2 and vertebrate orthologues. Mapping of the *Tbx2* cDNA sequence to the available genome sequence identified a 14,129bp region containing the complete cDNA sequence divided amongst seven exons (Fig. A1.1b).

Xenopus tropicalis Tbx5 is encoded by a 1557nt open reading frame. Alignment of this sequence with the *Xenopus laevis Tbx5* cDNA (Genbank Acc. # AF133036) identified 93% nucleotide sequence identity between the coding regions of the two orthologues. The *Xenopus tropicalis Tbx5* cDNA encodes a product exhibiting a high degree of evolutionary conservation amongst vertebrate species (Table A1.1). Results obtained from *in silico* analysis of the *Tbx5* genomic locus are shown in Figure A1.1c.

The *Tbx20* cDNA clone obtained consists of 2117bp, containing a 1320nt open reading frame with 93% sequence identity to that of *Xenopus laevis Tbx20* (Genbank Acc. # AY154394) (75% identity in untranslated regions). Table A1.1 shows the degree of sequence identity and similarity between conceptually translated *Xenopus tropicalis* Tbx20 and its orthologues in other vertebrates. The *Tbx20* sequence was found to be divided amongst eight exons within a 19,354bp region of a single genomic scaffold (Fig. A1.1d).

Analysis of *Tbx1* expression during embryogenesis

Tbx1 function is required for normal heart development in vertebrates. It is thought to act indirectly, influencing the differentiation of migrating cardiac neural crest cells by regulating the expression of one or more intercellular signals emanating from *Tbx1*-expressing cells in the pharyngeal endoderm and the mesenchymal core of the pharyngeal arches (Kochilas et al., 2005). The cardiac neural crest cells contribute to the formation of the outflow tract of the heart and the development of this region is severely affected in DiGeorge patients and in mouse models of the syndrome. Initial analysis of the phenotype of a hypomorphic $Tbx1^{neo}$ allele in the mouse suggests that the observed alignment and septation defects of the outflow tract are independent, thus underscoring the value of analyzing more subtle alleles in addition to single gene knockouts and larger deletions in vertebrate models (Xu et al., 2005). To determine the spatial patterns of *Tbx1* mRNA expression during the course of *X.tropicalis* embryogenesis, whole mount in situ hybridization was performed. At the earliest stage analyzed, stage 10.5 (early gastrula), no expression of *Tbx1* was detected. In early neurulae (stage 13), regionally restricted expression was clearly detected in a broad anterior domain surrounding the anterior end of the medio-dorsal groove of the neural plate (Fig. A1.2a). Within this broad ectodermal domain, two bilateral patches of strong *Tbx1* expression were detected flanking the medio-dorsal groove (Fig. A1.2a,c). These patches marked the posterior boundary of the *Tbx1* expression domain. In late neurulae (stage 19), strong expression was detected in the anterior ectoderm (Fig. A1.2d-f). This expression domain

appeared to largely exclude the central nervous system, commonly defined by the expression of pan-neural markers such as the neural cell adhesion molecule (N-CAM) (Eagleson et al., 1995). Expression was not detected in the developing eye anlagen and cement gland, and was only weakly detected in the region of the neural tube posterior to the eye anlagen. Instead, expression of *Tbx1* was found to immediately abut these regions of the ectoderm. As at stage 13, two distinct bilateral regions of strong staining were observed within the *Tbx1* expression domain at stage 19, extending as approximately dorsoventral stripes in the ectoderm on either side of the anterior CNS. It is unclear whether this *Tbx1* expression domain corresponds to the location of the proposed primordium of the ectodermal (neurogenic) placodes (Schlosser and Ahrens, 2004; Schlosser and Northcutt, 2000). At early tailbud stage (stage 25), *Tbx1* was found to be expressed in three distinct areas within the pharyngeal region and in the ventral region of each otic vesicle (Fig. A1.2g,h). At stage 33, expression within the otic vesicles extended further laterally (Fig. A1.2n). However, in subsequent stages (stages 40, 47) expression remained restricted to the ventral and lateral regions of the vesicles. This differs from the pattern reported for *X.laevis*, in which *Tbx1* appeared to be expressed throughout the vesicles (Ataliotis et al., 2005).

Expression of *Tbx1* orthologues in the pharyngeal region is broadly conserved amongst vertebrate species. Between stages 25 and 33, the elaboration of the expression pattern of *Tbx1* in this region of the *X.tropicalis* embryo reflects the morphogenesis of the pharyngeal arches. In this region, the

cells expressing *Tbx1* lay beneath the overlying epidermis. At stages 25 and 26, expression was detected in the mandibular and hyoid arches (Fig. A1.2g,h,i) and in a third domain corresponding to the future branchial arches, posterior to the hyoid arch. At stage 27, at which the first branchial arch becomes fully formed, *Tbx1* expression was detected in four distinct pharyngeal domains – the mandibular, hyoid and first branchial arches and a more posterior branchial region (Fig. A1.2j,k). By stage 33, expression was also detected in the second branchial arch (Fig. A1.2n). At this stage, *Tbx1* appears to mark distinct dorsal and ventral regions within the hyoid, first branchial, second branchial and forming third branchial arches.

Analysis of *Tbx2* expression during embryogenesis

In situ hybridization showed that, as in *X.laevis* (Hayata T, 1999), *Tbx2* is expressed ventrally in *X.tropicalis* early gastrulae (stage 10.5) (Fig. A1.3a,b). However, in contrast to the reported expression in *X.laevis*, *Tbx2* is expressed most strongly in the outer layer of ectodermal cells in *X.tropicalis* (Fig. A1.3c). In dissected wholemount embryos and in cryosectioned embryos (Fig. A1.3c), very faint staining was observed in the underlying ventral mesoderm. At the late gastrula stage (stage 12), expression appeared to be consistently upregulated in a small group of cells clustered around the ventral edge of the closing blastopore (Fig. A1.3d). At the early neurula stage (stage 13), four regions of ectodermal expression were clearly detected. Strong staining was observed in the developing cement gland (Fig. A1.3e) and in a U-shaped domain around the

proctodeum at the posterior of the embryo (Fig. A1.3g). Two bilateral patches of expression were seen in the head, at the edge of the neural plate, in the region of the future neurogenic placodes caudal to the eye anlagen (Fig. A1.3f,g). It is unclear whether this domain includes both the profundal-trigeminal placodal area and the dorsolateral placodes. In *Xenopus*, the dorsolateral placodes give rise to the lateral line placodes and the otic placodes at later stages (Schlosser and Northcutt, 2000). Finally, a diffuse pattern of *Tbx2*-positive cells was seen in the ventral epidermis (Fig. A1.3h, j-l). At stage 19 (late neurula), expression persists in the cement gland, the ventral epidermis, the proctodeal region, the lens placodes, and in a broad placodal area caudal to the eye anlagen (Fig. A1.3h-l). In addition, expression was detected in the dorsal root ganglia of the future spinal cord (Fig. A1.3i). At stage 21/22, *Tbx2* expression was seen in a wishbone-shaped group of cells situated dorsal and caudal to each developing optic vesicle (Fig. A1.3m), corresponding to the cranial (profundal and trigeminal) ganglia. Expression was found to persist in these cells through tailbud and into early tadpole stages (Fig. A1.3n-r). From stage 21/22 onwards, the bilateral expression of *Tbx2* in the ectodermal placodes became restricted primarily to the otic placode and the developing otic vesicles. Unlike *Tbx1*, *Tbx2* was found to be expressed throughout the otic vesicles, and this expression was detected at all subsequent stages analyzed (stages 24 to 40). At stage 24, additional staining was observed in the precursors of the hypaxial muscles and the pronephric duct in the trunk, in the developing branchial arches, and in the primordium of the heart (Fig. A1.3o,p). A small group of cells within the telencephalon is also

stained at this stage (Fig. A1.3o-r). In stage 29 embryos, expression was clearly detected in the frontonasal process (Fig. A1.3q). *Tbx2* continues to be expressed in the same regions of the embryo at stage 33, although its expression becomes clearly regionalized in the looping heart. A higher level of expression was clearly detected in the ventricle compared with the atrium, as reported in other organisms (Fig. A1.3r).

Analysis of *Tbx5* expression during embryogenesis

The expression pattern of *Tbx5* was analyzed at developmental stages from mid-gastrula (stage 11) to early tadpole (st40). No expression was detected at stage 11. In late neurulae (stage 19), a gradient of *Tbx5* expression was present within the eye anlagen, with higher levels dorsally (Fig. A1.4a,b). At this stage, two small patches of cells on either side of the embryo were also stained, corresponding to regions within the migrating bilateral heart primordia. At early tailbud stage (stage 25), this pattern of expression was maintained in a dorsal region of each developing eye (Fig. A1.4c) and in the heart primordia, located ventrally (Fig. A1.4c,d). In stage 26 embryos, the *Tbx5*-expressing cells of the heart primordia were seen to converge at the ventral midline (Fig. A1.4f), while expression was also detected in two bilateral groups of cells continuous with and extending dorsally from the heart primordia. These cells likely correspond to the progenitors of the right and left branches of the sinus venosus and common cardinal veins (Horb and Thomsen, 1999; Nieuwkoop and Faber, 1967). In other organisms, *Tbx5* has been shown to play an important role in eye development,

particularly in guiding the projection of neurons between the retina and tectum (Koshiba-Takeuchi et al., 2000). In *X.tropicalis*, expression in the dorsal region of the eye was found to be maintained until early tadpole stages (stage 40), although its expression becomes greatly restricted between stages 33 and 40 (Fig. A1.4h,i). At stage 31/32, strong expression was detected in the posterior region of the heart tube in cleared embryos (Fig. A1.4g). Following looping of the heart, a higher level of expression was detected in the ventricle (situated ventrally and offset to the left side of the embryo) than in the atrium (Fig. A1.4j). The regional differences in the expression of *Tbx5* within the hearts of *X.tropicalis* tadpoles were seen consistently in both wholemount and sectioned embryos. Transverse sections through the heart at stages following heart looping showed expression of *Tbx5* in the ventricular myocardium, while staining was not detected in the atrial region of the heart (Fig. A1.6b).

Analysis of *Tbx20* expression during embryogenesis

The expression pattern of *X.tropicalis Tbx20* was analyzed in embryos between stages 13 (neural plate stage) and 40 (early tadpole). Although expressed weakly in the developing cement gland as early as stage 13 in *X.laevis* (Brown et al., 2003), we did not detect expression at this stage in *X.tropicalis*. At late neurula stage (stage 20), *Tbx20* was strongly expressed in the developing cement gland and in the bilateral heart primordia (Fig. A1.5a-c). Expression in the cement gland was found to decrease from stage 25 onwards, while expression continued to be strongly detected in the developing heart. In

the heart-forming region at stage 25, a single domain of expression was detected, corresponding to the heart field formed by fusion of the bilateral heart primordial (Fig. A1.5e). This fusion of the *Tbx20*-expressing domains appears to occur earlier in *X.tropicalis* than in *X.laevis*. Notably, this pattern of expression differs considerably from that of *Tbx5*, in which fusion of the bilateral pre-cardiac expression domains begins at around stage 26 (see above). In addition to this cardiac expression, two small domains of expression were observed in the hindbrain (rhombencephalon) at this stage, corresponding to the second and fourth rhombomeres. At stage 29/30, expression persisted in these regions and was also weakly detected in a more posterior region of the hindbrain (Fig. A1.5f). The hindbrain expression of *Tbx20* was found to be upregulated in embryos at subsequent stages and, as in more anterior regions, was detected in distinct paired subdomains (Fig. A1.5g,j,k,m,n). At stage 33, when heart looping is initiated, *Tbx20* was found to be broadly expressed in the heart tube, with strong staining detected in the ventricle, atrium and both branches of the sinus venosus (inflow tract) (Fig. A1.5g,i). Thus, the expression domain of *Tbx20* in the developing chambers of the heart tube only partially overlaps that of *Tbx5*. This is consistent with the patterns of *Tbx20* expression reported in other vertebrates (Ahn et al., 2000; Brown et al., 2003; Kraus et al., 2001; Plageman and Yutzey, 2004; Yamagishi et al., 2004). During heart looping (stage 36), *Tbx20* was expressed at a higher level in the atrium than in the ventricle (Fig. A1.5l). This regional difference in the expression level of *Tbx20* was maintained in early

tadpole stage embryos (stage 40) and was clearly seen both in whole embryos and in transverse sections through the heart (Fig. A1.5o., 6c).

Table A.1 Sequence conservation of T-domain protein orthologues in vertebrates

X.tropicalis Tbx1, *Tbx2*, *Tbx5* and *Tbx20* were analyzed by pairwise alignment with their orthologues in *X.laevis* (African clawed frog), *Danio rerio* (zebrafish), *Gallus gallus* (chicken), *Mus musculus* (mouse) and *Homo sapiens* (human). Overall sequence identity and similarity (in parentheses) between amino acid sequences are shown as percentages. Where putative full-length sequences were not available, these comparisons were omitted (N/A).

	Xenopus laevis	***Danio rerio***	***Gallus gallus***	***Mus musculus***	***Homo sapiens***
Tbx1	97% (98%)	80% (87%)	N/A	71% (79%)	69% (77%)
Tbx2	96% (97%)	77% (84%)	N/A	70% (77%)	70% (77%)
Tbx5	95% (96%)	64% (73%)	81% (87%)	78% (85%)	78% (85%)
Tbx20	97% (98%)	85% (92%)	90% (95%)	90% (95%)	N/A

Figure A1.1 Genomic locus structure of *Tbx1*, *Tbx2*, *Tbx5* and *Tbx20* in *X.tropicalis*

Tbx1, *Tbx2*, *Tbx5* and *Tbx20* cDNAs and their corresponding genomic loci are shown in diagrammatic form (not to scale). Coding regions of each cDNA are shown (boxes) together with their nucleotide positions and the position of the T-box (defined by alignment of the encoded proteins with the T-domain of Xbra) is also indicated. The exons corresponding to the cDNA sequences are shown together with their sizes (in base pairs) plus those of the intervening introns. Note that as the size of the first exon of each gene is predicted based on the available cDNA sequence, the sizes of these exons may be underestimated here.

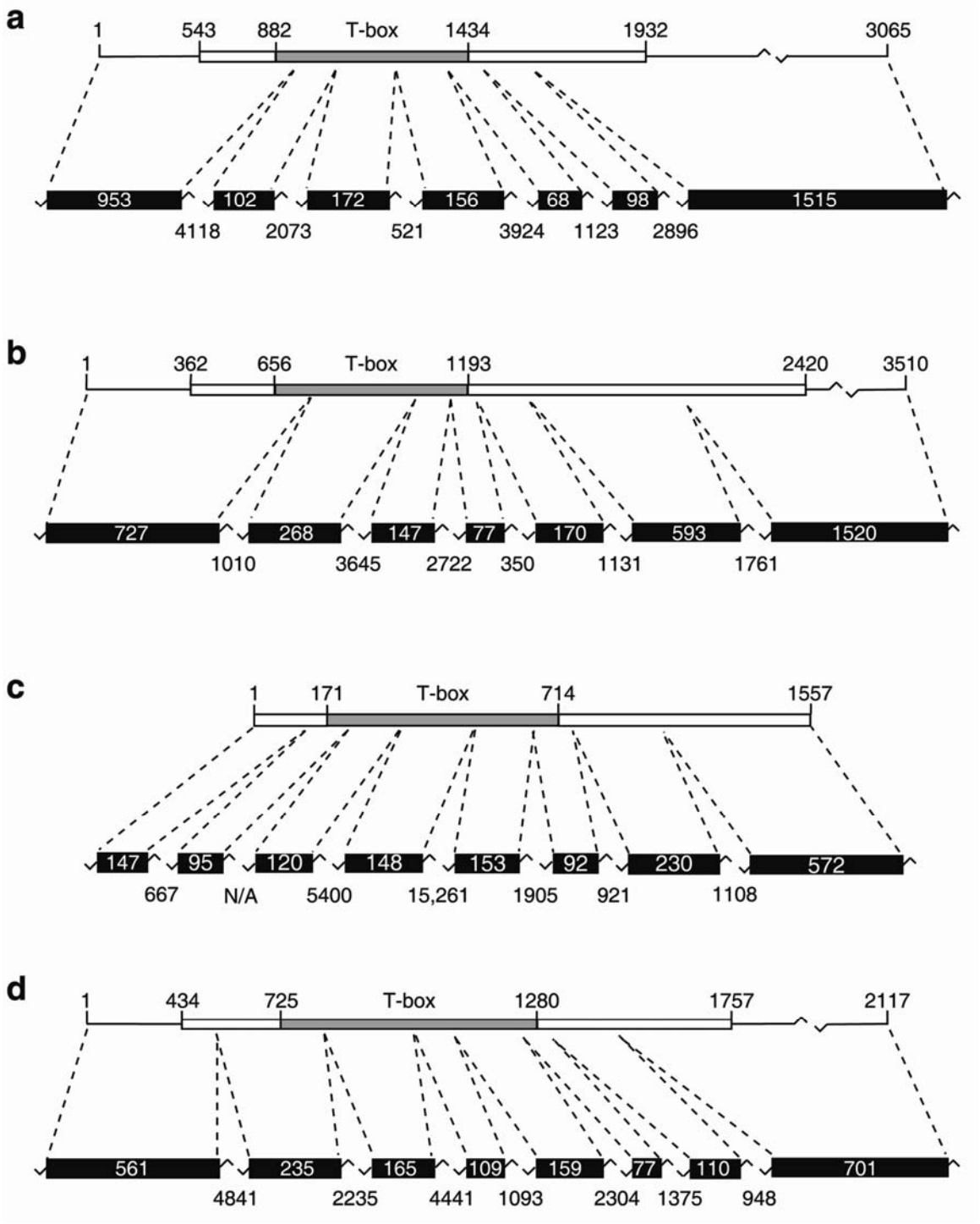
a
1
543
882
T-box
1434
1932
3065
953
102
172
156
68
98
1515
4118
2073
521
3924
1123
2896
b
1
362
656
T-box
1193
2420
3510
727
268
147
77
170
593
1520
1010
3645
2722
350
1131
1761
c
1
171
T-box
714
1557
147
95
120
148
153
92
230
572
667
N/A
5400
15,261
1905
921
1108
d
1
434
725
T-box
1280
1757
2117
561
235
165
109
159
77
110
701
4841
2235
4441
1093
2304
1375
948

Figure A1.2 Expression pattern of *Tbx1* in *X.tropicalis*

The results of in situ hybridizations for *Tbx1* expression from early neurula to late tailbud stages are shown (embryos uncleared). Except for the anterior views shown in a) and d), all embryos are oriented with anterior to the left. Stage 13 is shown in anterior (a), lateral (b) and dorsal (c) views. Bilateral patches of stronger expression are indicated in a) by arrowheads. Stage 19 is shown in anterior (d), lateral (e) and dorsal (f) views. Bilateral stripes of stronger expression are indicated in f) by an asterisk. *Tbx1* expression through tailbud stages is shown as follows: Stage 25 lateral (g) and ventral (h), stage 26 lateral (i), stage 27 lateral (j) and ventral (k), stage 28 lateral (l) and ventral (m), stage 33 lateral (n). *ba1* first branchial arch, *ba2* second branchial arch, *cg* cement gland, *ea* eye anlagen, *ha* hyoid arch, *ma* mandibular arch, *ov* otic vesicle.

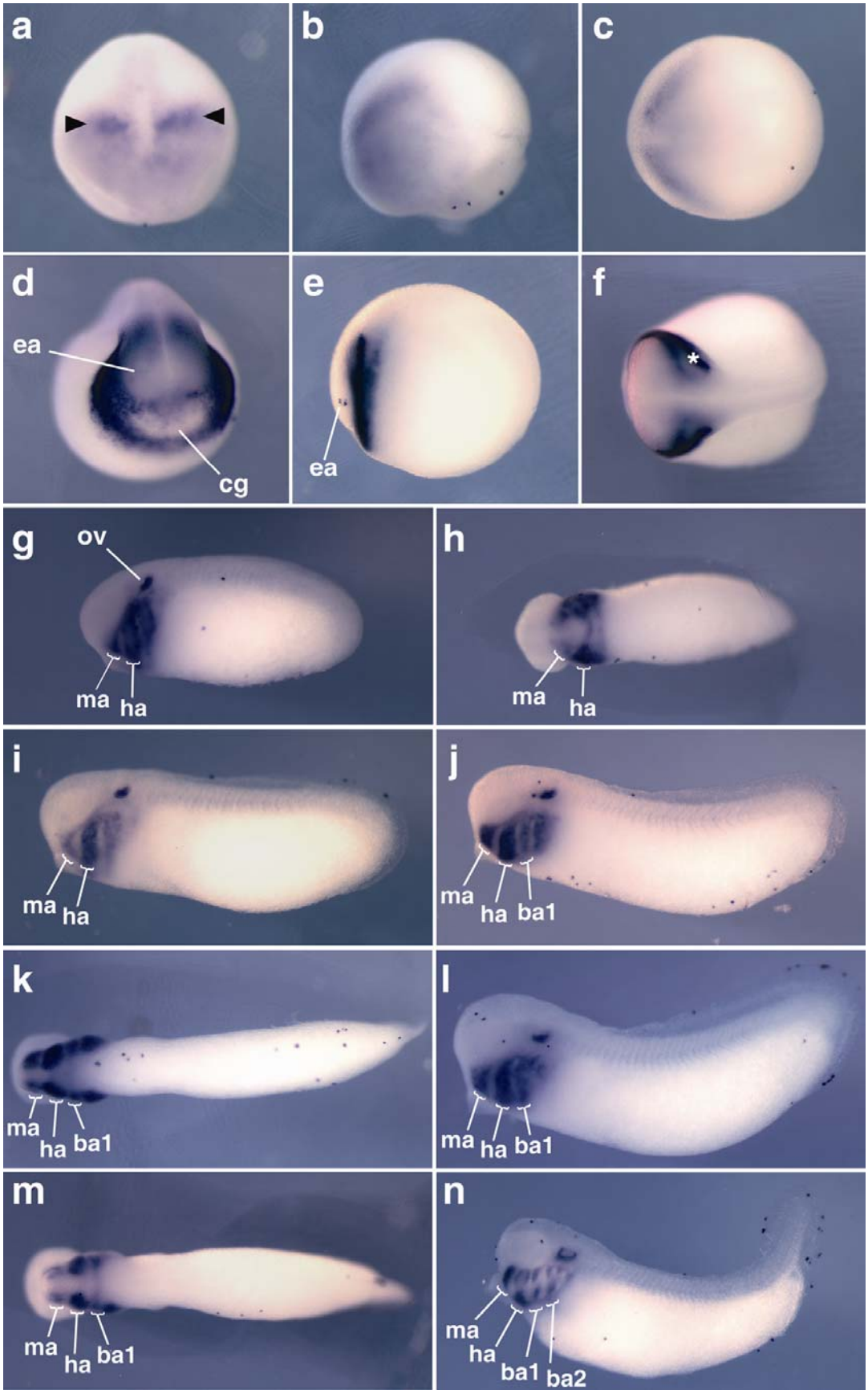
a
b
c
d
ea
cg
e
ea
f
*
g
ov
ma
ha
h
ma
ha
i
ma
ha
j
ma
ha
ba1
k
ma
ha
ba1
l
ma
ha
ba1
m
ma
ha
ba1
n
ma
ha
ba1
ba2

Figure A1.3 Expression pattern of *Tbx2* in *X.tropicalis*

In-situ hybridization results are shown for *Tbx2* (embryos uncleared). Expression at early gastrula (stage 10.5) is shown in lateral (a) and vegetal (b) views of wholemount embryos, and in transverse section (c; ventral to the right). In both a) and b), the embryo is oriented with dorsal to the left and the dorsal blastopore lip is indicated by an arrowhead in a). A vegetal view of a late gastrula (st12) is shown in d), ventral side uppermost. Expression at early neurula (stage 13) (e-g) late neurula (stage 19) (h,l) and tailbud stages 21/22 (m), 25 (n), 26 (o,p), 29 (q) and 33 (r) are also shown. Expression in the forebrain (telencephalon) at tailbud stages is indicated by an asterisk (o-r). Except for anterior (d,j) and posterior (l) views, all embryos are oriented with anterior to the left. *cg* cement gland, *crg* cranial ganglia, *drg* dorsal root ganglia, *fn* frontonasal process, *hm* hypaxial muscle, *ht* heart tube, *lp* lens placode, *ov* otic vesicle, *pd* pronephric duct, *pr* proctodeum.

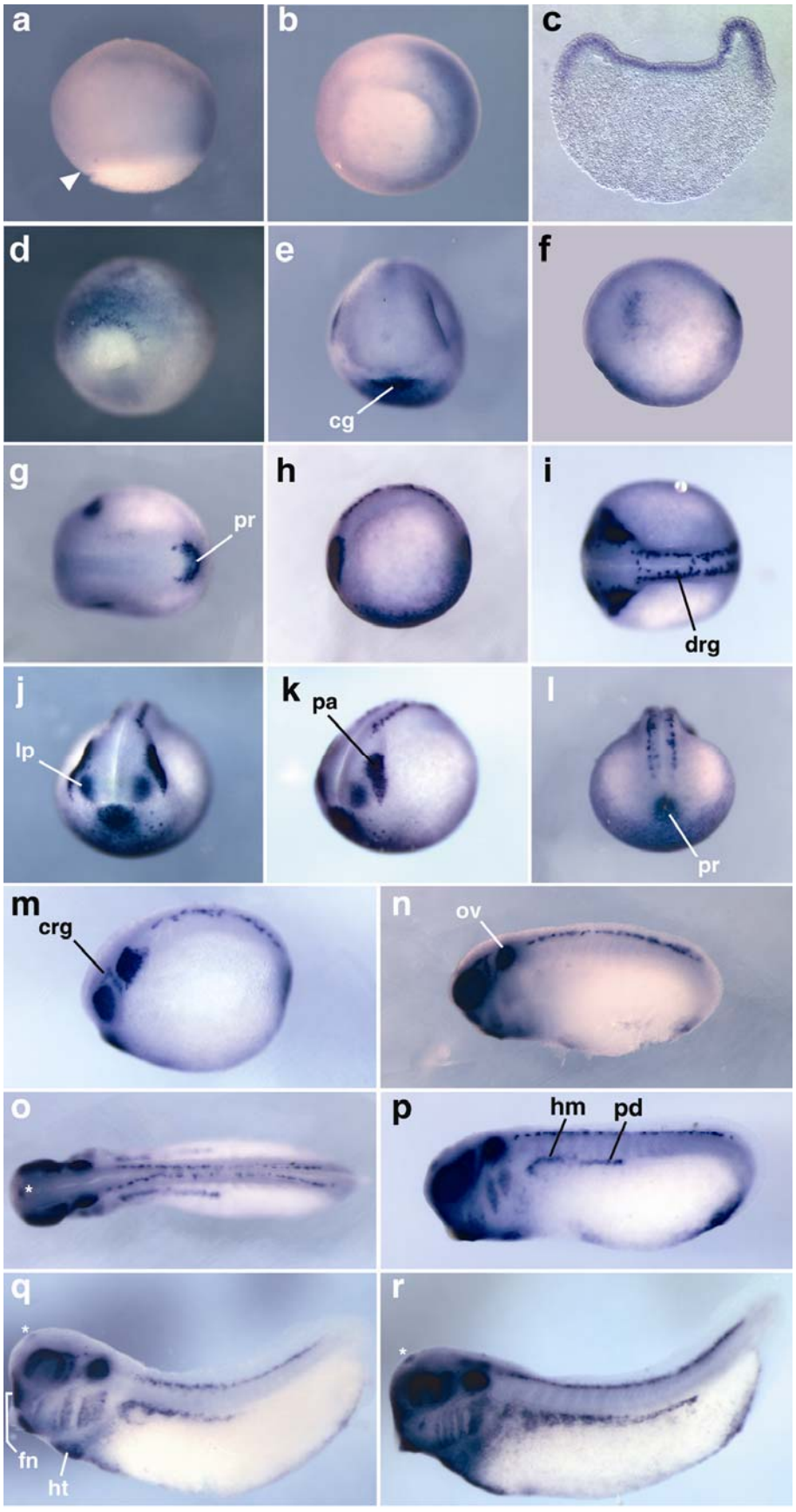
a
b
c
d
e
cg
f
g
pr
h
i
drg
j
lp
k
pa
l
pr
m
crg
n
ov
o
*
p
hm
pd
q
*
fn
ht
r
*

Figure A1.4 Expression pattern of *Tbx5* in *X.tropicalis*

The expression pattern of *Tbx5* detected by in situ hybridization between late neurula and early tadpole stages is shown (uncleared except for g). Stages are as follows: Stage 19 (a,b), stage 25 (c,d), stage 26 (e,f), stage 31/32 (g) (cleared), stage 33 (h), and stage 40 (i,j). Except for the anterior view in b) and the ventral view in j), embryos are oriented with anterior to the left. Anterior is to the top in j). *ea* eye anlagen, *hp* heart primordium, *v* ventricle.

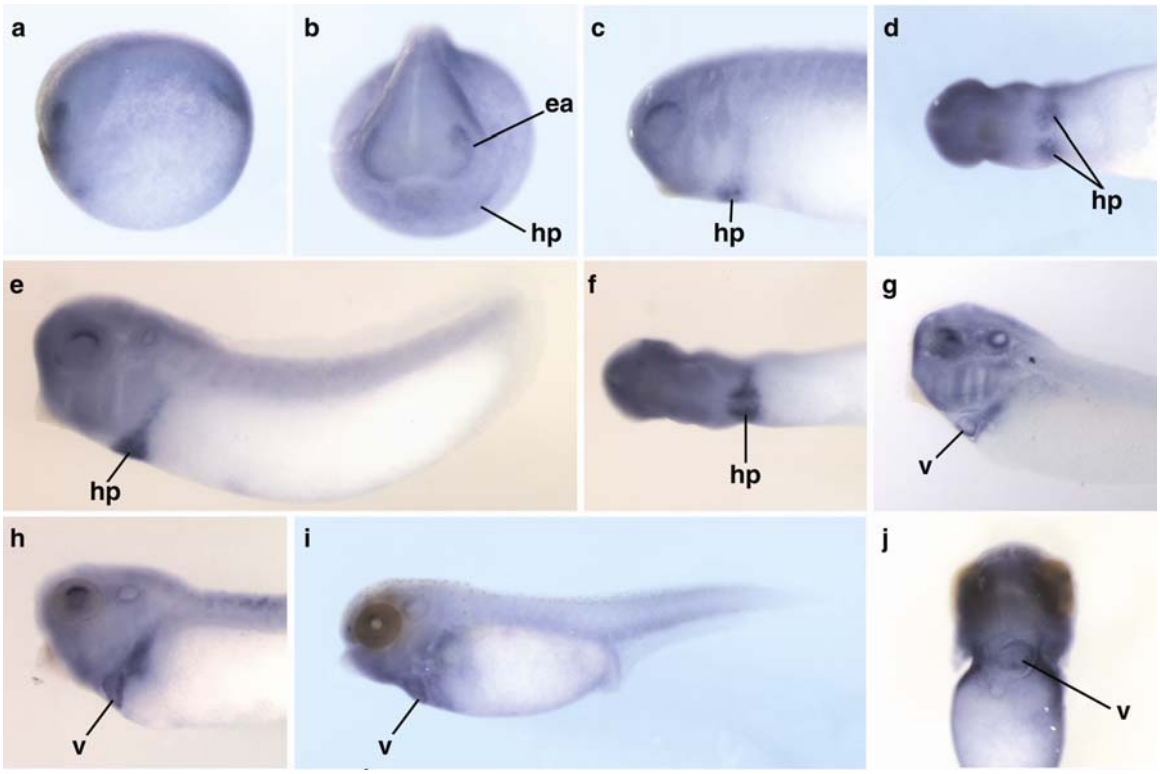

Figure A1.5 Expression pattern of *Tbx20* in *X.tropicalis*

The expression pattern of *Tbx20* detected by in situ hybridization between late neurula and early tadpole stages is shown (embryos uncleared). Stages are as follows: Stage 20 (a-c), stage 25 (d, e), stage 29/30 (f), stage 33 (g-i), stage 36 (j-l), and stage 40 (m-o). Except for the anterior view in a), embryos are oriented with anterior to the left. *a* atrium, *cg* cement gland, *h* heart, *hb* hindbrain, *hp* heart primordium, *ht* heart tube, *sv* sinus venosus, *v* ventricle.

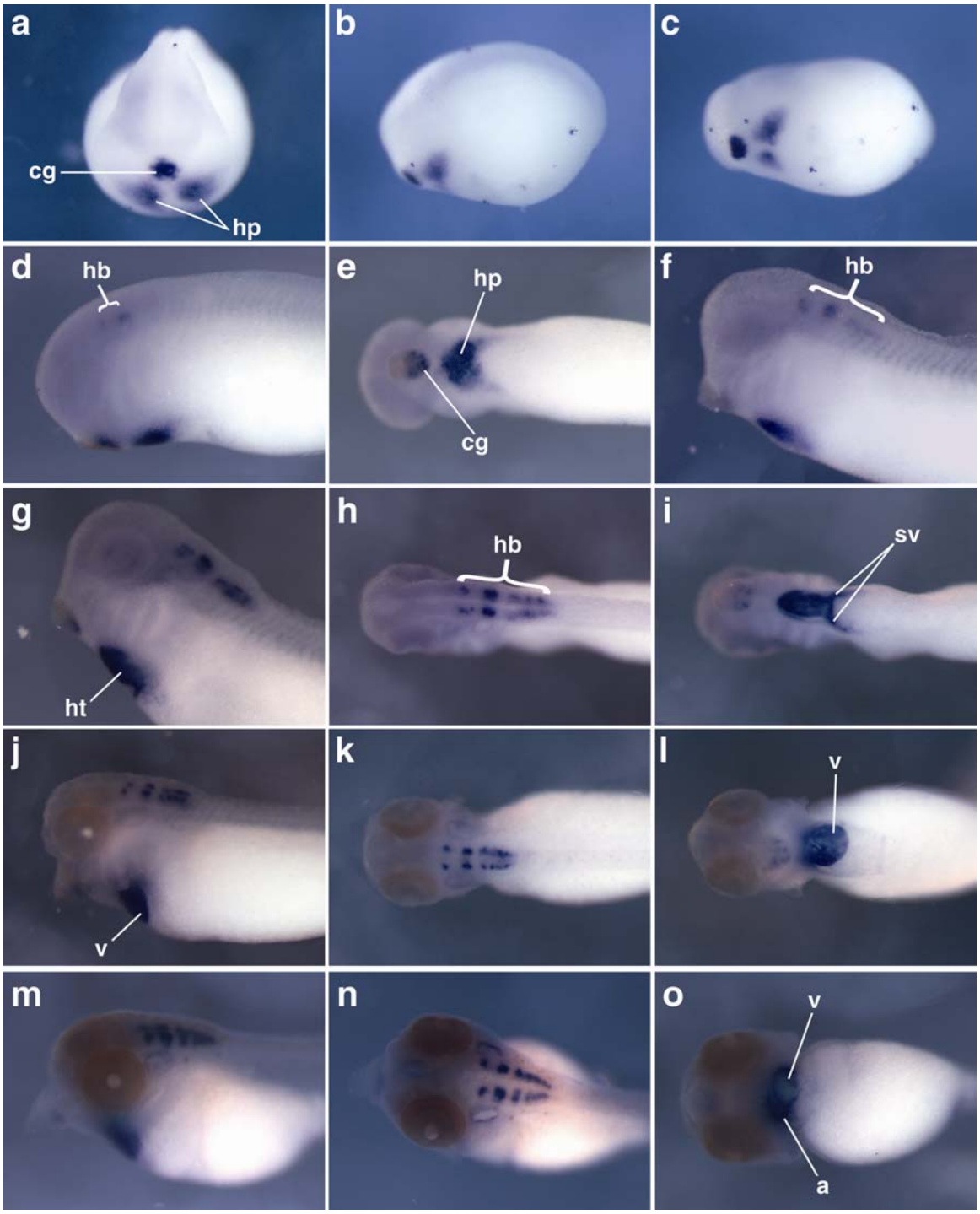
a
cg
hp
b
c
d
hb
e
hp
cg
f
hb
g
ht
h
hb
i
sv
j
v
k
l
v
m
n
o
v
a

Figure A1.6 Cardiac expression of *Tbx2, Tbx5* and *Tbx20*

The *in situ* hybridization patterns of *Tbx2*, *Tbx5* and *Tbx20* in the forming cardiac chambers were examined in transverse sections through the tadpole heart after looping. a) *Tbx2* expression was seen in the myocardium of both the atrial (*am*) and ventricular (*vm*) regions of the looped heart at stage 36. b) Expression of *Tbx5* was restricted primarily to the developing ventricular myocardium at stage 38. c) In contrast to *Tbx5*, high levels of *Tbx20* expression were seen in the atrial region but not in the ventricle (stage 40). Magnification: 100X.

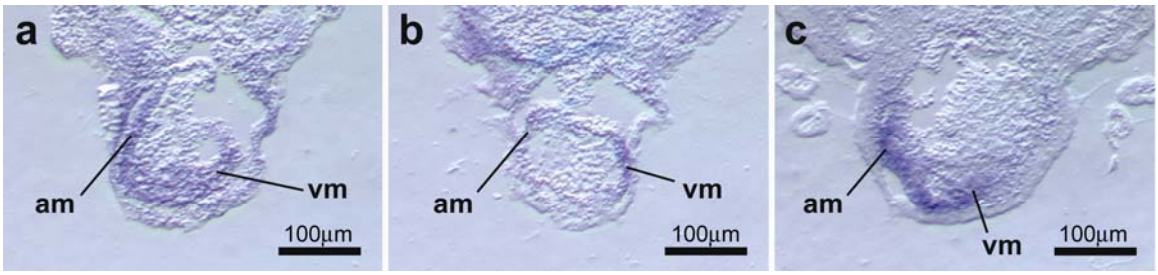

REFERENCES

Ahn, D. G., Ruvinsky, I., Oates, A. C., Silver, L. M., and Ho, R. K. (2000). tbx20, a new vertebrate T-box gene expressed in the cranial motor neurons and developing cardiovascular structures in zebrafish. Mech Dev *95*, 253-258.

Altschul, S. F., Gish, W., Miller, W., Myers, E. W., and Lipman, D. J. (1990). Basic local alignment search tool. J Mol Biol *215*, 403-410.

Ataliotis, P., Ivins, S., Mohun, T. J., and Scambler, P. J. (2005). XTbx1 is a transcriptional activator involved in head and pharyngeal arch development in Xenopus laevis. Dev Dyn *232*, 979-991.

Basson, C. T., Bachinsky, D. R., Lin, R. C., Levi, T., Elkins, J. A., Soults, J., Grayzel, D., Kroumpouzou, E., Traill, T. A., Leblanc Straceski, J.*, et al.* (1997). Mutations in human cause limb and cardiac malformation in Holt-Oram syndrome. Nat Genet *15*, 30-35.

Brown, D. D., Binder, O., Pagratis, M., Parr, B. A., and Conlon, F. L. (2003). Developmental expression of the Xenopus laevis Tbx20 orthologue. Dev Genes Evol *212*, 604-607.

Brown, D. D., Martz, S. N., Binder, O., Goetz, S. C., Price, B. M. J., Smith, J. C., and Conlon, F. L. (2005). Tbx5 and Tbx20 act synergistically to control vertebrate heart morphogenesis. Development *132*, 553-563.

Cai, C. L., Zhou, W., Yang, L., Bu, L., Qyang, Y., Zhang, X., Li, X., Rosenfeld, M. G., Chen, J., and Evans, S. (2005). T-box genes coordinate regional rates of proliferation and regional specification during cardiogenesis. Development *132*, 2475-2487.

Eagleson, G., Ferreiro, B., and Harris, W. A. (1995). Fate of the Anterior Neural Ridge and the Morphogenesis of the *Xenopus* Forebrain. Journal of Neurobiology *28*, 146-158.

Gilchrist, M. J., Zorn, A. M., Voigt, J., Smith, J. C., Papalopulu, N., and Amaya, E. (2004). Defining a large set of full-length clones from a *Xenopus tropicalis* EST project. Developmental Biology, 498-516.

Hayata T, K. H., Eisaki A, Asashima M (1999). Expression of *Xenopus* T-box transcription factor, *Tbx2* in *Xenopus* embryo. Development Genes and Evolution, 625-628.

Horb, M. E., and Thomsen, G. H. (1999). Tbx5 is essential for heart development. Development *126*, 1739-1751.

Hu, N., Sedmera, D., Yost, H. J., and Clark, E. B. (2000). Structure and function of the developing zebrafish heart. Anat Rec *260*, 148-157.

Islam, N., Moss, T. (1996). Enzymatic removal of vitelline membrane and other protocol modifications for whole mount *in situ* hybridization of *Xenopus* embryos. Trends in Genetics *12*, 459.

Izpisúa-Belmonte, J.-C., De Robertis, E. M., Storey, K. G., and Stern, C. D. (1993). The homeobox gene goosecoid and the origin of organizer cells in the early chick blastoderm. Cell.

Jerome, L. A., and Papaioannou, V. E. (2001). DiGeorge syndrome phenotype in mice mutant for the T-box gene, Tbx1. Nat Genet *27*, 286-291.

Khokha, M. K., Chung, C., Bustamante, E. L., Gaw, L. W., Trott, K. A., Yeh, J., Lim, N., Lin, J. C., Taverner, N., Amaya, E.*, et al.* (2002). Techniques and probes for the study of Xenopus tropicalis development. Dev Dyn *225*, 499-510.

Kochilas, L., Liao, J., Merscher-Gomez, S., Kucherlapati, R., Morrow, B., and Epstein, J. A. (2005). New insights into the role of *Tbx1* in the DiGeorge mouse model, In Cardiovascular Development and Congenital Malformations: Molecular and Genetic Mechanisms, M. Artman, D. W. Benson, D. Srivastava, and M. Nakazawa, eds. (Blackwell Publishing).

Koshiba-Takeuchi, K., Takeuchi, J. K., Matsumoto, K., Momose, T., Uno, K., Hoepker, V., Ogura, K., Takahashi, N., Nakamura, H., Yasuda, K., and Ogura, T. (2000). Tbx5 and the retinotectum projection. Science *287*, 134-137.

Kraus, F., Haenig, B., and Kispert, A. (2001). Cloning and expression analysis of the mouse T-box gene tbx20. Mech Dev *100*, 87-91.

Li, Q. Y., Newbury-Ecob, R. A., Terrett, J. A., Wilson, D. I., Curtis, A. R., Yi, C. H., Gebuhr, T., Bullen, P. J., Robson, S. C., Strachan, T.*, et al.* (1997). Holt-Oram syndrome is caused by mutations in TBX5, a member of the Brachyury (T) gene family. Nat Genet *15*, 21-29.

Liao, J., Kochilas, L., Nowotschin, S., Arnold, J. S., Aggarwal, V. S., Epstein, J. A., Brown, M. C., Adams, J., and Morrow, B. E. (2004). Full spectrum of malformations in velo-cardio-facial syndrome/DiGeorge syndrome mouse models by altering Tbx1 dosage. Hum Mol Genet *13*, 1577-1585.

Lindsay, E. A., Vitelli, F., Su, H., Morishima, M., Huynh, T., Pramparo, T., Jurecic, V., Ogunrinu, G., Sutherland, H. F., Scambler, P. J.*, et al.* (2001). Tbx1 haploinsufficieny in the DiGeorge syndrome region causes aortic arch defects in mice. Nature *410*, 97-101.

Lindsey, E. A., Vitelli, F., Su, H., Morishima, M., Huynh, T., Pramparo, T., Jurecic, V., Ogunrinu, G., Sutherland, H. F., Scrambler, P. J.*, et al.* (2001). Tbx1 haploinsufficiency in the DiGeorge syndrome region causes aortic arch defects in mice. Nature *410*, 97-101.

Mandel, E. M., Callis, T. E., Wang, D. Z., and Conlon, F. L. (2005). Transcriptional mechanisms of congenital heart disease. Drug Discovery Today: Disease Mechanisms *2*, 33-38.

Mohun, T. J., Leong, L. M., Weninger, W. J., and Sparrow, D. B. (2000). The morphology of heart development in Xenopus laevis. Dev Biol *218*, 74-88.

Moraes, F., Novoa, A., Jerome-Majewska, L. A., Papaioannou, V. E., and Mallo, M. (2005). Tbx1 is required for proper neural crest migration and to stabilize spatial patterns during middle and inner ear development. Mech Dev *122*, 199-212.

Nieuwkoop, P. D., and Faber, J., eds. (1967). Normal Table of *Xenopus laevis (Daudin)*, 2nd edn (Amsterdam: North-Holland Pub. Co.).

Packham, E. A., and Brook, J. D. (2003). T-box genes in human disorders. Hum Mol Genet *12 Spec No 1*, R37-44.

Piotrowski, T., Ahn, D. G., Schilling, T. F., Nair, S., Ruvinsky, I., Geisler, R., Rauch, G. J., Haffter, P., Zon, L. I., Zhou, Y.*, et al.* (2003). The zebrafish van

gogh mutation disrupts tbx1, which is involved in the DiGeorge deletion syndrome in humans. Development *130*, 5043-5052.

Plageman, T. F., Jr., and Yutzey, K. E. (2004). Differential expression and function of tbx5 and tbx20 in cardiac development. J Biol Chem *279*, 19026-19034.

Plageman, T. F., Jr., and Yutzey, K. E. (2005). T-box genes and heart development: putting the "T" in heart. Dev Dyn *232*, 11-20.

Raft, S., Nowotschin, S., Liao, J., and Morrow, B. E. (2004). Suppression of neural fate and control of inner ear morphogenesis by Tbx1. Development *131*, 1801-1812.

Ryan, K., and Chin, A. J. (2003). T-box genes and cardiac development. Birth Defects Res Part C Embryo Today *69*, 25-37.

Schlosser, G., and Ahrens, K. (2004). Molecular anatomy of placode development in *Xenopus laevis*. Developmental Biology, 439-466.

Schlosser, G., and Northcutt, R. G. (2000). Development of Neurogenic Placodes in *Xenopus laevis*. Journal of Comparative Neurology, 121-146.

Showell, C., Binder, O., and Conlon, F. L. (2004). T-box genes in early embryogenesis. Dev Dyn *229*, 201-218.

Singh, M. K., Christoffels, V. M., Dias, J. M., Trowe, M. O., Petry, M., Schuster-Gossler, K., Burger, A., Ericson, J., and Kispert, A. (2005). Tbx20 is essential for cardiac chamber differentiation and repression of Tbx2. Development *132*, 2697-2707.

Sive, H. L., Grainger, R. M., and Harland, R. M. (2000). Early development of Xenopus laevis: a laboratory manual.: Cold Spring Harbor Press;).

Stemple, D. L., Solnica-Krezel, L., Zwartkruis, F., Neuhauss, S. C. F., Schier, A. F., Malicki, J., Stainier, D. Y. R., Abdelilah, S., Rangini, Z., Mountcastle-Shah, E., and Driever, W. (1996). Mutations affecting development of the notochord in zebrafish. Development *123*, 117-128.

Stennard, F. A., Costa, M. W., Lai, D., Biben, C., Furtado, M. B., Solloway, M. J., McCulley, D. J., Leimena, C., Preis, J. I., Dunwoodie, S. L.*, et al.* (2005). Murine T-box transcription factor Tbx20 acts as a repressor during heart development, and is essential for adult heart integrity, function and adaptation. Development *132*, 2451-2462.

Xu, H., Morishima, M., and Baldini, A. (2005). *Tbx1* and DiGeorge syndrome: a genetic link between cardiovascular and pharyngeal development, In Cardiovascular Development and Congenital Malformations: Molecular and Genetic Mechanisms (Blackwell Publishing).

Yamagishi, T., Nakajima, Y., Nishimatsu, S., Nohno, T., Ando, K., and Nakamura, H. (2004). Expression of tbx20 RNA during chick heart development. Dev Dyn *230*, 576-580.

Appendix 2

Small heat shock protein *Hsp27* is required for proper heart tube formation

Small Heat Shock Protein *Hsp27* Is Required for Proper Heart Tube Formation, Daniel D. Brown, Kathleen S. Christine, Christopher Showell, and Frank Conlon, Genesis, Volume 45, 667-678, 2007. Reprinted with permission of Wiley-Liss, Inc. a subsidiary of John Wiley & Sons, Inc.

ABSTRACT

The small heat shock protein *Hsp27* has been shown to be involved in a diverse array of cellular processes, including cellular stress response, protein chaperone activity, regulation of cellular glutathione levels, apoptotic signaling, and regulation of actin polymerization and stability. Furthermore, mutation within *Hsp27* has been associated with the human congenital neuropathy Charcot-Marie Tooth (CMT) disease. *Hsp27* is known to be expressed in developing embryonic tissues; however, little has been done to determine the endogenous requirement for *Hsp27* in developing embryos. In this study, we show that depletion of XHSP27 protein results in a failure of cardiac progenitor fusion

resulting in cardia bifida. Furthermore, we demonstrate a concomitant disorganization of actin filament organization and defects in myofibril assembly. Moreover, these defects are not associated with alterations in specification or differentiation. We have thus demonstrated a critical requirement for XHSP27 in developing cardiac and skeletal muscle tissues.

INTRODUCTION

Formation of a functioning heart requires the organization and synchronization of many cellular and tissue-level processes, including proper cell movements and polarity establishment, specification and differentiation of cardiac precursors, and morphogenesis of the heart. During gastrulation a bilaterally symmetric pair of fields within the anterior lateral plate mesoderm (LPM) is initially specified as cardiac precursors. Once the cardiac precursor fields are specified, they undergo two separate migration events as neurulation proceeds. The large-scale tissue movements involved in neurulation result in the anterior movement of the cardiac progenitors toward more anterior regions. This process seems to be largely controlled by FGF family members, including FGF8 and FGF4 (Beiman et al., 1996; Ciruna and Rossant, 1999; Gisselbrecht et al., 1996; Sun et al., 1999) as well as G-coupled proteins (Quertermous, 2007; Scott et al., 2007; Zeng et al., 2007). Soon after migration to more anterior positions in the embryo, the cardiac progenitors migrate ventrally as an epithelial sheet towards the anterior ventral midline where they proceed to fuse, proliferate and form a

linear heart tube (DeHaan, 1963; Goetz and Conlon, 2007; Kolker et al., 2000; Mohun et al., 2003; Trinh and Stainier, 2004).

Several requirements for the ventral migration and fusion of the cardiac fields have thus far been identified, including proper cardiomyocyte differentiation (Reiter et al., 1999; Yelon et al., 2000), interaction or signaling from the endoderm (Alexander et al., 1999; Kikuchi et al., 2000; Reiter et al., 1999; Schier et al., 1997), epithelial organization of the cardiac fields, and migration cues from the midline (Trinh and Stainier, 2004). Recent work by Trihn and Stainier (2004) has demonstrated a requirement for *fibronectin* (*Fn*) in the migrating cardiac precursor fields in zebrafish; fish mutant for *Fn* exhibit cardia bifida, which is characterized by unfused cardiac progenitors that independently differentiate into cardiac tissue (Trinh and Stainier, 2004). Their results indicate that *Fn* at the junction between the endoderm and mesoderm is required for epithelial integrity within the cardiac fields. Furthermore, deposition of *Fn* at the ventral midline regulates the timing of migration. Other studies have shown that mutant mice lacking *Fn* display defects in cardiogenesis, despite normal specification of the cardiac precursors (George et al., 1997; George et al., 1993). It is also well established that the anterior endoderm is required for cardiac progenitor migration (reviewed in (Lough and Sugi, 2000). For example, many genes involved in endoderm differentiation and maturation, including *Gata4*, *Gata5*, *one-eyed pinhead* (*oep*), *casanova*, and *miles apart* result in cardia bifida when mutated in mice or fish (Kuo et al., 1997; Kupperman et al., 2000; Reiter et al.,

1999; Stainier, 2001). Furthermore, studies have shown that abrogation of proper myocardial differentiation can also result in cardia bifida (Reiter et al., 1999; Yelon et al., 2000). In the present study we report a requirement for the small heat shock protein, *Hsp27*, in proper cardiac fusion.

Hsp27, also called *Hsp25* in mice and *HspB1* in humans, is one of the most widely distributed and most studied of the small heat shock proteins (sHSPs; reviewed in (Ferns et al., 2006). Changes in *Hsp27* expression have been observed in cells and tissues exposed to numerous stress conditions, including oxidative damage (Arrigo, 2001; Baek et al., 2000; Dalle-Donne et al., 2001; Escobedo et al., 2004; Huot et al., 1996; Komatsuda et al., 1999; Mehlen et al., 1995), metal toxicity (Bonham et al., 2003; Leal et al., 2002; Somji et al., 1999), and ischemia (Hollander et al., 2004; Reynolds and Allen, 2003; Shelden et al., 2002; Vander Heide, 2002), as well as in disease states such as cardiac hypertrophy (Knowlton et al., 1998; Scheler et al., 1999), and muscle myopathies (Benndorf and Welsh, 2004). In addition, a role for HSP27 function has been implicated in cellular processes, including protein chaperone activity (Jakob et al., 1993), regulation of cellular glutathione levels (Arrigo, 2001; Baek et al., 2000), apoptotic signaling (Bruey et al., 2000; Paul et al., 2002), inhibition of actin polymerization (Benndorf et al., 1994; Miron et al., 1991; Rahman et al., 1995), and stabilization of actin filament arrays (Huot et al., 1996; Lavoie et al., 1993a; Lavoie et al., 1993b; Lavoie et al., 1995). Furthermore, mutation within *Hsp27* has been associated with the human congenital disorder Charcot-Marie-Tooth

disease (CMT; (Evgrafov et al., 2004). CMT is a progressive neuropathy of the peripheral nervous system, and is the single most-common inherited neuropathy at an estimated prevalence of 1 in 2,500 (Skre, 1974).

Hsp27 is known to be expressed during both skeletal and cardiac muscle development in several organisms, including human (Shama et al., 1999), mouse (Gernold et al., 1993), pig (David et al., 2000) and zebrafish (Mao et al., 2005; Mao and Shelden, 2006). A role for Hsp27 in heart development has been implied by studies over-expression of Hsp27 can protect mice from induced heart failure (Brundel et al., 2006; Liu et al., 2007). However, the precise requirement for Hsp27 during normal cardiac development is not known. Here we report the sequence and expression of the *X. laevis* orthologue of *heat shock protein 27* (*XHsp27*). We demonstrate using anti-sense morpholinos that XHSP27 is required for proper fusion of cardiac precursors and for actin organization in developing cardiac and skeletal muscle. We further demonstrate that cardiac specification and differentiation appear unaltered as assayed by several markers of cardiac precursor and differentiated cardiomyocyte populations.

MATERIAL AND METHODS

Embryo culture and injections

Preparation and injection of *X. laevis* embryos was carried out as previously described (Wilson and Hemmati-Brivanlou, 1995). Embryos were staged according to Nieuwkoop and Faber (Nieuwkoop and Faber, 1967). An

antisense morpholino oligonucleotide was designed against the translation start site of *XHsp27*. XHSP27 morpholinos were obtained from Gene Tools, LLC. with the following sequence: 5' AAT TCT GCG TTC TGA CAT TTT CTC T 3'. The human β-globin splice-mutant standard control morpholino from Gene Tools was used as control. For the *in vitro* translation studies, TBX20MO was used to show specificity of the HSP27MO (Brown et al., 2005). HSP27MO was injected at 60ng/embryo.

Translation inhibition by morpholinos

In vitro translations were performed using TNT Coupled Reticulocyte Lysate System (Promega) following the manufacturer's protocol. Reactions were carried out in the presence or absence of HSP27MO or TBX20MO. A carboxy-terminal hemagluttin tagged version of HSP27 was generated using the pSP64T-HA vector (generous gift of Masazuma Tada). An HA-tagged TBX20 was also used in the *in vitro* translation study (Brown et al., 2005). We have recently demonstrated that *X. laevis* SHP2 is uniformly expressed throughout early development (Brown et al., 2005) and anti-PTP1D/SHP2 primary antibody was used at 1:2500 (Transduction Laboratories) as a loading control with peroxidase-conjugated AffiniPure donkey anti-mouse (H+L) 2° antibody (1:10,000). HA-tagged proteins were probed with anti-HA primary antibody (Covance) at 1:1000 dilution, and peroxidase-conjugated AffiniPure Donkey anti-mouse (H+L) secondary antibody (Jackson ImmunoResearch Laboratories) at 1:10,000 dilution. For *in vivo* translation analyses, embryos were injected with MOs and

mRNA at the one-cell stage. At stage 19, 40 embryos per treatment were collected and lysed in 300 □l of lysis buffer: 140 mM NaCl, 50 mM Tris (pH 7.6), 10 mM EDTA, 1% Surfact-Amps Triton-100 (Pierce), Complete EDTA-free Protease Inhibitor (Roche), and 25mM PMSF (Roche). Lysates were resolved on 12% SDS-PAGE gels, and visualization was carried out using luminol-based chemi-luminescence solutions at 1:1 ratio: solution A: 100mM Tris pH8.5, 2.5mM Luminol (Sigma), 0.4 mM p-Coumaric acid (Sigma); solution B: 100 mM Tris pH 8.5, 0.02% H_2O_2 (Sigma).

Whole-mount *in situ* hybridization

Whole-mount *in situ* hybridization was performed as previously described (Harland, 1991). Probes used include *Tbx20* (Brown et al., 2003), *Nkx2.5* (Brown et al., 2005), *Gata4* and *Gata6* (generous gifts of Roger Patient; (Jiang and Evans, 1996), *Mlc1v'* (IMAGE clone 4408657, GenBank Accession No.: BG884964), and *Titin Novex 3* (Brown et al., 2006).

Immunodetection

Embryos were prepared for whole-mount immunohistochemistry as previously described (Kolker et al., 2000). Briefly, fixed embryos were incubated overnight at 4°C with an antibody against *myosin heavy chain* □ (Abcam), at a dilution of 1:500. Following washes, the embryos were incubated overnight at 4°C with a Cy3-conjugated anti-mouse secondary antibody (Sigma) at a dilution of 1:100. For imaging, embryos were cleared with 2:1 benzyl benzoate: benzyl

alcohol and viewed on a Leica MZFLIII fluorescence dissecting microscope. For immunostaining of histological sections, embryos were collected at the indicated stages, fixed for 2 hours in 4% paraformaldehyde, and embedded in OCT cryosectioning medium (Tissue Tek). Cryostat sections (14 □m) were rinsed with wash buffer (PBS with 1% Triton and 1% heat inactivated calf serum), and incubated at 4°C overnight, as indicated, with mouse anti-*myosin heavy chain* □ (Abcam), at a dilution of 1:500 or anti-tropomyosin 1:50 (Developmental Studies Hybridoma Bank), and phalloidin conjugated to Alexa 488 flourophore (Molecular Probes). Sections were then rinsed with wash buffer and incubated with anti-mouse Cy3-conjugated secondary antibody (1:200; Sigma). Sections were rinsed and incubated for 20 minutes at room temperature with DAPI, cover slipped and visualized on either a Zeiss LSM410 confocal microscope or a Nikon Eclipse E800 fluorescent microscope.

For western blot analysis, stage 29 and 33 embryos (N=10) per treatment were collected, lysed, and sonicated in 100 µl of lysis buffer used in the *in vivo* morpholino studies above. 10 µg of each lysate was run on a 4-12% SDS-PAGE gel and transferred. Western blots were probed with antibodies against actin (Santa Cruz) and α-tubulin (Abcam) at dilutions of 1:100 and 1:1000, respectively, in 5% non-fat milk in TBS-T. Actin was detected using peroxidase-conjugated AffiniPure donkey anti-mouse (H+L) secondary antibody (Jackson ImmunoResearch Laboratories). α-tubulin was detected using was detected using peroxidase-conjugated AffiniPure donkey anti-rabbit (H+L) secondary

antibody (Jackson ImmunoResearch Laboratories). Both secondary antibodies were used at 1:10,000 dilution. Visualization was carried out using Super Signal West Pico Chemiluminescent Substrate (Pierce).

Transmission electron microscopy

Briefly, stage 37 embryos were fixed in 2% paraformaldehyde/2.5% gluteraldehyde overnight (Goetz et al., 2006). Embryos were post-fixed in ferrocyanide-reduced osmium and embedded in Spurr's epoxy resin. Transverse ultra-thin (70 nm) sections were mounted on copper grids, and post-stained with 4% aqueous uranyl acetate followed by Reynolds' lead citrate. Sections were imaged with a LEO EM-910 transmission electron microscope.

RESULTS

XHsp27 expression is developmentally regulated in differentiating cardiac and skeletal muscle.

XHsp27, the *X. laevis* orthologue of *Hsp27* (HSP25, HspB1; GenBank Accession No.: EF066483) was initially identified in a screen for differentially expressed cardiac genes as an expressed sequence tag (GenBank Accession No.: AW766262) identified in the developing heart (D. Brown and F.L.C., unpublished data). This EST was subsequently sequenced and a BLASTn search revealed that the EST is highly similar to several members of the small heat shock protein 27 subfamily. The *X. laevis Hsp27* transcript consists of at

least 1123 nucleotides and encodes for 213 putative amino acids (Fig. A2.1A). The *XHsp27* transcript appears to align with a single locus within the *Xenopus tropicalis* (*X. tropicalis*) genome (JGI, ver. 4.1, scaffold 72), consisting of 3 exons separated by two introns. This organization appears to mirror that of mouse *Hsp27* (Ferns et al., 2006), which also consists of three exons. In addition, a synteny search using Metazome (www.metazome.net) reveals that the genomic locus within *X. tropicalis* is highly syntenic with the *Hsp27* orthologue locus on human chromosome 7, mouse chromosome 5, rat chromosome 12, and chick chromosome 19. (Fig. A2.1C). Protein alignments performed against *Hsp27* orthologues in human (GenBank Accession No.: BC073768), rat (GenBank Accession No.: NM_031970), mouse (GenBank Accession No.: AK003119), pig (GenBank Accession No.: NM_001007518), dog (GenBank Accession No.: NM_001003295), chick (GenBank Accession No.: NM_205290), and zebrafish (GenBank Accession No.: NM_001008615) reveal conservation of identities in the range of 64-70% (Fig. A2.1A-B). An “alpha-crystallin-hsps” domain within the transcript is conserved between the *Hsp27* orthologues, as identified by the NCBI conserved domain search (cd#: cd00298; Fig. A2.1A). The crystallin domain is critical in homo- and heterodimerization between various sHSPs (Feil et al., 2001). Furthermore, one of two putative actin interacting domains appears to be highly conserved between *XHsp27* and the various orthologues, with a second domain showing a smaller degree of conservation (Fig A2.1A; Mao et al., 2005). Thus, this transcript is likely the *X. laevis* orthologue of *Hsp27* and we refer to this transcript as *XHsp27*.

By whole-mount *in situ* hybridization, *XHsp27* appears to be expressed diffusely throughout the developing embryo during gastrulation, consistent with recent findings in zebrafish (Fig. A2.2; (Mao and Shelden, 2006). Shortly after gastrulation *XHsp27* becomes restricted to thin dorsal-ventral stripes within a subdomain of each developing myotome within the somitic mesoderm (Fig. A2.2C). This expression initially begins in the anterior most somites and proceeds in a wave towards the posterior end, mirroring the wave of somitic formation and development (Fig A2.2B-L). As myogenesis progresses, the thickness of each vertical stripe expands to encompass the entire myotome and this expression remains in the developing muscle until at least stage 40 (Fig A2.2B-I). During cardiac precursor fusion and linear heart tube formation, *XHsp27* expression commences throughout the developing myocardium and remains expressed throughout the developing heart at all stages examined (Fig A2.2G-I, L, M). Furthermore, as muscle development continues during early tadpole stages, *XHsp27* expression becomes evident in other muscle domains such as those in the developing jaw and the body wall (Fig A2.2I). Expression is also detected in the brain of tadpole stage embryos (Fig A2.2I). These results indicate that *XHsp27* is a developmentally regulated gene and may be involved in gastrulation, cardiac and skeletal myogenesis, and neural development.

XHSP27 morpholinos specifically inhibit HSP27 translation

In order to test whether *XHsp27* protein is required during embryogenesis, we sought to knock down endogenous XHSP27 protein levels using antisense

morpholino oligonucleotides. To this end we designed morpholinos targeted against the start site of *XHsp27*, which we refer to as HSPMO (Fig. A2.3A). Unfortunately, attempts to detect endogenous or *in vitro* translated *X. laevis* HSP27 were unsuccessful using several of the available commercial HSP27 antibodies. Thus we sought to test the efficiency and specificity of morpholino translation inhibition using a hemagglutinin (HA) epitope-tagged version of XHSP27 both *in vitro* and *in vivo*. For the *in vitro* inhibition study, transcription/translation reactions were incubated with HA-HSP27 construct alone and together with increasing concentrations of HSP27MO (Fig. A2.3B). TBX20MO was included as a negative control (Brown et al., 2005). Furthermore, HSPMO was incubated with HA-*Tbx20* to show specificity of the HSP27MO. Results from these assays show that HSP27MO efficiently blocks translation of HA-*XHsp27 in vitro* while TBX20MO and ControlMO do not. In contrast, HSP27MO does not block translation of HA-TBX20 (Fig. A2.3B).

In order to test whether HSP27MO can knock down XHSP27 translation *in vivo*, HA-Hsp27 capped mRNA was injected into one-cell stage embryos along with HSP27MO. To insure that the MOs did not bind the mRNA prior to injection, embryos were first injected with 30ng or 60ng HSPMO or 60ng ControlMO. Embryos were then re-injected with 100pg HA-HSP27 capped mRNA prior to first cleavage. Embryos were then collected at stage 20, lysed, submitted to Western blotting with an anti-HA antibody, and with an antibody against the protein phosphatase, SHP2, as loading control (Brown et al., 2005; Langdon et al.,

submitted). As shown in Figure A2.3C, embryos injected with HSPMO completely lack HA-HSP27 protein, in contrast to ControlMO injected embryos, which display no inhibition of HA-HSP27 translation.

Knockdown of XHSP27 protein translation results in partial cardia bifida.

To determine the requirement for XHSP27 during development, we injected HSP27MO into one-cell stage embryos. Despite *XHsp27* expression in gastrula embryos, no defects in gastrulation were observed, suggesting that XHSP27 is not required for this process. However, by linear heart tube formation stage (stage 33), defects in heart tube fusion became apparent as assayed by myosin heavy chain (MHC) whole-mount antibody staining (Fig. A2.4J-L). As shown in Figure A2.4, XHSP27 morphants display a bifurcation in the posterior inflow region of the linear heart tube. The degree of bifurcation varies between embryos, and in the most severe cases the hearts appear to be almost entirely divided, resulting in complete cardia bifida (Fig. A2.4P-R). Additional Hsp27 morphoinos designed against either the 5-prime UTR or splice donor/junctions led to partial reduction of HSP27 and a similar albeit weaker phenotype while mis-match splice morpholinos gave no phenotype (data not shown). Attempts to rescue the phenotype by mis-expression of Hsp27 lead to developmental abnormalities at gastrulation and early embryonic lethality precluding analysis of heart development.

Despite aberrant morphogenesis of the heart, the extant cardiac tissue becomes rhythmically contractile; however, XHSP27 morphant embryos arrest development shortly thereafter (stage 40). These results suggest that XHSP27 is critical for proper cardiac morphogenesis.

The cardiac transcriptional program appears to be unaltered in XHSP27 morphants.

To assess whether the cardiac and skeletal muscle precursors are properly specified and differentiate, whole-mount *in situ* hybridizations were performed on XHSP27 morphant embryos using a panel of cardiac and skeletal muscle markers. *Tbx20*, *Nkx2.5*, *Gata4*, and *Gata6* probes were used to mark both early cardiac precursors and terminally differentiated cardiomyocytes, while *titin novex-3* (*XTn3*) and myosin light chain 1v' (*Mlc1v'*) were used to mark differentiated skeletal and cardiac muscle. As shown in Figure A2.5, the cardiac and skeletal muscle domains appeared normal in all cases. This data, combined with the observation that the hearts are contractile, suggests that the cardiac and skeletal muscle precursors are properly specified, migrate to the correct location within the embryo and can initiate terminal differentiation.

XHSP27 morphants display actin filament disorganization in the developing heart and somites.

Recent studies have shown that in addition to a requirement for cardiac differentiation and endoderm maturation in heart tube formation, proper epithelial

organization, adhesion and migration are absolutely critical for heart tube formation. Furthermore, HSP27 has been shown to stabilize the actin cytoskeleton in response to stress (Huot et al., 1996; Lavoie et al., 1993a; Lavoie et al., 1993b; Lavoie et al., 1995). Thus considering that the cardiomyocytes are apparently specified and differentiate properly, that *XHsp27* is not detected in endoderm tissue, and that *XHsp27* is known to be involved in cytoskeletal dynamics, we hypothesized that actin organization may be disrupted in the developing myotomes and heart of XHSP27 morphants. To address this possibility we injected HSP27MO into one-cell stage embryos and collected the embryos at stages during cardiac fusion (stage 28), linear heart tube formation (stage 33), and cardiac looping (stage 37). Embryos were then transversely cryosectioned and cardiac sections were immunostained for *myosin heavy chain* (*MHC*) using a *MHC*-specific antibody and F-actin using phalloidin. Somitic sections were stained for F-actin and with DAPI to mark nuclei in somitic sections. In control hearts, actin staining is most apparent at the basal and apical surfaces of the cells in the forming heart tube, which consists of a single layer of cardiac cells, as well as in fibers perpendicular to the lumen, which appear to correspond with the lateral membranes of cardiac cells (Fig. A2.6A-C, G-I). However, in XHSP27 morphant hearts, actin staining appears diffuse and disorganized (Fig. A2.6D-F, J-L). Few distinct fibers are apparent within the morphant hearts, except where lumen formation occurs (Fig. A2.6L). A similar and more dramatic defect in actin organization is evident within the developing somites. In control morpholino-injected embryos, the somites display thick,

highly organized actin bundles oriented along the anterior-posterior axis (Fig. A2.6M-O, S-U). However, in XHSP27 morphants, the actin appears disorganized and scattered throughout the somites (Fig. A2.6P-R, V-X). Furthermore, the somitic domain itself appears to be larger and less well-defined (Fig. A2.6P-R, V-X). This appearance is similar to the appearance of the somites at earlier stages, after which the somites normally become smaller and more compact, possibly due to the formation of the thick actin bundles. These alteration in actin organization are not due to the levels of actin as western blots with a actin specific antibody show equal levels of actin in control and Hsp27MO embryos (Fig. A2.7) therefore, suggesting that *XHsp27* is required for proper regulation of cytoskeletal dynamics during myogenesis.

In order to gain further insight into the nature of microfilament disorganization in XHSP27 morphants, embryos were injected with control or XHSP27 morpholinos, collected at stage 38 and visualized using transmission electron microscopy (TEM). As shown in Figure A2.8, ControlMO hearts display many myofibril bundles, the majority of which were found to be oriented along the anterior-posterior axis, as demonstrated by transversely sectioned myofibers (Fig. A2.8). In regions where longitudinal sections of myofibers are present, clear z-lines are evident showing the fusion between individual sarcomeres (Fig. A2.8A, B). Furthermore, in transverse myofiber sections, the highly organized myosin structure can be seen (Fig. A2.8C inset). In contrast, XHSP27 morphant hearts show very few myofiber structures (Fig. A2.8D-E). In addition, the

occasional myofibers are very short and no z-lines or connections between multiple fibers were apparent, indicating a lack of sarcomeric assembly (Fig. A2.8D-E). In some sections, large aggregates of bodies are apparent that appear very similar to cross-sectional views of myosin in control myofibrils (Fig. A2.8F inset). However, these aggregates lack any of the obvious structure in spacing or organization characteristic of myofibrils (Fig. A2.8F inset). Similar results are observed within the developing myotomes in the somitic region of XHSP27 morphants. In the forming skeletal muscle, all myofibers analyzed appeared to be sectioned transversely, indicating that these fibers are arranged along the anterior-posterior axis. ControlMO injected myotomes display thick myofiber structures that generally extend throughout the entire cell (Fig. A2.8G, H). In higher magnifications, the myofibril structure is visible as highly ordered arrays of microfilaments (Fig. A2.8H). In contrast, XHSP27 morphants display much fewer apparent myofibers and most of these appear abnormal in morphology (Fig. A2.8I, J). Magnification of these myofibers reveal a less-ordered structure and an apparent lack of thick myosin filaments in these structures (Fig. A2.8J). These observations suggest that the lack in actin organization is accompanied by a failure of myofibril assembly and sarcomere formation. Collectively, these results indicate that XHSP27 is required for normal cardiac precursor fusion and muscle formation, and that these defects are accompanied by a failure in actin organization and proper myofibril assembly.

DISCUSSION

Developmental regulation of Hsp27 expression

Hsp27 has been shown to be involved in a diverse array of cellular processes. In general, the majority of functional data on *Hsp27* comes from experiments performed both *in vitro* and in cell culture, and much of this research has focused on the function of *Hsp27* in response to various cellular stressors. However, surprisingly little has been done to address the potential role of *Hsp27* in developing embryos. In this study, we report the identification of *X. laevis Hsp27* and demonstrate that this orthologue is expressed in a developmentally regulated manner throughout developing gastrula, skeletal muscle and cardiac tissues. The temporal and spatial expression appears to be highly conserved between *X. laevis* and zebrafish (Mao and Shelden, 2006; Tuttle et al., 2007). In frogs and fish, *XHsp27* is initially detected diffusely throughout the gastrulating embryo, suggesting that *Hsp27* may be involved in gastrulation. However, embryos depleted of *XHsp27* protein by antisense morpholinos did not display any defects in gastrulation, suggesting either that XHSP27 is not required for gastrulation or that a functionally redundant sHSP is present in *X. laevis*. During neurulation, *XHsp27* expression commences in the anterior most developing somites, followed by a posterior wave of expression in newly forming somites. As development proceeds, expression within the somitic myotomes expands to encompass the entire myotome, suggesting that XHSP27 may be involved in morphogenesis or differentiation of muscle tissue. However, our data from XHSP27-depleted embryos suggest that XHSP27 functions in cytoskeletal

dynamics but is not involved in differentiation. In addition to its role in skeletal muscle, *XHsp27* is expressed in developing cardiac tissue, beginning at heart tube formation, with this expression continuing through stage 40. During tadpole stages, additional domains of expression within developing jaw and body wall muscles also become evident, suggesting that XHSP27 may be involved in general mechanisms of muscle formation and development.

Hsp27 in cardiogenesis and myogenesis

Formation of a linear heart tube requires the coordination of cardiac specification, differentiation, and cell behavior within defined spatial and temporal domains. In the present study, we identify the small heat shock protein, Hsp27, as being integral to this process. Several studies have shown that *Hsp27* is expressed in developing muscle tissues. While it is clear that *Hsp27* is critical in mediating the cellular response to a wide variety of stressors, it is unclear what role *Hsp27* may be playing during cardiogenesis and myogenesis under un-stressed physiological conditions. Evidence from studies of embryonic stem cell differentiation has suggested that *Hsp27* can function as a molecular switch between differentiation and apoptosis (Mehlen et al., 1997). Furthermore, it is known that proper cardiomyocyte differentiation is necessary for cardiac fusion and heart tube formation (Reiter et al., 1999; Yelon et al., 2000). However, while our data does not rule this out as a possible function for *XHsp27*, it at least suggests that a primary function of *Hsp27* may be to regulate actin dynamics in the context of myogenesis. Our results show that the cardiac and skeletal

muscle appears to be specified and to differentiate normally, at least as assayed by several markers of specification and terminal myocyte differentiation. Furthermore, the total amount of cardiac and skeletal tissue appears grossly normal in *XHsp27*-depleted embryos. With the exception of actin, all markers examined appear to be normally expressed and the defects in heart development appear to be primarily morphogenetic in nature. These data suggest that the cause of the cardiac defect is not a failure of cardiomyocyte differentiation. It remains formally possible that the cardiac fusion defects may result from a loss of differentiation or an increase in apoptosis in a subset of cardiac precursors at the midline, essentially creating a barrier between the two cardiac fields. However, further studies must be conducted to precisely define whether *Hsp27* can influence differentiation or apoptosis in the developing embryo.

Abrogation of *XHsp27* function in *X. laevis* embryos results in improper fusion of the cardiac progenitors, resulting in two unfused or partially fused contractile hearts. Our data suggest that the primary role of *Hsp27* in cardiogenesis is to regulate actin dynamics, and thus cell motility or adhesion. In support of this hypothesis, previous research has shown that cardiac epithelial integrity and cell motility and adhesion are critical for proper fusion of the cardiac primordia (Trinh and Stainier, 2004). In addition, the precardiac field was shown to consist of a single polarized epithelial layer. Our results demonstrate that actin fibers are visible primarily at the cell membrane in the single-cell layered cardiac precursors. However, in XHSP27-depleted embryos, few discrete fibers are

visible. These results suggest that epithelial organization or polarization is defective in the cardiac fields and that XHSP27 is required for this organization. Actin fiber organization appears to be morphologically different in developing skeletal muscle. Within the developing myotomes, thick actin fibers are arranged in an anterior-posterior orientation and do not appear to delineate the membranes in an epithelial manner. However, similar to what is seen in cardiac primordia, actin protein appears to be completely disorganized in XHSP27 morphant embryos, again suggesting that cell polarity or tissue integrity is affected by HSP27 loss.

ACKNOWLEDGEMENTS

This work is supported by grants to F.L.C. from the NIH/NHLBI, RO1 HL075256 and R21 HL083965 and by an award from the UNC Medical Alumni Association. D.D.B is supported by a UNC Graduate School Dissertation Completion Fellowship. KC was supported by a trainee in the Integrative Vascular Biology program T32HL69768 from the NIH. We would like to thank Roger Patient for providing the *Gata4* and *Gata6* probe constructs.

Figure A2.1 *XHsp27* is a conserved member of the *Hsp27* subfamily of proteins.

(A) Protein sequence alignments of *X. laevis Hsp27* with various *Hsp27* orthologues. Alignment was performed using the GeneDoc program. Blue underline indicates conserved crystallin domain. Red underline indicates putative actin interacting domains. (B) Percent identity and similarity between *Hsp27* orthologues. (C) Synteny between *X. tropicalis*, human, mouse, rat, and chick *Hsp27* loci as revealed by Metazome. *Hsp27* is indicated in black. Upstream and downstream genes are colored as indicated.

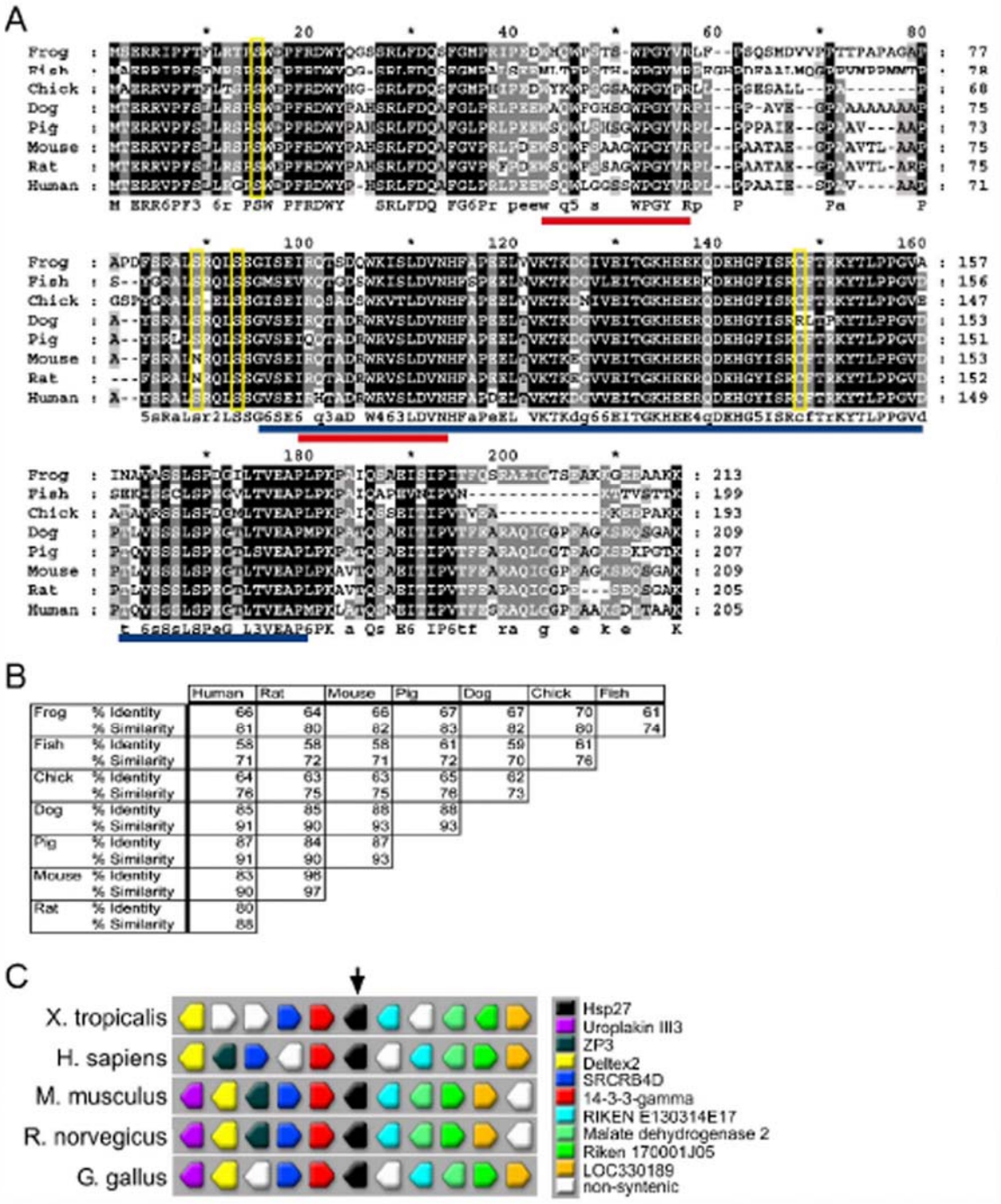

		Human	Rat	Mouse	Pig	Dog	Chick	Fish
Frog	% Identity	66	64	66	67	67	70	61
	% Similarity	81	80	82	83	82	80	74
Fish	% Identity	58	58	58	61	59	61	
	% Similarity	71	72	71	72	70	76	
Chick	% Identity	64	63	63	65	62		
	% Similarity	76	75	75	76	73		
Dog	% Identity	85	85	88	88			
	% Similarity	91	90	93	93			
Pig	% Identity	87	84	87				
	% Similarity	91	90	93				
Mouse	% Identity	83	98					
	% Similarity	90	97					
Rat	% Identity	80						
	% Similarity	88						

Figure A2.2 *XHsp27* is expressed in the gastrula, and developing skeletal and cardiac muscle.

Whole mount *in situ* hybridization of *X. laevis* embryos using an antisense probe specific for *XHsp27* at the indicated stages. (A) Dorsal is to the top. (B-I) Anterior is to the left. (J-M) transverse sections through somitic (J, K) and cardiac (L, M) regions. Dorsal is to the top. *b*, body muscle; *br*, brain; *h*, heart; *j*, jaw muscle, *m*, myotome; *mc*, myocardium.

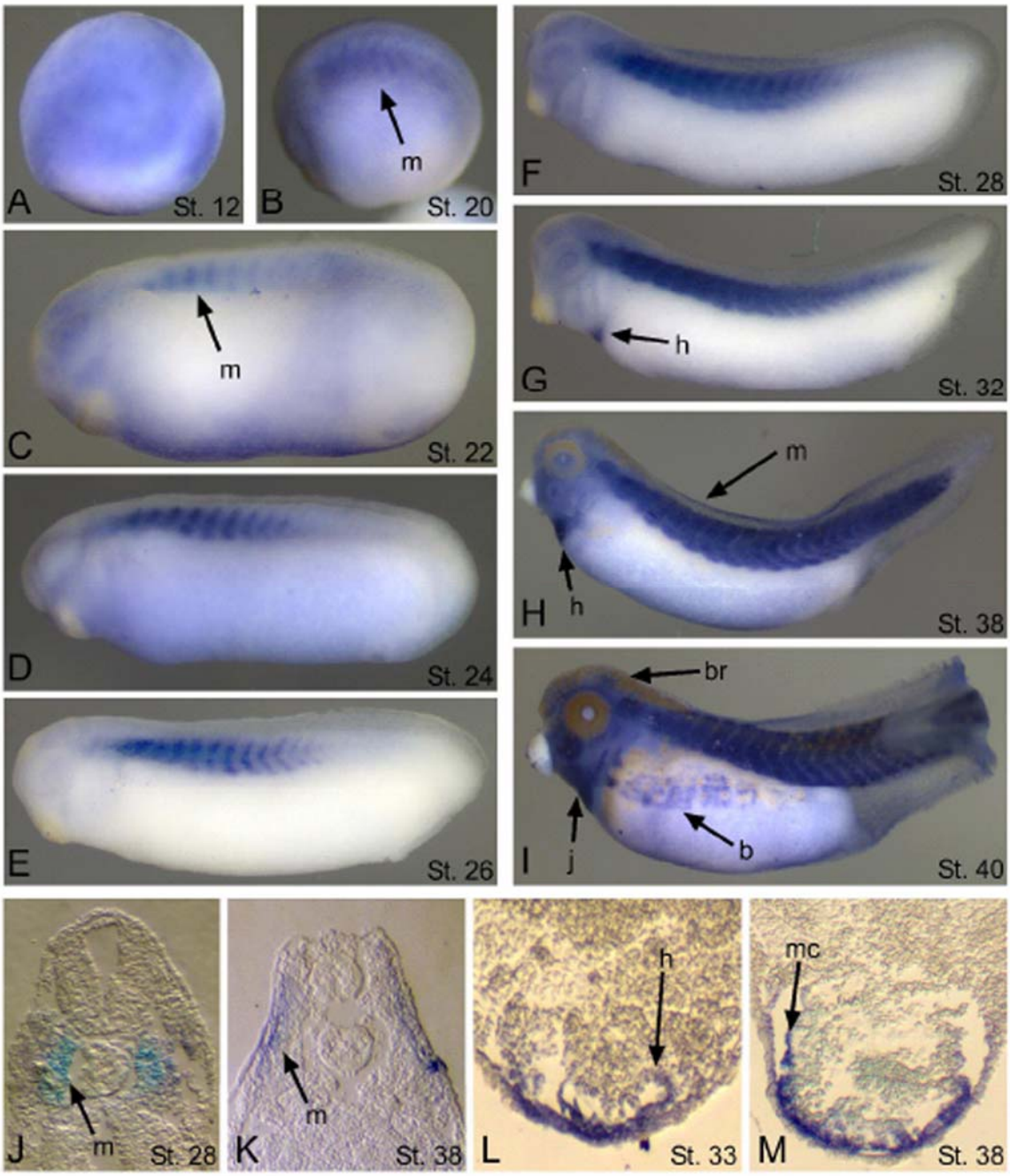
A
St. 12
B
m
St. 20
C
m
St. 22
D
St. 24
E
St. 26
F
St. 28
G
h
St. 32
H
m
h
St. 38
I
br
j
b
St. 40
J
m
St. 28
K
m
St. 38
L
h
St. 33
M
mc
St. 38

Figure A2.3 HSP27 morpholinos specifically block translation *in vitro*.

(A) Diagram depicting *XHsp27* mRNA structure and morpholino-targeted region. (B) Western blot demonstrating translation inhibition *in vitro* using rabbit reticulocyte lysate. Reactions were incubated with the indicated total amounts of HA-*Hsp27* mRNA and/or HSP27MO. TBX20MO was included as a negative control. HSP27MO was incubated with HA-*Tbx20* mRNA to show specificity of the HSP27MO. HA-HSP27 and HA-TBX20 was visualized using anti-HA antibody, and SHP2 antibody was used as loading control. (C) Western blot demonstrating translation inhibition *in vivo* by coinjection of HA-*Hsp27* mRNA with HSP27MO. Embryos were injected with the indicated amount of HSP27MO, ControlMO, and/or HA-*Hsp27* mRNA. Embryos were collected at stage 20. Western blotting was performed on lysate using anti-HA antibody. SHP2 antibody was used as loading control.

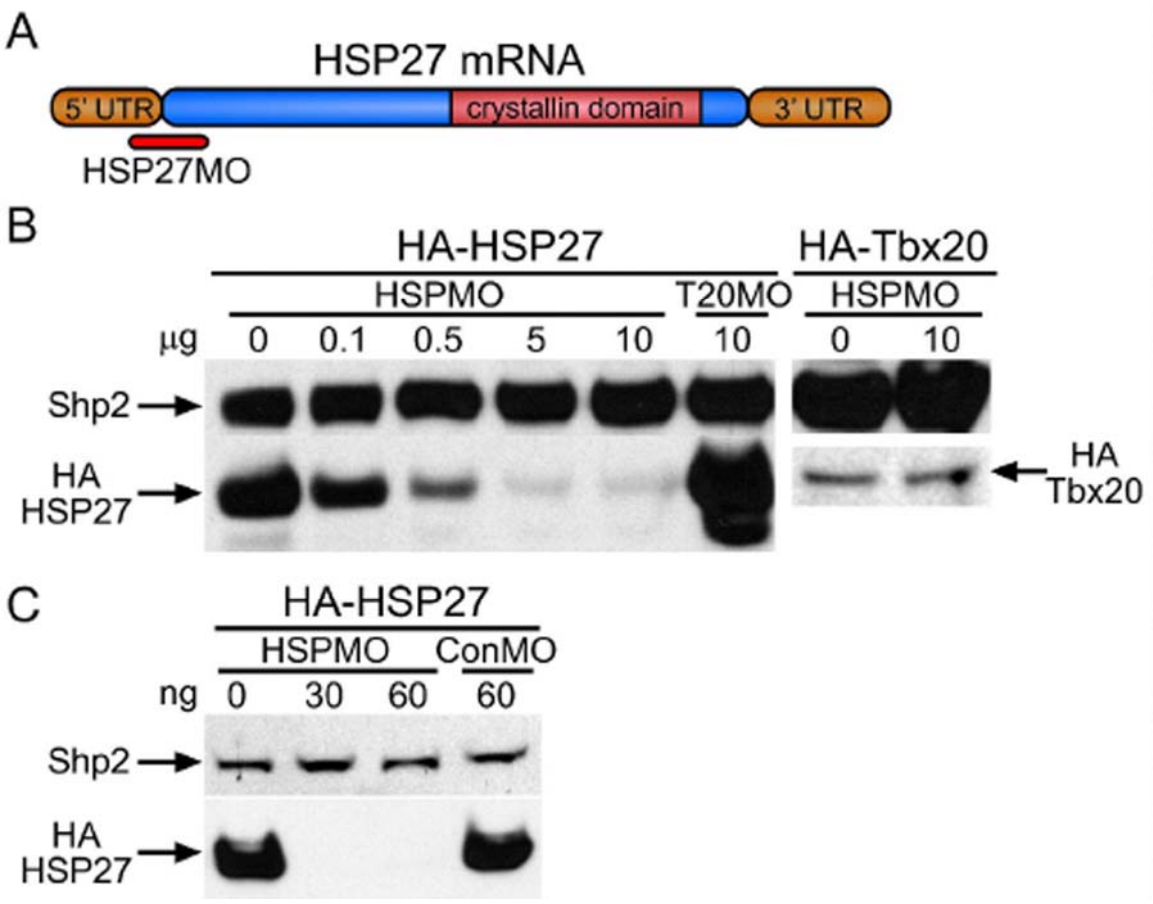
A
HSP27 mRNA
5' UTR
crystallin domain
3' UTR
HSP27MO
B
HA-HSP27
HA-Tbx20
HSPMO
T20MO
HSPMO
μg
0
0.1
0.5
5
10
10
0
10
Shp2
HA
HSP27
HA
Tbx20
C
HA-HSP27
HSPMO
ConMO
ng
0
30
60
60
Shp2
HA
HSP27

Figure A2.4 Depletion of XHSP27 results in unfused or partially fused hearts.

Whole-mount antibody staining using anti-myosin heavy chain α (MHC). Embryos were injected at the one-cell stage with either HSPMO or ConMO, fixed, and stained for MHC at the indicated stages. All views are ventral with anterior upwards. Arrows indicate separation between the two cardiac fields or developing hearts. a, atrium; i, inflow tract; o, outflow tract; v, ventricle.

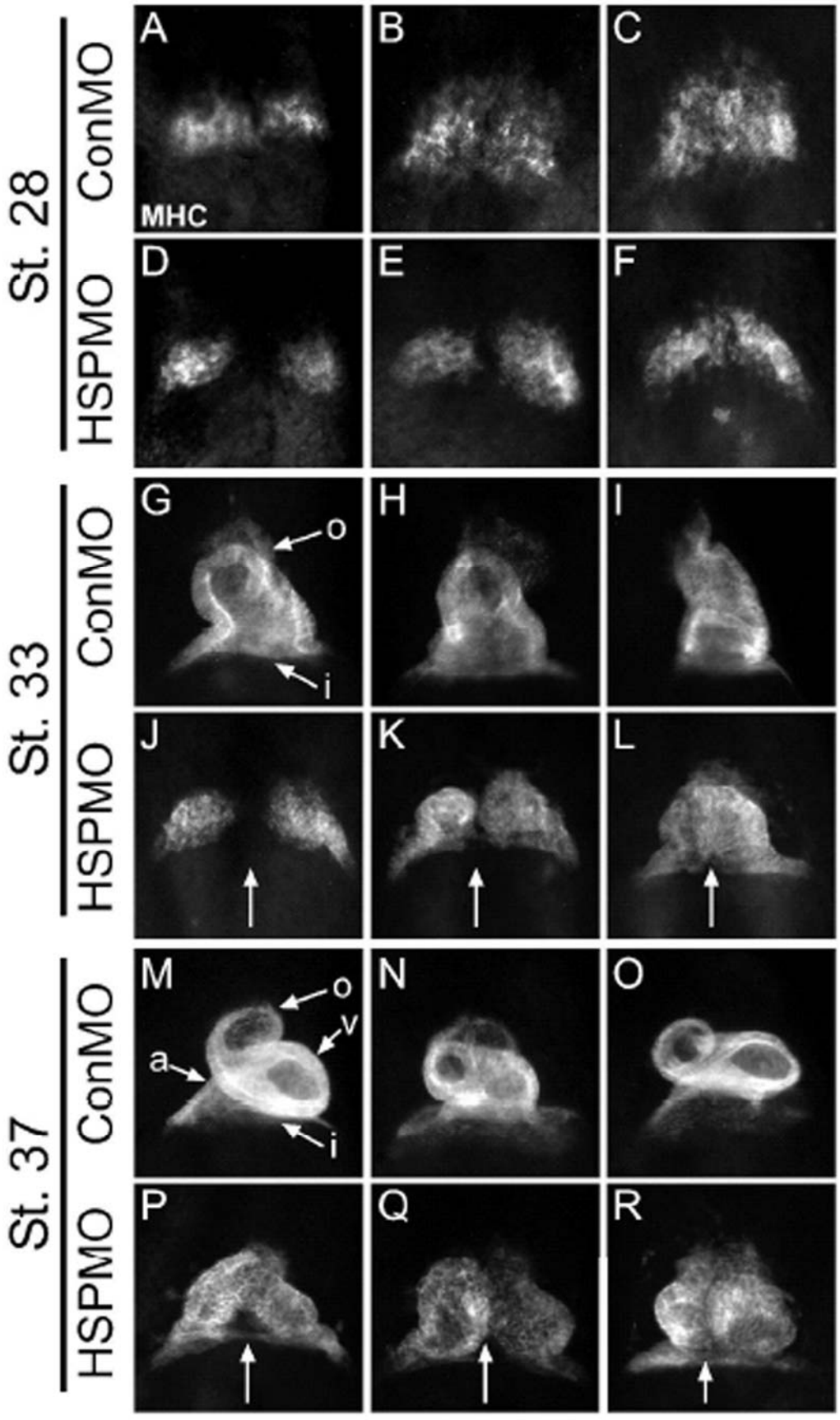
St. 28
ConMO
HSPMO
St. 33
ConMO
HSPMO
St. 37
ConMO
HSPMO
A
B
C
MHC
D
E
F
G
o
i
H
I
J
K
L
M
o
v
a
i
N
O
P
Q
R

Figure A2.5 Specification and differentiation of cardiac and skeletal muscle appear unaltered in HSP27 morphants.

Whole-mount *in situ* hybridizations using antisense probes against (A) *Nkx2.5*, (B) *Tbx20*, (C) *Gata4*, (D) *Gata6*, (E) *Mlc1v'*, and (F) *Titin novex 3* (*Tn3*). Embryos were injected with either HSP27MO or ControlMO and fixed at the indicated stages. (A-F) Ventral views with anterior upward. (E, F) Stage 37 embryos shown laterally with anterior to the left. All markers analyzed appear normal between control and HSP27 morphant embryos.

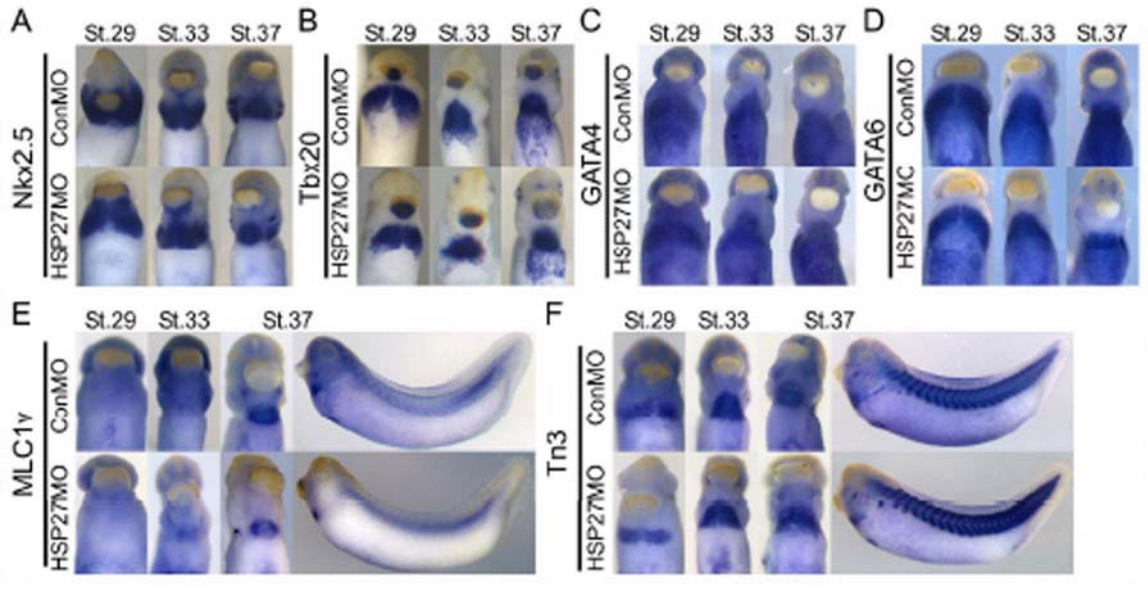

Figure A2.6 Depletion of XHSP27 results in actin disorganization in developing skeletal and cardiac muscle.

Transverse 12 □m sections through the heart (A-L) and somite (M-X). All sections are shown with dorsal upward. Heart sections were immunostained for F-actin using phalloidin (A, D, G, J) and MHC using anti-MHC antibody (B, E, H, K). Overlays are shown in (C, F, I, L). Somite sections were immunostained for F-actin using phalloidin (M, P, S, V) and stained with DAPI to visualize the nuclei (N, Q, T, W). Overlays are shown in (O, R, U, X).

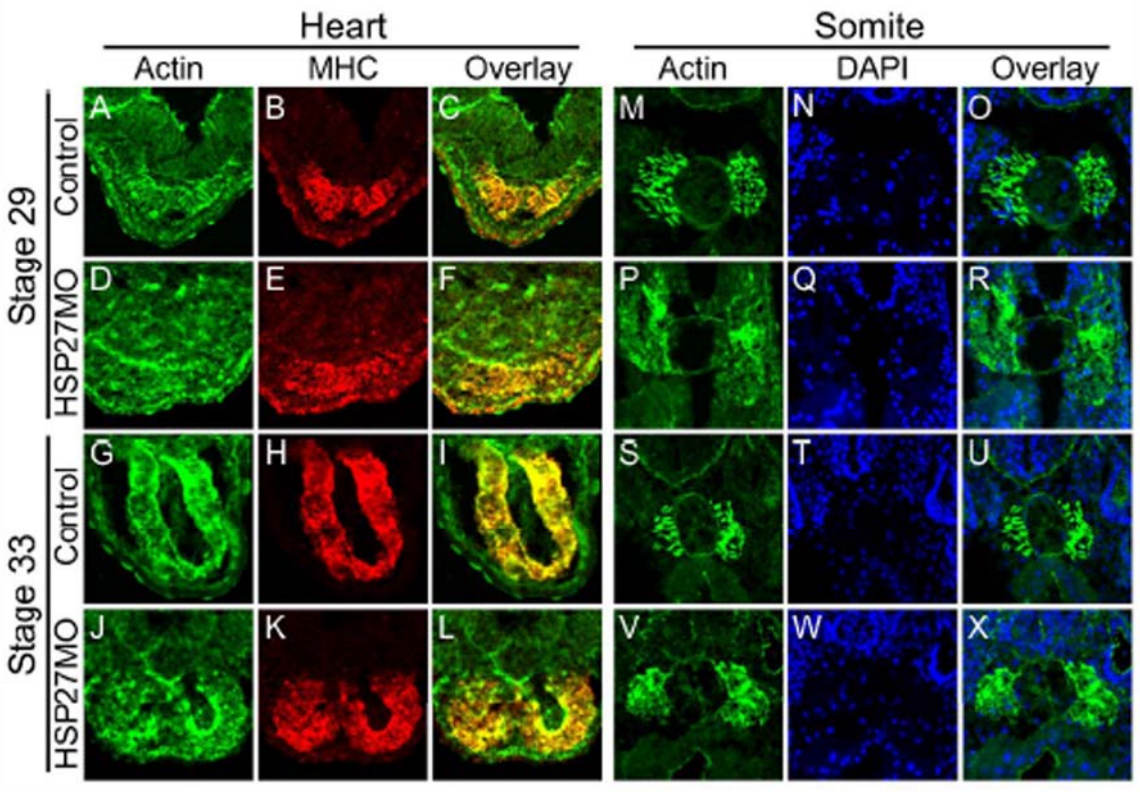
Heart
Somite
Actin
MHC
Overlay
Actin
DAPI
Overlay
Stage 29
Control
HSP27MO
Stage 33
Control
HSP27MO
A
B
C
M
N
O
D
E
F
P
Q
R
G
H
I
S
T
U
J
K
L
V
W
X

Figure A2.7 HSP-depletion does not alter levels of actin.

Western blot demonstrating actin levels in control and *Hsp27*-depleted embryos (Hsp27MO) at the indicated stages. α-tubulin antibody staining was used as a loading control.

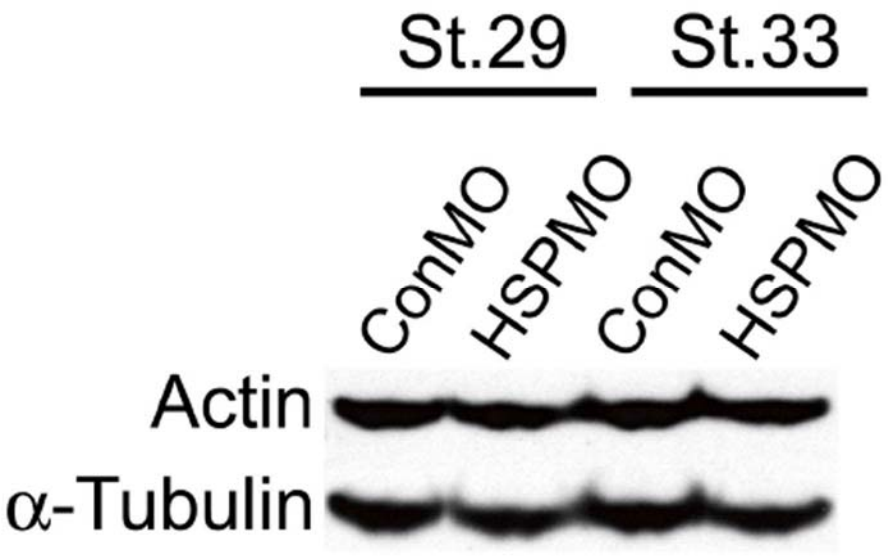

Figure A2.8 XHSP27 morphant ultrastructure analysis reveals a lack in myofibril assembly.

Transmission electron microscopy of ventral myocardium in stage 38 control and XHSP27 morphant hearts. (A-C) Ventral myocardium of ConMO injected embryo. (D-F) Ventral myocardium of XHSP27MO injected embryo. Cardiac muscle fibrils are shown pseudo-colored in yellow. Inset in (C) shows magnification of myofibril structure and inset in (F) shows magnification of apparent myosin aggregates. (G, H) Muscle fibers within the myotome in stage 38 control morpholino injected embryos. (I, J) Muscle fibers within the myotome in stage 38 *XHsp27* morpholino injected embryos. *l*, longitudinal myofibers section; *t*, transverse myofibers section; *z*, z-line.

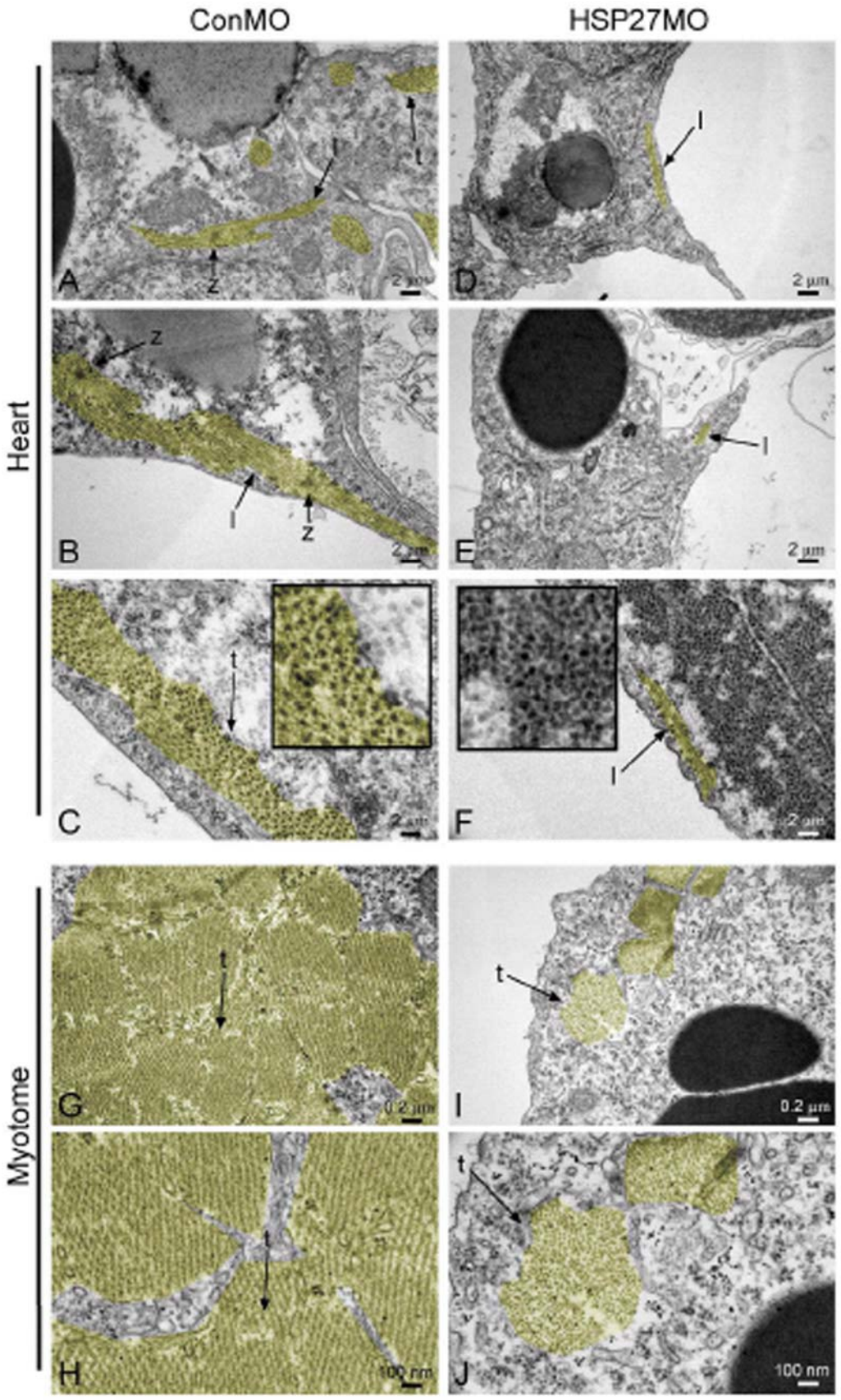
ConMO
HSP27MO
Heart
Myotome
A
B
C
D
E
F
G
H
I
J
z
t
l
2 μm
0.2 μm
100 nm

REFERENCE

Alexander, J., Rothenberg, M., Henry, G. L. and Stainier, D. Y. (1999). casanova plays an early and essential role in endoderm formation in zebrafish. *Dev Biol* 215, 343-57.

Arrigo, A. P. (2001). Hsp27: novel regulator of intracellular redox state. *IUBMB Life* 52, 303-7.

Baek, S. H., Min, J. N., Park, E. M., Han, M. Y., Lee, Y. S., Lee, Y. J. and Park, Y. M. (2000). Role of small heat shock protein HSP25 in radioresistance and glutathione-redox cycle. *J Cell Physiol* 183, 100-7.

Beiman, M., Shilo, B. and T., V. (1996). Heartless, a Drosophila FGF receptor homolog, is essential for cell migration and establishment of several mesodermal lineages. *Genes Dev.* 10, 2993-3002.

Benndorf, R., Hayess, K., Ryazantsev, S., Wieske, M., Behlke, J. and Lutsch, G. (1994). Phosphorylation and supramolecular organization of murine small heat shock protein HSP25 abolish its actin polymerization-inhibiting activity. *J Biol Chem* 269, 20780-4.

Benndorf, R. and Welsh, M. J. (2004). Shocking degeneration. *Nat Genet* 36, 547-8.

Bonham, R. T., Fine, M. R., Pollock, F. M. and Shelden, E. A. (2003). Hsp27, Hsp70, and metallothionein in MDCK and LLC-PK1 renal epithelial cells: effects of prolonged exposure to cadmium. *Toxicol Appl Pharmacol* 191, 63-73.

Brown, D. D., Binder, O., Pagratis, M., Parr, B. A. and Conlon, F. L. (2003). Developmental expression of the Xenopus laevis Tbx20 orthologue. *Dev Genes Evol* 212, 604-7.

Brown, D. D., Davis, A. C. and Conlon, F. L. (2006). Xtn3 is a developmentally expressed cardiac and skeletal muscle-specific novex-3 titin isoform. *Gene Expr Patterns* 6, 913-918.

Brown, D. D., Martz, S. N., Binder, O., Goetz, S. C., Price, B. M. J., Smith, J. C. and Conlon, F. L. (2005). Tbx5 and Tbx20 act synergistically to control vertebrate heart morphogenesis. *Development* 132, 553-563.

Bruey, J. M., Ducasse, C., Bonniaud, P., Ravagnan, L., Susin, S. A., Diaz-Latoud, C., Gurbuxani, S., Arrigo, A. P., Kroemer, G., Solary, E. et al. (2000). Hsp27 negatively regulates cell death by interacting with cytochrome c. *Nat Cell Biol* 2, 645-52.

Brundel, B. J., Shiroshita-Takeshita, A., Qi, X., Yeh, Y. H., Chartier, D., van Gelder, I. C., Henning, R. H., Kampinga, H. H. and Nattel, S. (2006). Induction of

heat shock response protects the heart against atrial fibrillation. *Circ Res* 99, 1394-402.

Ciruna, B. G. and Rossant, J. (1999). Expression of the T-box gene Eomesodermin during early mouse development. *Mech Dev* 81, 199-203.

Dalle-Donne, I., Rossi, R., Milzani, A., Di Simplicio, P. and Colombo, R. (2001). The actin cytoskeleton response to oxidants: from small heat shock protein phosphorylation to changes in the redox state of actin itself. *Free Radic Biol Med* 31, 1624-32.

David, J. C., Landry, J. and Grongnet, J. F. (2000). Perinatal expression of heat-shock protein 27 in brain regions and nonneural tissues of the piglet. *J Mol Neurosci* 15, 109-20.

DeHaan, R. L. (1963). Migrating patterns of precardiac mesoderm in the early chick embryo. *Exp. cell Res.* 29, 544-560.

Escobedo, J., Pucci, A. M. and Koh, T. J. (2004). HSP25 protects skeletal muscle cells against oxidative stress. *Free Radic Biol Med* 37, 1455-62.

Evgrafov, O. V., Mersiyanova, I., Irobi, J., Van Den Bosch, L., Dierick, I., Leung, C. L., Schagina, O., Verpoorten, N., Van Impe, K., Fedotov, V. et al. (2004). Mutant small heat-shock protein 27 causes axonal Charcot-Marie-Tooth disease and distal hereditary motor neuropathy. *Nat Genet* 36, 602-6.

Feil, I. K., Malfois, M., Hendle, J., van Der Zandt, H. and Svergun, D. I. (2001). A novel quaternary structure of the dimeric alpha-crystallin domain with chaperone-like activity. *J Biol Chem* 276, 12024-9.

Ferns, G., Shams, S. and Shafi, S. (2006). Heat shock protein 27: its potential role in vascular disease. *Int J Exp Pathol* 87, 253-74.

George, E. L., Baldwin, H. S. and Hynes, R. O. (1997). Fibronectins are essential for heart and blood vessel morphogenesis but are dispensable for initial specification of precursor cells. *Blood* 90, 3073-81.

George, E. L., Georges-Labouesse, E. N., Patel-King, R. S., Rayburn, H. and Hynes, R. O. (1993). Defects in mesoderm, neural tube and vascular development in mouse embryos lacking fibronectin. *Development* 119, 1079-91.

Gernold, M., Knauf, U., Gaestel, M., Stahl, J. and Kloetzel, P. M. (1993). Development and tissue-specific distribution of mouse small heat shock protein hsp25. *Dev Genet* 14, 103-11.

Gisselbrecht, S., Skeath, J., Doe, C. and Michelson, A. (1996). heartless encodes a fibroblast growth factor receptor (DFR1/DFGF-R2) involved in the

directional migration of early mesodermal cells in the Drosophila embryo. *Genes Dev..* 1, 3003-3017.

Goetz, S. and Conlon, F. L. (2007). Cardiac Progenitors and the Embryonic Cell Cycle. *Cell Cycle* In Press.

Goetz, S. C., Brown, D. D. and Conlon, F. L. (2006). TBX5 is required for embryonic cardiac cell cycle progression. *Development* 133, 2575-84.

Harland, R. M. (1991). In situ hybridization: an improved whole mount method for Xenopus embryos. *Meth. Cell Biol.* 36, 675-685.

Hollander, J. M., Martin, J. L., Belke, D. D., Scott, B. T., Swanson, E., Krishnamoorthy, V. and Dillmann, W. H. (2004). Overexpression of wild-type heat shock protein 27 and a nonphosphorylatable heat shock protein 27 mutant protects against ischemia/reperfusion injury in a transgenic mouse model. *Circulation* 110, 3544-52.

Huot, J., Houle, F., Spitz, D. R. and Landry, J. (1996). HSP27 phosphorylation-mediated resistance against actin fragmentation and cell death induced by oxidative stress. *Cancer Res* 56, 273-9.

Jakob, U., Gaestel, M., Engel, K. and Buchner, J. (1993). Small heat shock proteins are molecular chaperones. *J Biol Chem* 268, 1517-20.

Jiang, Y. and Evans, T. (1996). The Xenopus GATA-4/5/6 genes are associated with cardiac specification and can regulate cardiac-specific transcription during embryogenesis. *Dev Biol* 174, 258-70.

Kikuchi, Y., Trinh, L. A., Reiter, J. F., Alexander, J., Yelon, D. and Stainier, D. Y. (2000). The zebrafish bonnie and clyde gene encodes a Mix family homeodomain protein that regulates the generation of endodermal precursors. *Genes Dev* 14, 1279-89.

Knowlton, A. A., Kapadia, S., Torre-Amione, G., Durand, J. B., Bies, R., Young, J. and Mann, D. L. (1998). Differential expression of heat shock proteins in normal and failing human hearts. *J Mol Cell Cardiol* 30, 811-8.

Kolker, S., Tajchman, U. and Weeks, D. L. (2000). Confocal Imaging of early heat development in Xenopus laevis. *Dev. Biol.* 218, 64-73.

Komatsuda, A., Wakui, H., Oyama, Y., Imai, H., Miura, A. B., Itoh, H. and Tashima, Y. (1999). Overexpression of the human 72 kDa heat shock protein in renal tubular cells confers resistance against oxidative injury and cisplatin toxicity. *Nephrol Dial Transplant* 14, 1385-90.

Kuo, C. T., Morrisey, E. E., Anandappa, R., Sigrist, K., Lu, M. M., Parmacek, M. S., Soudais, C. and Leiden, J. M. (1997). GATA4 transcription factor is required for ventral morphogenesis and heart tube formation. *Genes Dev* 11, 1048-60.

Kupperman, E., An, S., Osborne, N., Waldron, S. and Stainier, D. Y. (2000). A sphingosine-1-phosphate receptor regulates cell migration during vertebrate heart development. *Nature* 406, 192-5.

Langdon, Y. G., Duddy, J. and Conlon, F. L. (submitted). An evolutionarily conserved role for SHP-2 signalling in early heart development.

Lavoie, J. N., Gingras-Breton, G., Tanguay, R. M. and Landry, J. (1993a). Induction of Chinese hamster HSP27 gene expression in mouse cells confers resistance to heat shock. HSP27 stabilization of the microfilament organization. *J Biol Chem* 268, 3420-9.

Lavoie, J. N., Hickey, E., Weber, L. A. and Landry, J. (1993b). Modulation of actin microfilament dynamics and fluid phase pinocytosis by phosphorylation of heat shock protein 27. *J Biol Chem* 268, 24210-4.

Lavoie, J. N., Lambert, H., Hickey, E., Weber, L. A. and Landry, J. (1995). Modulation of cellular thermoresistance and actin filament stability accompanies phosphorylation-induced changes in the oligomeric structure of heat shock protein 27. *Mol Cell Biol* 15, 505-16.

Leal, R. B., Cordova, F. M., Herd, L., Bobrovskaya, L. and Dunkley, P. R. (2002). Lead-stimulated p38MAPK-dependent Hsp27 phosphorylation. *Toxicol Appl Pharmacol* 178, 44-51.

Liu, L., Zhang, X., Qian, B., Min, X., Gao, X., Li, C., Cheng, Y. and Huang, J. (2007). Over-expression of heat shock protein 27 attenuates doxorubicin-induced cardiac dysfunction in mice. *Eur J Heart Fail*.

Lough, J. and Sugi, Y. (2000). Endoderm and heart development. *Dev Dyn* 217, 327-42.

Mao, L., Bryantsev, A. L., Chechenova, M. B. and Shelden, E. A. (2005). Cloning, characterization, and heat stress-induced redistribution of a protein homologous to human hsp27 in the zebrafish Danio rerio. *Exp Cell Res* 306, 230-41.

Mao, L. and Shelden, E. A. (2006). Developmentally regulated gene expression of the small heat shock protein Hsp27 in zebrafish embryos. *Gene Expr Patterns* 6, 127-33.

Mehlen, P., Kretz-Remy, C., Briolay, J., Fostan, P., Mirault, M. E. and Arrigo, A. P. (1995). Intracellular reactive oxygen species as apparent modulators of heat-shock protein 27 (hsp27) structural organization and phosphorylation in basal

and tumour necrosis factor alpha-treated T47D human carcinoma cells. *Biochem J* 312 (Pt 2), 367-75.

Mehlen, P., Mehlen, A., Godet, J. and Arrigo, A. P. (1997). hsp27 as a switch between differentiation and apoptosis in murine embryonic stem cells. *J Biol Chem* 272, 31657-65.

Miron, T., Vancompernolle, K., Vandekerckhove, J., Wilchek, M. and Geiger, B. (1991). A 25-kD inhibitor of actin polymerization is a low molecular mass heat shock protein. *J Cell Biol* 114, 255-61.

Mohun, T., Orford, R. and Shang, C. (2003). The origins of cardiac tissue in the amphibian, Xenopus laevis. *Trends Cardiovasc Med* 13, 244-8.

Nieuwkoop, P. D. and Faber, J. (1967). Normal Table of *Xenopus laevis* (Daudin). Amsterdam: North Holland.

Paul, C., Manero, F., Gonin, S., Kretz-Remy, C., Virot, S. and Arrigo, A. P. (2002). Hsp27 as a negative regulator of cytochrome C release. *Mol Cell Biol* 22, 816-34.

Quertermous, T. (2007). Apelin and its g protein-coupled receptor regulate cardiac development as well as cardiac function. *Dev Cell* 12, 319-20.

Rahman, D. R., Bentley, N. J. and Tuite, M. F. (1995). The Saccharomyces cerevisiae small heat shock protein Hsp26 inhibits actin polymerisation. *Biochem Soc Trans* 23, 77S.

Reiter, J. F., Alexander, J., Rodaway, A., Yelon, D., Patient, R., Holder, N. and Stainier, D. Y. (1999). Gata5 is required for the development of the heart and endoderm in zebrafish. *Genes Dev* 13, 2983-95.

Reynolds, L. P. and Allen, G. V. (2003). A review of heat shock protein induction following cerebellar injury. *Cerebellum* 2, 171-7.

Scheler, C., Li, X. P., Salnikow, J., Dunn, M. J. and Jungblut, P. R. (1999). Comparison of two-dimensional electrophoresis patterns of heat shock protein Hsp27 species in normal and cardiomyopathic hearts. *Electrophoresis* 20, 3623-8.

Schier, A. F., Neuhauss, S. C., Helde, K. A., Talbot, W. S. and Driever, W. (1997). The one-eyed pinhead gene functions in mesoderm and endoderm formation in zebrafish and interacts with no tail. *Development* 124, 327-42.

Scott, I. C., Masri, B., D'Amico, L. A., Jin, S. W., Jungblut, B., Wehman, A. M., Baier, H., Audigier, Y. and Stainier, D. Y. (2007). The g protein-coupled receptor agtrl1b regulates early development of myocardial progenitors. *Dev Cell* 12, 403-13.

Shama, K. M., Suzuki, A., Harada, K., Fujitani, N., Kimura, H., Ohno, S. and Yoshida, K. (1999). Transient up-regulation of myotonic dystrophy protein kinase-binding protein, MKBP, and HSP27 in the neonatal myocardium. *Cell Struct Funct* 24, 1-4.

Shelden, E. A., Borrelli, M. J., Pollock, F. M. and Bonham, R. (2002). Heat shock protein 27 associates with basolateral cell boundaries in heat-shocked and ATP-depleted epithelial cells. *J Am Soc Nephrol* 13, 332-41.

Skre, H. (1974). Genetic and clinical aspects of Charcot-Marie-Tooth's disease. *Clin Genet* 6, 98-118.

Somji, S., Sens, D. A., Garrett, S. H., Sens, M. A. and Todd, J. H. (1999). Heat shock protein 27 expression in human proximal tubule cells exposed to lethal and sublethal concentrations of CdCl2. *Environ Health Perspect* 107, 545-52.

Stainier, D. Y. (2001). Zebrafish genetics and vertebrate heart formation. *Nat Rev Genet.* 2, 39-48.

Sun, X., Meyers, E. N., Lewandoski, M. and Martin, G. R. (1999). Targeted disruption of Fgf8 causes failure of cell migration in the gastrulating mouse embryo. *Genes Dev* 13, 1834-46.

Trinh, L. A. and Stainier, D. Y. (2004). Fibronectin regulates epithelial organization during myocardial migration in zebrafish. *Dev Cell* 6, 371-82.

Tuttle, A. M., Gauley, J., Chan, N. and Heikkila, J. J. (2007). Analysis of the expression and function of the small heat shock protein gene, hsp27, in Xenopus laevis embryos. *Comp Biochem Physiol A Mol Integr Physiol* 147, 112-21.

Vander Heide, R. S. (2002). Increased expression of HSP27 protects canine myocytes from simulated ischemia-reperfusion injury. *Am J Physiol Heart Circ Physiol* 282, H935-41.

Wilson, P. A. and Hemmati-Brivanlou, A. (1995). Induction of epidermis and inhibition of neural fate by Bmp-4. *Nature* 376, 331-333.

Yelon, D., Ticho, B., Halpern, M. E., Ruvinsky, I., Ho, R. K., Silver, L. M. and Stainier, D. Y. (2000). The bHLH transcription factor hand2 plays parallel roles in zebrafish heart and pectoral fin development. *Development* 127, 2573-82.

Zeng, X. X., Wilm, T. P., Sepich, D. S. and Solnica-Krezel, L. (2007). Apelin and its receptor control heart field formation during zebrafish gastrulation. *Dev Cell* 12, 391-402.